NASA Contractor Report 3102

Rotary Balance Data for a Typical Single-Engine General Aviation Design for an Angle-of-Attack Range of 8° to 35°

III - Effect of Wing Leading-Edge Modifications Model A

William Bihrle, Jr., and William Mulcay

CONTRACT NAS1-14849
NOVEMBER 1979

NASA

NASA Contractor Report 3102

Rotary Balance Data for a Typical Single-Engine General Aviation Design for an Angle-of-Attack Range of 8° to 35°

III - Effect of Wing Leading-Edge Modifications Model A

William Bihrle, Jr., and William Mulcay
Bihrle Applied Research, Inc.
Jericho, New York

Prepared for
Langley Research Center
under Contract NAS1-14849

NASA
National Aeronautics
and Space Administration

Scientific and Technical
Information Branch

1979

SUMMARY

Aerodynamic characteristics obtained in a rotational flow environment utilizing a rotary balance located in the Langley spin tunnel are presented in plotted form for a 1/5-scale, single-engine, low-wing, general aviation airplane model. The configurations tested included the basic airplane, sixteen wing leading-edge modifications and lateral-directional control settings. Data are presented for all configurations without analysis for an angle-of-attack range of 8° to 35° and clockwise and counter-clockwise rotations covering an $\frac{\Omega b}{2V}$ range from 0 to 0.85. Also, data are presented above 35° angle of attack for some configurations.

INTRODUCTION

The NASA Langley Research Center has initiated a broad general aviation stall/spin research program which includes spin-tunnel and free-flight radio control model tests, as well as full-scale flight tests for a number of configurations typical of light, general aviation airplanes. To support this effort, rotary balance wind tunnel force tests covering these same configurations will be conducted to establish a data base for analysis of model and full-scale flight results, and to develop design charts for desirable stall/spin characteristics.

A 1/5-scale, single-engine, general aviation airplane model, referred to as model A, having a low-wing location was tested in a rotational flow environment utilizing a rotary balance located in the Langley spin tunnel. This report presents the data obtained for the basic configuration, sixteen wing leading-edge modifications, and lateral-directional control settings.

SYMBOLS

The units for physical quantities used herein are presented in the International System of Units (SI) and U.S. Customary Units. The measurements were made in the U.S. Customary Units; equivalent dimensions were determined by using the conversion factors given in reference 1.

b wing span

$\bar{c}$ mean aerodynamic chord, cm (in.)

C_L lift-force coefficient, $\frac{\text{Lift force}}{qS}$

C_ℓ rolling-moment coefficient, $\frac{\text{Rolling moment}}{qSb}$

C_m pitching-moment coefficient, $\frac{\text{Pitching moment}}{qS\bar{c}}$

C_n yawing-moment coefficient, $\frac{\text{Yawing moment}}{qSb}$

q free-stream dynamic pressure, N/m^2 (lb/ft^2)

S wing area, m^2 (ft^2)

V free-stream velocity, m/sec (ft/sec)

α angle of attack, deg

β angle of sideslip, deg

Ω angular velocity about spin axis, rad/sec

$\frac{\Omega b}{2V}$ spin coefficient, positive for clockwise spin

δ_a aileron deflection, positive when right aileron is down

$(\delta_{a_{right}} - \delta_{a_{left}})/2$, deg

δ_e elevator deflection, positive when trailing edge is down, deg

δ_r rudder deflection, positive when trailing edge is to left, deg

Abbreviations:

cg center of gravity

LE leading edge

SR spin radius

TEST EQUIPMENT

A rotary balance measures the forces and moments acting on an airplane while subjected to rotational flow conditions; the background for this apparatus is discussed in reference 2. A photograph and sketch of the rotary balance apparatus installed in the Langley spin tunnel are shown in figures 1 and 2, respectively. The rotating portion of the balance system, mounted on a horizontal supporting boom which is hinged at the wall, is moved from the wall to the center of the tunnel by cables. The rotary arm of the balance system, which rotates about a vertical axis, is attached to the outer end of the horizontal supporting boom and is driven by a drive shaft through couplings and gears.

A test model is mounted on a strain gauge balance which is affixed to the bottom of the rotary balance apparatus. Controls located outside the tunnel are used to activate motors on the rig which position the model to the desired attitude. The angle-of-attack range of the rig is 8 to 90 degrees and the sideslip angle range is ±15 degrees. The spin radius and the lateral displacement motors allow the operator to position the moment center of the balance on the spin axis or at a specific distance from the spin axis. This is done for each combination of angle of attack and sideslip angle. The general practice is to mount the moment center of the balance at the cg location about which

the aerodynamic moments are desired. Electrical current from the balance, and to the motors on the rig, is conducted through slip-rings located at the rig head. Examples of how the rig is positioned for different angle of attack and sideslip angles are shown in figures 2a and 2b, respectively.

The model can be rotated up to 90 rpm in either direction. By using different rotational speeds and a specific airflow in the tunnel, the motions of a steady spinning airplane can be simulated. The aerodynamic forces and moments can then be measured for values of $\frac{\Omega b}{2V}$, including the case of $\frac{\Omega b}{2V} = 0$, where static aerodynamic forces and moments can be obtained.

A NASA six-component strain gauge balance is mounted inside the model and measures the normal, lateral and longitudinal forces and the yawing, rolling and pitching moments acting about the model body axis. The interactions that exist between the six components are available from balance calibration tests and are accounted for after the balance voltages are converted to forces and moments.

The data acquisition, reduction and presentation system for the rotary balance set-up is composed of a 12-channel scanner/voltmeter, a mini-computer and a plotter. With this equipment, on-line digital print-out and/or graphical plots of data are possible.

TEST PROCEDURES

Rotary aerodynamic data are obtained in two steps. The first step is to record the inertial forces and moments (tares) acting on the model at different attitudes and rotational speeds.

To accomplish this, a covered bird-cage like structure is mounted to the upper rig which encloses the model without touching it. In this manner, the air immediately surrounding the model is rotated with it. As the rig is rotated at the desired attitude and rate, the inertial forces and moments generated by the model are measured and stored on magnetic tape for later use.

The second step in the data-gathering process is to measure aerodynamic and inertial forces at different attitudes and rotational speeds for a selected tunnel velocity with, of course, the cage structure removed. The tares are subtracted from these values, and the remaining aerodynamic forces and moments are then converted to coefficient form and stored on magnetic tape.

MODEL

A 1/5-scale fiberglass/aluminum model of a configuration considered to be a typical low-wing, single-engine, light general aviation airplane was tested in the present study. A three-view drawing of this model is shown in figure 3, dimensional characteristics of the model are presented in Table I, and a photograph of the model installed on the rotary balance located in the Langley spin tunnel is presented in figure 1.

The model control surfaces could be set at any position prior to the test. The maximum deflections for the control surfaces were:

Rudder, deg	25 right, 25 left
Aileron, deg	25 up, 20 down

TEST CONDITIONS

The tests were conducted in the spin tunnel at a tunnel velocity of 7.62m/sec (25 ft/sec) which corresponds to a Reynolds number of 128,000 based on the model mean aerodynamic chord. Unless noted otherwise in Table II, all the configurations were tested through an angle-of-attack range of 8 to 35° at a zero sideslip angle with the spin axis located 76.2cm (30in) forward of the full-scale airplane cg location of .255$\bar{c}$. At each spin attitude, measurements were obtained for nominal $\frac{\Omega b}{2V}$ values of .1, .2, .3, .4, .45, .55, .65, .75 and .85 in both clockwise and counter-clockwise directions, as well as for $\frac{\Omega b}{2V} = 0$ (static value).

DATA PRESENTATION

Table II identifies the configurations tested and the corresponding appendix figure numbers which present the aerodynamic data. The aerodynamic coefficients vs. $\frac{\Omega b}{2V}$ are presented for each configuration in three sequentially numbered figures in the following order: C_n, C_ℓ, and C_m. Each figure, in turn, consists of two pages which present the subject aerodynamic coefficient vs. $\frac{\Omega b}{2V}$ for the following angles of attack and spin radius.

a) α= 8, 10, 12, 14, 16 deg SR= 76cm (30in)

b) α= 18, 20, 25, 30, 35 deg SR= 76cm (30in)

As noted in Table II, data is also available for some configurations between 30 and 90° angle of attack. This data is presented for the following angles of attack and spin radius:

c) α= 30, 35, 40, 45, 50 deg SR= 0

d) α= 55, 60, 70, 80, 90 deg SR= 0

All the moment data are presented for a cg position of 0.255$\bar{c}$.

Lift coefficient as a function of angle of attack for zero rotation rate is presented at the end of the Appendix for the configurations cited in Table II.

REFERENCES

1. Mechtly, E.A.: The International System of Units - Physical Constants and Conversion Factors. NASA SP-7012, 1973.

2. Bihrle, William, Jr.; Hultberg, Randy S.; and Mulcay, William: Rotary Balance Data for a Typical Single-Engine Low-Wing General Aviation Design for an Angle-of-Attack Range of 30° to 90°. NASA CR 2972, 1978.

TABLE I.- DIMENSIONAL CHARACTERISTICS OF THE BASIC MODEL

Overall length, m (ft)	1.23 (4.05)
Wing:	
Span, m (ft)	1.46 (4.80)
Area, m^2 (ft^2)	0.36 (3.87)
Root chord, cm (in.)	24.54 (9.66)
Tip chord, cm (in.)	24.54 (9.66)
Mean aerodynamic chord, cm (in.)	24.54 (9.66)
Leading edge of $\bar{c}$, distance rearward of leading edge of root chord, cm (in.)	0
Aspect ratio	5.9
Dihedral, deg	5.0
Incidence:	
Root, deg	3.5
Tip, deg	3.5
Airfoil section	NACA 64_2-415 modified
Horizontal tail:	
Span, m (ft)	0.47 (1.53)
Incidence, deg	-3.0
Airfoil section	NACA 65_1-012
Vertical tail:	
Airfoil section	NACA 65_1-012

TABLE II.- CONFIGURATIONS TESTED AND FIGURE INDEX

(Unless noted otherwise, all configurations tested through α= 8 to 35° at β= 0° and SR= 76cm (30in).)

FIGURE NO.	CONFIGURATION	δ_e deg	δ_a deg	δ_r deg	REMARKS
[a]A1-A3	Basic	0	0	0	also α=30 to 90°,SR=0
A4-A6	↓		22.5	-25	
[a]A7-A9	Outboard LE wing droop		0	0	
A10-A12	↓		22.5	-25	
A13-A15	Inboard LE wing droop		0	0	
A16-A18	↓		22.5	-25	
[a]A19-A21	Full-span LE wing droop		0	0	also α=30 to 90°,SR=0
A22-A24	↓		22.5	-25	
[b]A25-A27	Full-span LE wing droop with large nose radius		0	0	
[b]A28-A30	Outboard LE wing droop with large nose radius				also α=30 to 90°,SR=0
[b]A31-A33	Outboard LE wing droop with large nose radius and uprigged ailerons				also α=30 to 90°,SR=0
[b]A34-A36	Outboard symmetrical wing slat extension				
[b]A37-A39	Full-span LE wing droop with outboard spoiler strip				
[c]A40-A42	Segmented LE wing droop with 16.3cm (6.4in) gap				
[c]A43-A45	Segmented LE wing droop with 12.2cm (4.8in) gap				
[c]A46-A48	Outboard LE wing droop extended inboard 12.2cm (4.8in)				
[c]A49-A51	Outboard LE wing droop extended inboard 12.2cm (4.8in) with a triangular fairing				
[d]A52-A54	4.1cm (1.6in) span LE wing tab				
[d]A55-A57	12.2cm (4.8in) span triangular planform LE wing tab				
[d]A58-A60	4.1cm (1.6in) span LE wing tab extended outboard 12.2cm (4.8in) with a triangular planform fairing				
[d]A61-A63	Full-span LE wing droop with a 12.2cm (4.8in) span triangular planform LE wing tab				

[a] C_L vs. α presented in figure A64.

[b] C_L vs. α presented in figure A65.

[c] C_L vs. α presented in figure A66.

[d] C_L vs. α presented in figure A67.

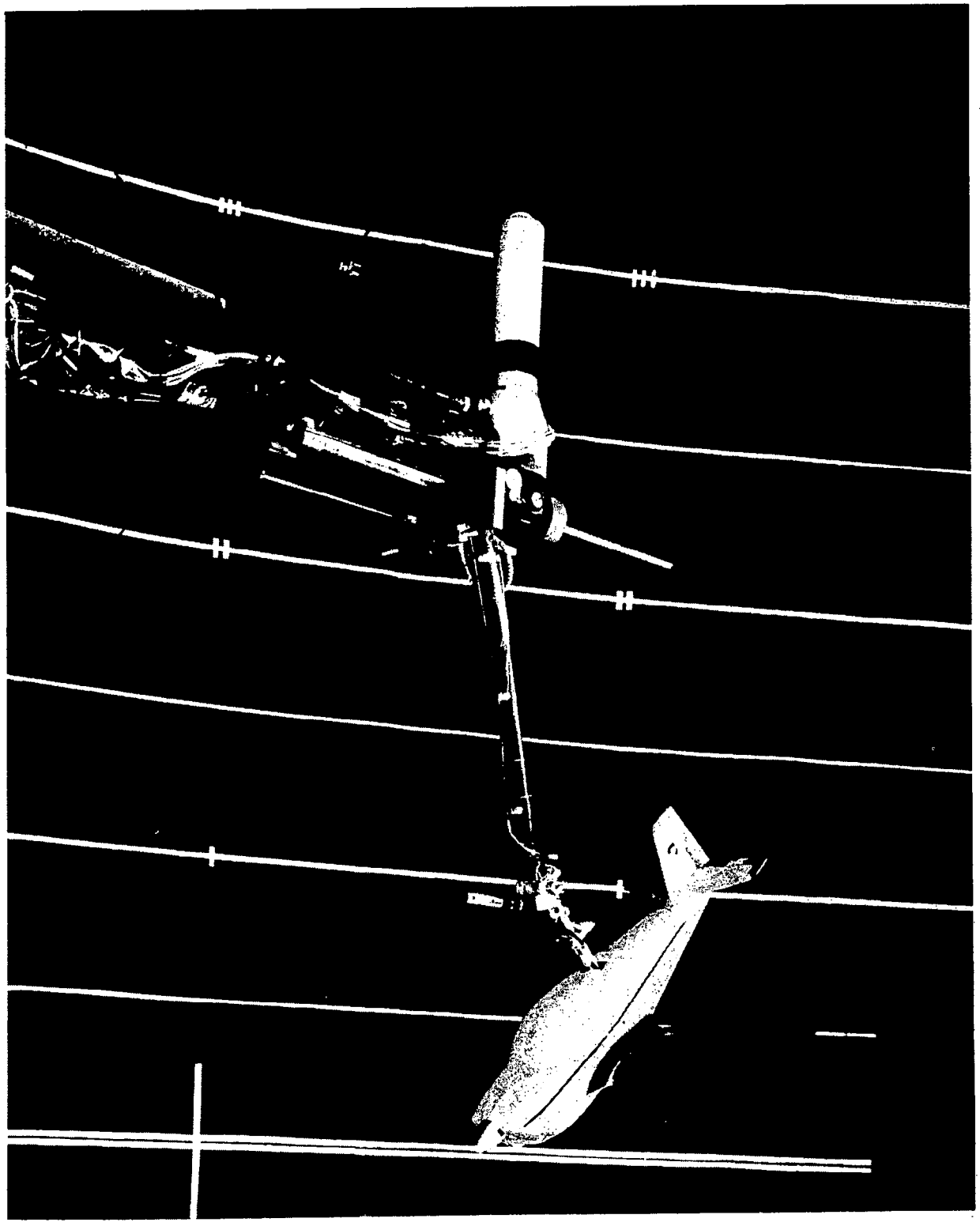

Figure 1.- Photograph of 1/5-scale model installed on rotary balance apparatus.

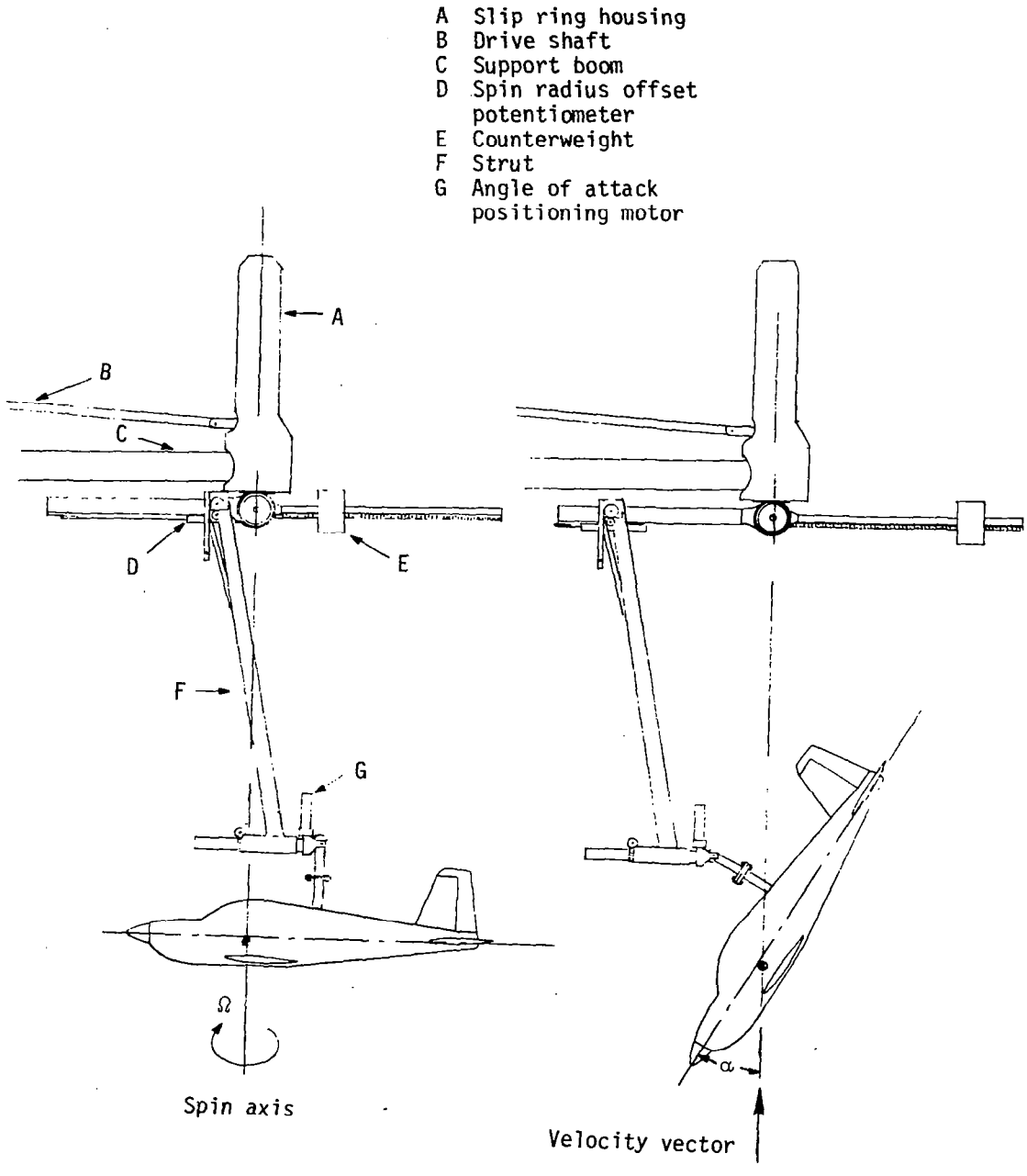

(a) Side view of model.

Figure 2.- Sketch of rotary balance apparatus.

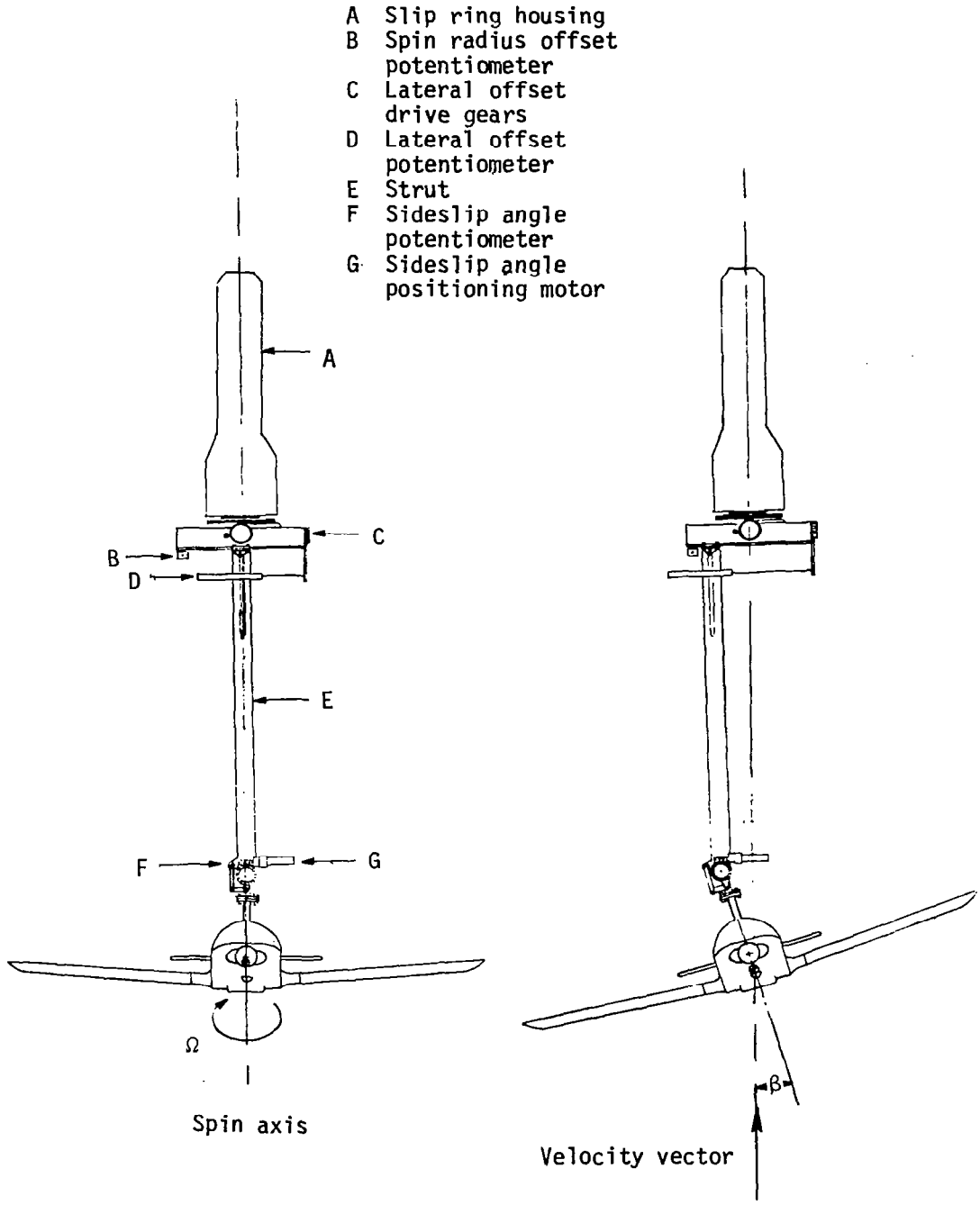

(b) Front view of model.

Figure 2.- Concluded.

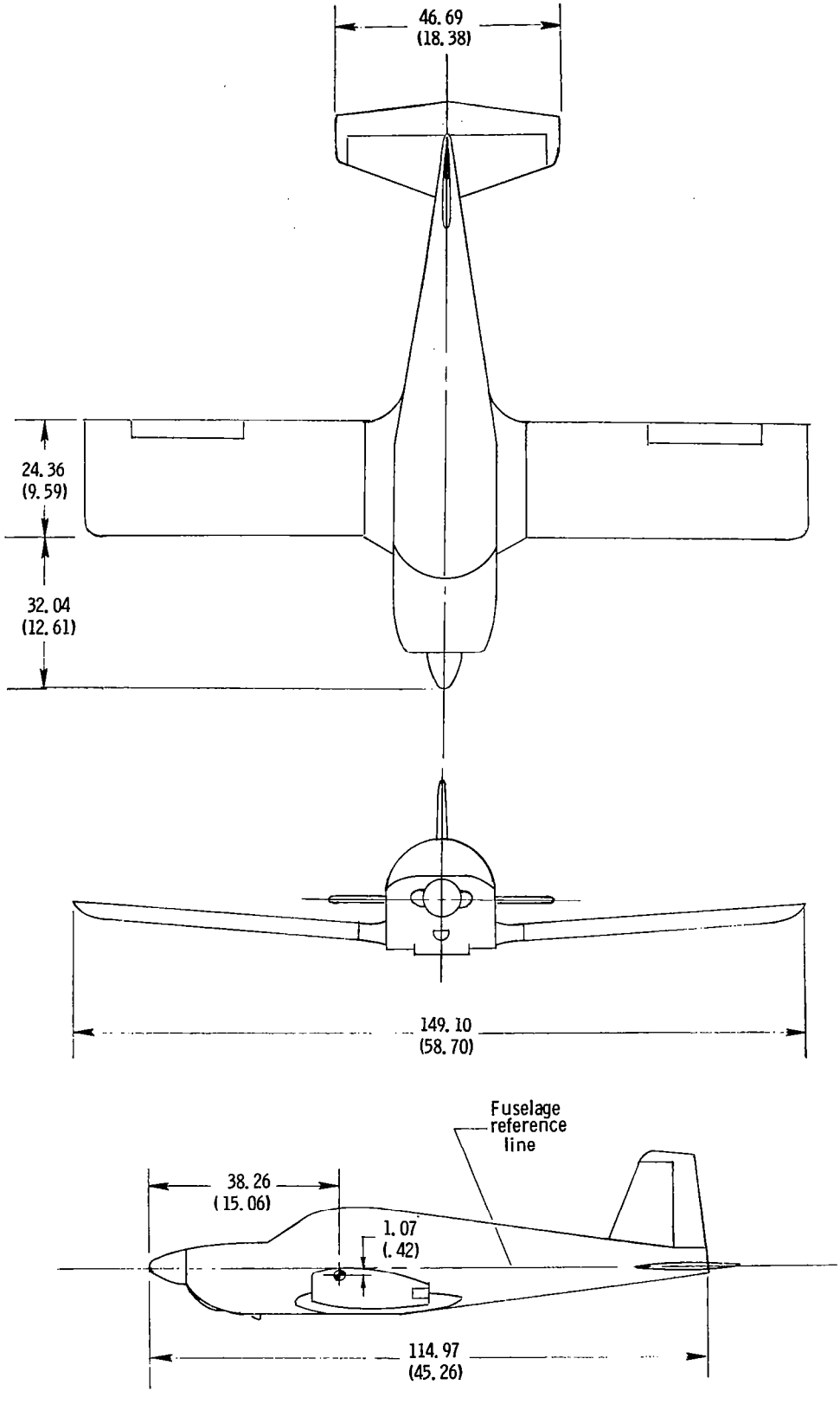

Figure 3. - Three-view drawing of 1/5-scale low-wing general aviation model A. Center-of-gravity positioned at 0.255c. Dimensions are given in centimeters(inches), model scale.

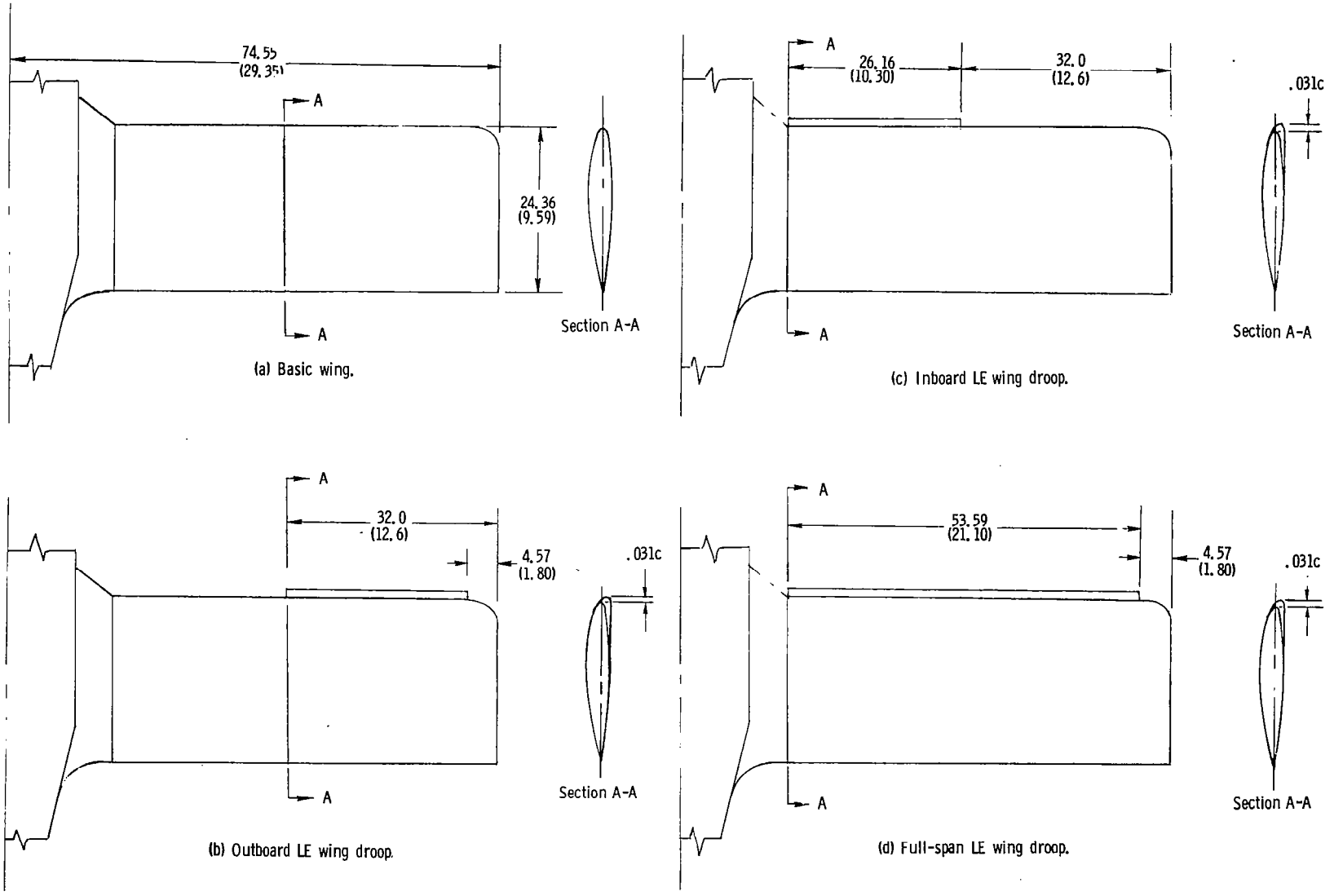

Figure 4. - Wing leading-edge modifications tested on model. Dimensions are given in centimeters(inches), model scale.

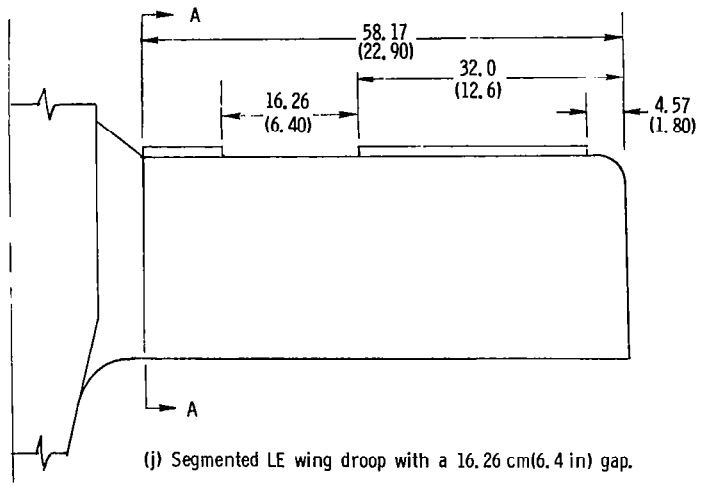

(j) Segmented LE wing droop with a 16.26 cm(6.4 in) gap.

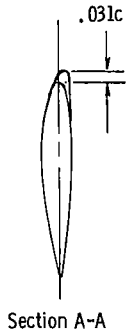

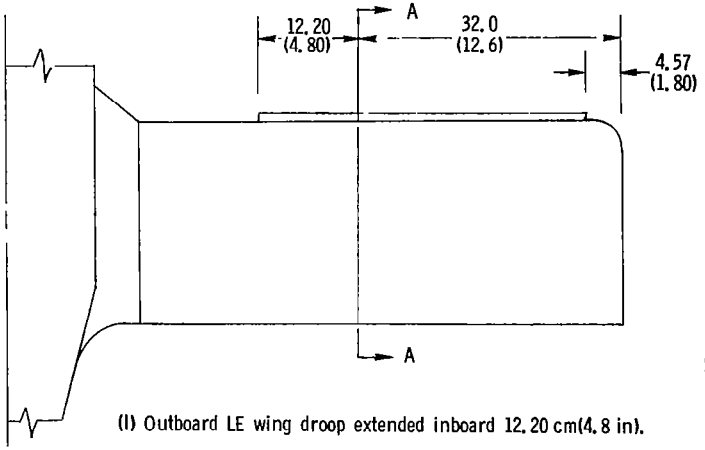

(l) Outboard LE wing droop extended inboard 12.20 cm(4.8 in).

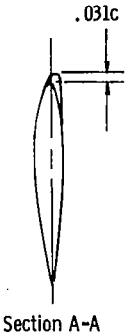

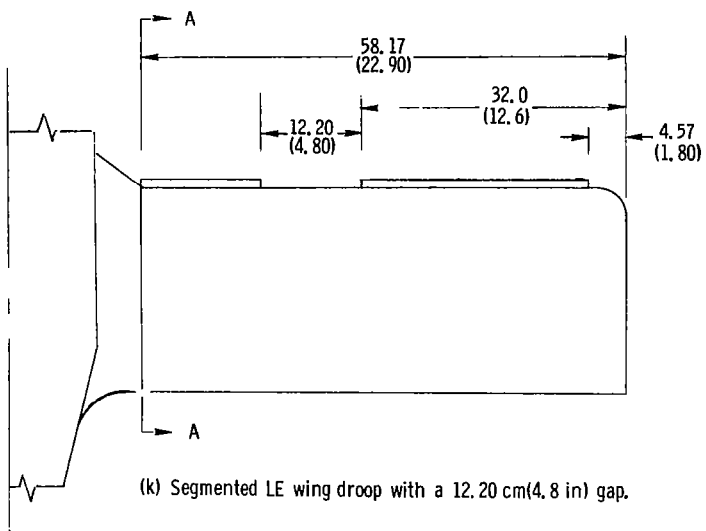

(k) Segmented LE wing droop with a 12.20 cm(4.8 in) gap.

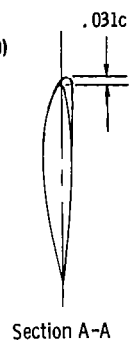

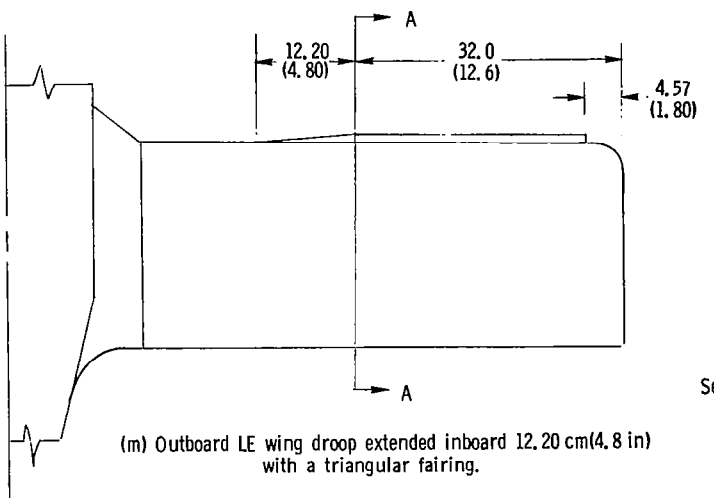

(m) Outboard LE wing droop extended inboard 12.20 cm(4.8 in) with a triangular fairing.

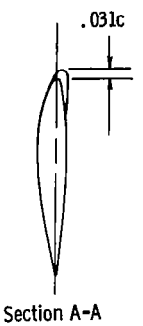

Figure 4. - Continued.

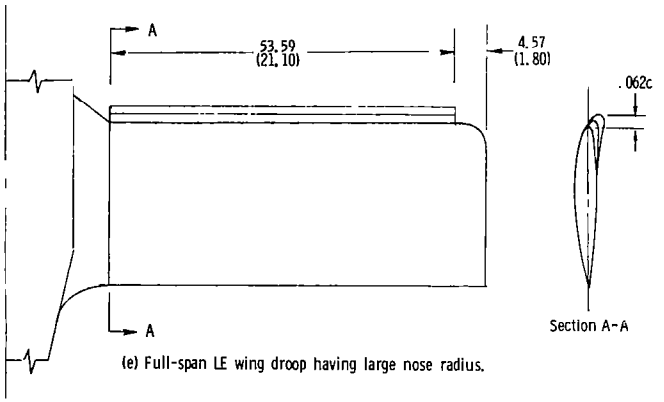

(e) Full-span LE wing droop having large nose radius.

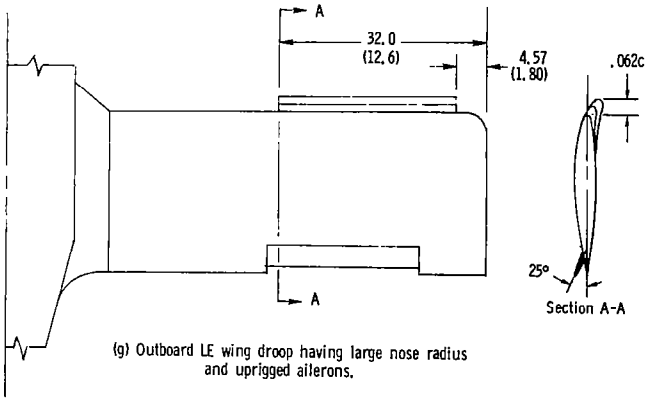

(g) Outboard LE wing droop having large nose radius and uprigged ailerons.

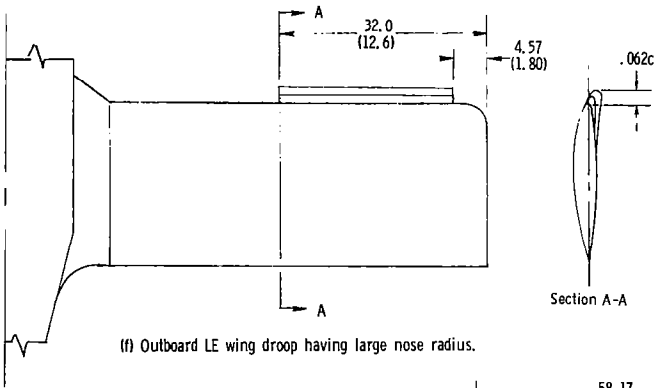

(f) Outboard LE wing droop having large nose radius.

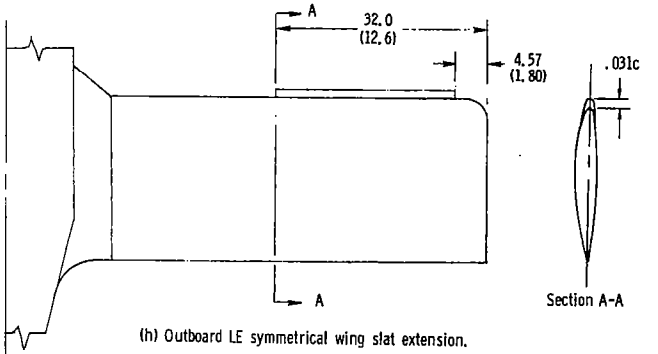

(h) Outboard LE symmetrical wing slat extension.

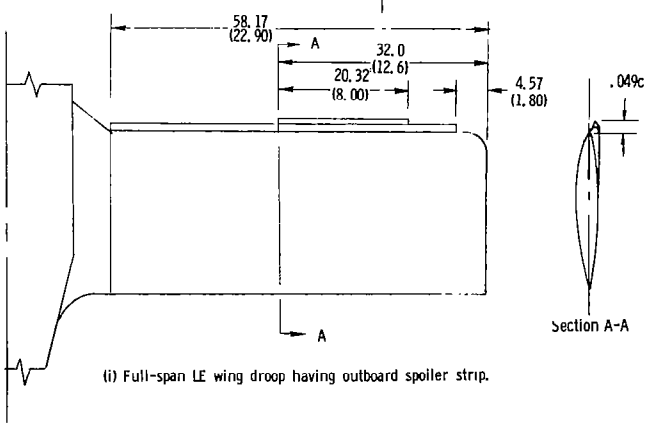

(i) Full-span LE wing droop having outboard spoiler strip.

Figure 4. - Continued.

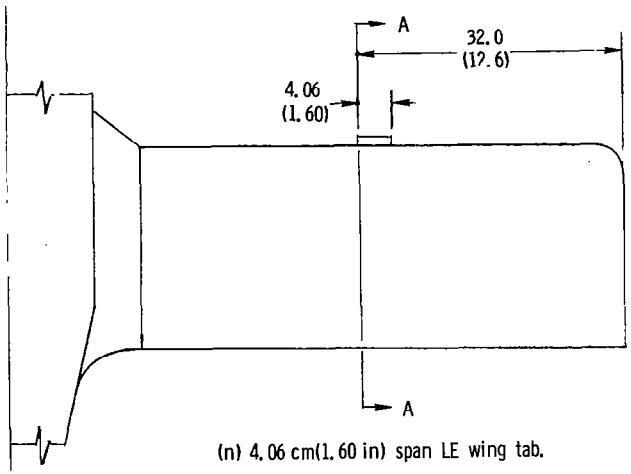

(n) 4.06 cm(1.60 in) span LE wing tab.

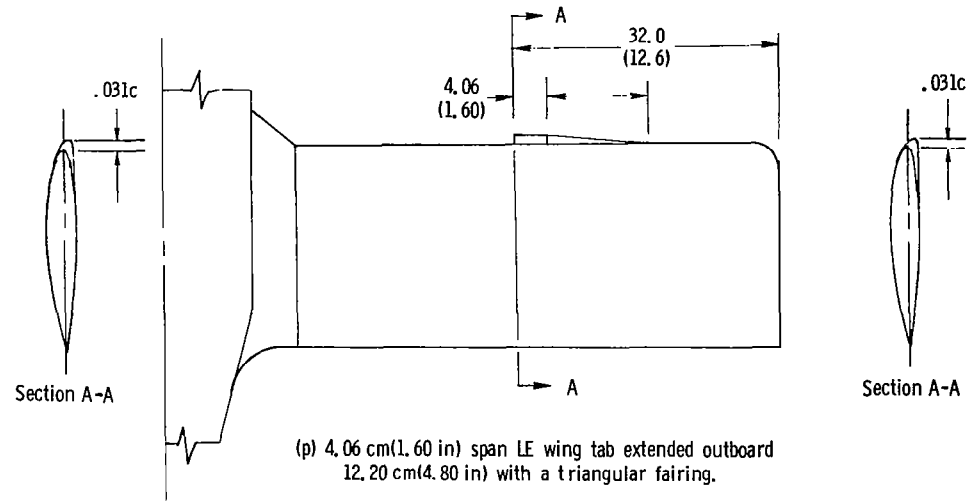

(p) 4.06 cm(1.60 in) span LE wing tab extended outboard 12.20 cm(4.80 in) with a triangular fairing.

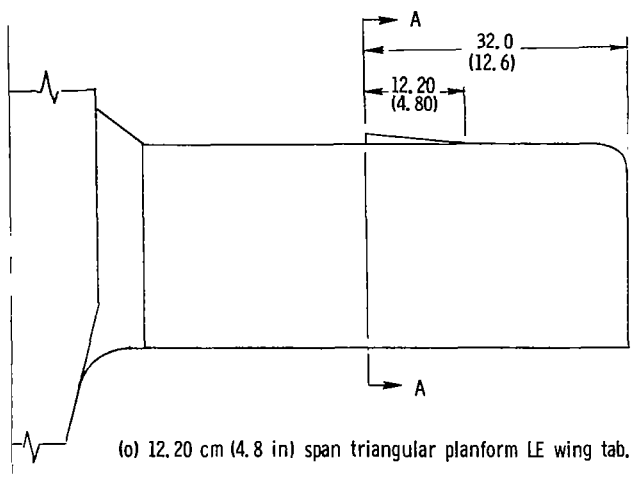

(o) 12.20 cm (4.8 in) span triangular planform LE wing tab.

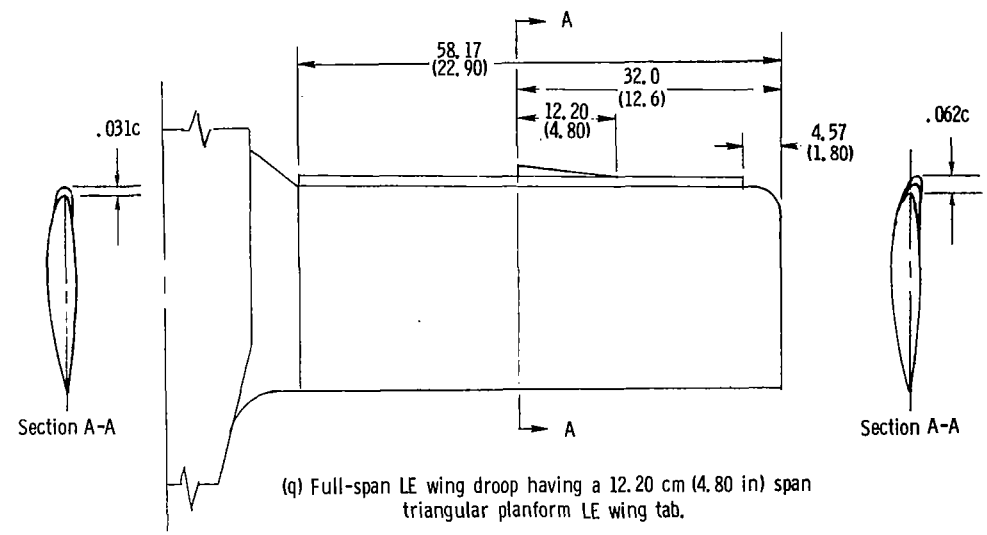

(q) Full-span LE wing droop having a 12.20 cm (4.80 in) span triangular planform LE wing tab.

Figure 4. - Concluded.

APPENDIX

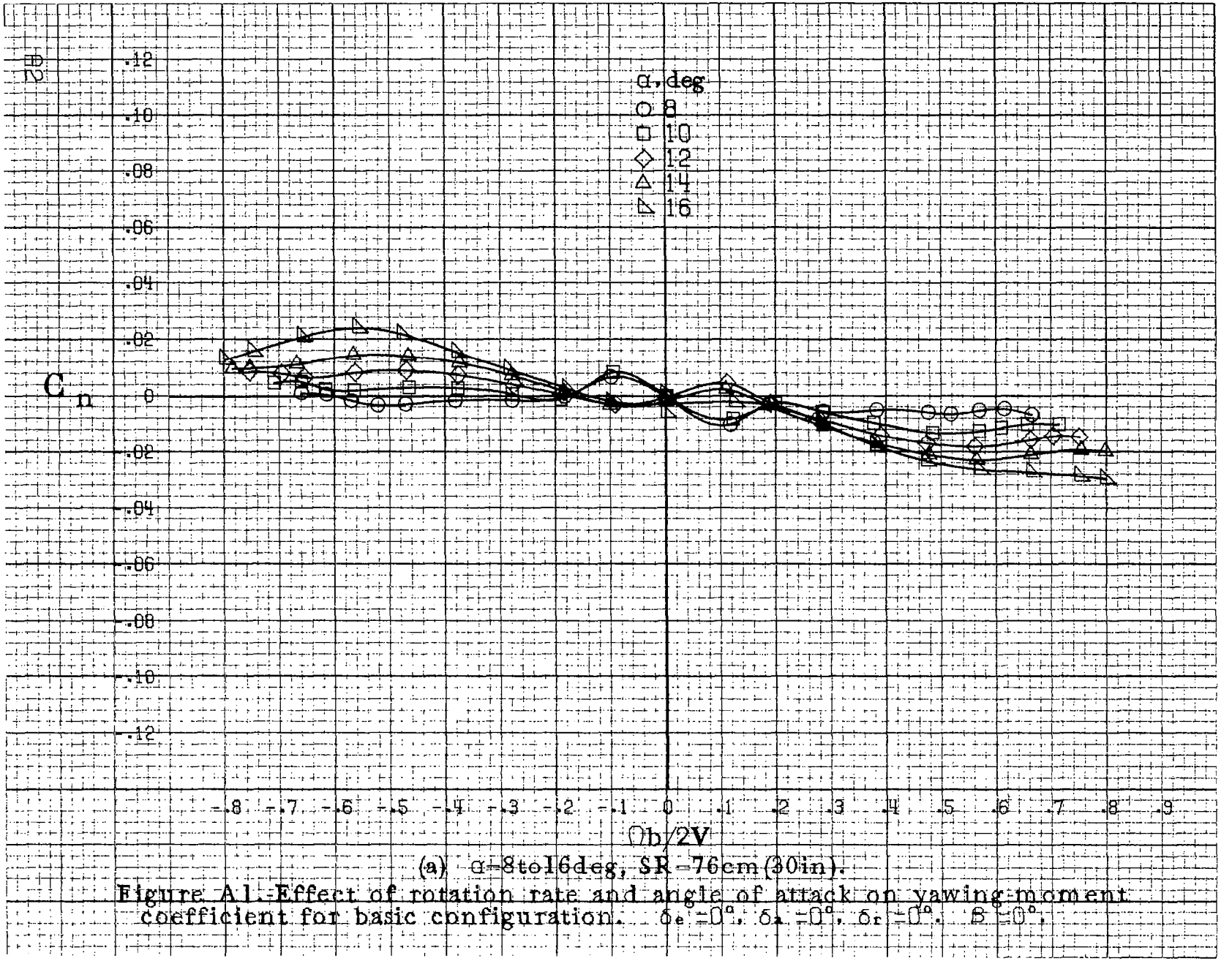

(a) α=8to16deg, SR=76cm(30in).

Figure A1.-Effect of rotation rate and angle of attack on yawing-moment coefficient for basic configuration. $\delta_e = 0°$, $\delta_a = 0°$, $\delta_r = 0°$, $\beta = 0°$.

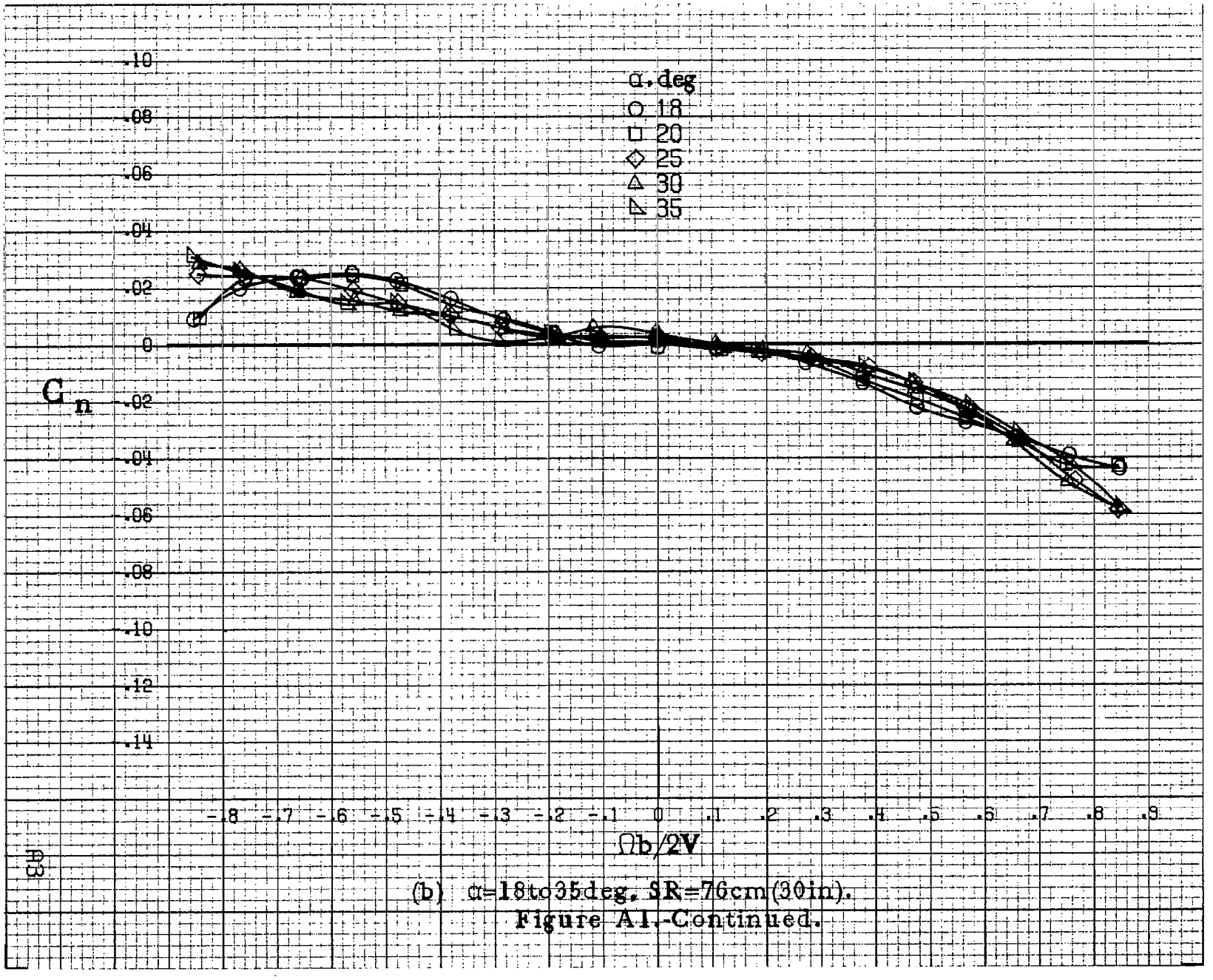

(b) α=18to35deg, SR=76cm(30in).

Figure A1.-Continued.

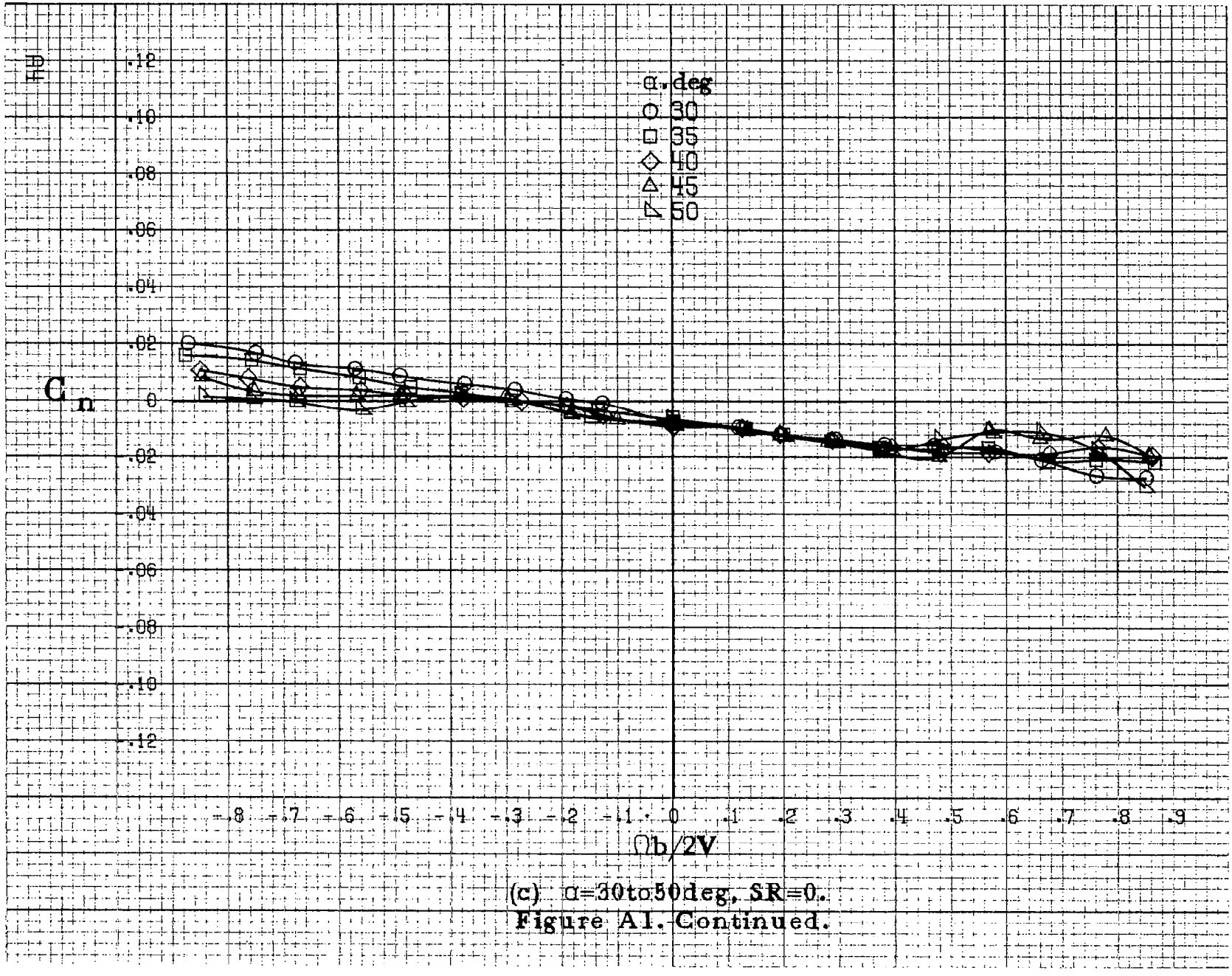

(c) α=30to50deg, SR=0.

Figure A1. Continued.

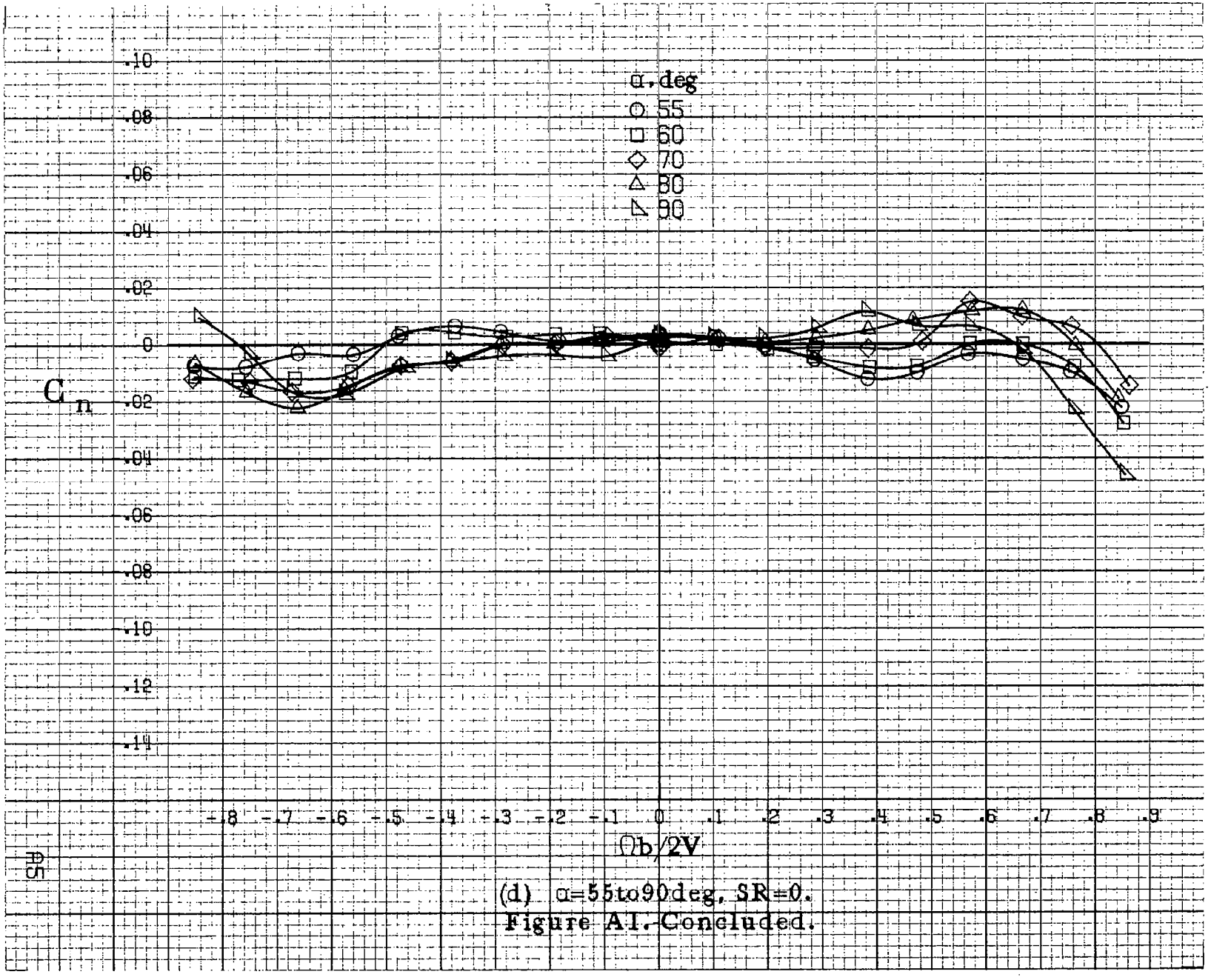

(d) α=55to90deg, SR=0.

Figure A1. Concluded.

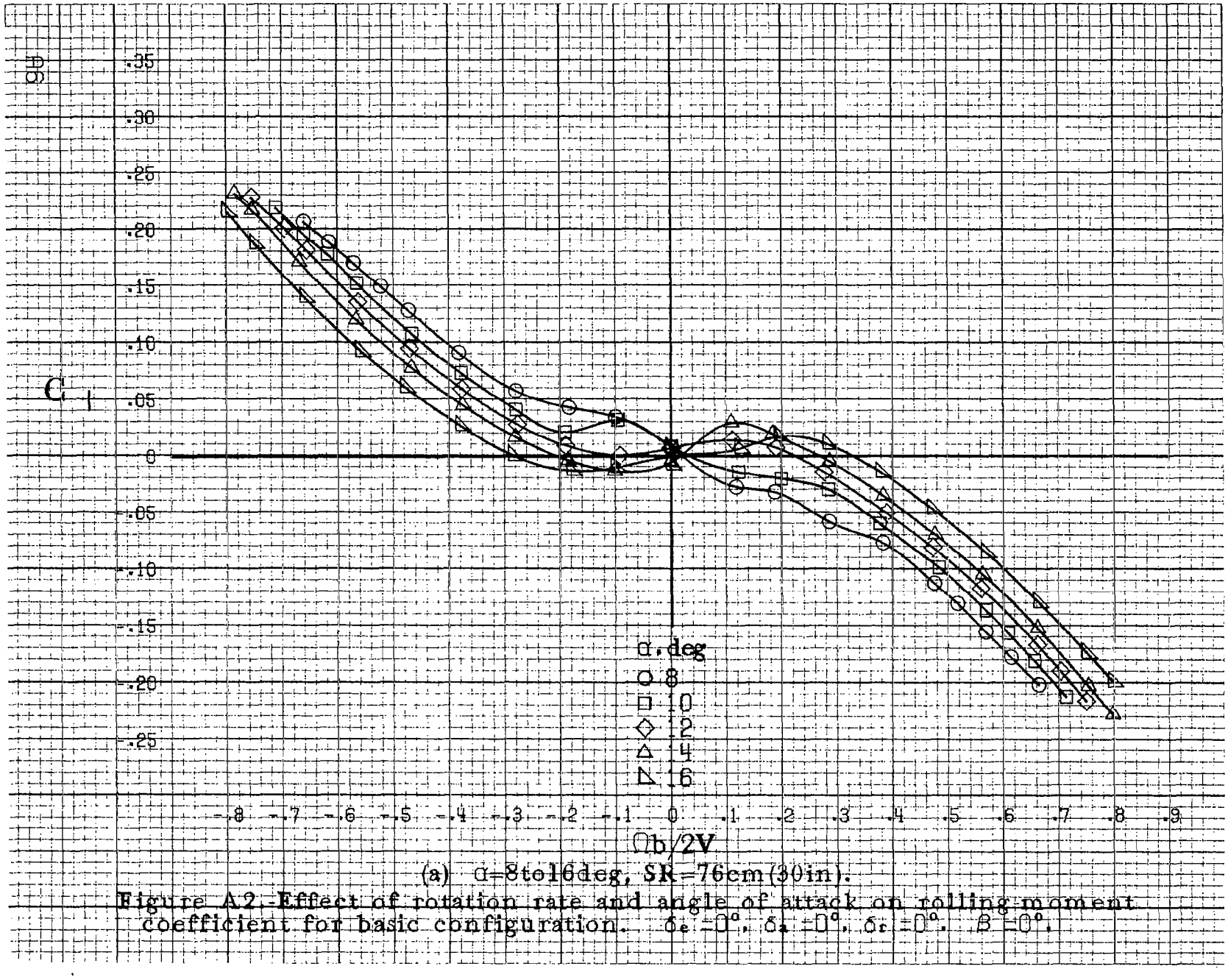

(a) α=8to16deg, SR=76cm(30in).

Figure A2.-Effect of rotation rate and angle of attack on rolling-moment coefficient for basic configuration. $\delta_e = 0°$, $\delta_a = 0°$, $\delta_r = 0°$, $\beta = 0°$.

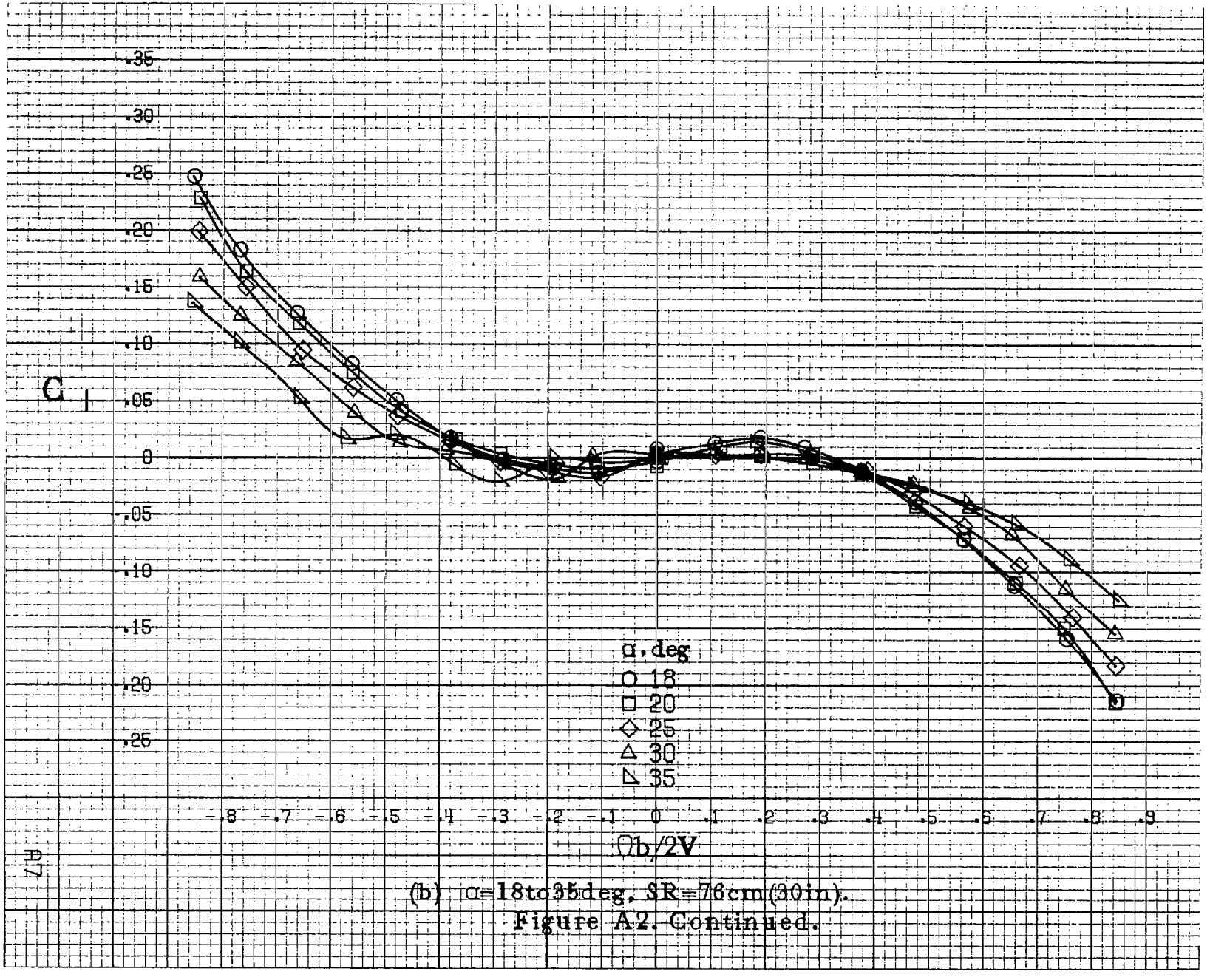

(b) α=18to35deg, SR=76cm(30in).

Figure A2. Continued.

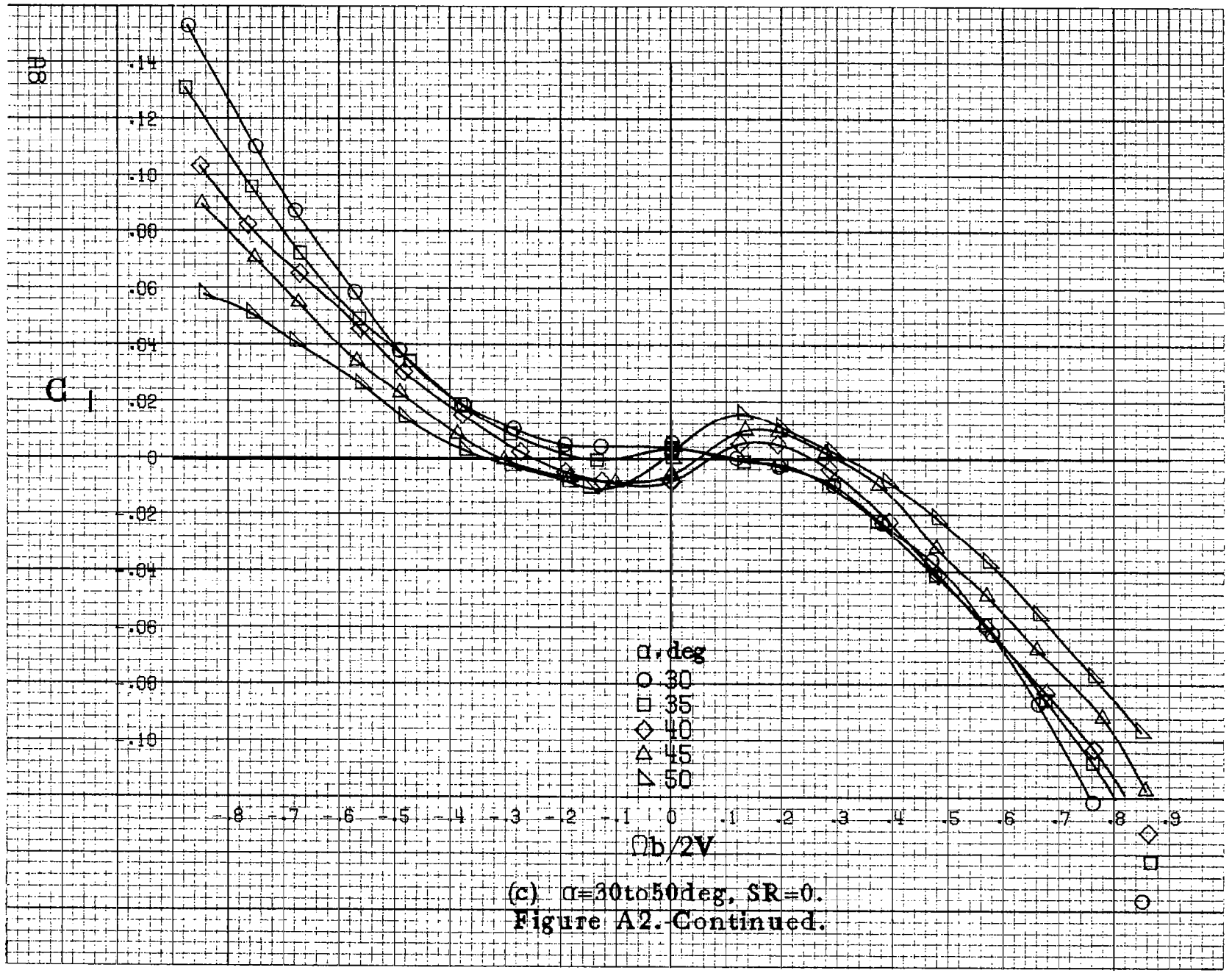

(c) α=30to50deg, SR=0.

Figure A2.-Continued.

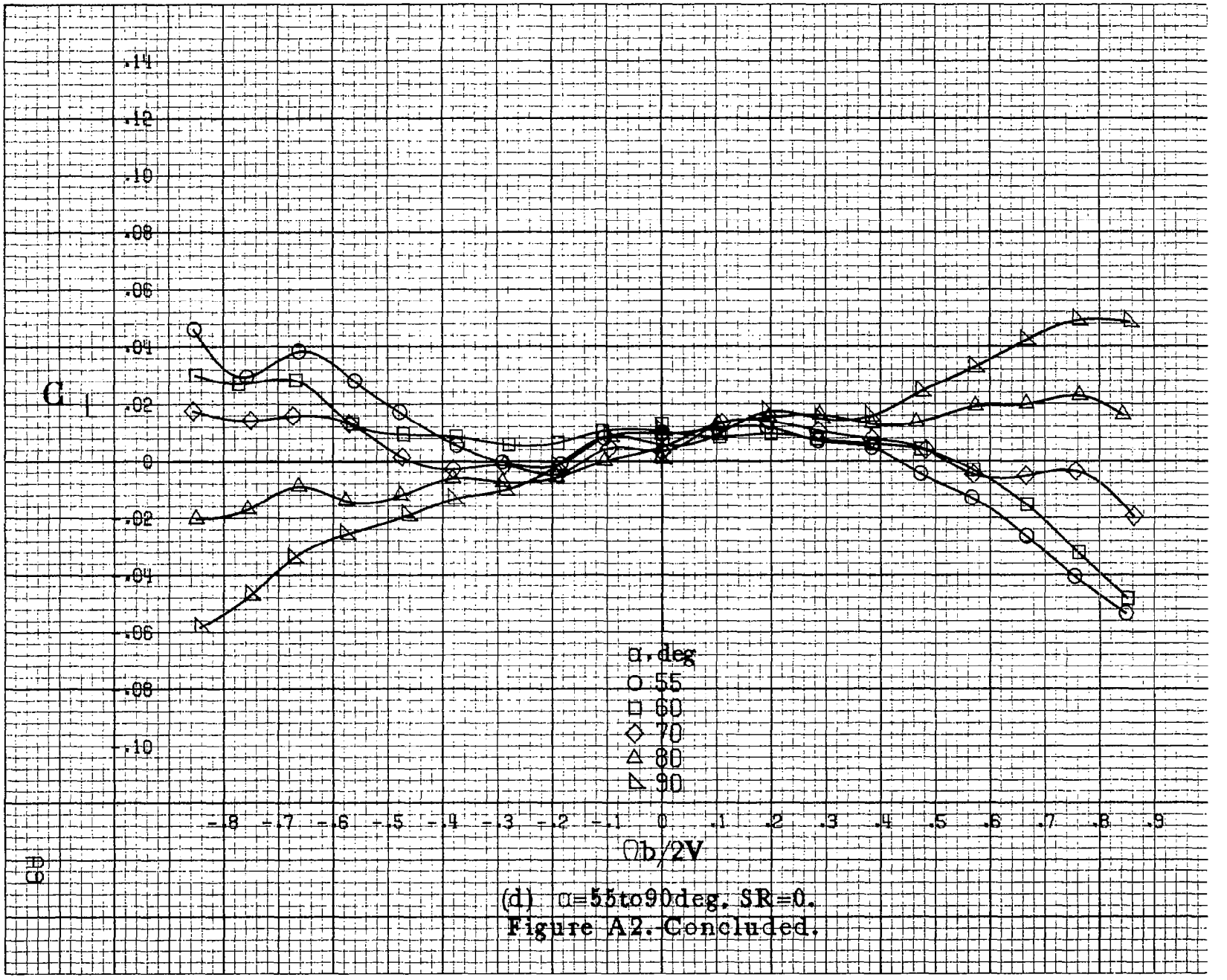

(d) α=55to90deg. SR=0.

Figure A2. Concluded.

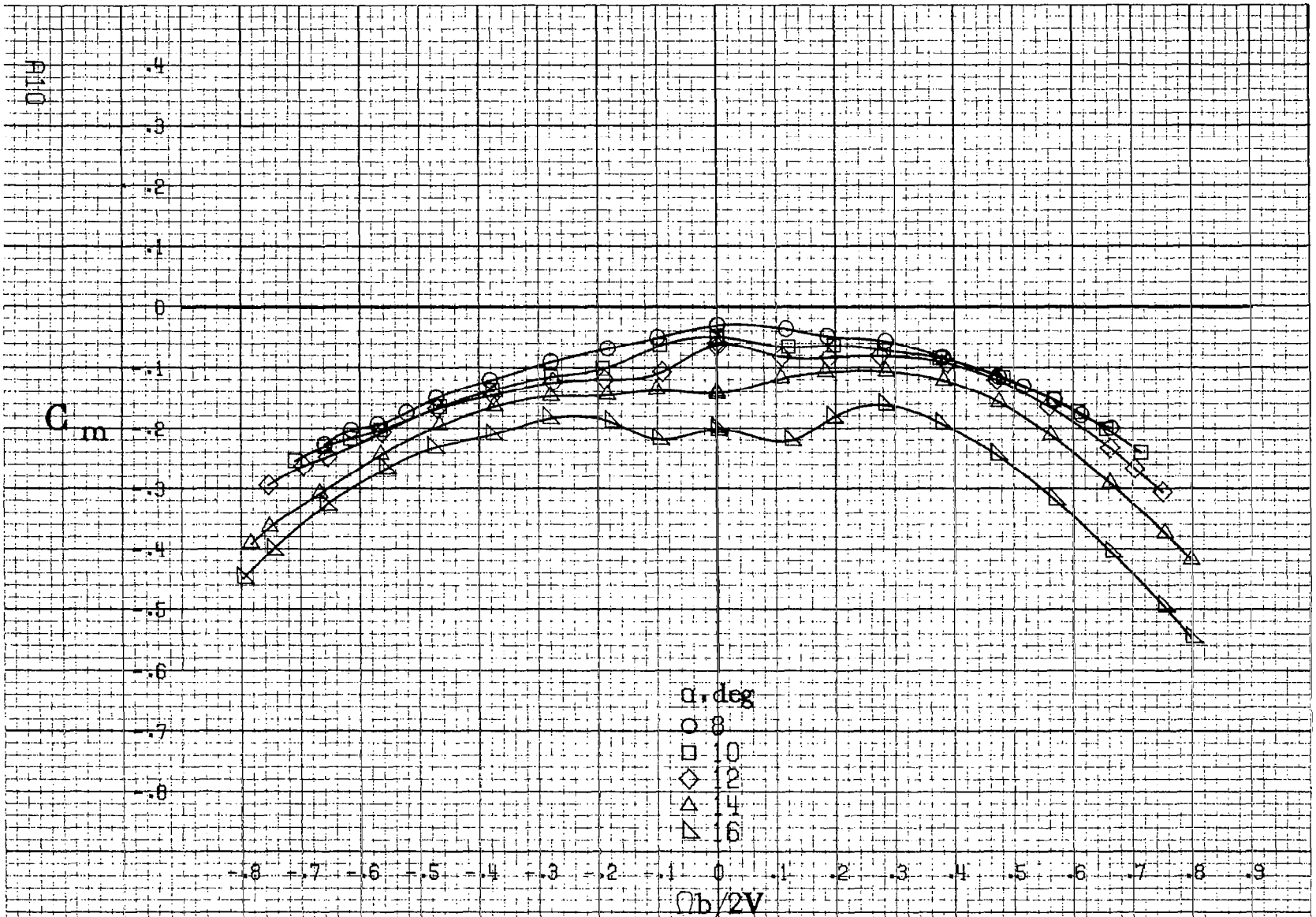

(a) α=8to16deg, SR=76cm(30in).

Figure A3.-Effect of rotation rate and angle of attack on pitching-moment coefficient for basic configuration. $\delta_e = 0°$, $\delta_a = 0°$, $\delta_r = 0°$, $\beta = 0°$.

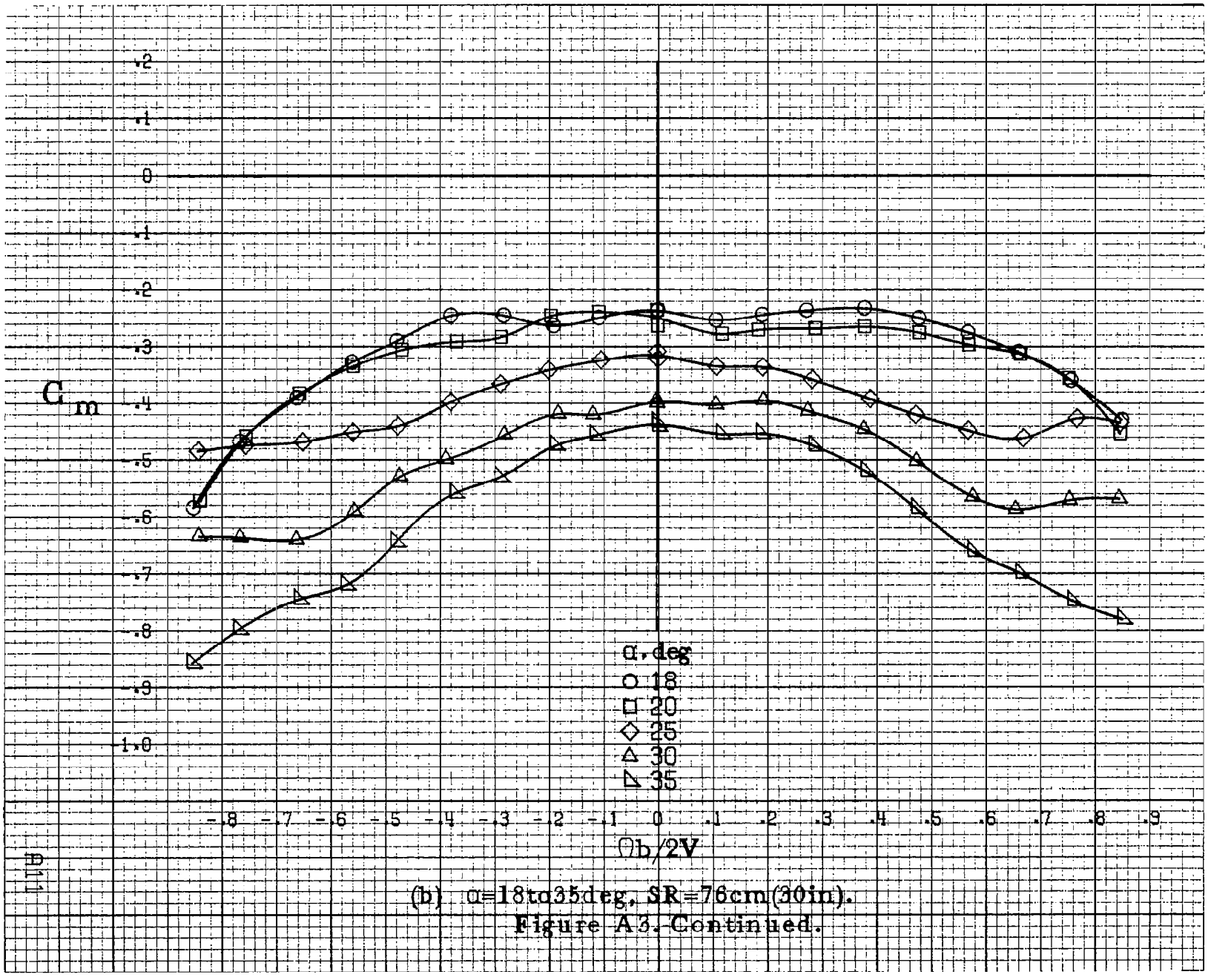

(b) α=18to35deg, SR=76cm(30in).

Figure A3. Continued.

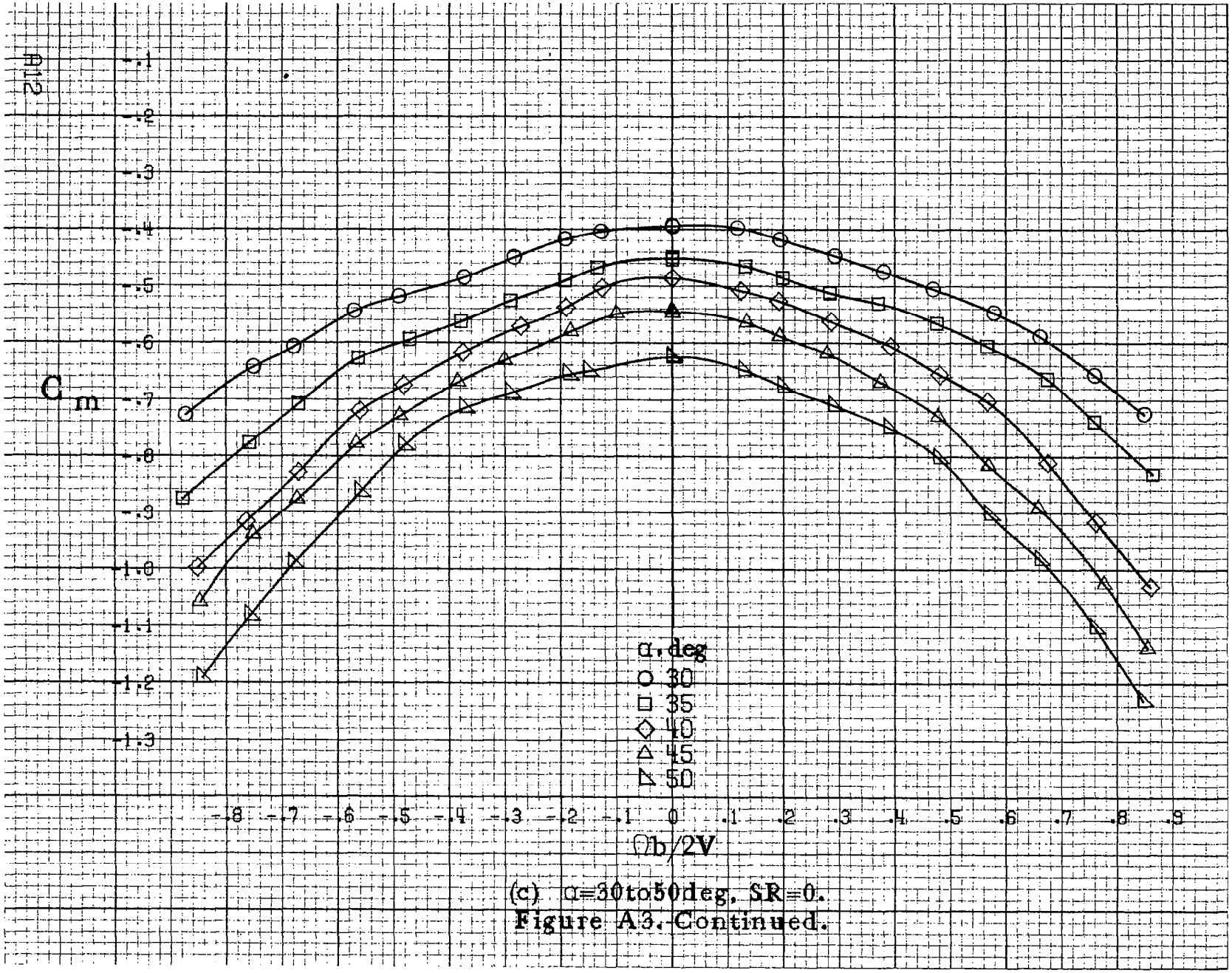

(c) α=30to50deg, SR=0.

Figure A3.-Continued.

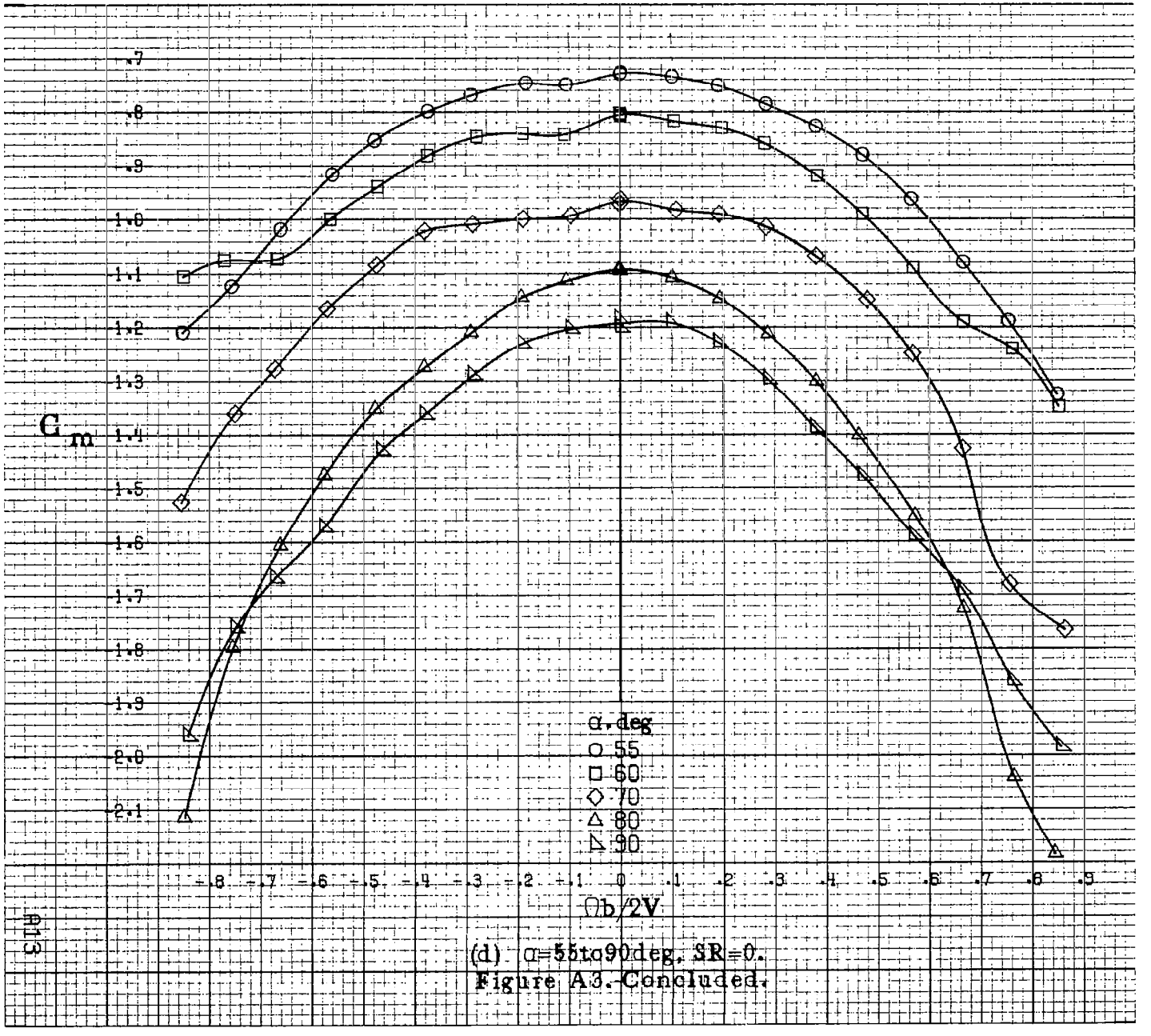

(d) α=55to90deg, SR=0.

Figure A3. Concluded.

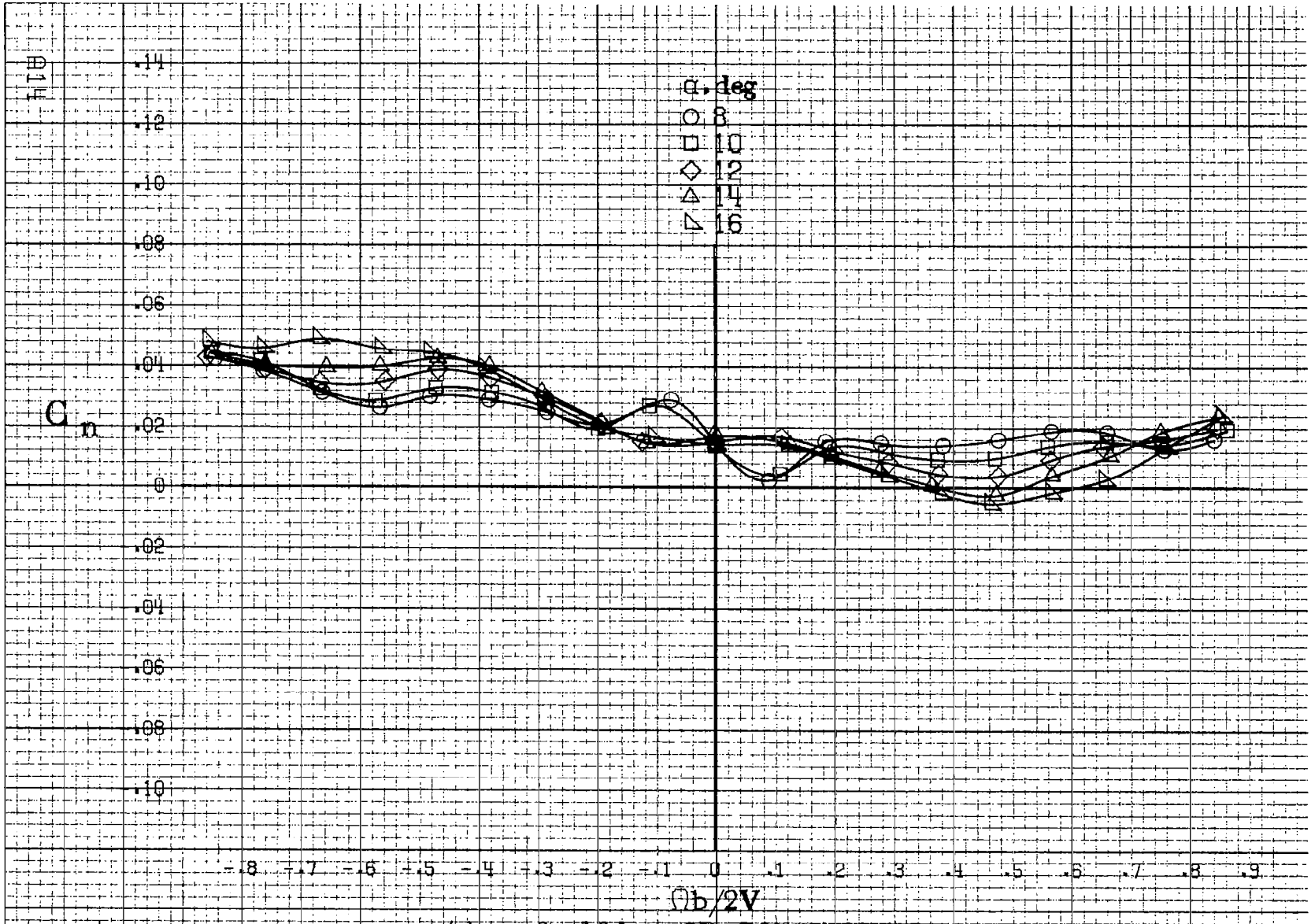

(a) α=8to16deg, SR=76cm(30in).

Figure A4.- Effect of rotation rate and angle of attack on yawing-moment coefficient for basic configuration. $\delta_e = 0°$, $\delta_a = 23°$, $\delta_r = -25°$, $\beta = 0°$.

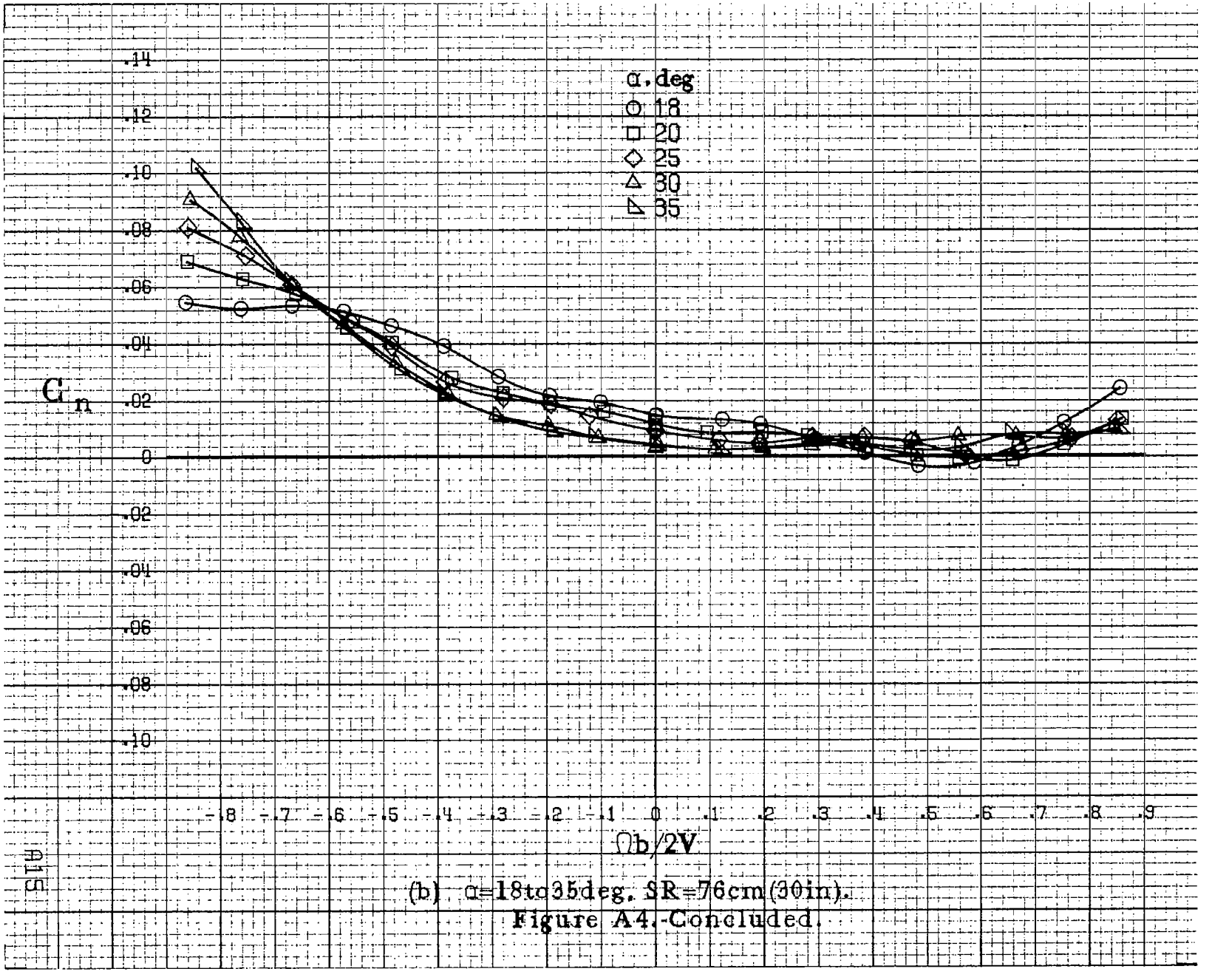

(b) α=18to35deg. SR=76cm(30in).

Figure A4.-Concluded.

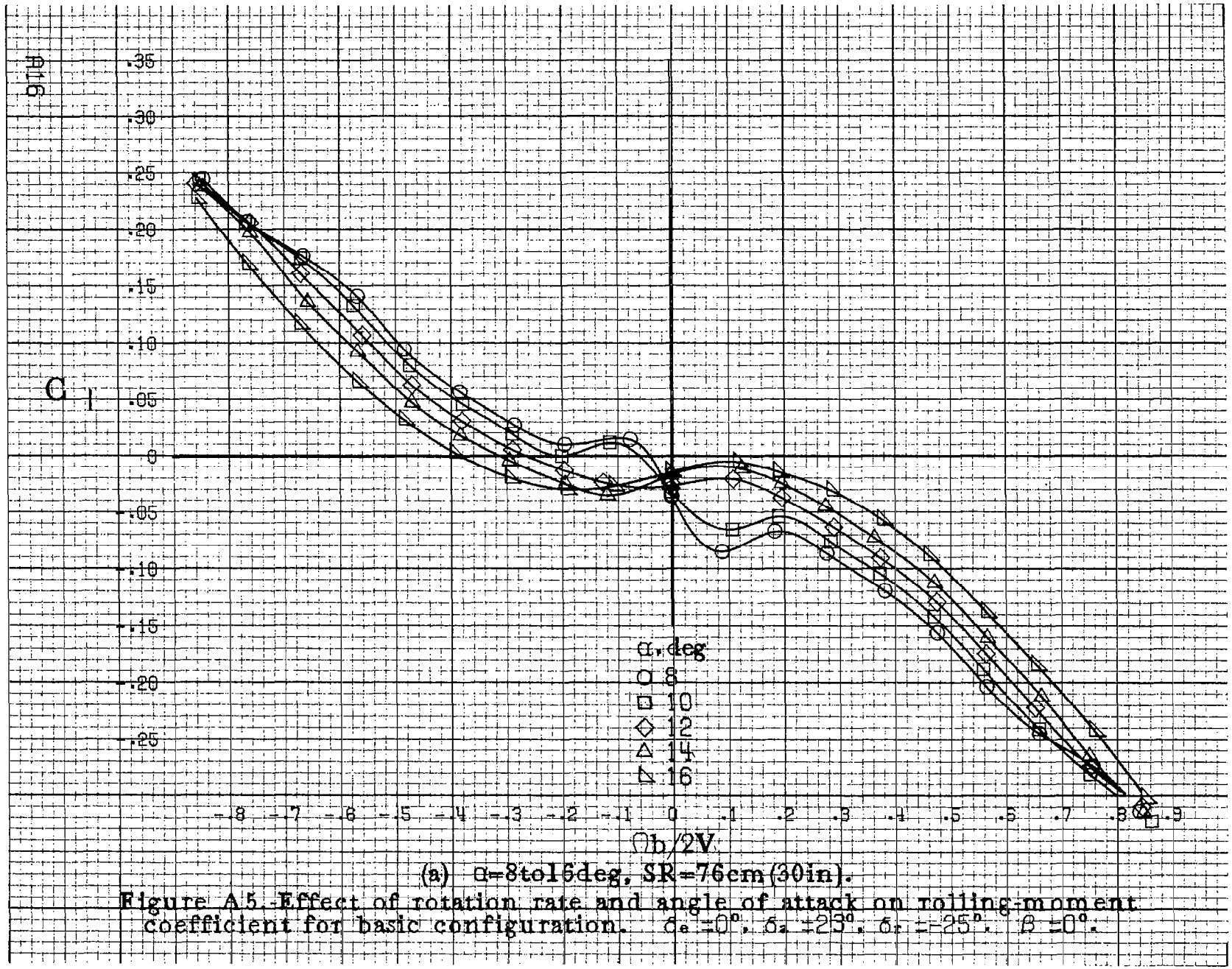

(a) α=8to16deg, SR=76cm(30in).

Figure A5.-Effect of rotation rate and angle of attack on rolling-moment coefficient for basic configuration. $\delta_e = 0°$, $\delta_a = 23°$, $\delta_r = -25°$, $\beta = 0°$.

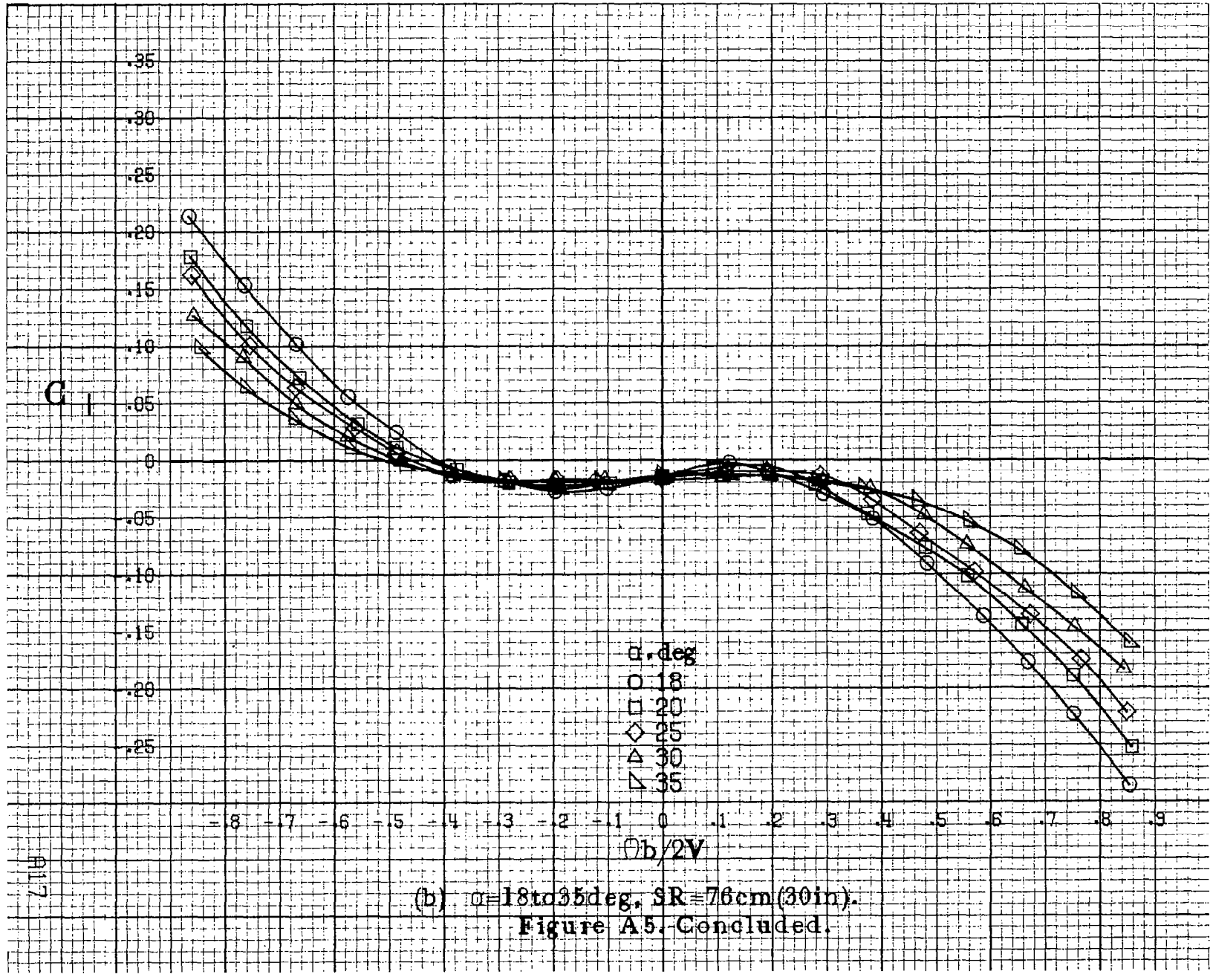

(b) α=18to35deg, SR=76cm(30in).

Figure A5.-Concluded.

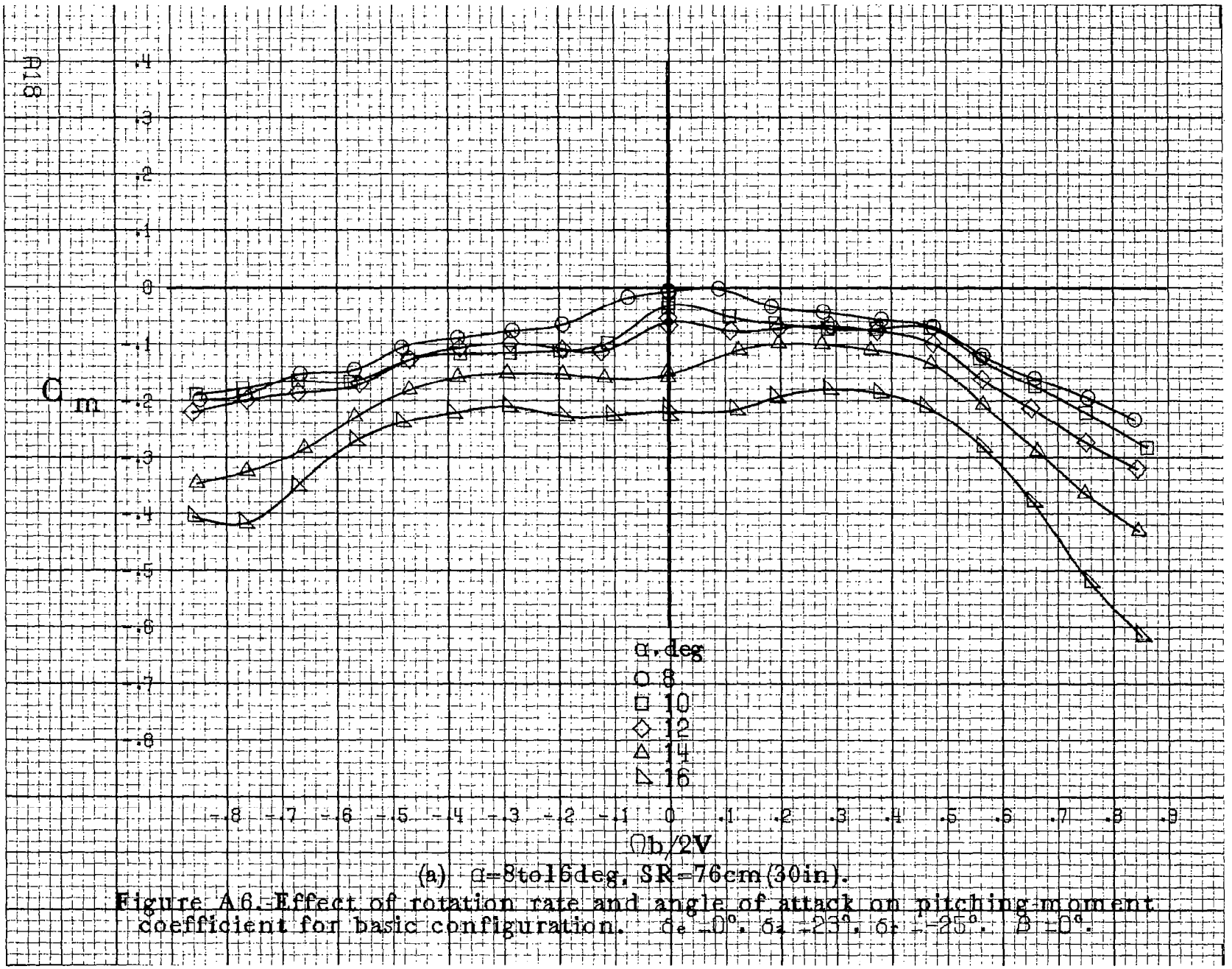

(a) α=8to16deg, SR=76cm(30in).

Figure A6.-Effect of rotation rate and angle of attack on pitching moment coefficient for basic configuration. $\delta_e = 0°$, $\delta_a = 23°$, $\delta_r = -25°$, $\beta = 0°$.

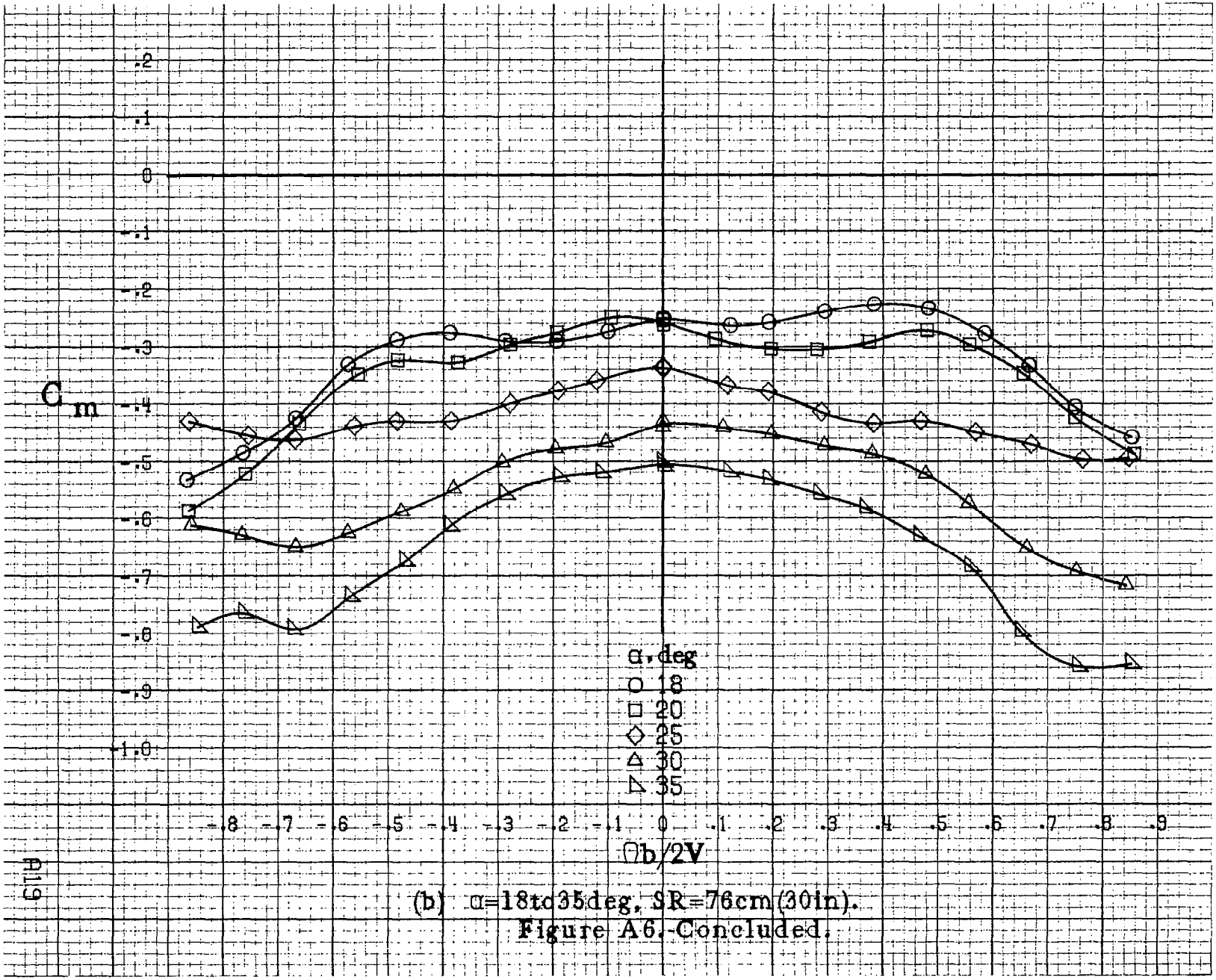

(b) α=18to35deg, SR=76cm(30in).

Figure A6.-Concluded.

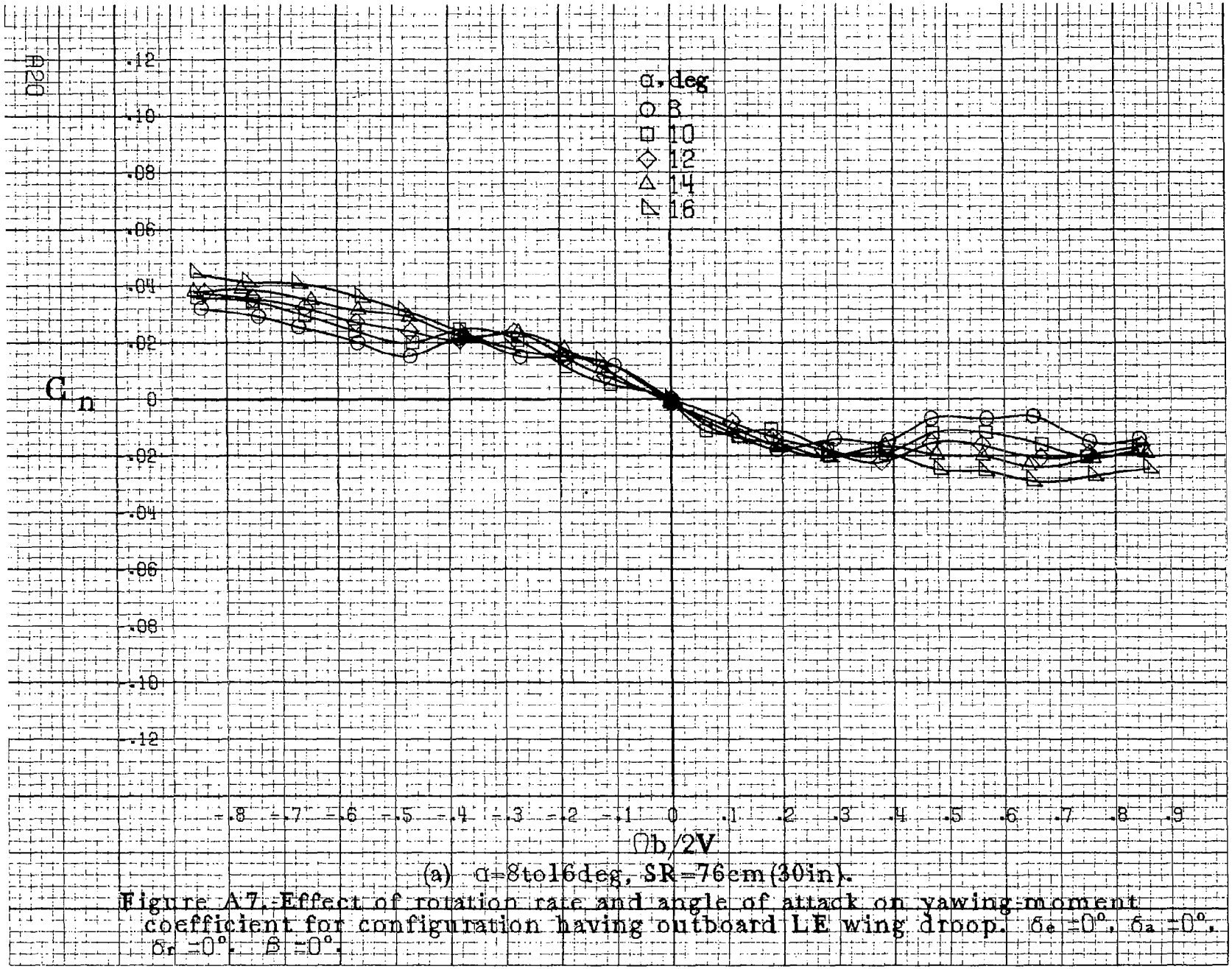

(a) α=8to16deg, SR=76cm(30in).

Figure A7. Effect of rotation rate and angle of attack on yawing-moment coefficient for configuration having outboard LE wing droop. δ_e =0°, δ_a =0°, δ_r =0°, β =0°.

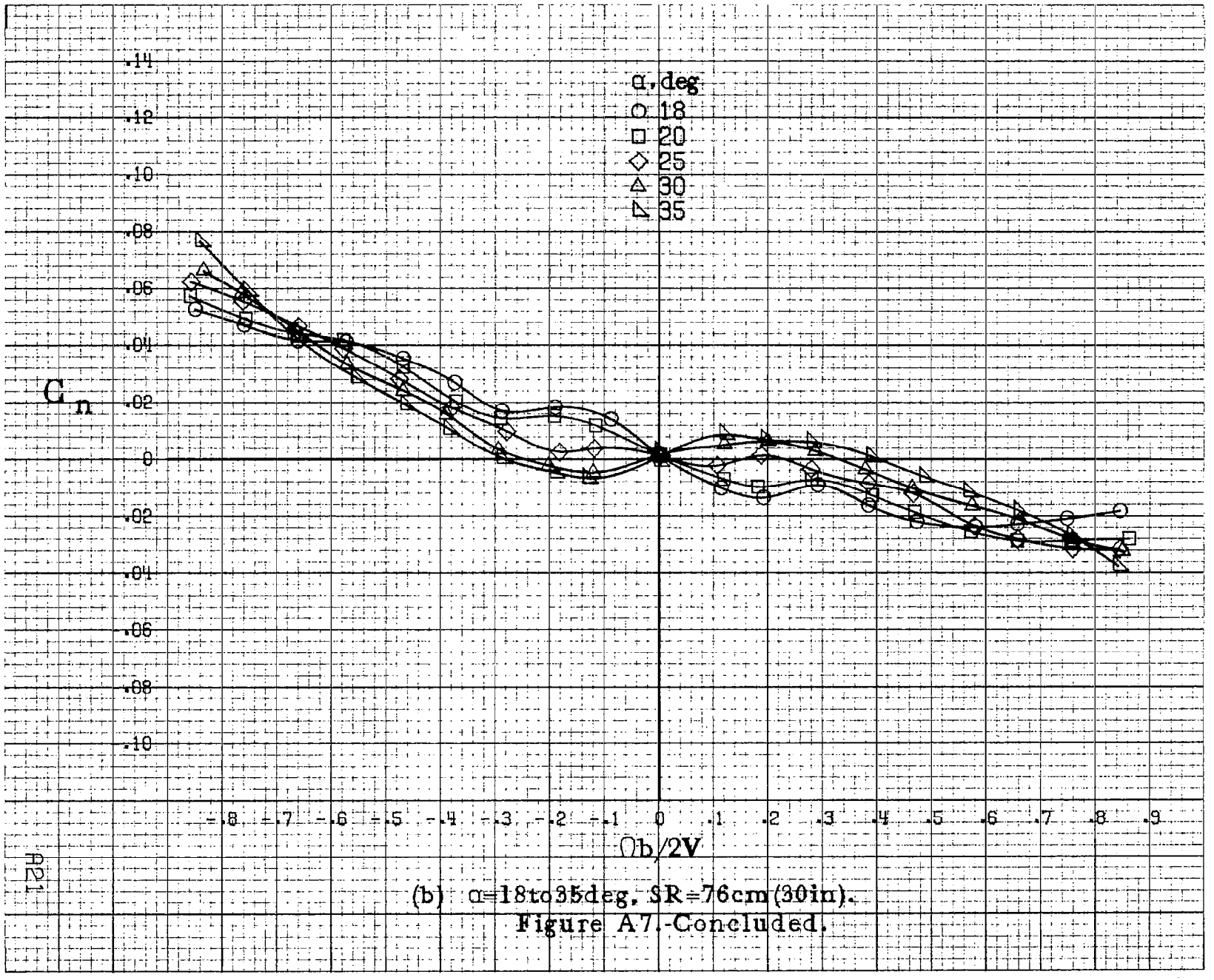

(b) α=18to35deg, SR=76cm(30in).

Figure A7.-Concluded.

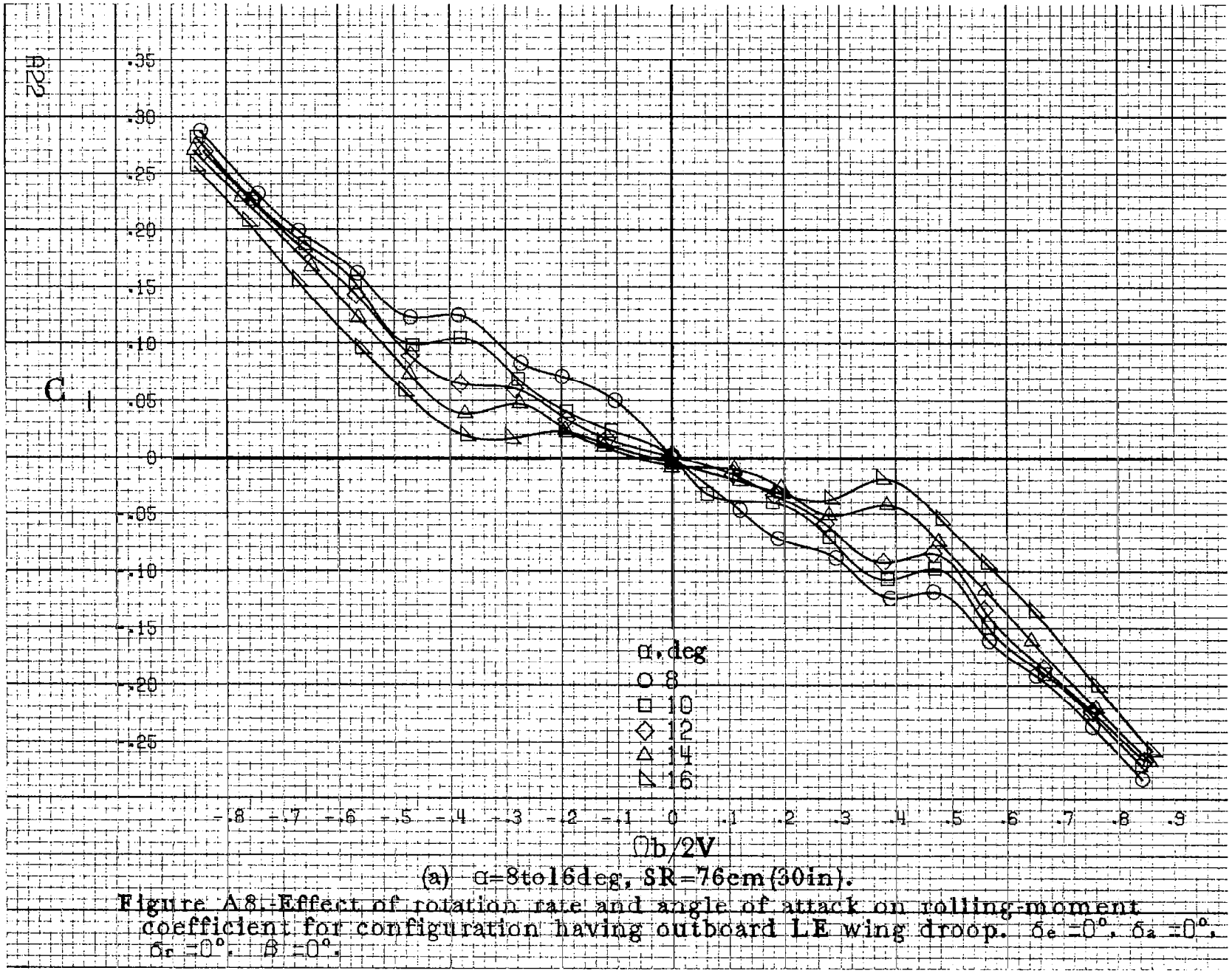

(a) α=8to16deg, SR=76cm(30in).

Figure A8.-Effect of rotation rate and angle of attack on rolling-moment coefficient for configuration having outboard LE wing droop. $\delta_e = 0°$, $\delta_a = 0°$, $\delta_r = 0°$, $\beta = 0°$.

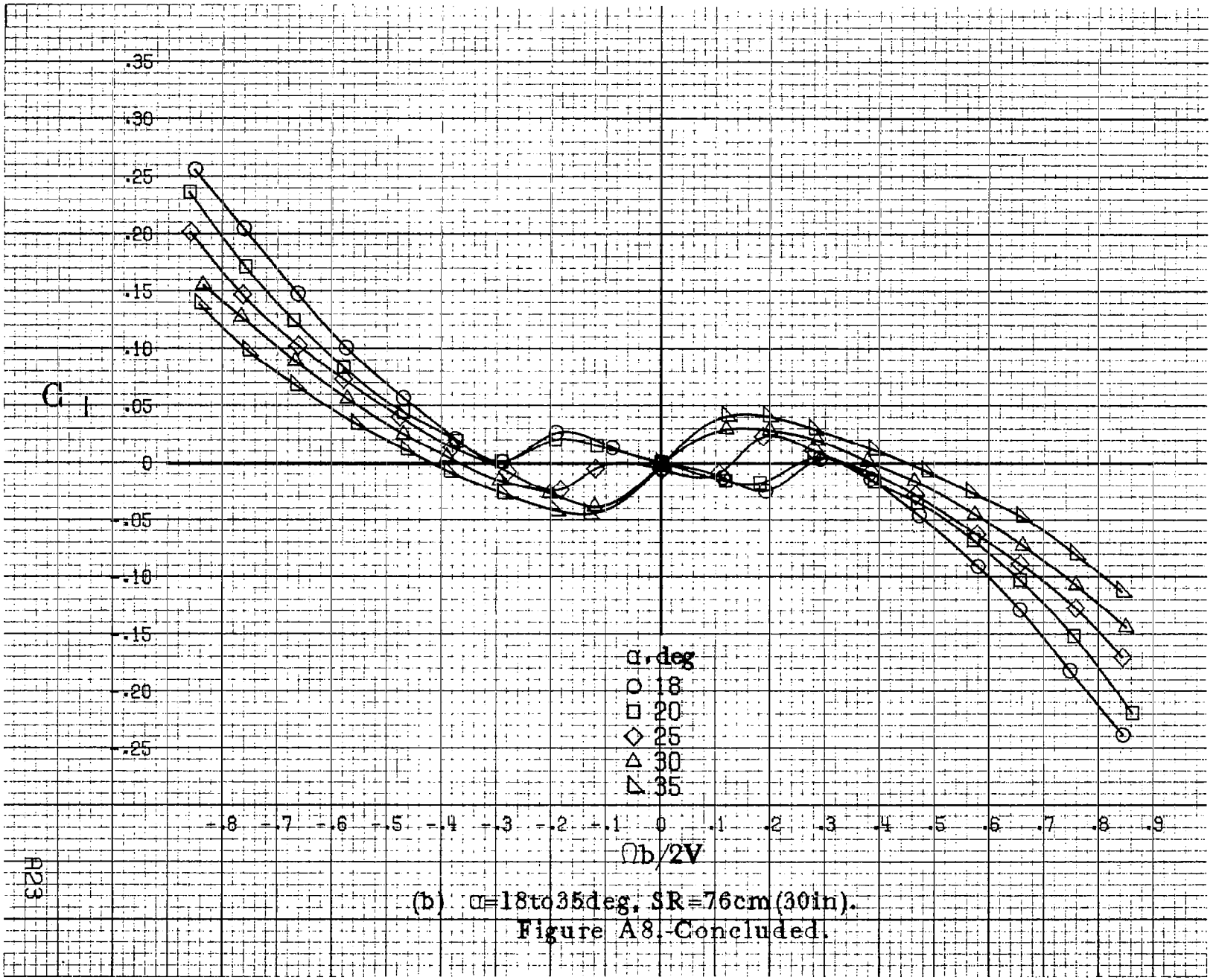

(b) α=18to35deg, SR=76cm(30in).

Figure A8.-Concluded.

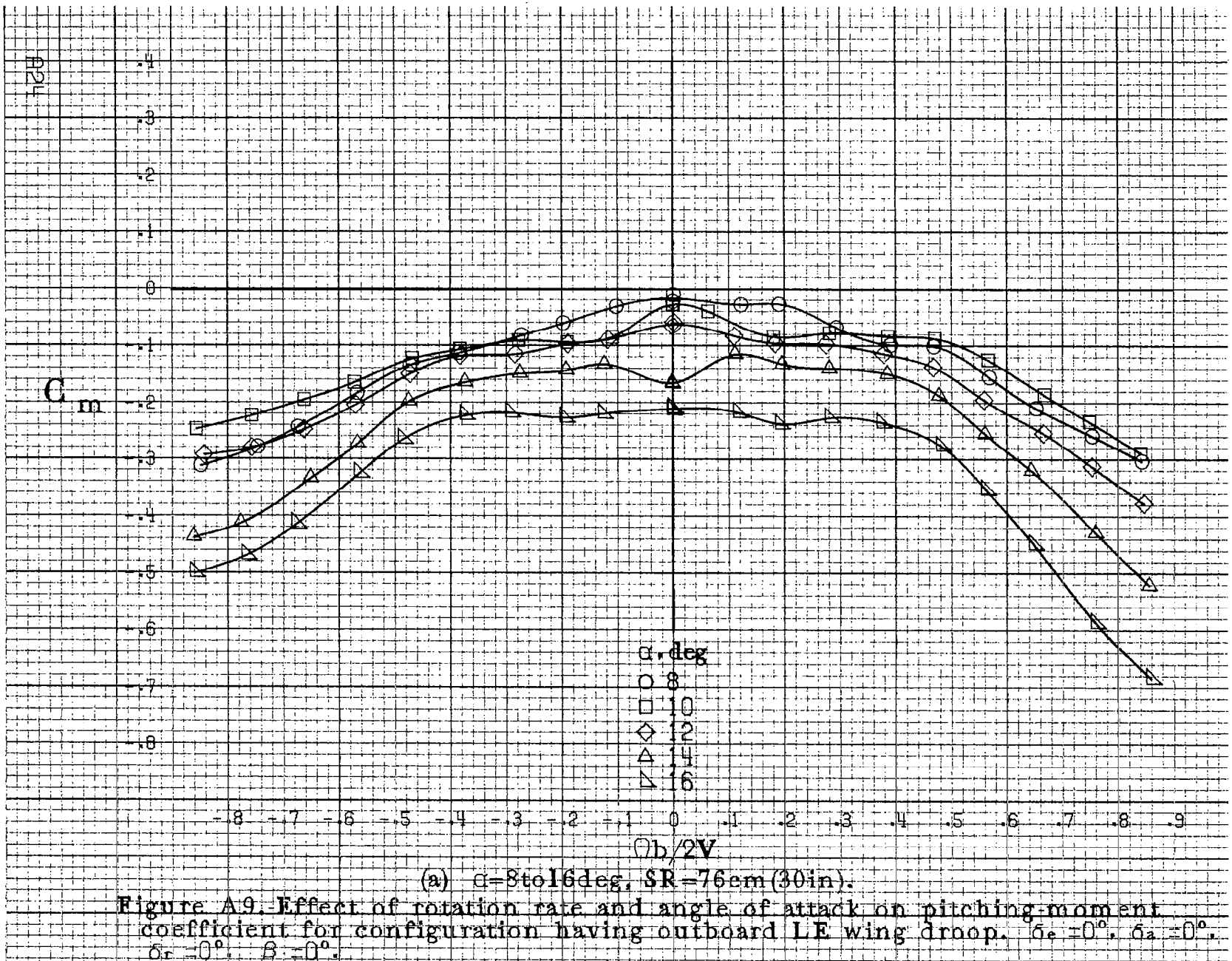

(a) α=8to16deg, SR=76cm(30in).

Figure A9. Effect of rotation rate and angle of attack on pitching-moment coefficient for configuration having outboard LE wing droop. $\delta_e = 0°$, $\delta_a = 0°$, $\delta_r = 0°$, $\beta = 0°$.

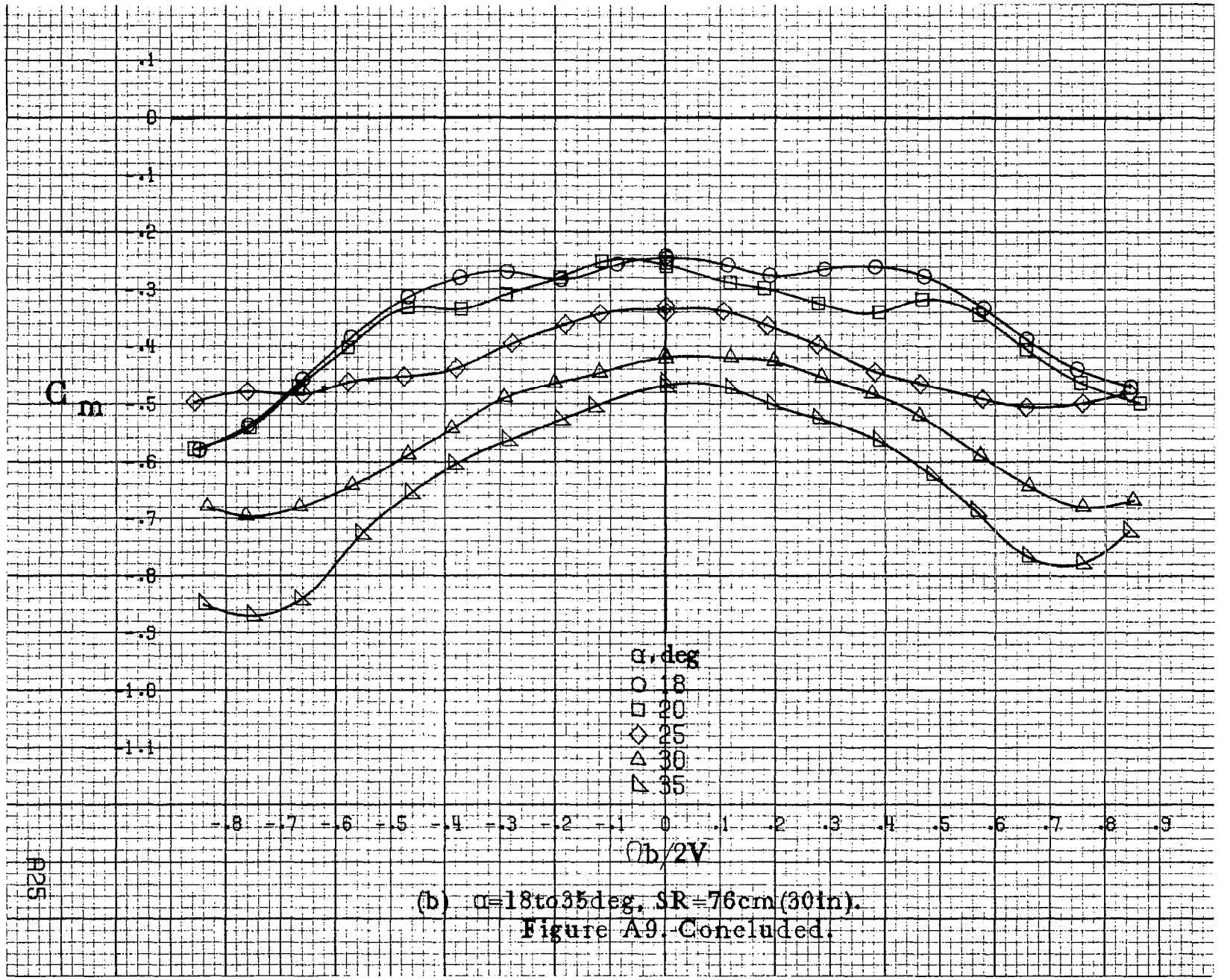

(b) α=18to35deg, SR=76cm(30in).

Figure A9.-Concluded.

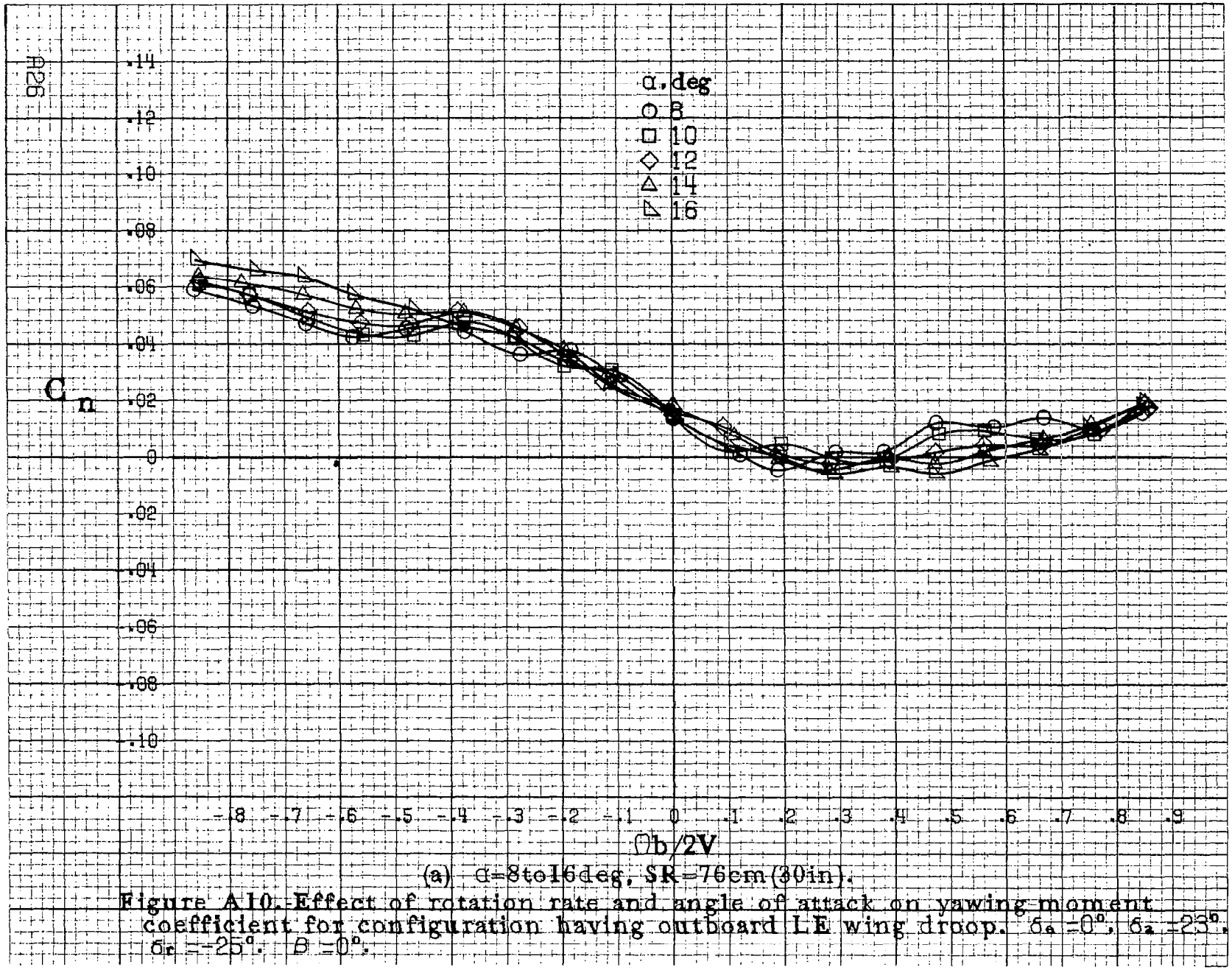

(a) α=8to16deg, SR=76cm(30in).

Figure A10.-Effect of rotation rate and angle of attack on yawing moment coefficient for configuration having outboard LE wing droop. $\delta_a = 0°$, $\delta_a = 23°$, $\delta_r = -25°$, $\beta = 0°$.

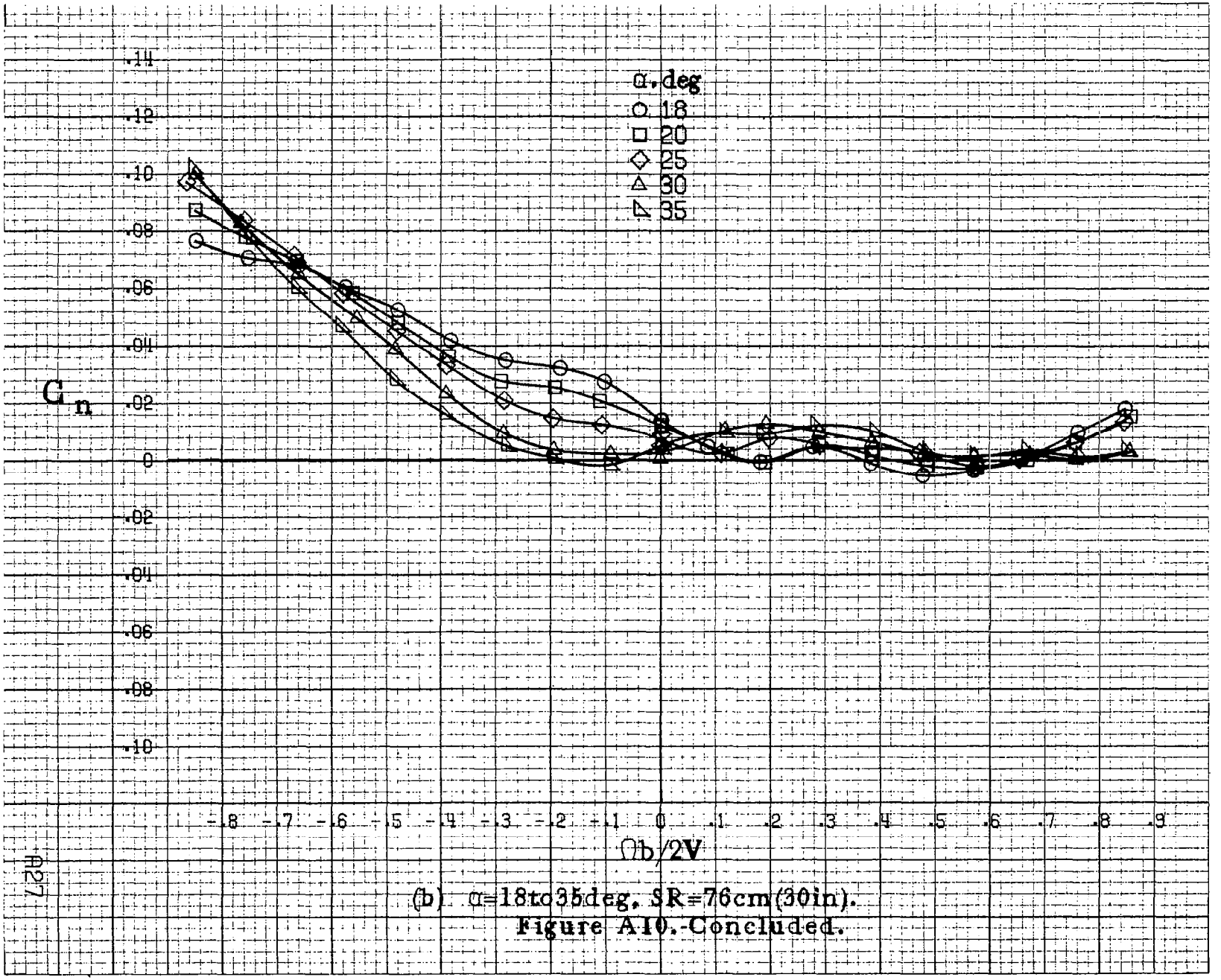

(b) α=18to35deg, SR=76cm(30in).

Figure A10.-Concluded.

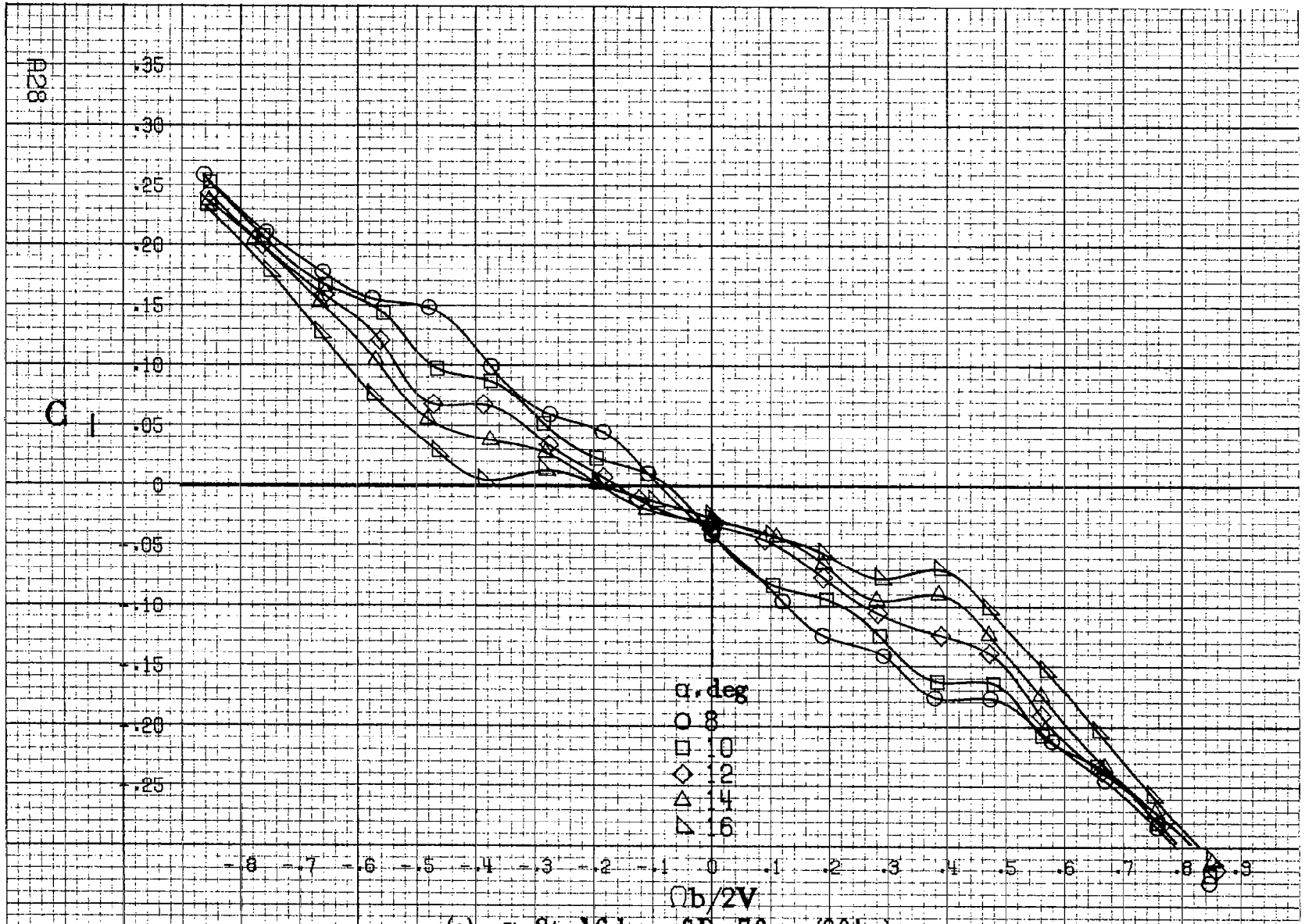

(a) α=8to16deg, SR=76cm(30in).

Figure A11.-Effect of rotation rate and angle of attack on rolling-moment coefficient for configuration having outboard LE wing droop. δ_e =0°, δ_a =23°, δ_r =-25°, β =0°.

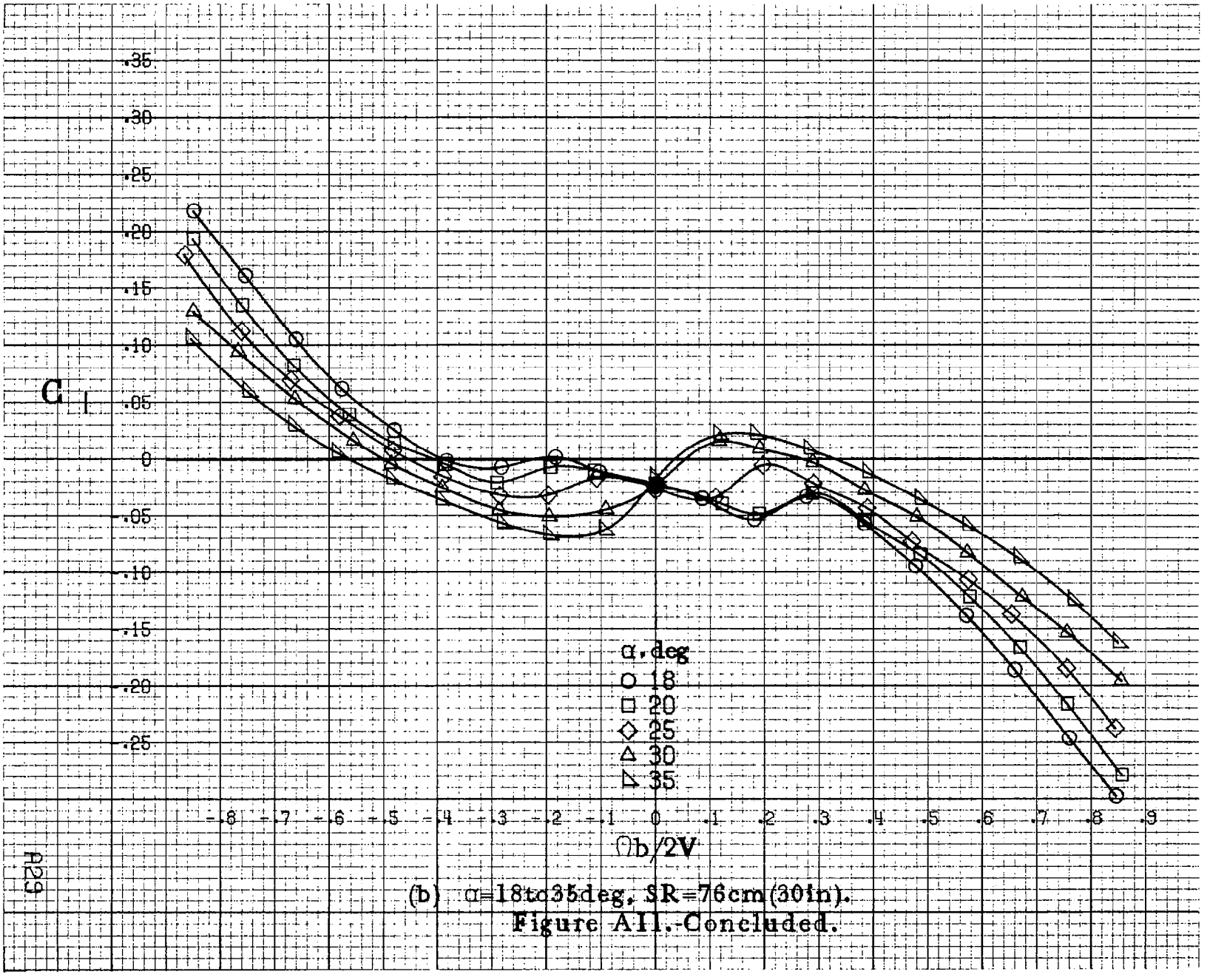

(b) α=18 to 35 deg, SR=76 cm (30 in).

Figure A11.-Concluded.

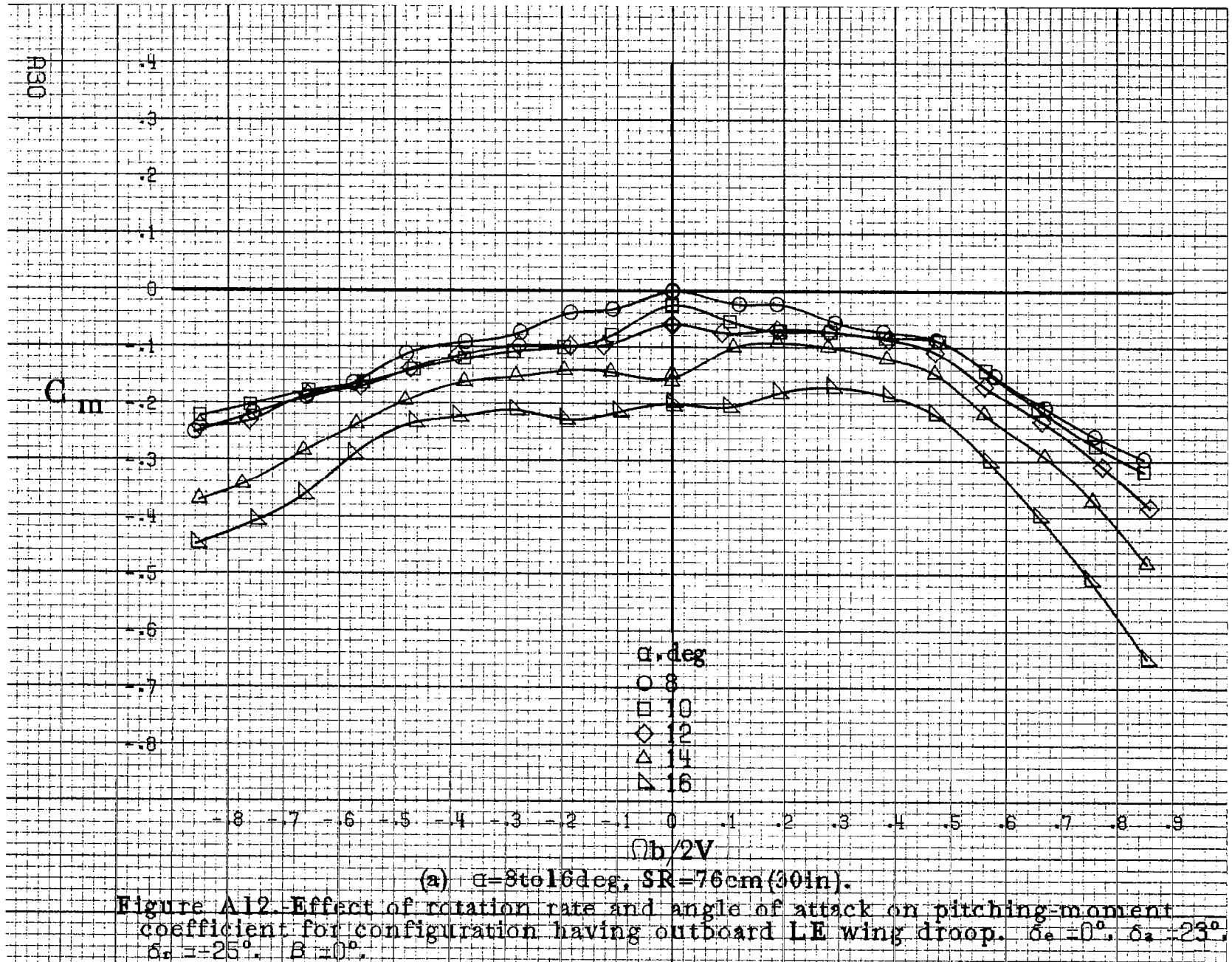

(a) α=8to16deg, SR=76cm(30in).

Figure A12.-Effect of rotation rate and angle of attack on pitching-moment coefficient for configuration having outboard LE wing droop. δ_e =0°, δ_a =-23°, δ_r =+25°, β =0°.

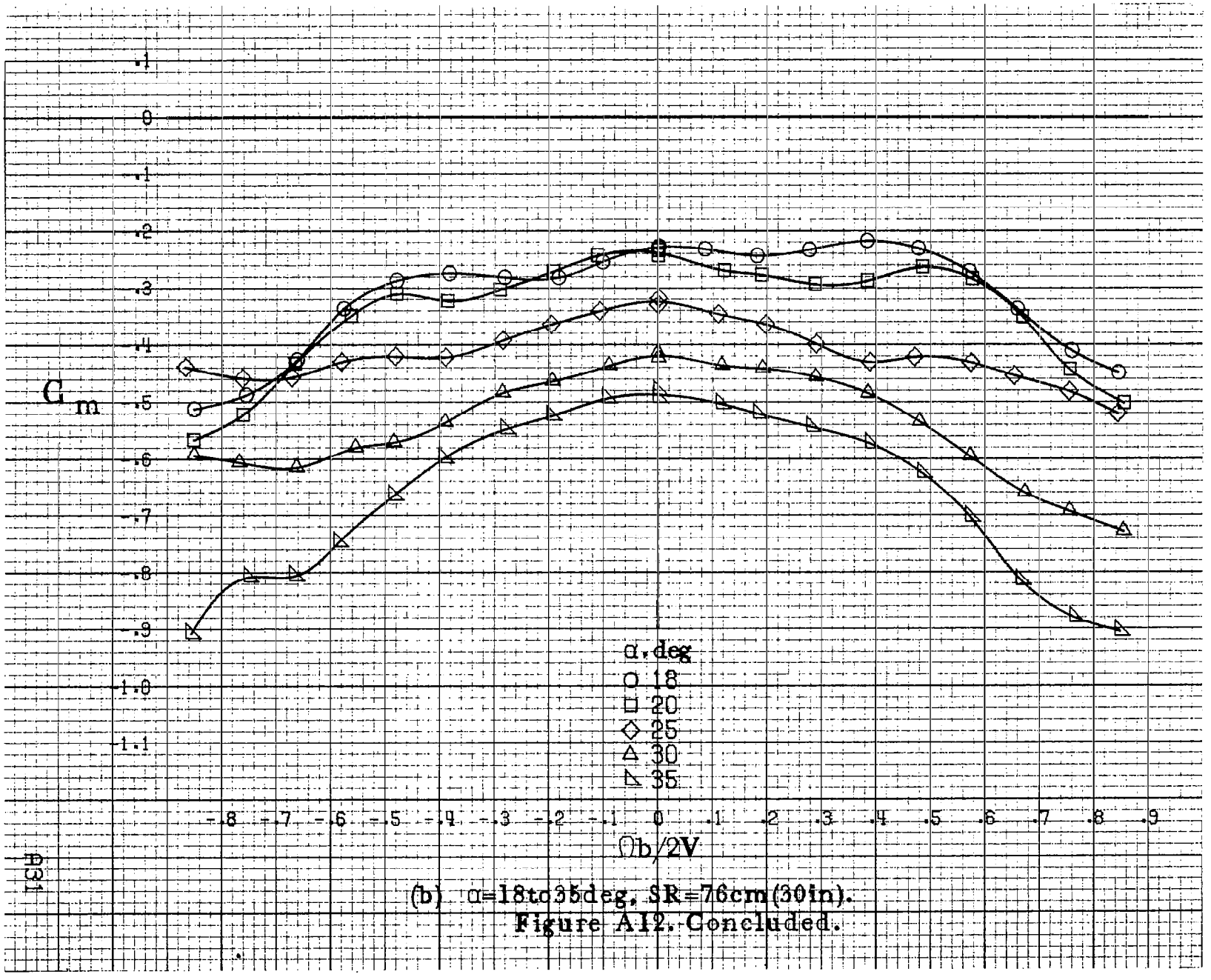

(b) α=18to35deg, SR=76cm(30in).

Figure A12. Concluded.

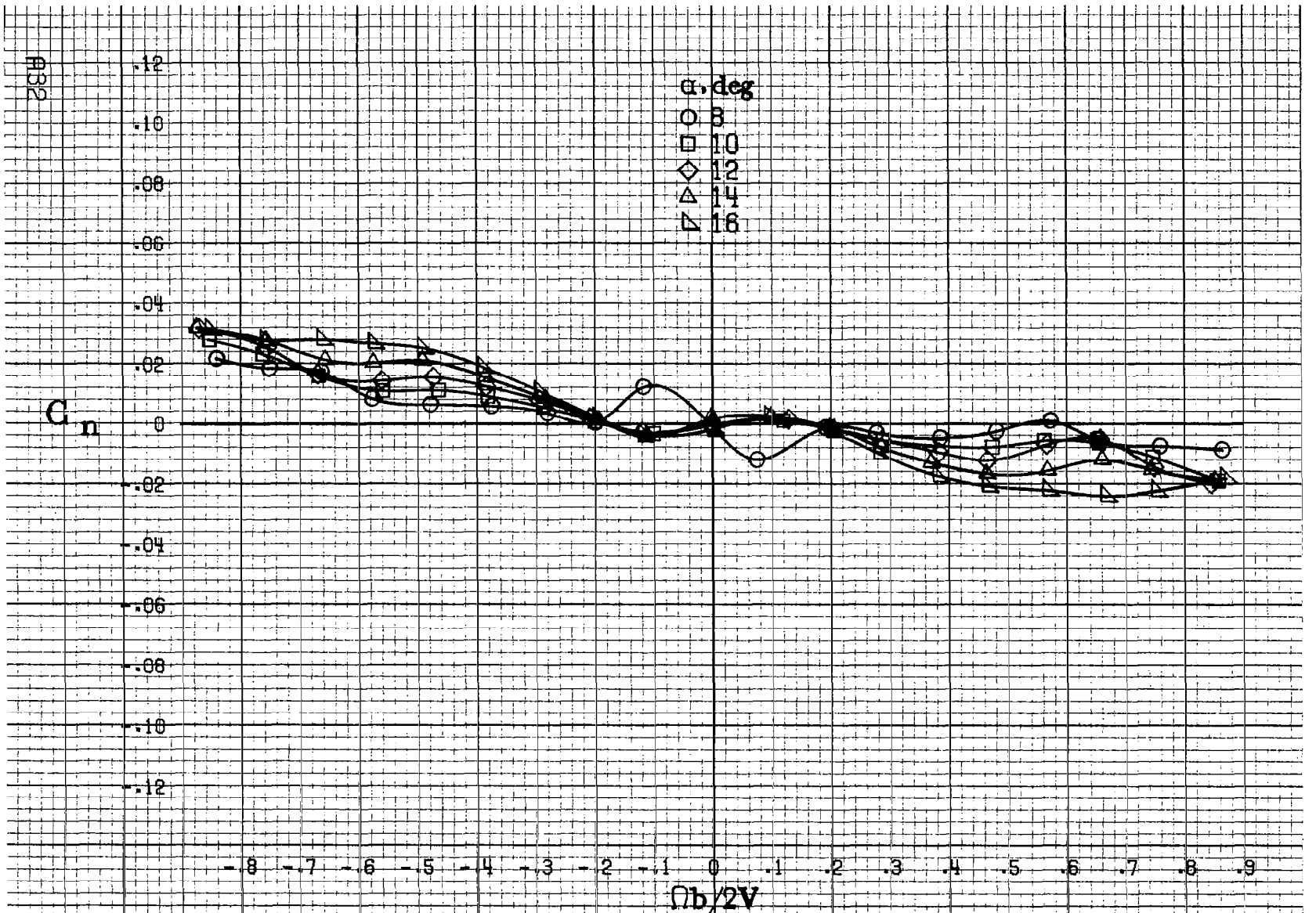

(a) α=8to16deg, SR=76cm(30in).

Figure A13.-Effect of rotation rate and angle of attack on yawing-moment coefficient for configuration having inboard LE wing droop. $\delta_e = 0°$, $\delta_a = 0°$, $\delta_r = 0°$, $\beta = 0°$.

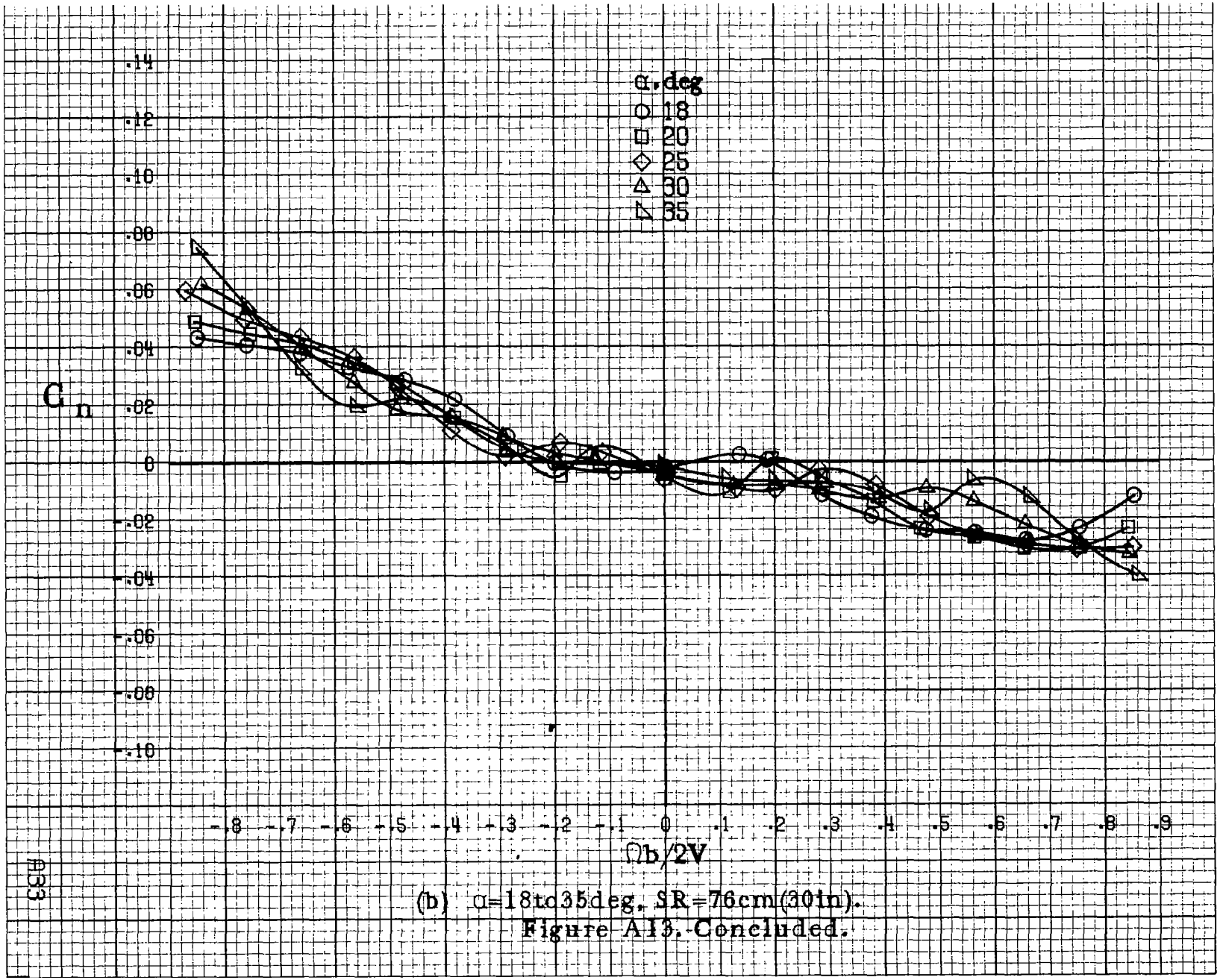

(b) α=18to35deg, SR=76cm(30in).

Figure A13. Concluded.

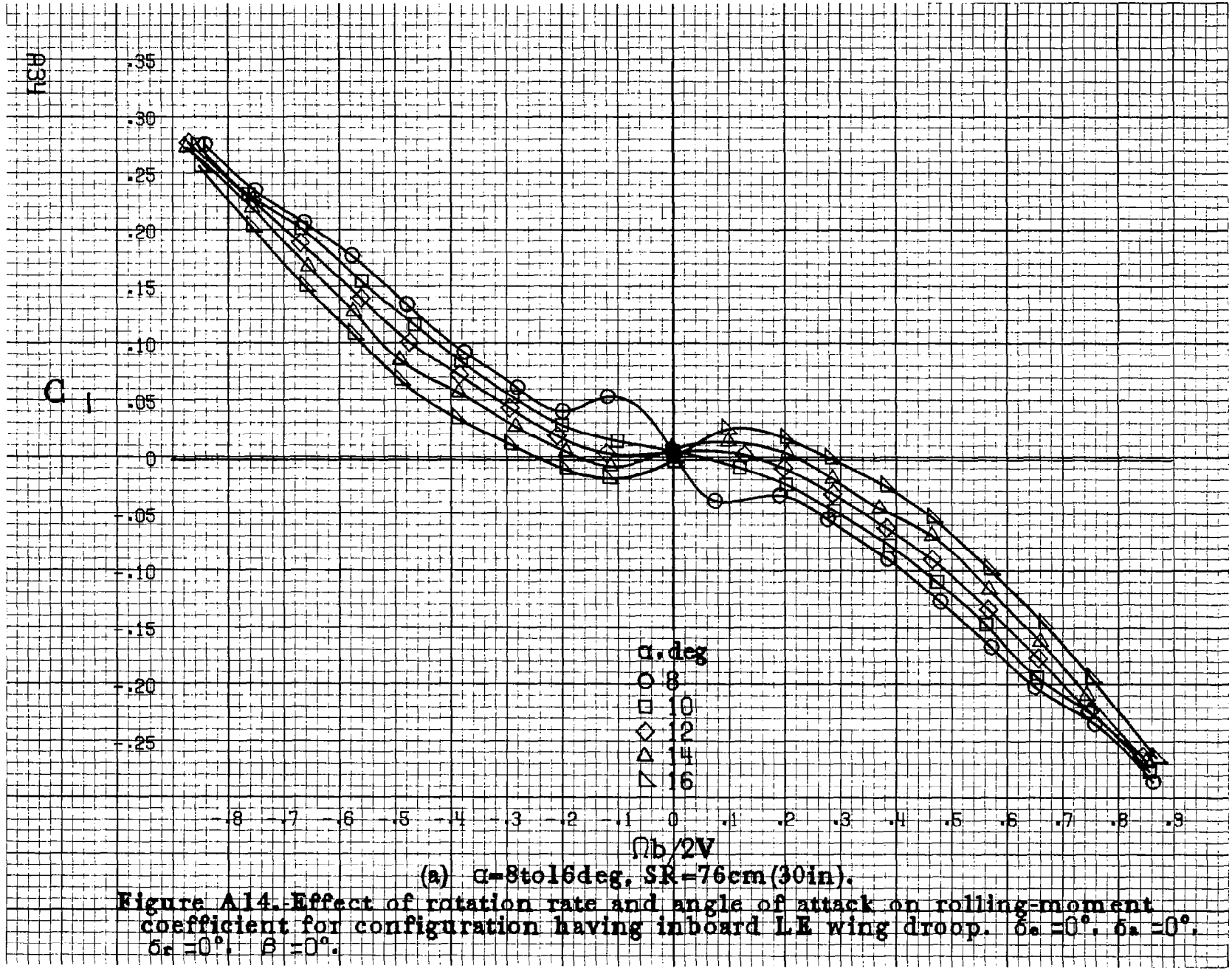

(a) α=8to16deg, SR=76cm(30in).

Figure A14.-Effect of rotation rate and angle of attack on rolling-moment coefficient for configuration having inboard LE wing droop. $\delta_e = 0°$, $\delta_a = 0°$, $\delta_r = 0°$, $\beta = 0°$.

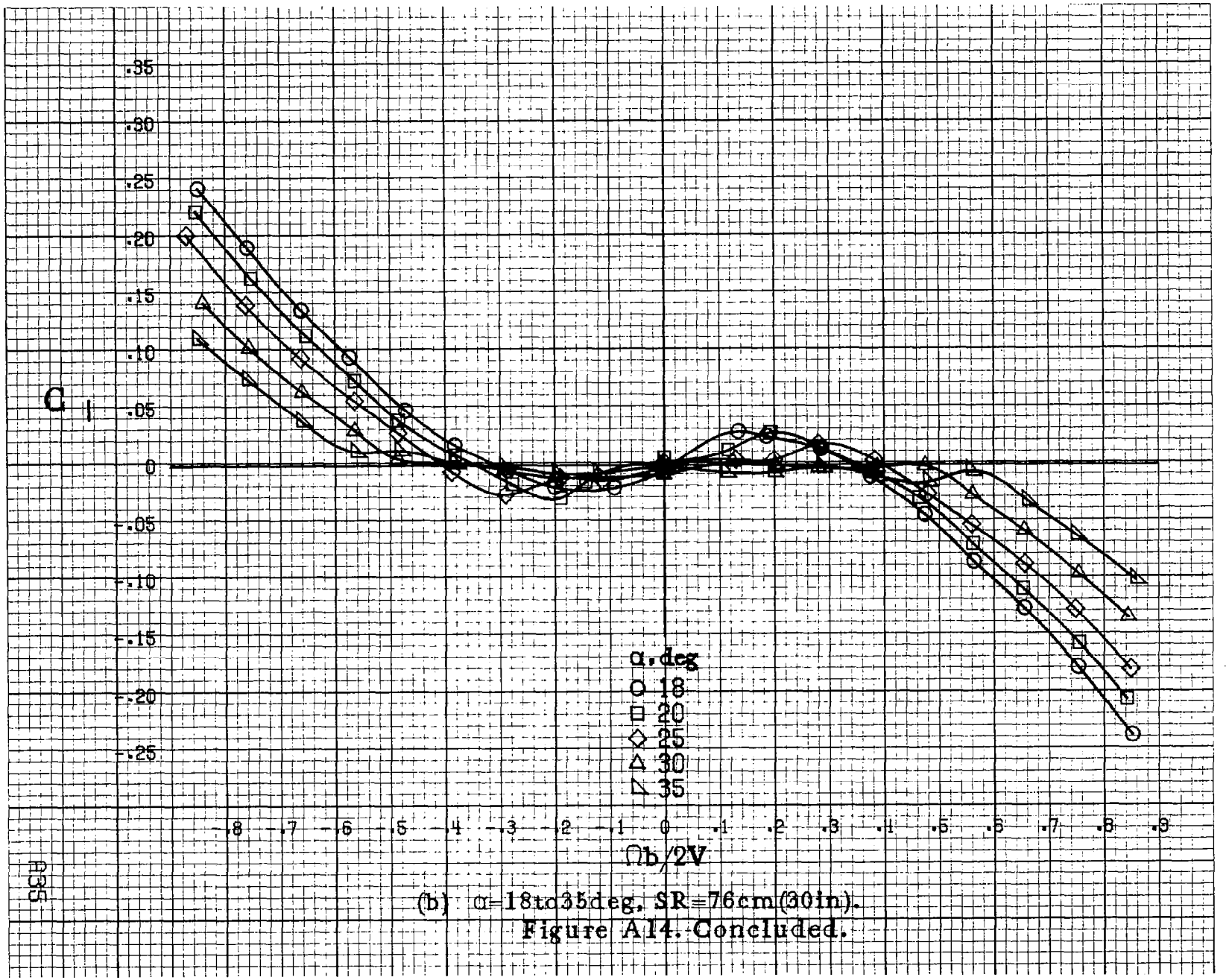

(b) α=18 to 35 deg, SR=76 cm (30 in).

Figure A14. Concluded.

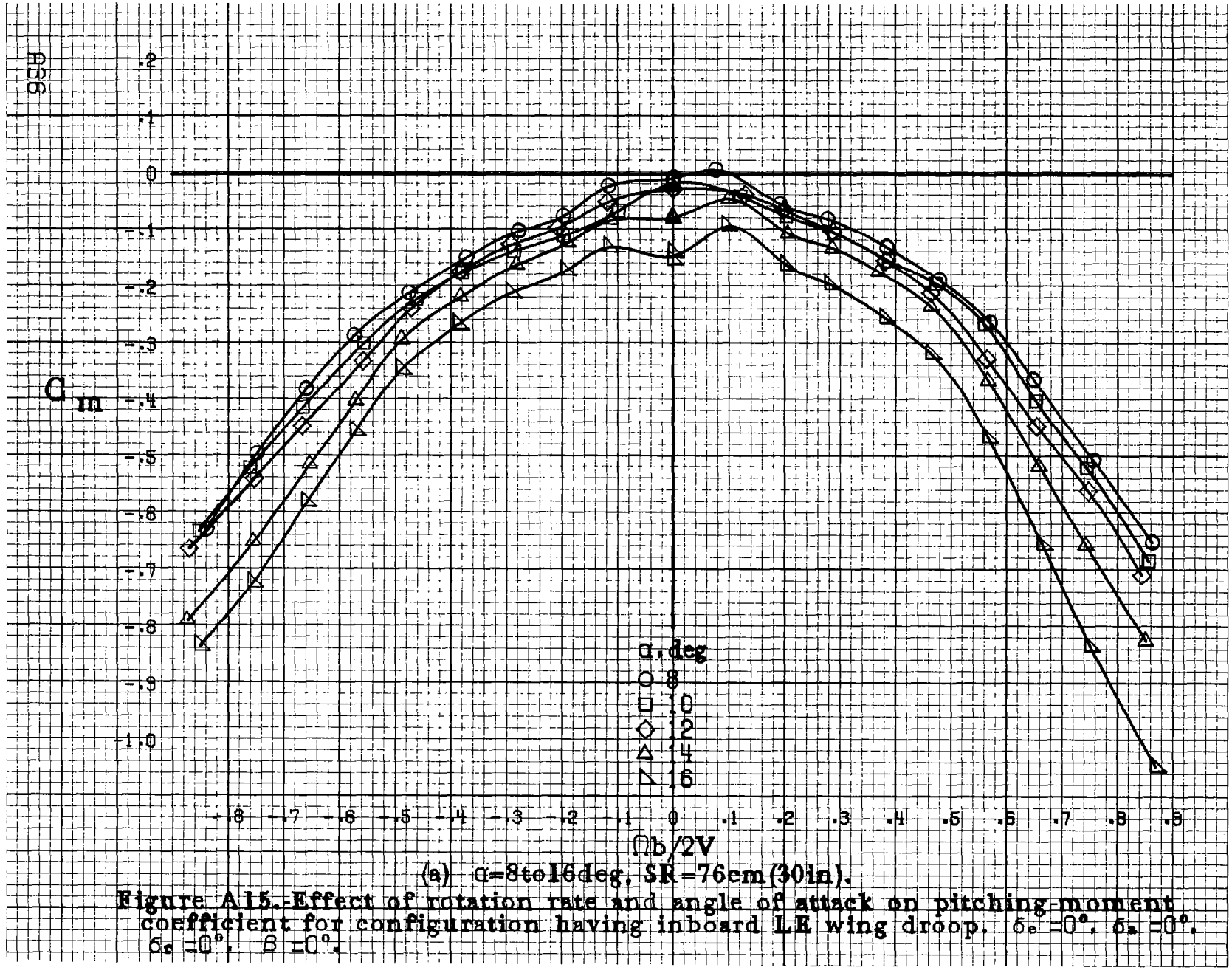

(a) α=8to16deg, $R=76cm(30in).

Figure A15.-Effect of rotation rate and angle of attack on pitching-moment coefficient for configuration having inboard LE wing droop. $\delta_e = 0°$, $\delta_a = 0°$, $\delta_r = 0°$, $\beta = 0°$.

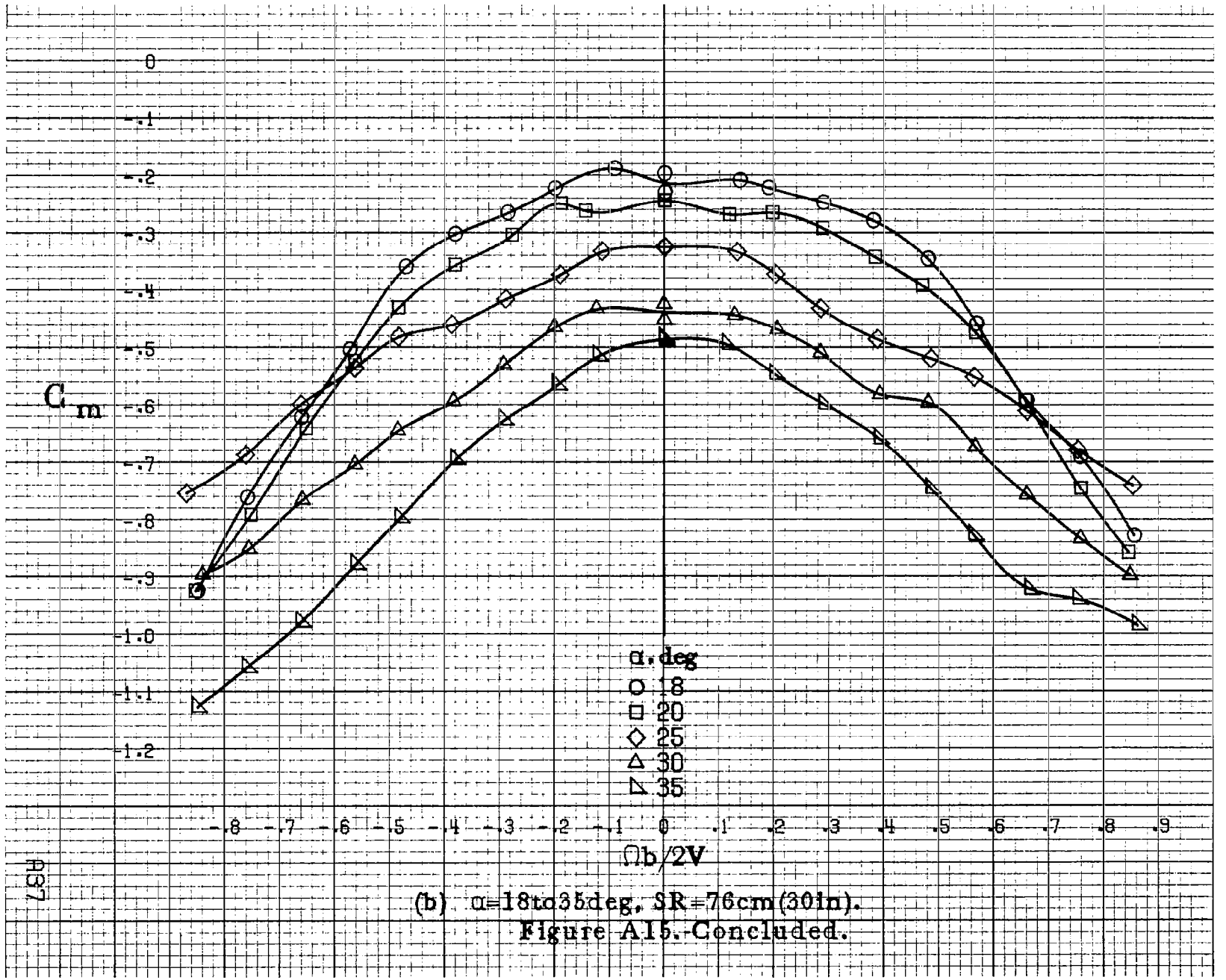

(b) α=18to35deg, SR=76cm(30in).

Figure A15.-Concluded.

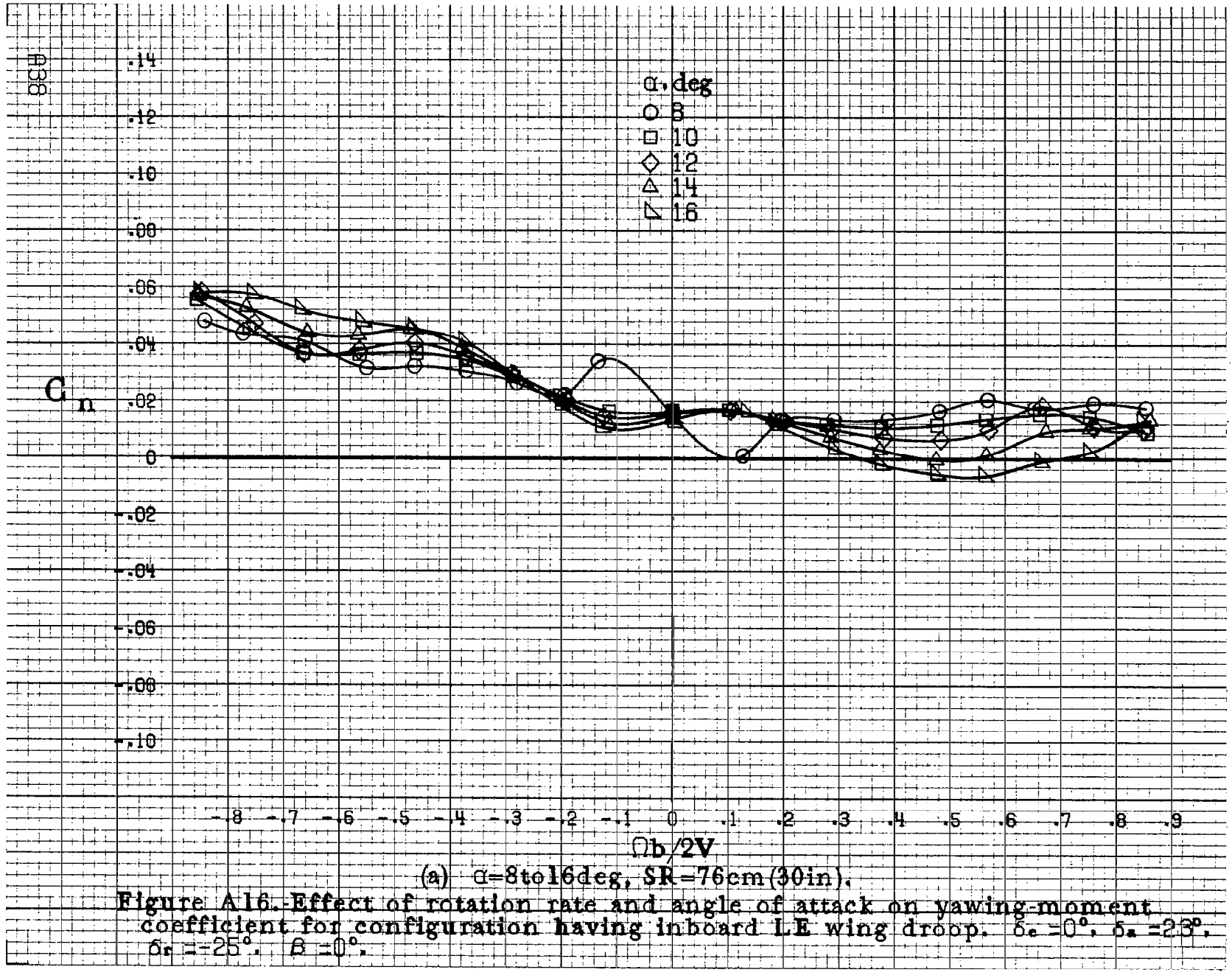

(a) α=8to16deg, SR=76cm(30in).

Figure A16.-Effect of rotation rate and angle of attack on yawing-moment coefficient for configuration having inboard LE wing droop. $\delta_e = 0°$, $\delta_a = 23°$, $\delta_r = -25°$, $\beta = 0°$.

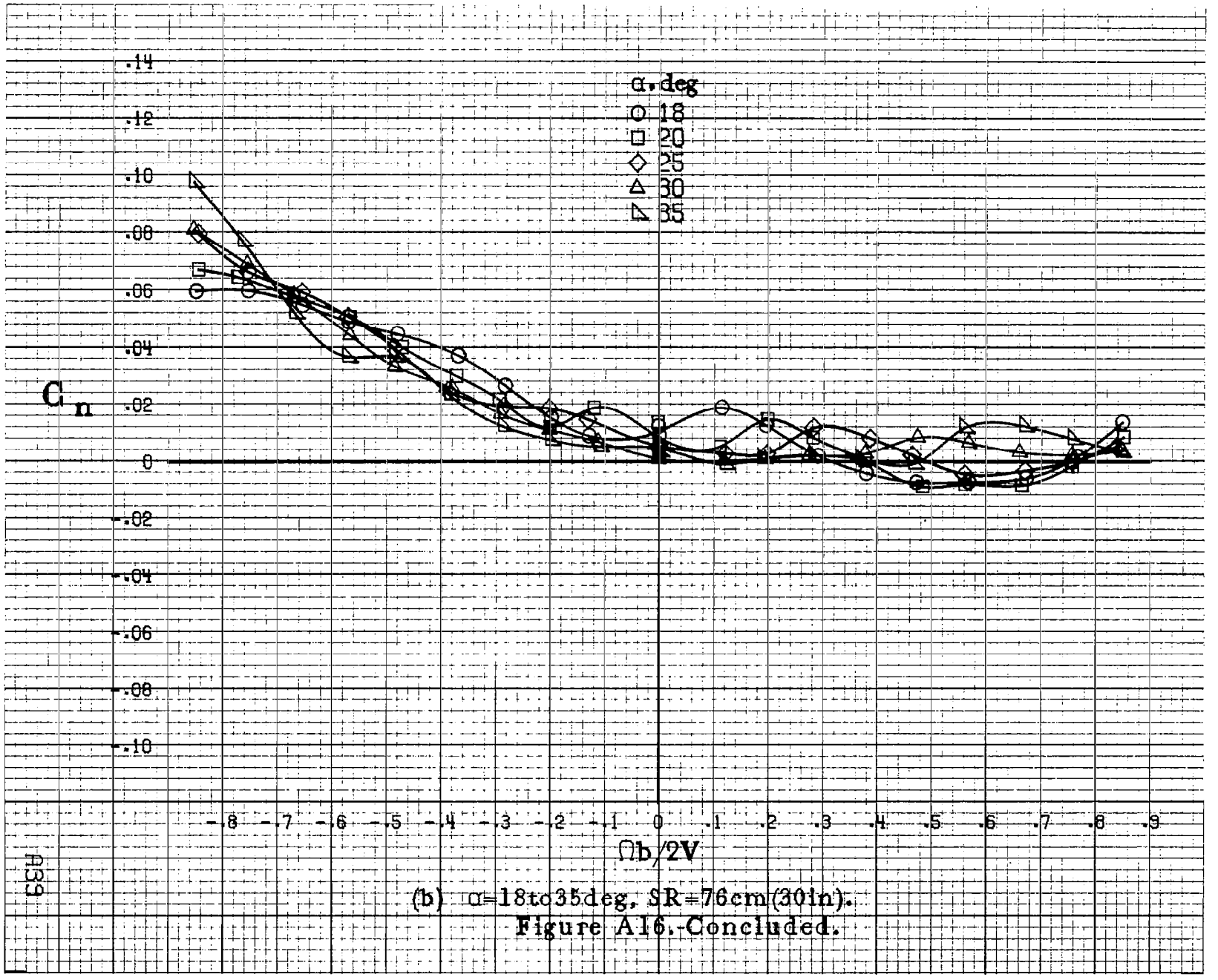

(b) α=18to35deg, SR=76cm(30in).

Figure A16.-Concluded.

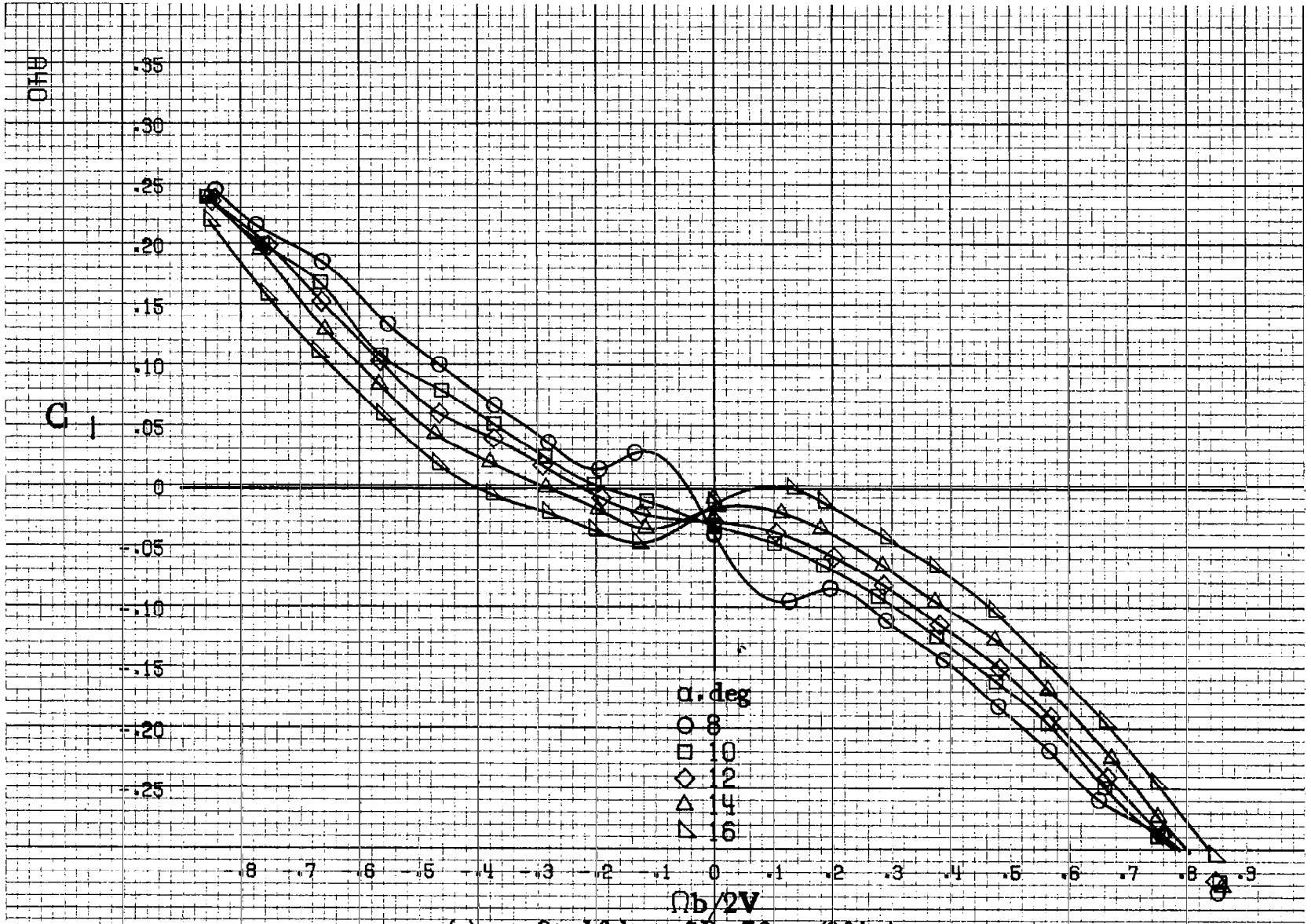

(a) α=8to16deg, SR=76cm(30in).

Figure A17.-Effect of rotation rate and angle of attack on rolling-moment coefficient for configuration having inboard LE wing droop. $\delta_e = 0°$, $\delta_a = 23°$, $\delta_r = -25°$, $\beta = 0°$.

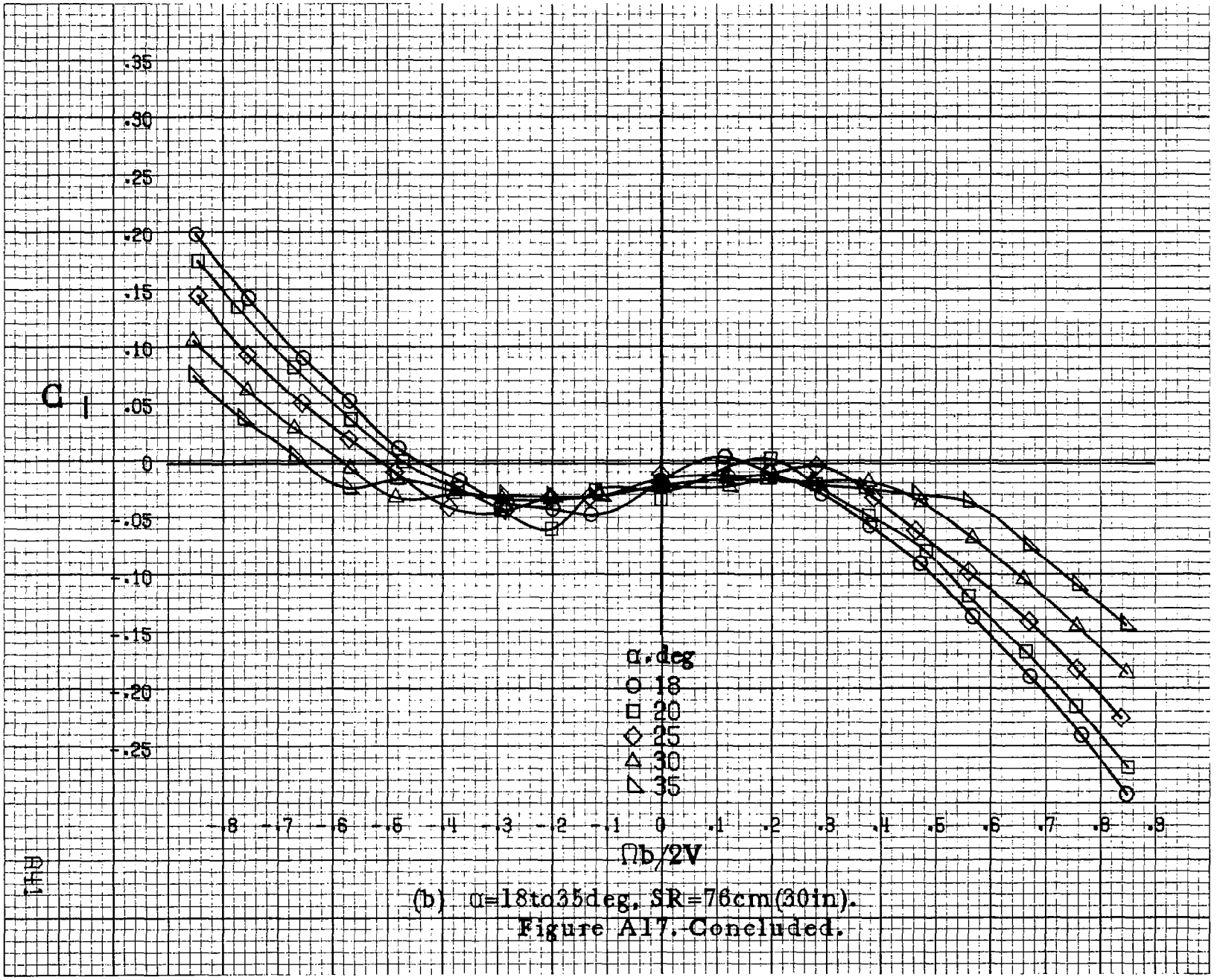

(b) α=18to35deg, SR=76cm(30in).

Figure A17. Concluded.

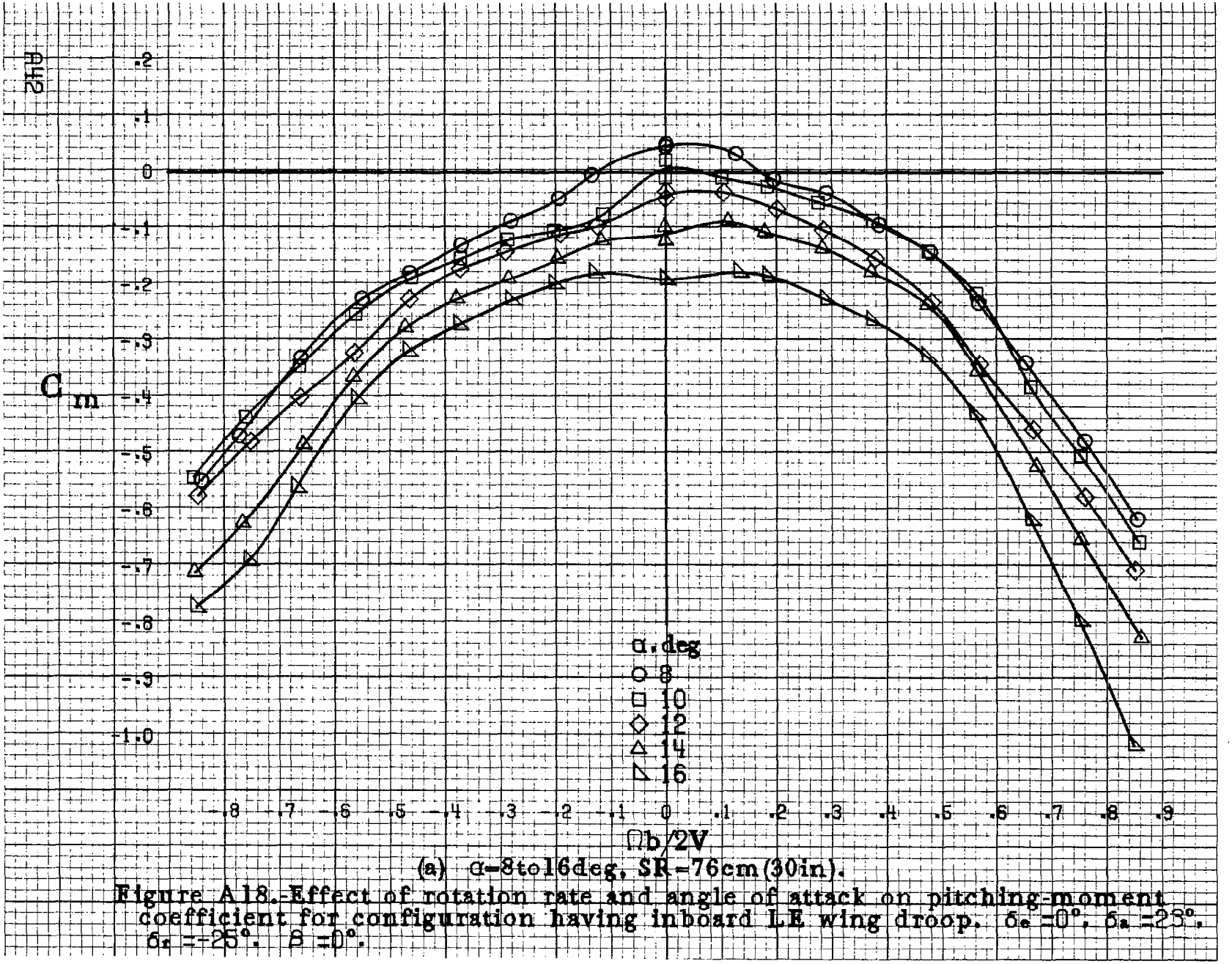

(a) α=8to16deg, $R=76cm(30in).

Figure A18.-Effect of rotation rate and angle of attack on pitching-moment coefficient for configuration having inboard LE wing droop. $\delta_e = 0°$, $\delta_a = 23°$, $\delta_r = -25°$, $\beta = 0°$.

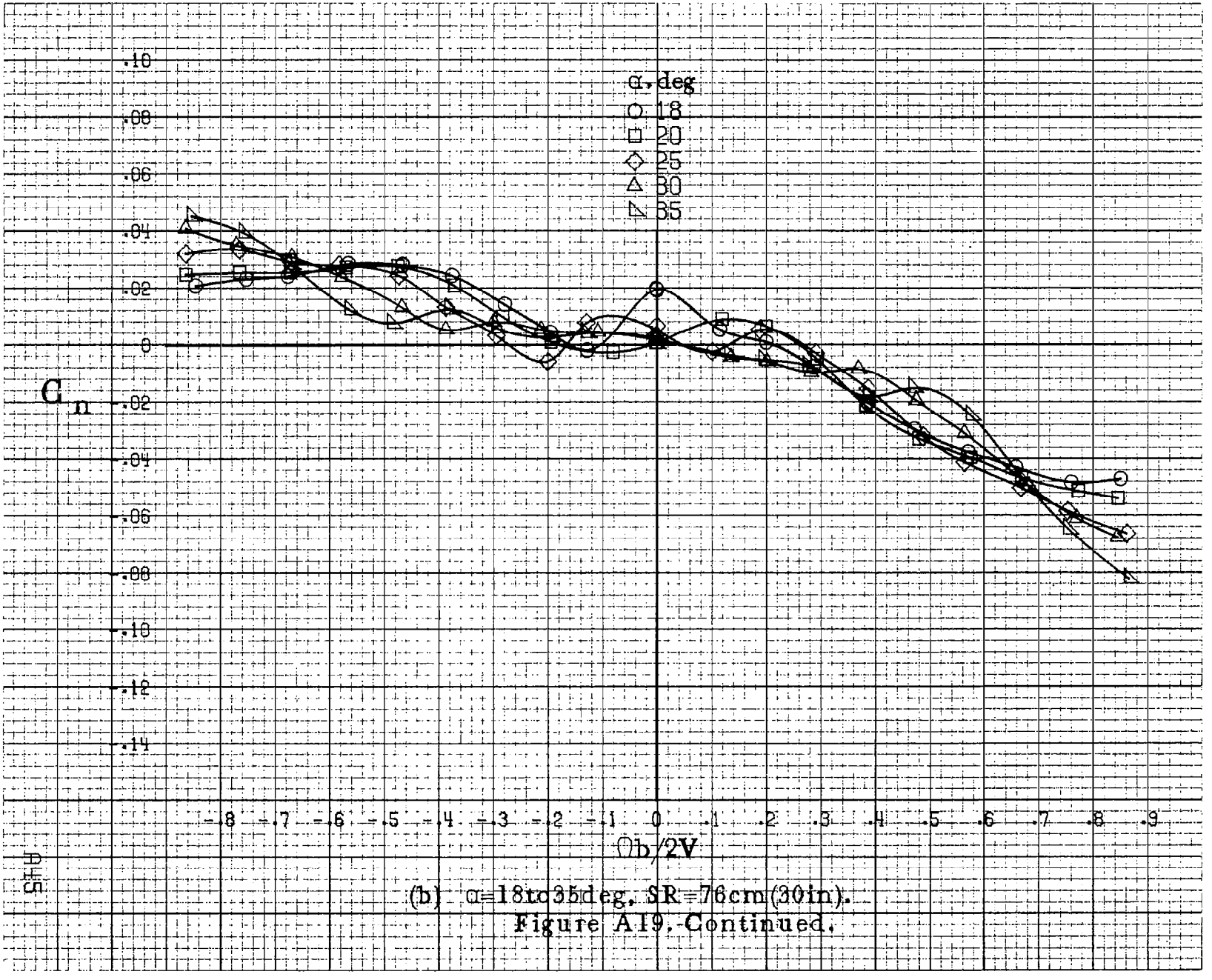

(b) α=18to35deg, SR=76cm(30in).

Figure A19.-Continued.

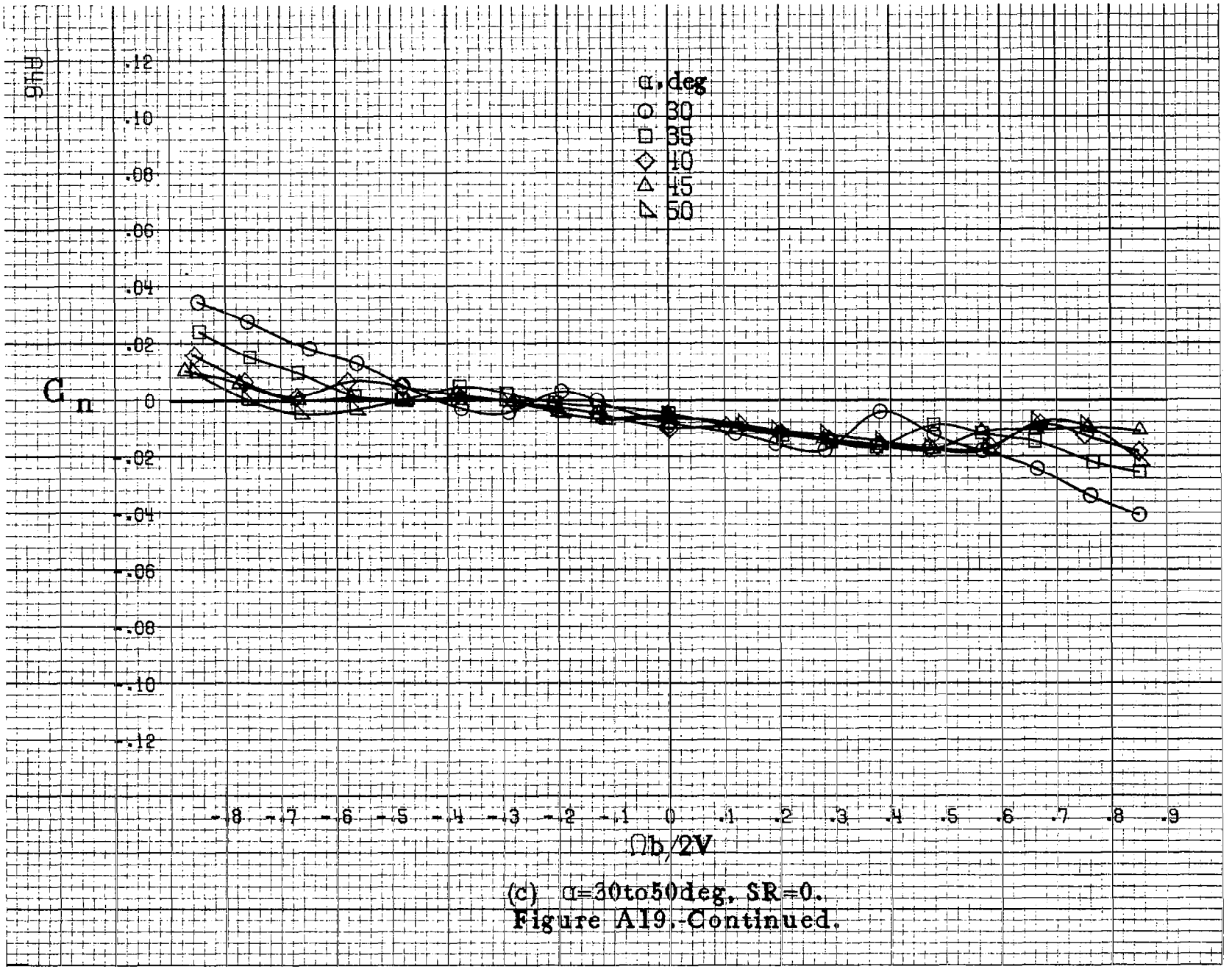

(c) α=30to50deg, SR=0.

Figure A19.-Continued.

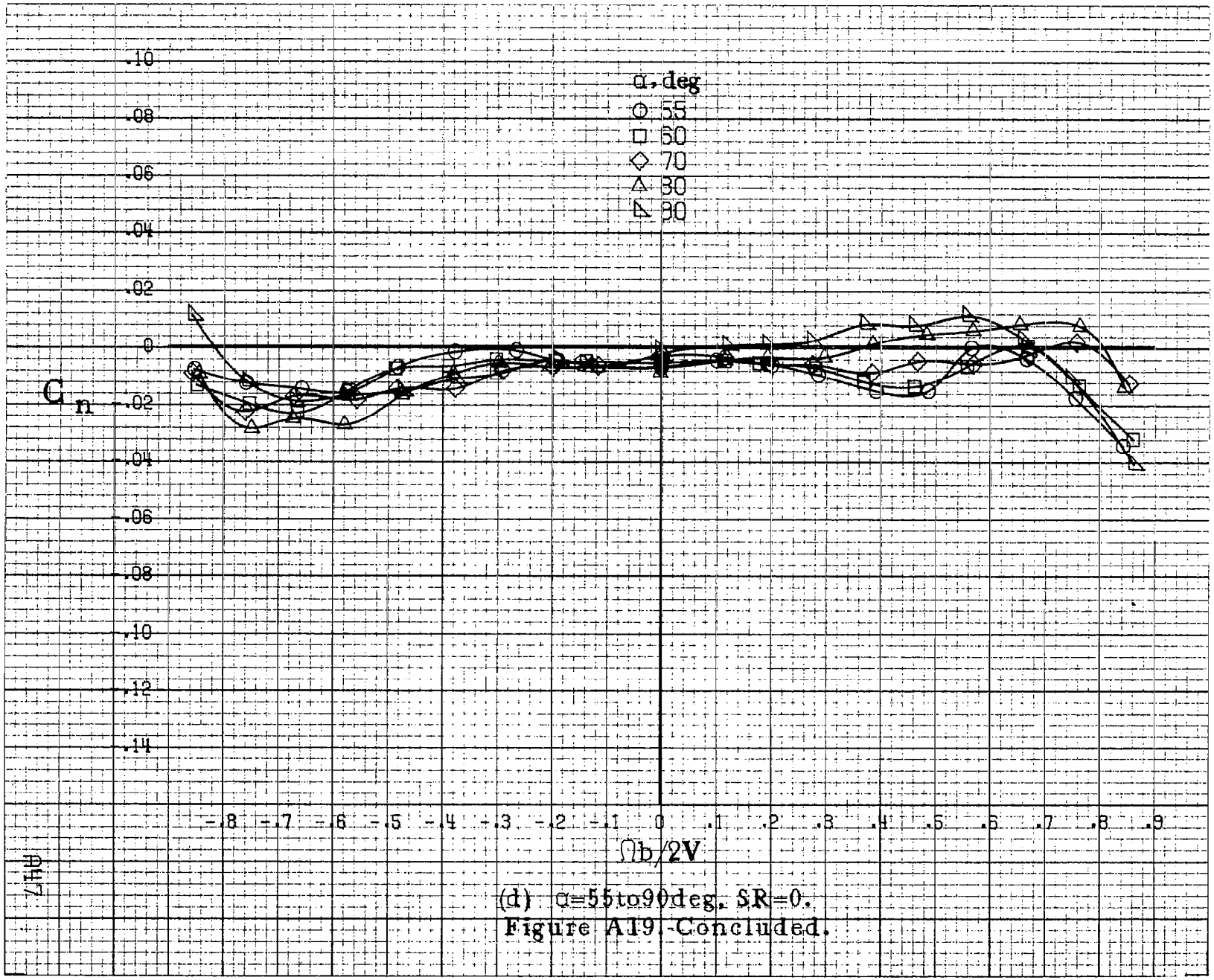

(d) α=55to90deg. SR=0.

Figure A19.-Concluded.

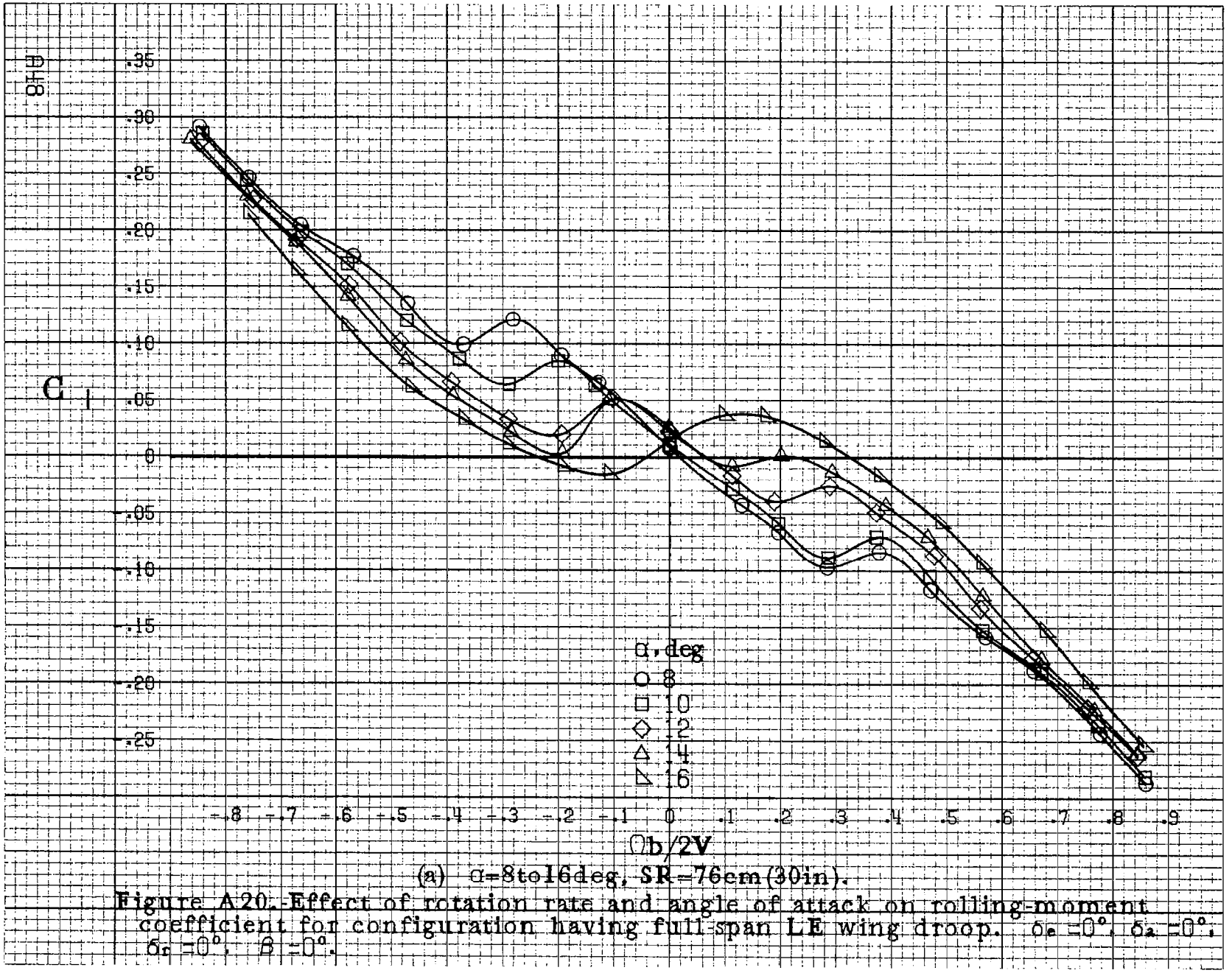

(a) α=8to16deg, SR=76cm(30in).

Figure A20.-Effect of rotation rate and angle of attack on rolling-moment coefficient for configuration having full-span LE wing droop. $\delta_e = 0°$, $\delta_a = 0°$, $\delta_r = 0°$, $\beta = 0°$.

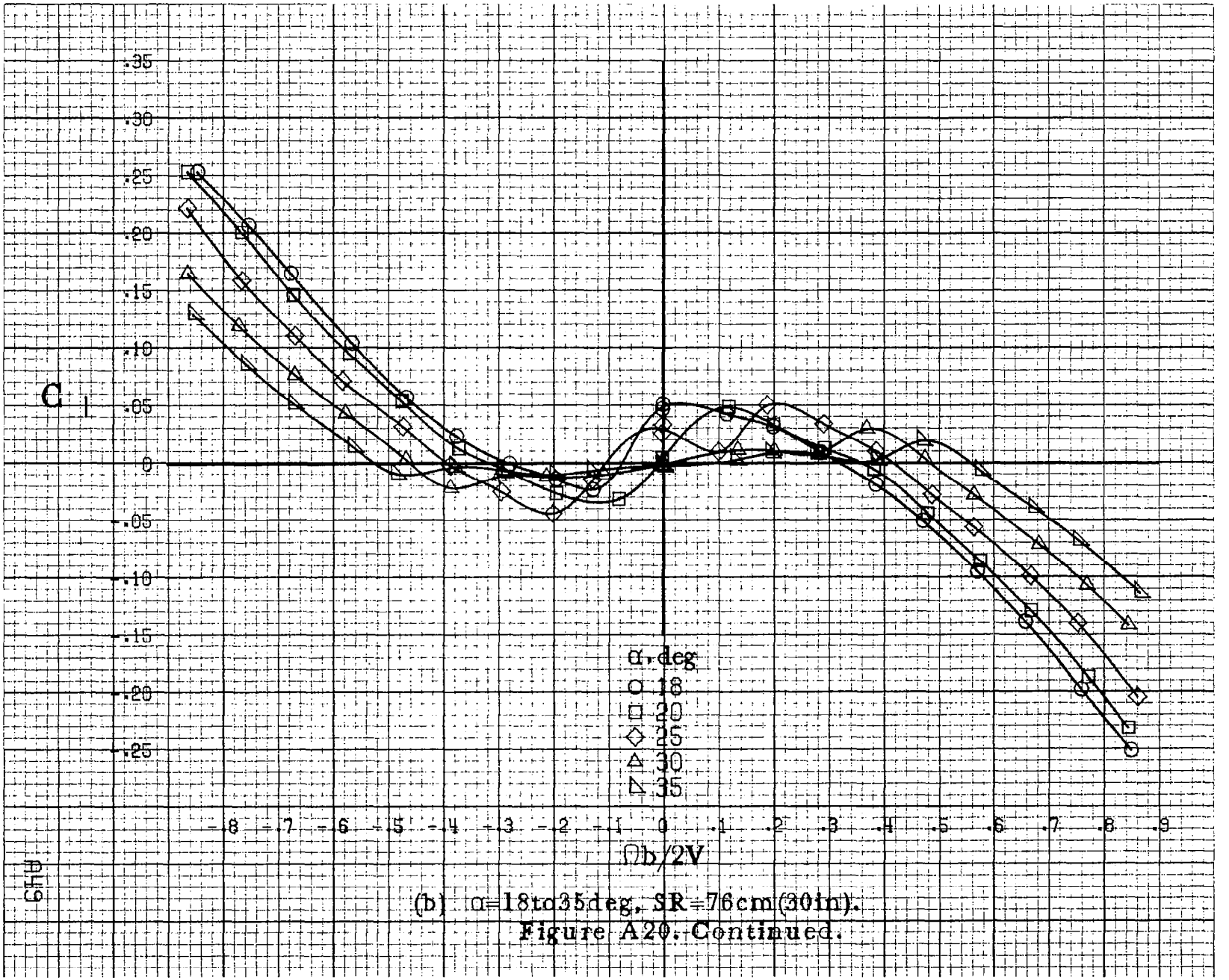

(b) α=18to35deg, SR=76cm(30in).

Figure A20. Continued.

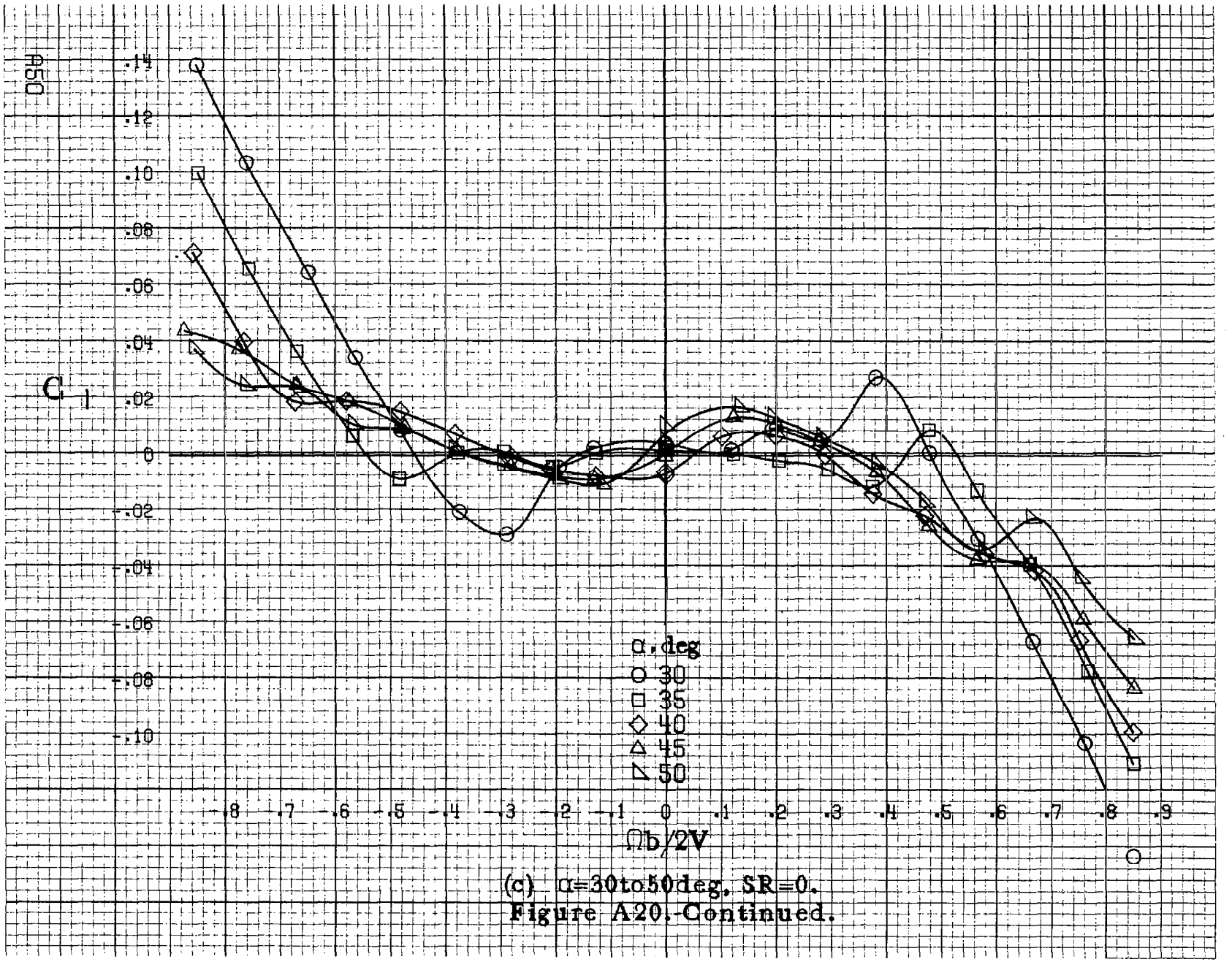

(c) α=30to50deg, SR=0.

Figure A20.-Continued.

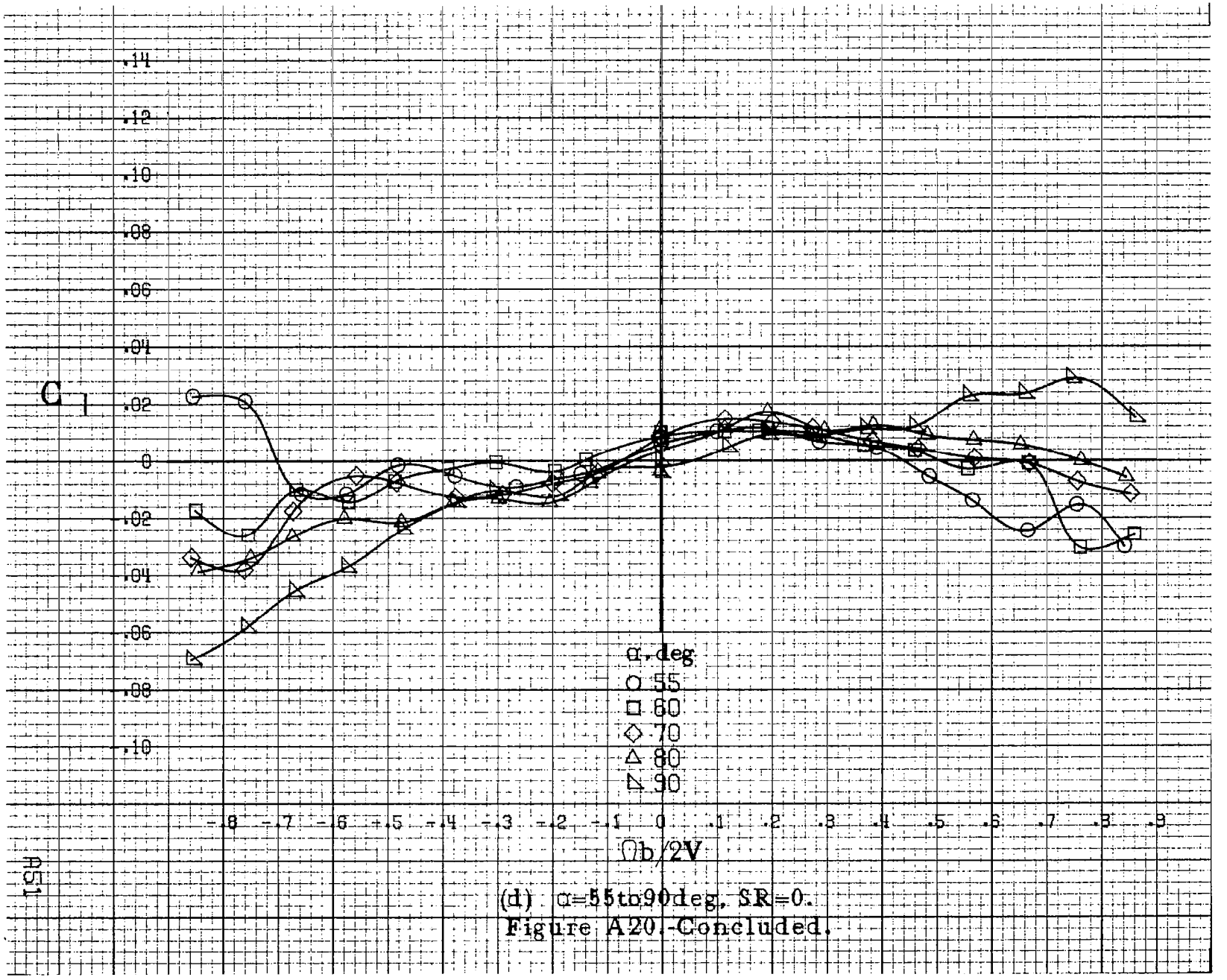

(d) α=55to90deg, SR=0.

Figure A20.-Concluded.

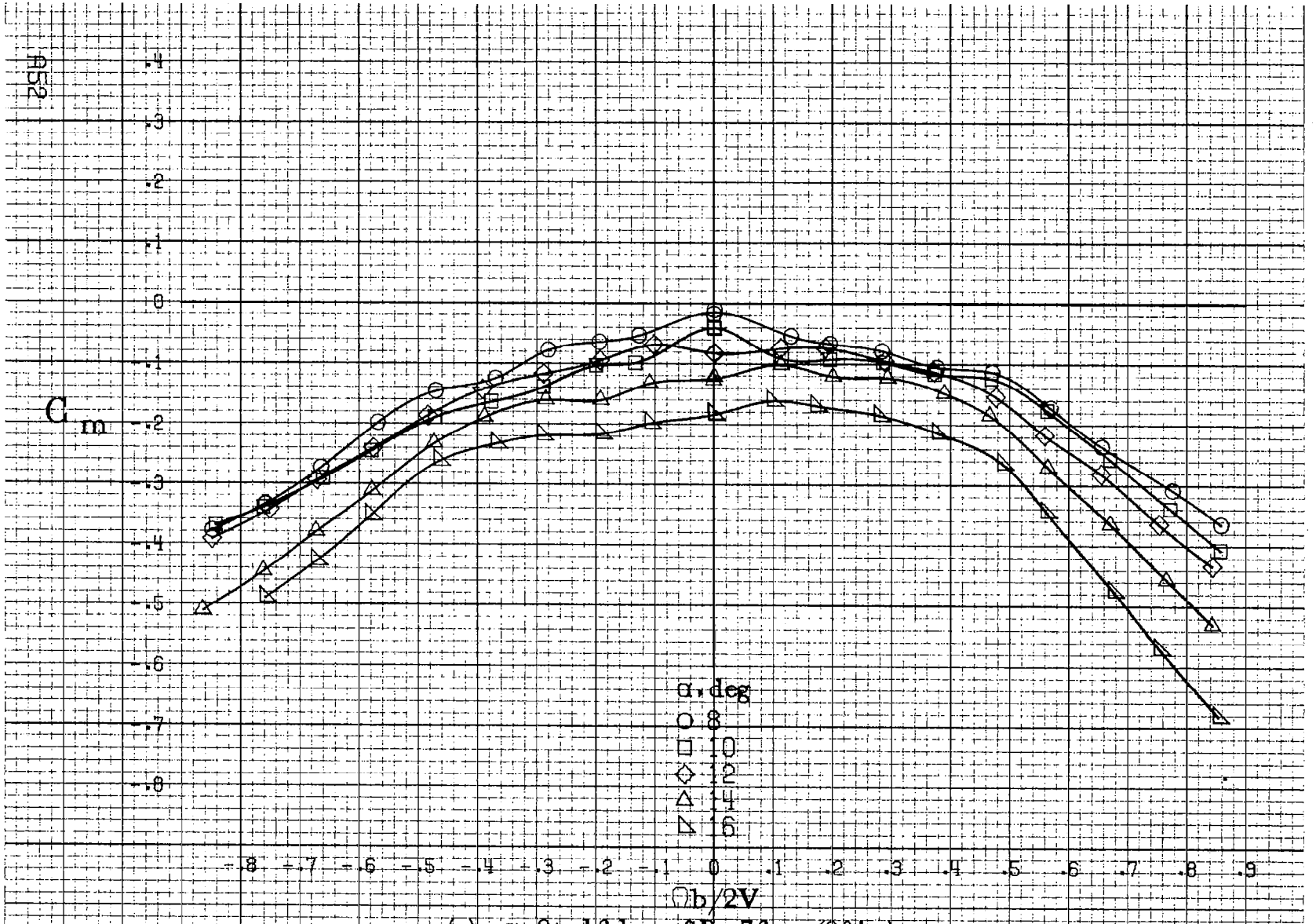

(a) α=8to16deg, SR=76cm(30in).

Figure A21.-Effect of rotation rate and angle of attack on pitching-moment coefficient for configuration having full-span LE wing droop. $\delta_e = 0°$, $\delta_a = 0°$, $\delta_r = 0°$, $\beta = 0°$.

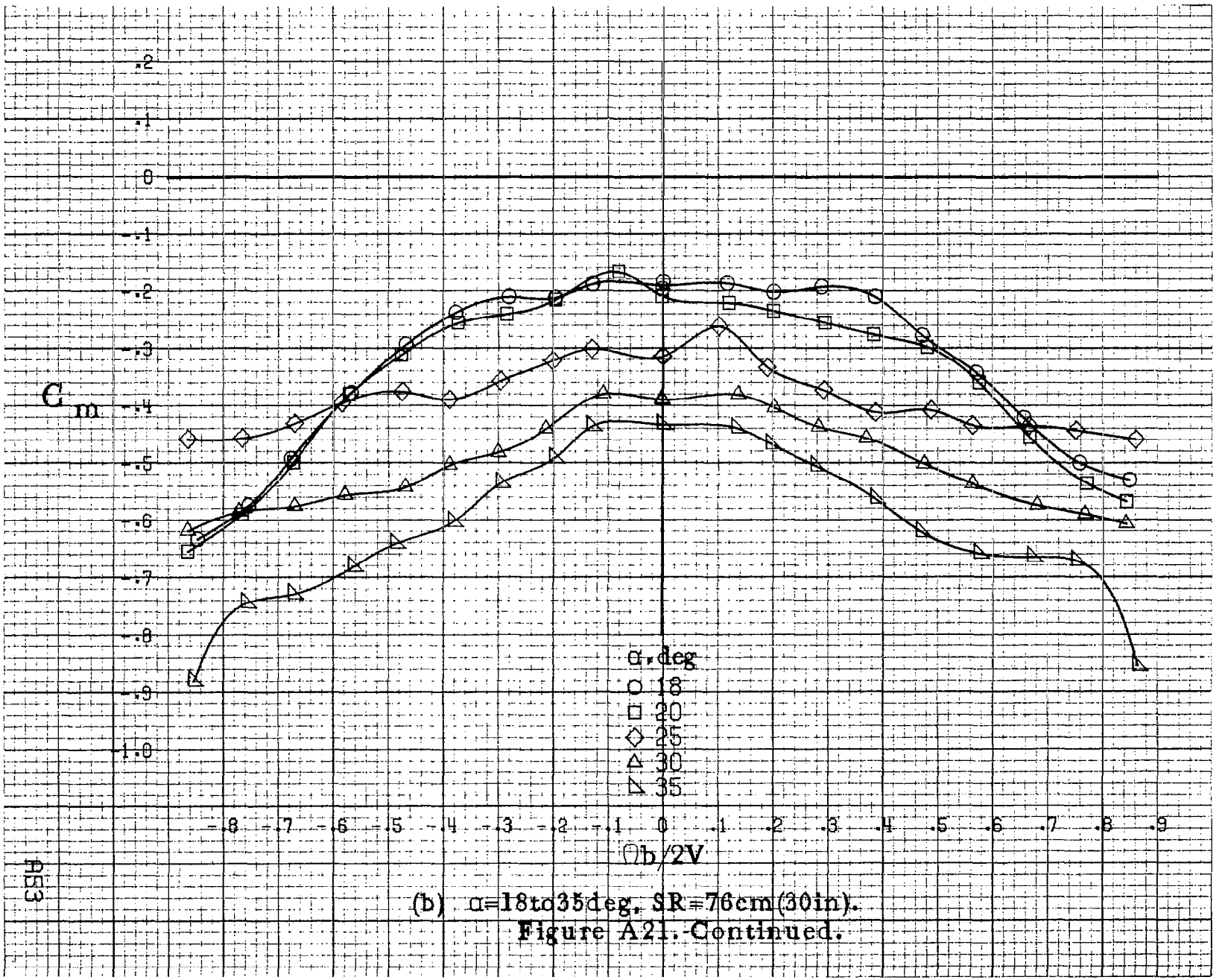

(b) α=18to35deg, SR=76cm(30in).

Figure A21.-Continued.

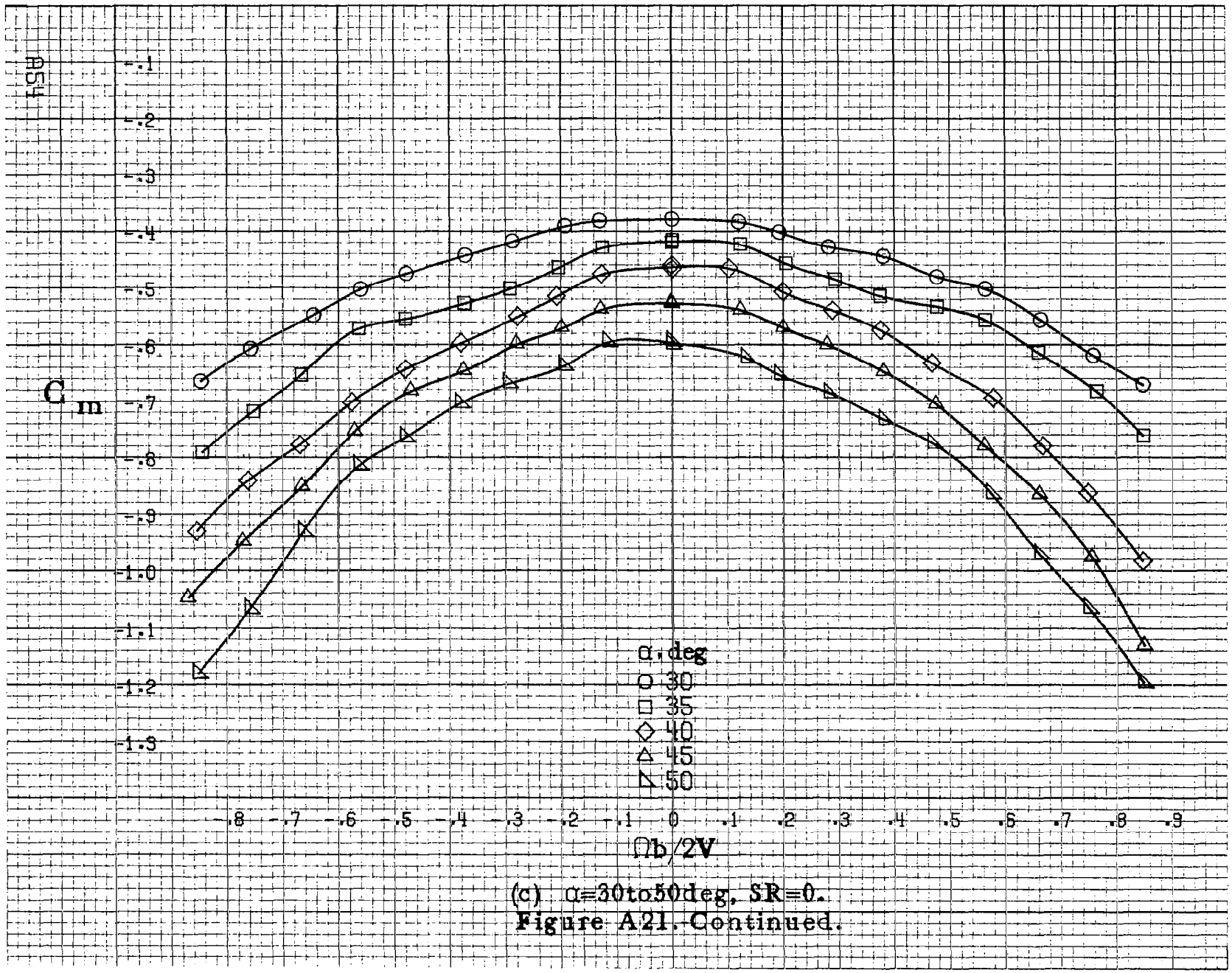

(c) α=30to50deg, SR=0.

Figure A21. Continued.

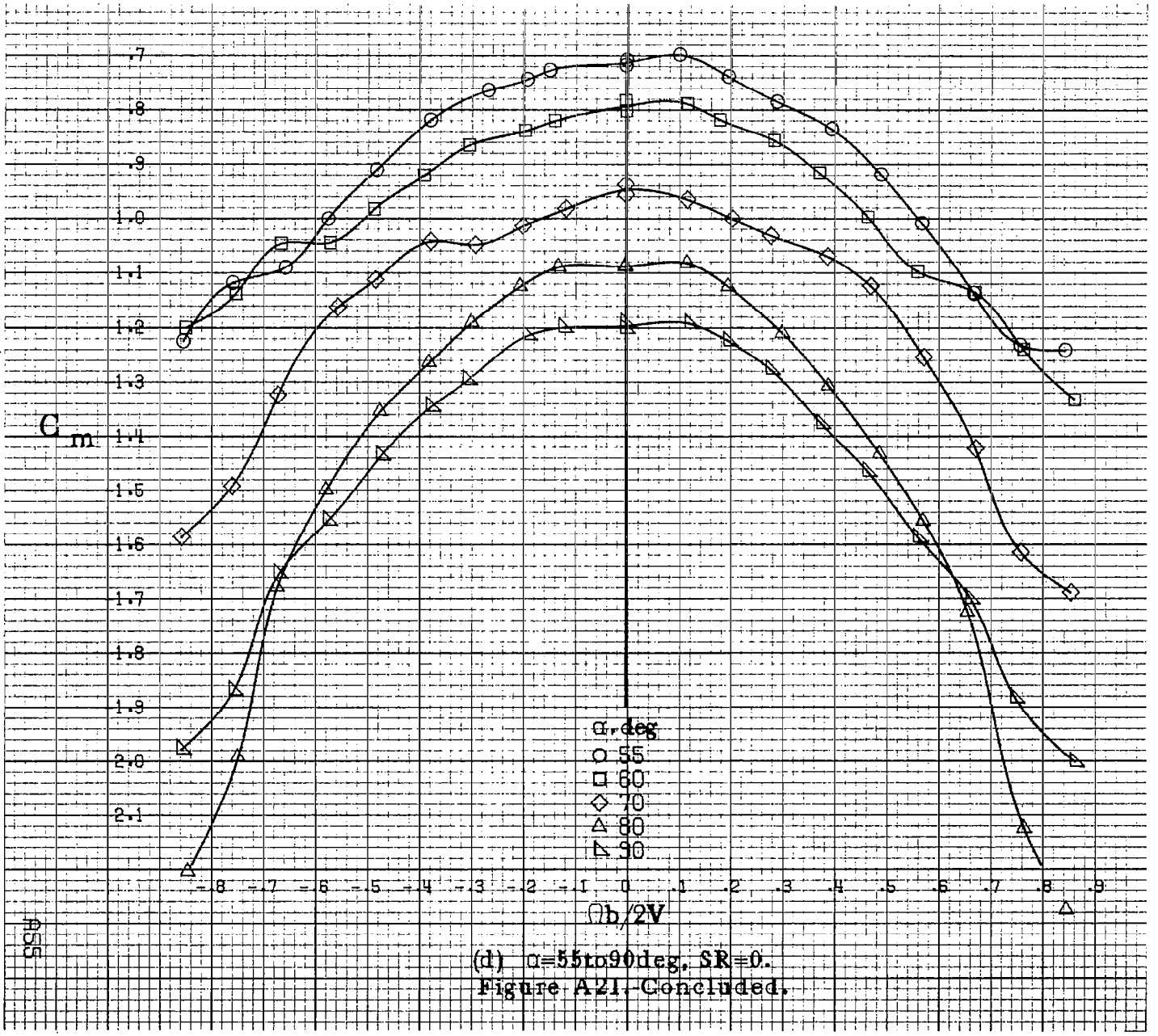

(d) α=55to90deg, SR=0.

Figure A21.-Concluded.

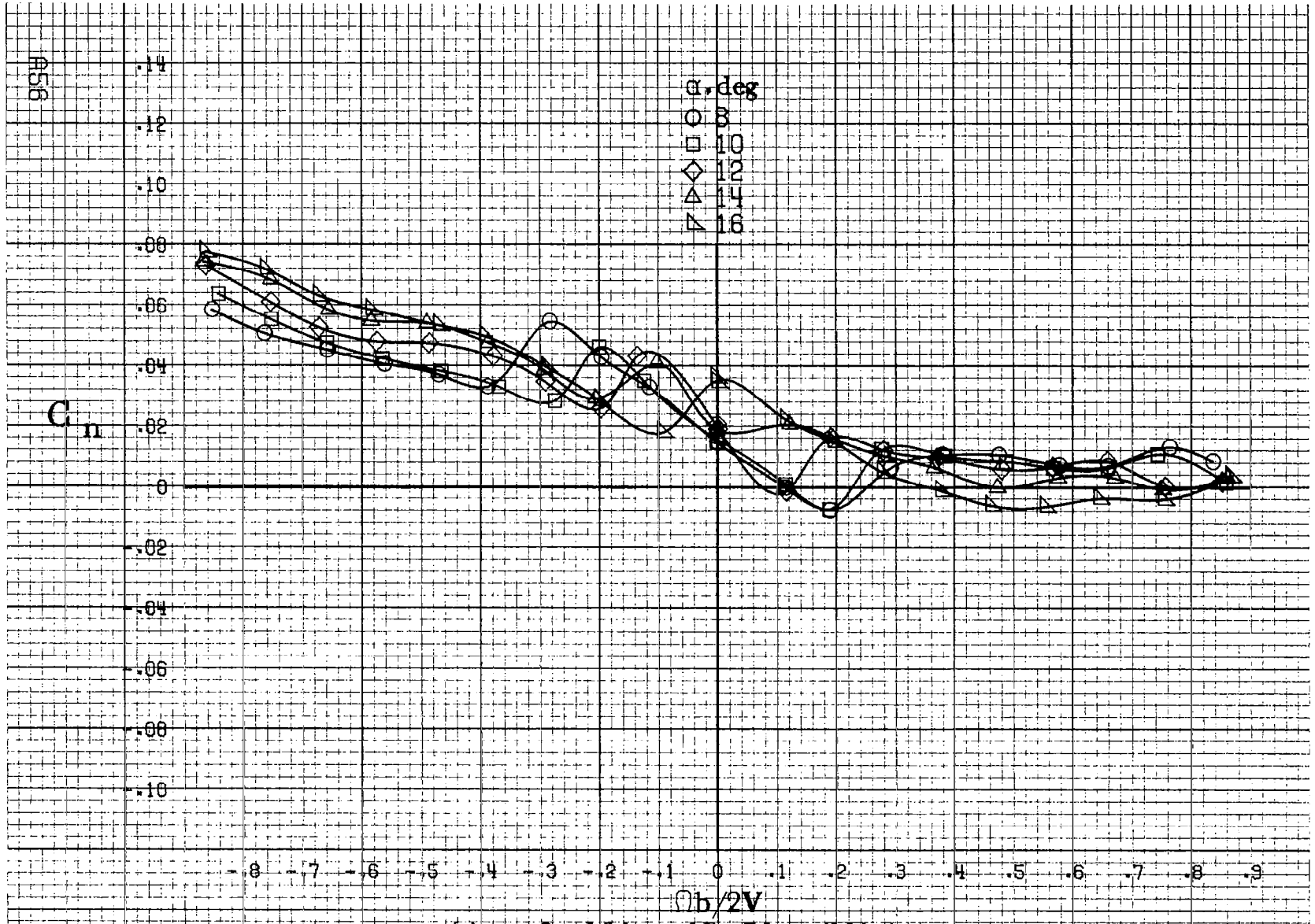

(a) α=8to16deg, SR=76cm(30in).

Figure A22. Effect of rotation rate and angle of attack on yawing-moment coefficient for configuration having full-span LE wing droop. $\delta_e = 0°$. $\delta_a = 23°$. $\delta_n = -25°$. $\beta = 0°$.

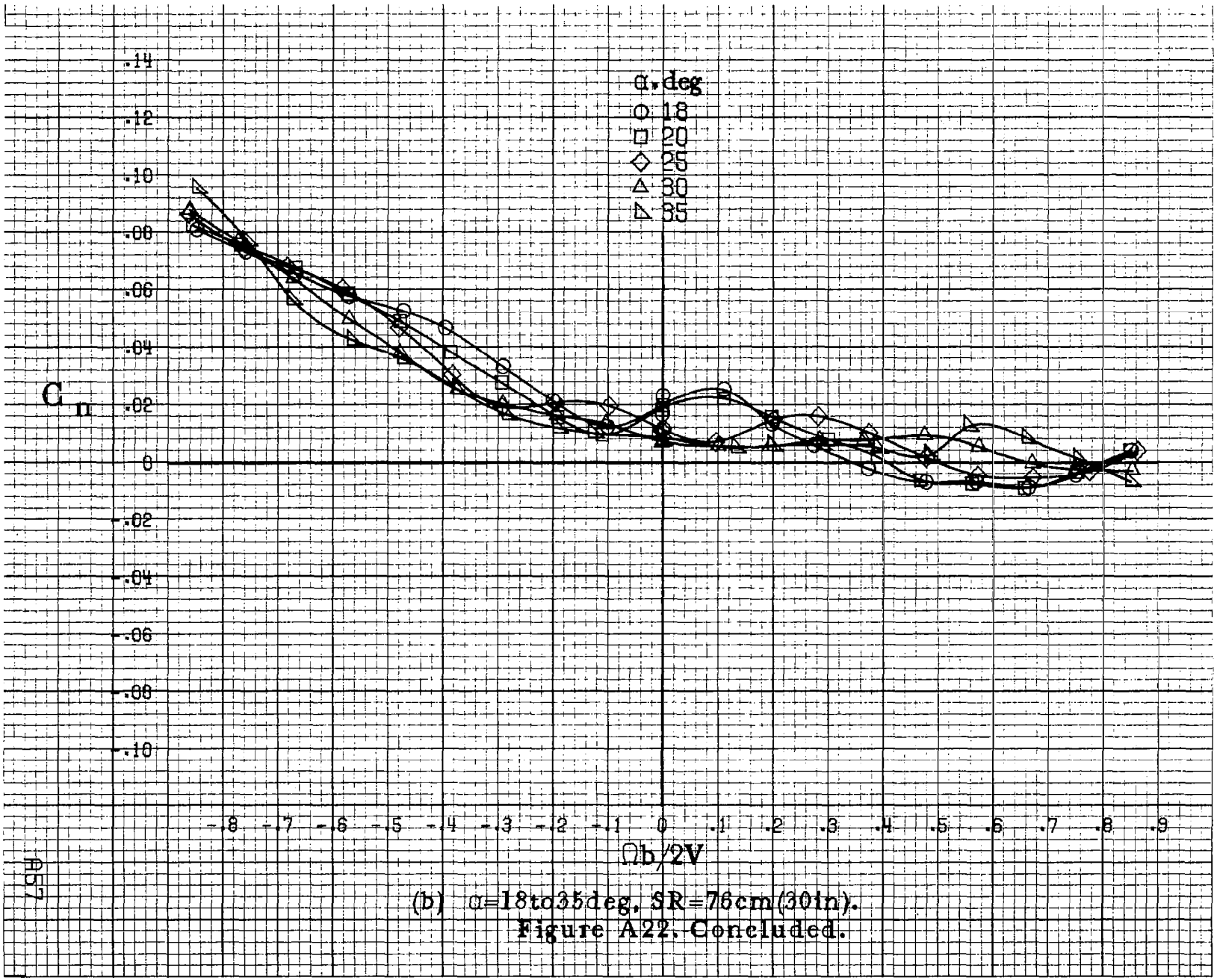

(b) α=18 to 35 deg, SR=76 cm (30 in).

Figure A22. Concluded.

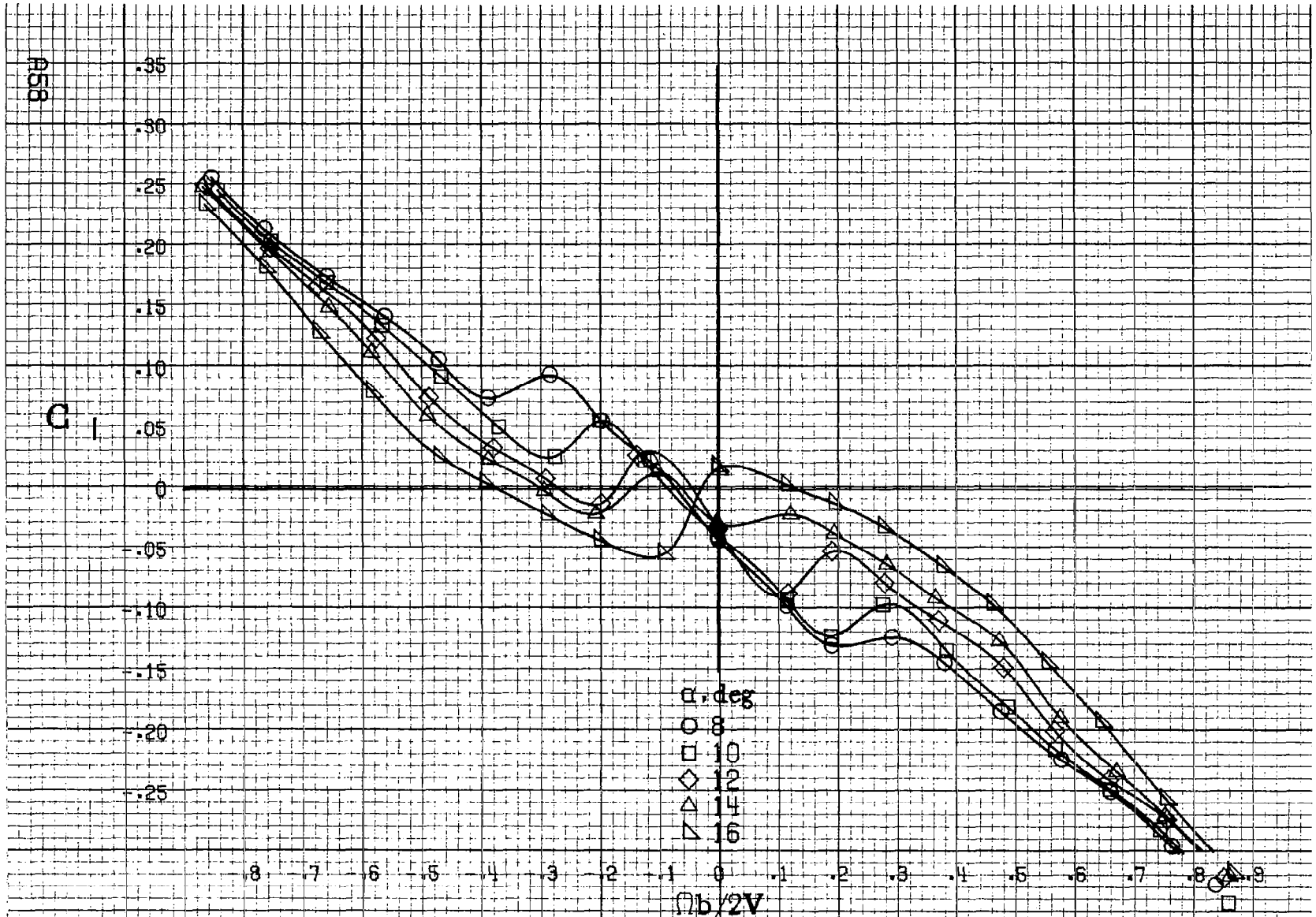

(a) α=8to16deg, SR=76cm(30in).

Figure A23.-Effect of rotation rate and angle of attack on rolling-moment coefficient for configuration having full-span LE wing droop. $\delta_e = 0°$, $\delta_a = 23°$, $\delta_r = -25°$, $\beta = 0°$.

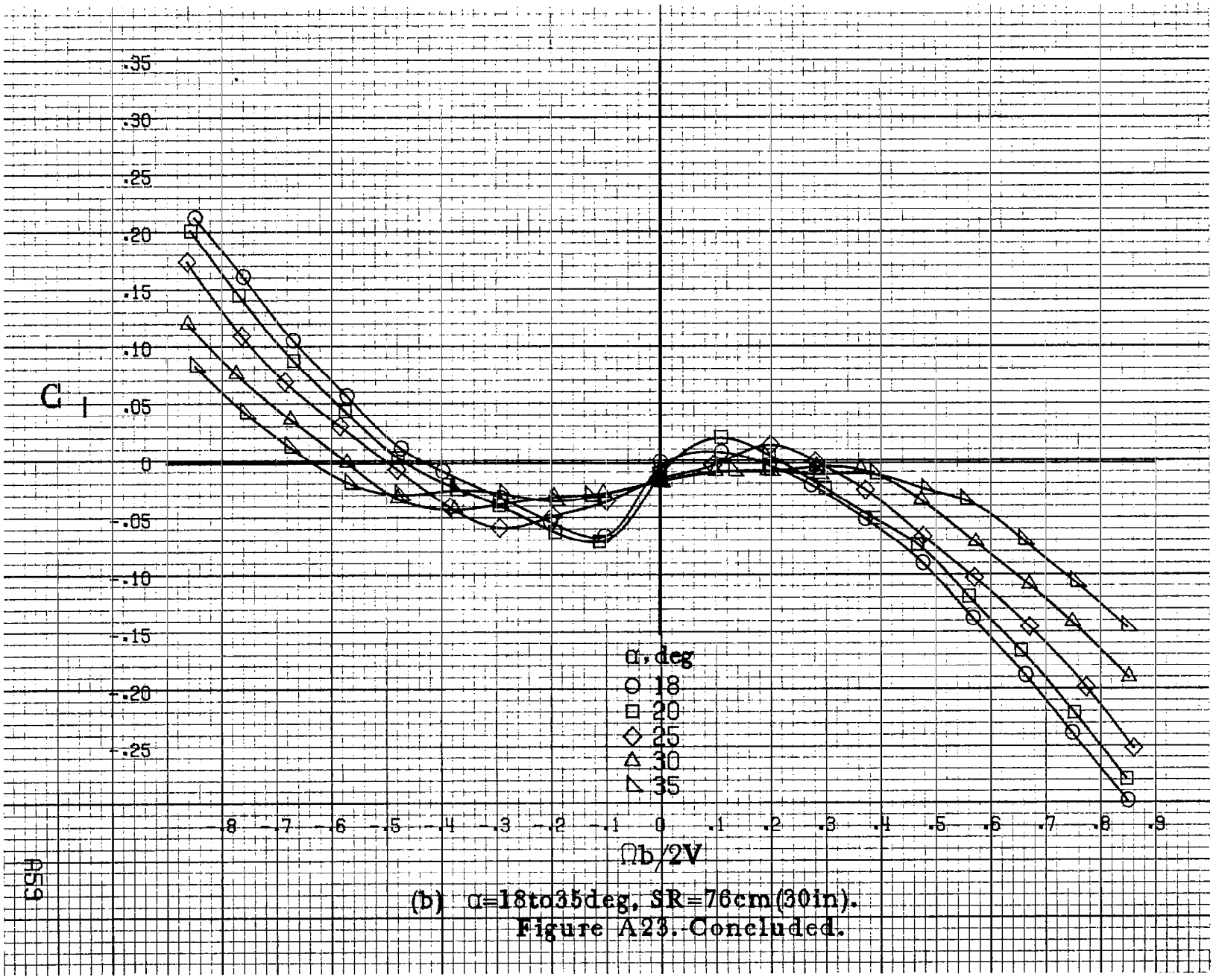

(b) α=18toα35deg, SR=76cm(30in).

Figure A23.-Concluded.

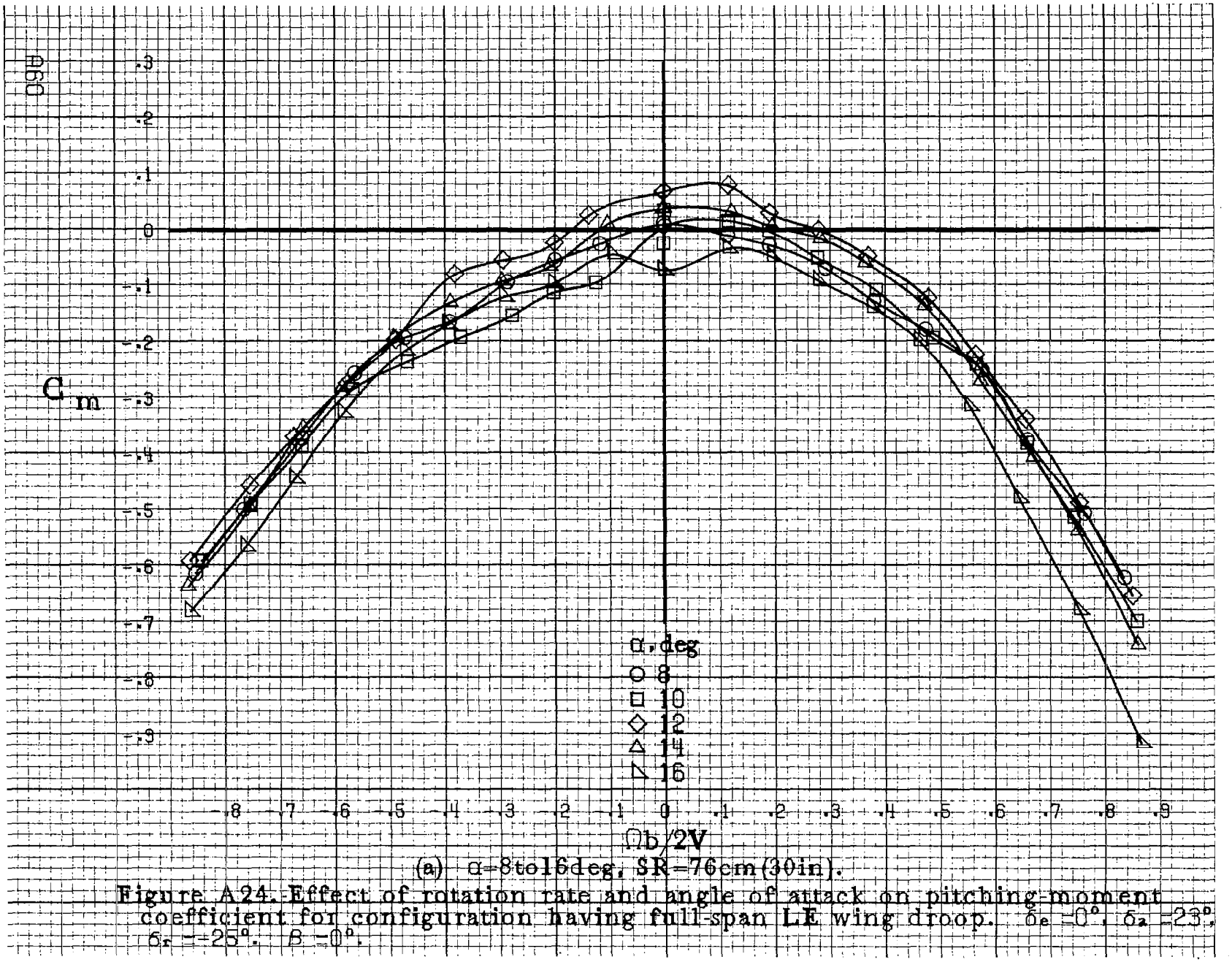

(a) α=8to16deg, SR=76cm(30in).

Figure A24. Effect of rotation rate and angle of attack on pitching-moment coefficient for configuration having full-span LE wing droop. $\delta_e = 0°$, $\delta_a = 23°$, $\delta_r = -25°$, $\beta = 0°$.

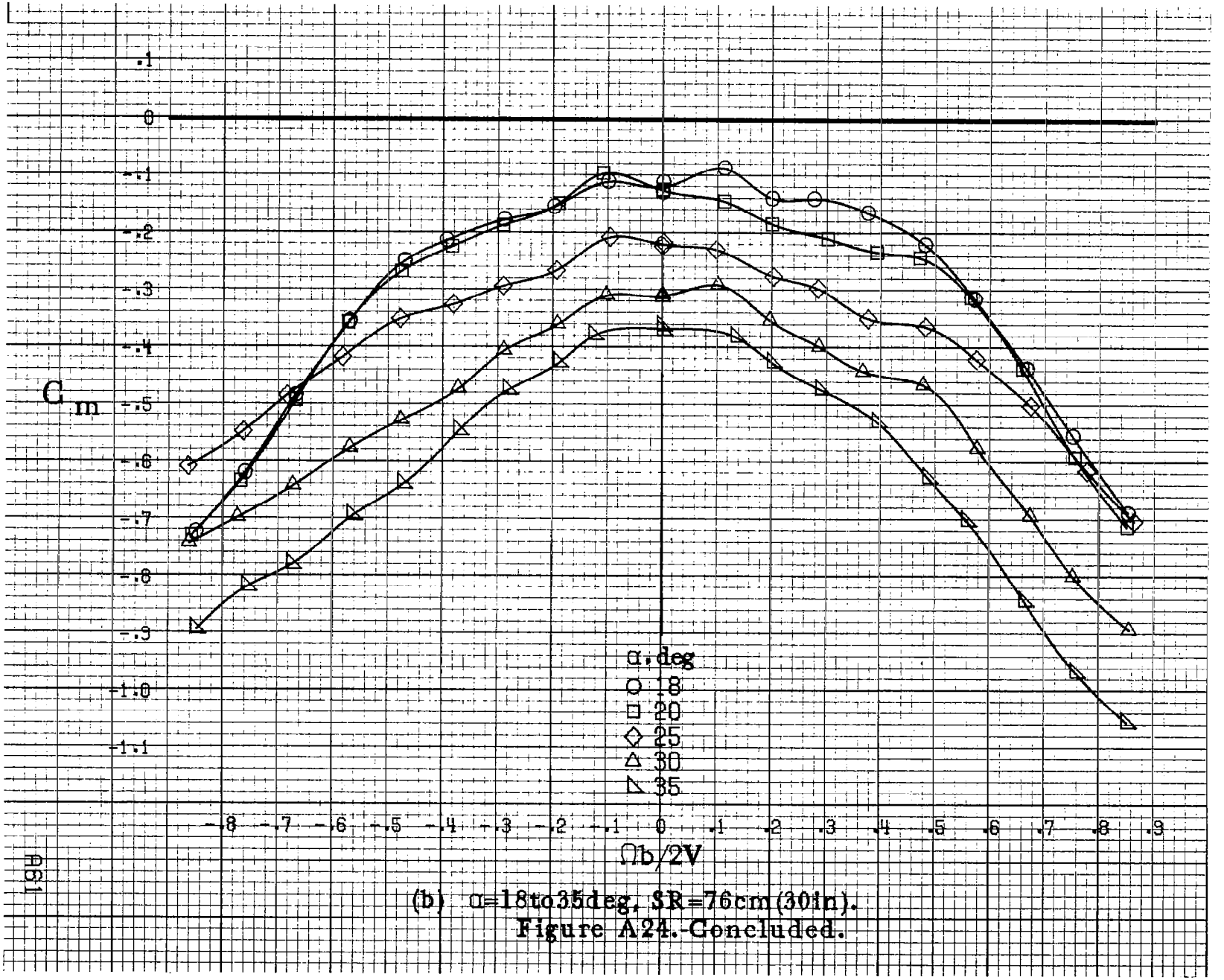

(b) α=18to35deg, SR=76cm(30in).

Figure A24.-Concluded.

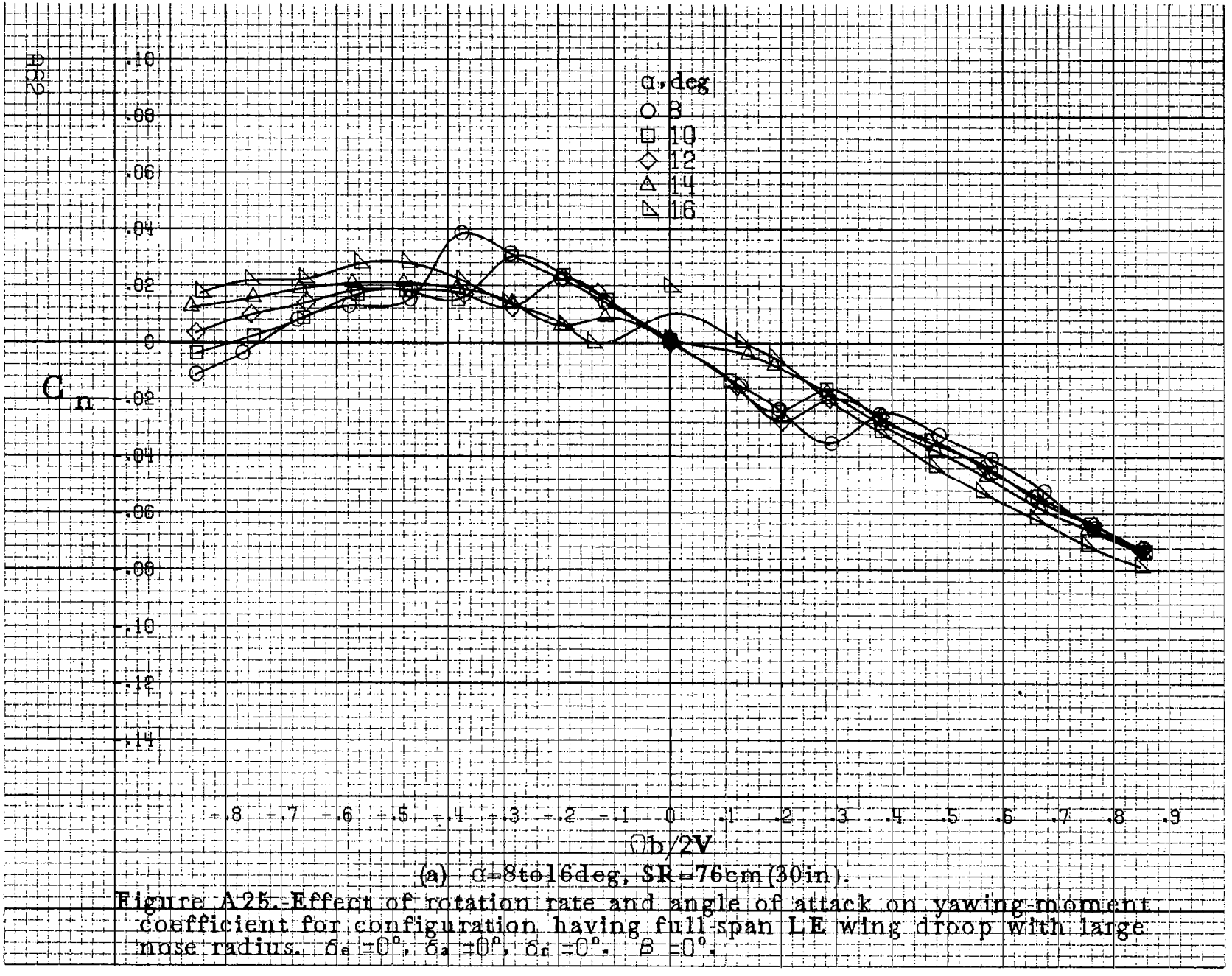

(a) α=8to16deg, $R=76cm(30in).

Figure A25.-Effect of rotation rate and angle of attack on yawing-moment coefficient for configuration having full-span LE wing droop with large nose radius. $\delta_e = 0^\circ$, $\delta_a = 0^\circ$, $\delta_r = 0^\circ$, $\beta = 0^\circ$.

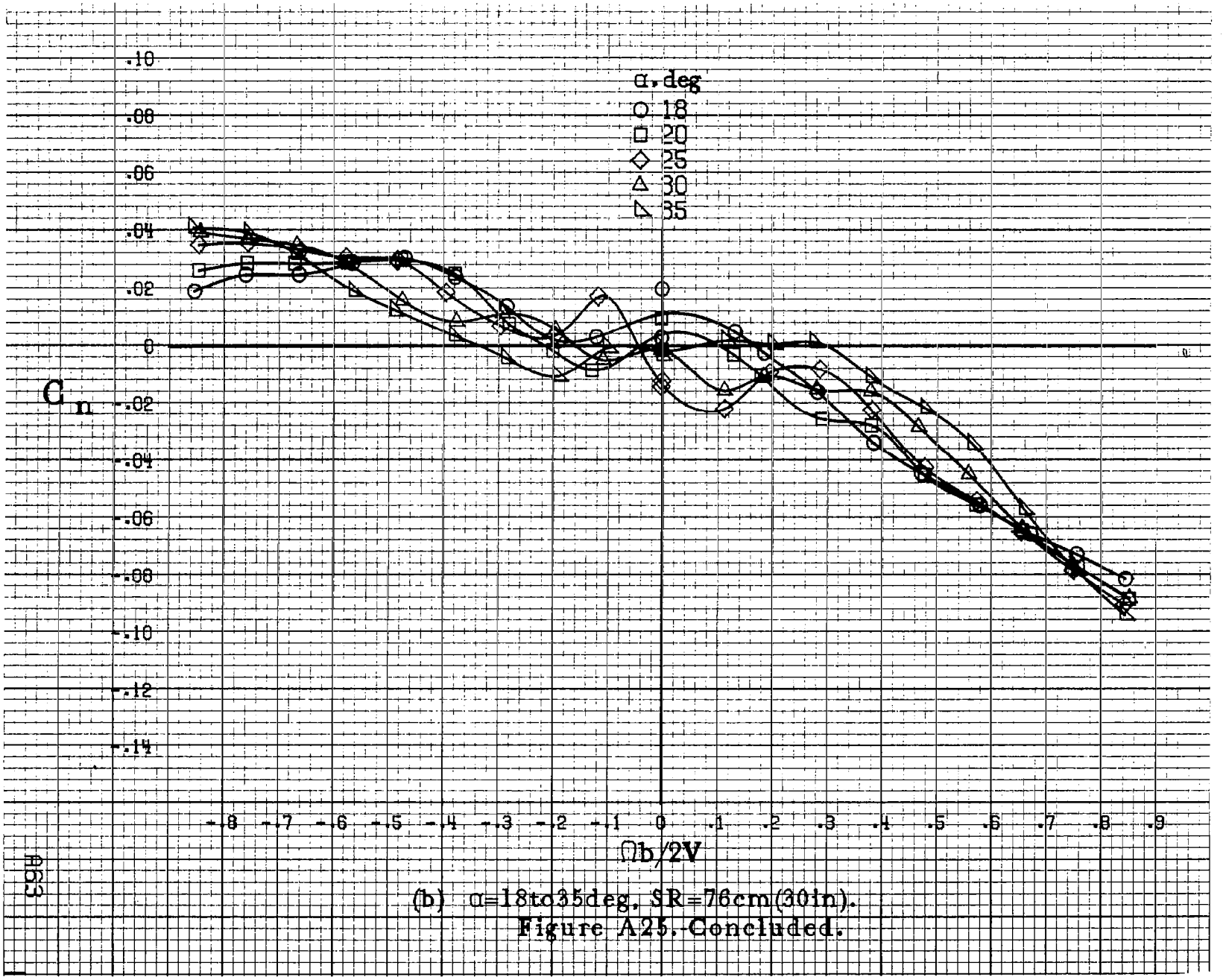

(b) α=18to35deg, SR=76cm(30in).

Figure A25.-Concluded.

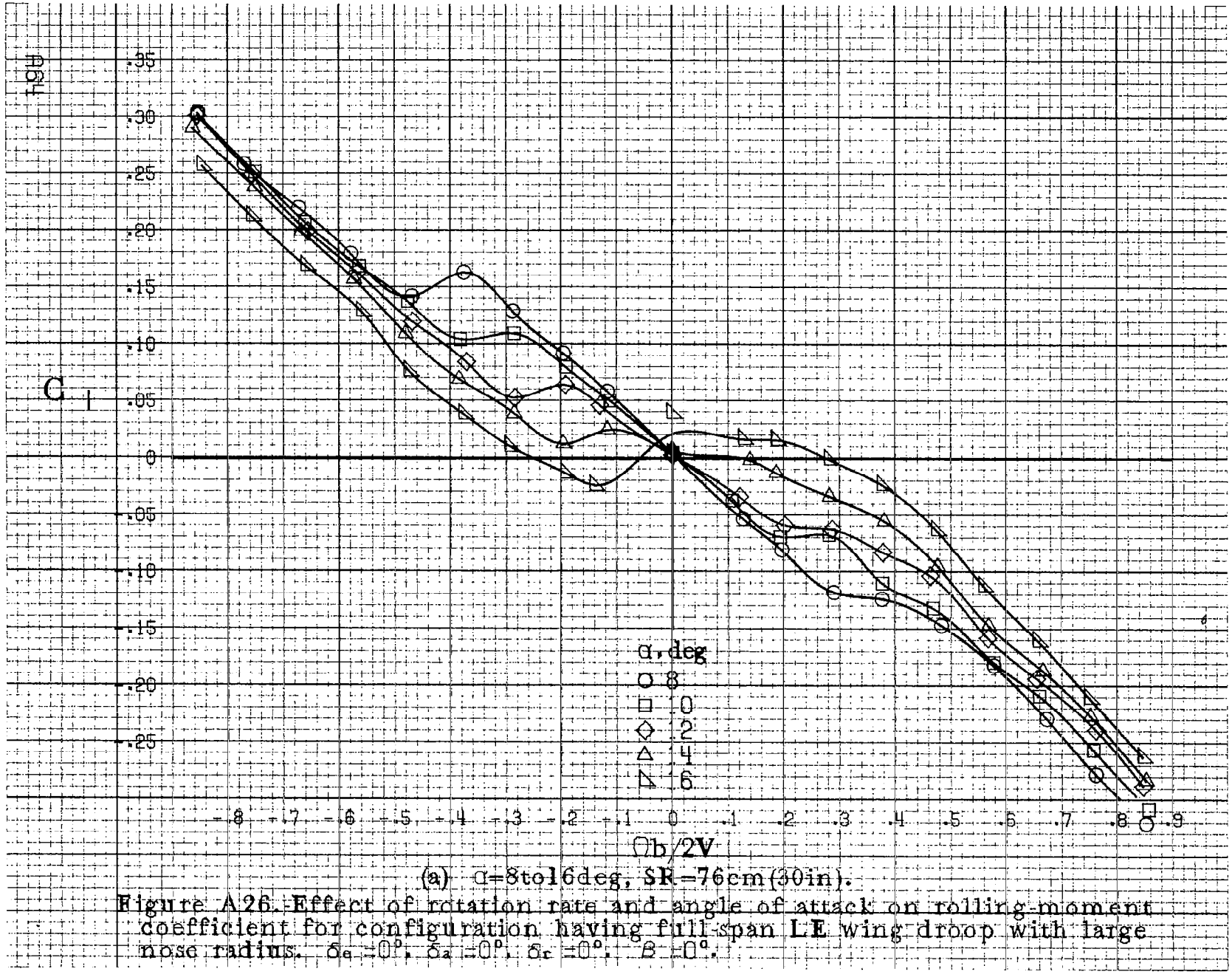

(a) α=8to16deg, S_R=76cm(30in).

Figure A26.-Effect of rotation rate and angle of attack on rolling-moment coefficient for configuration having full-span LE wing droop with large nose radius. $\delta_e = 0^o$, $\delta_a = 0^o$, $\delta_r = 0^o$, $\beta = 0^o$.

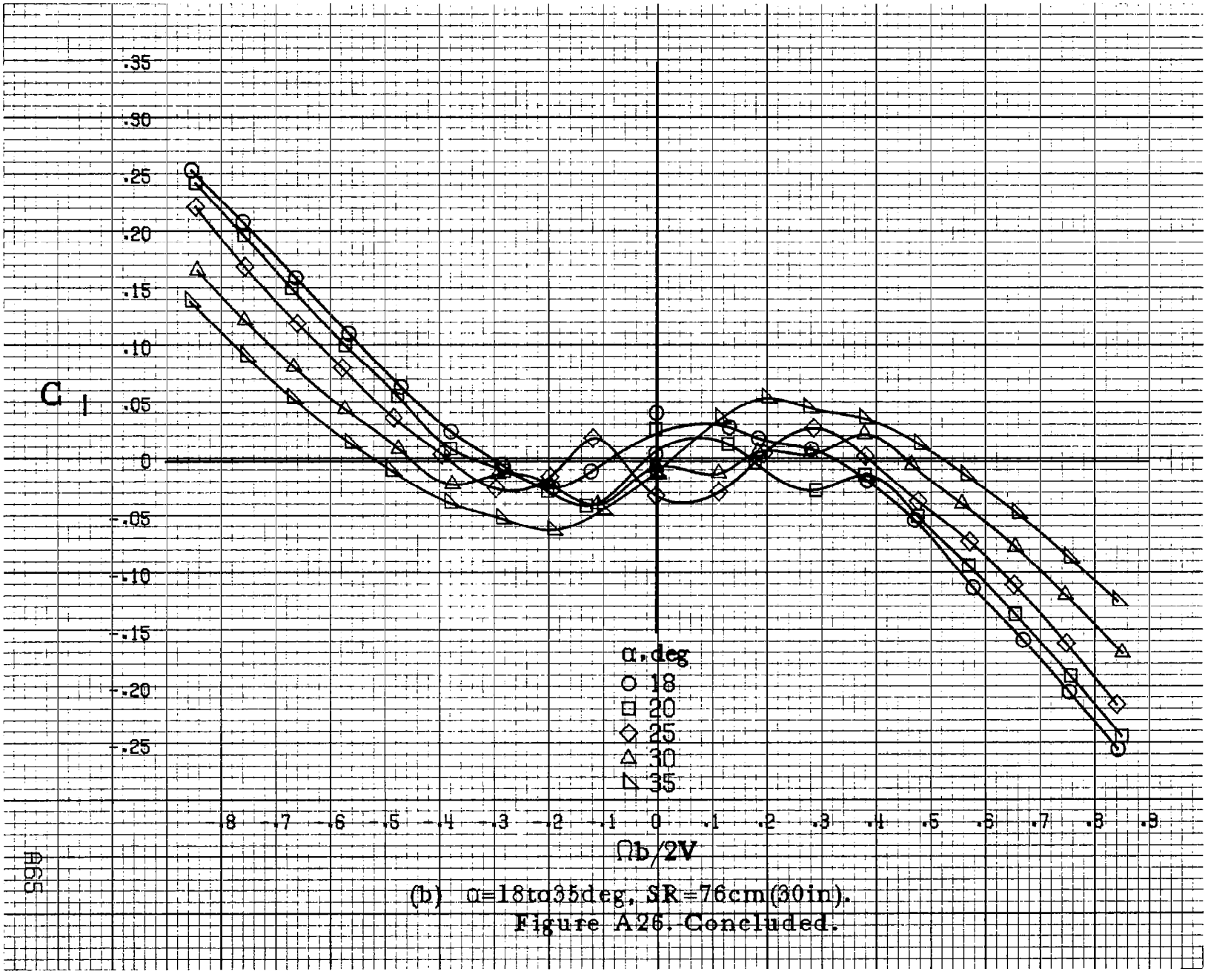

(b) α=18to35deg, SR=76cm(30in).

Figure A26. Concluded.

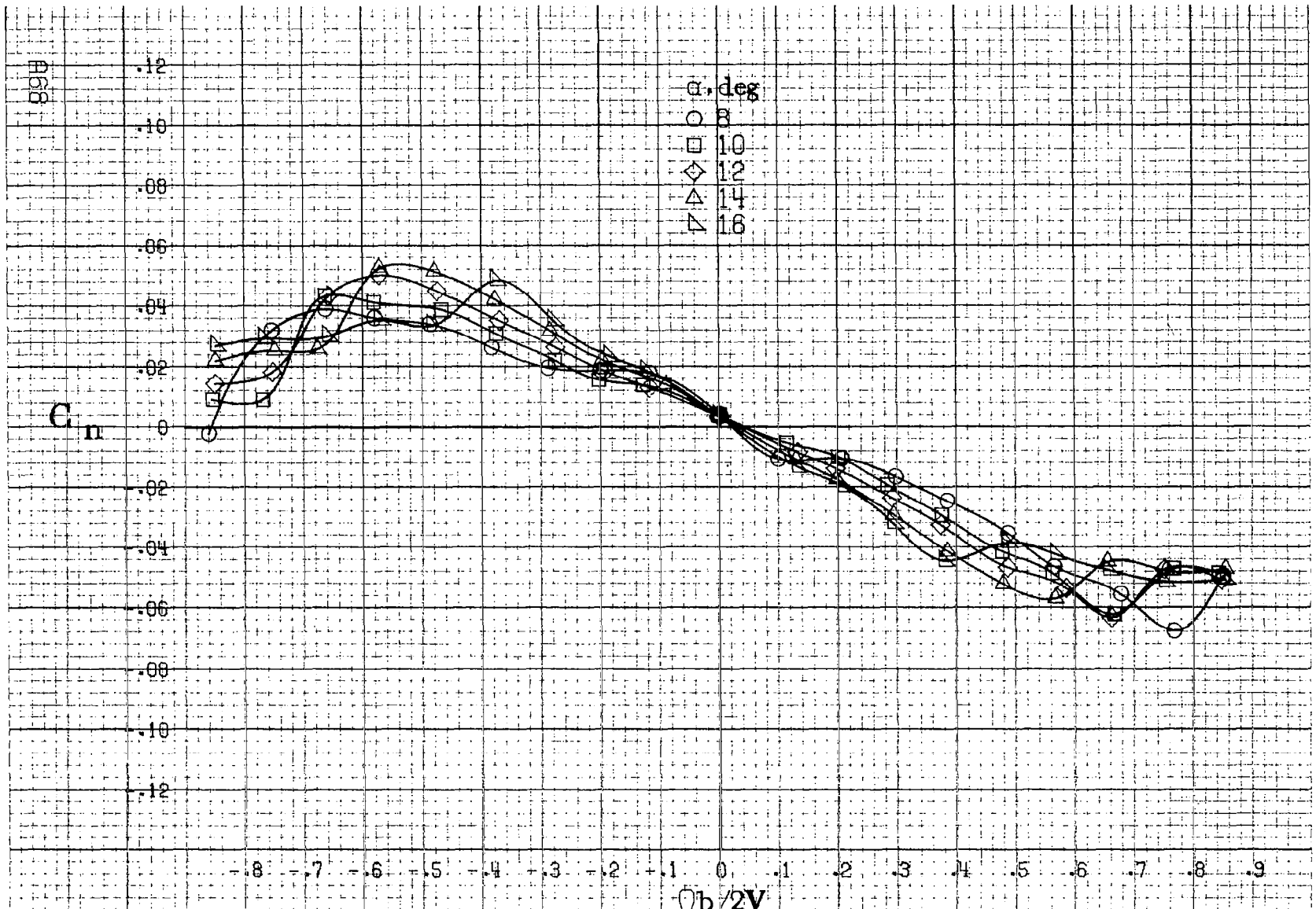

(a) α=8to16deg, SR=76cm(30in).

Figure A28. Effect of rotation rate and angle of attack on yawing-moment coefficient for configuration having outboard LE wing droop with large nose radius. $\delta_e = 0°$, $\delta_a = 0°$, $\delta_r = 0°$, $\beta = 0°$.

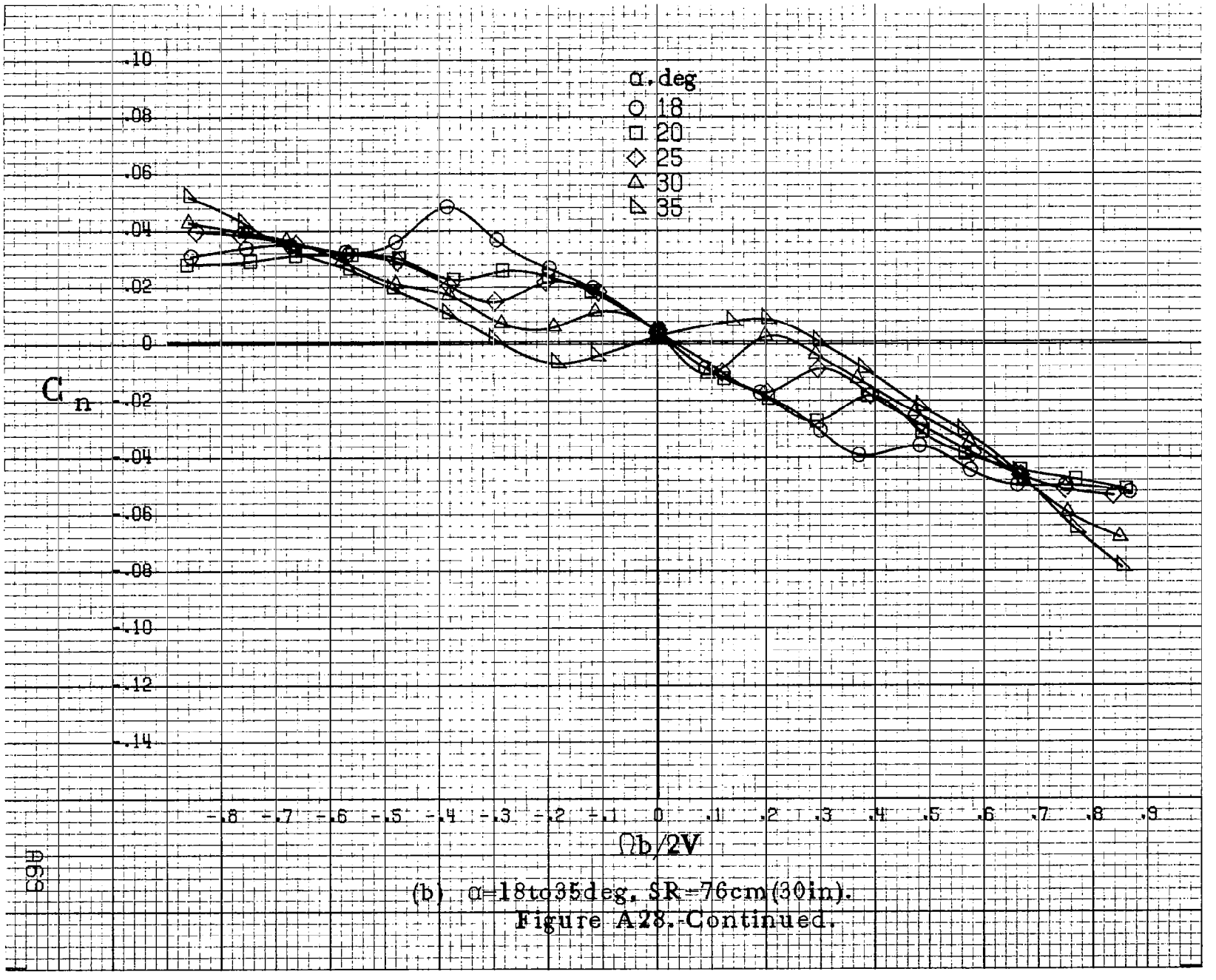

(b) α=18to35deg, SR=76cm(30in).

Figure A28.-Continued.

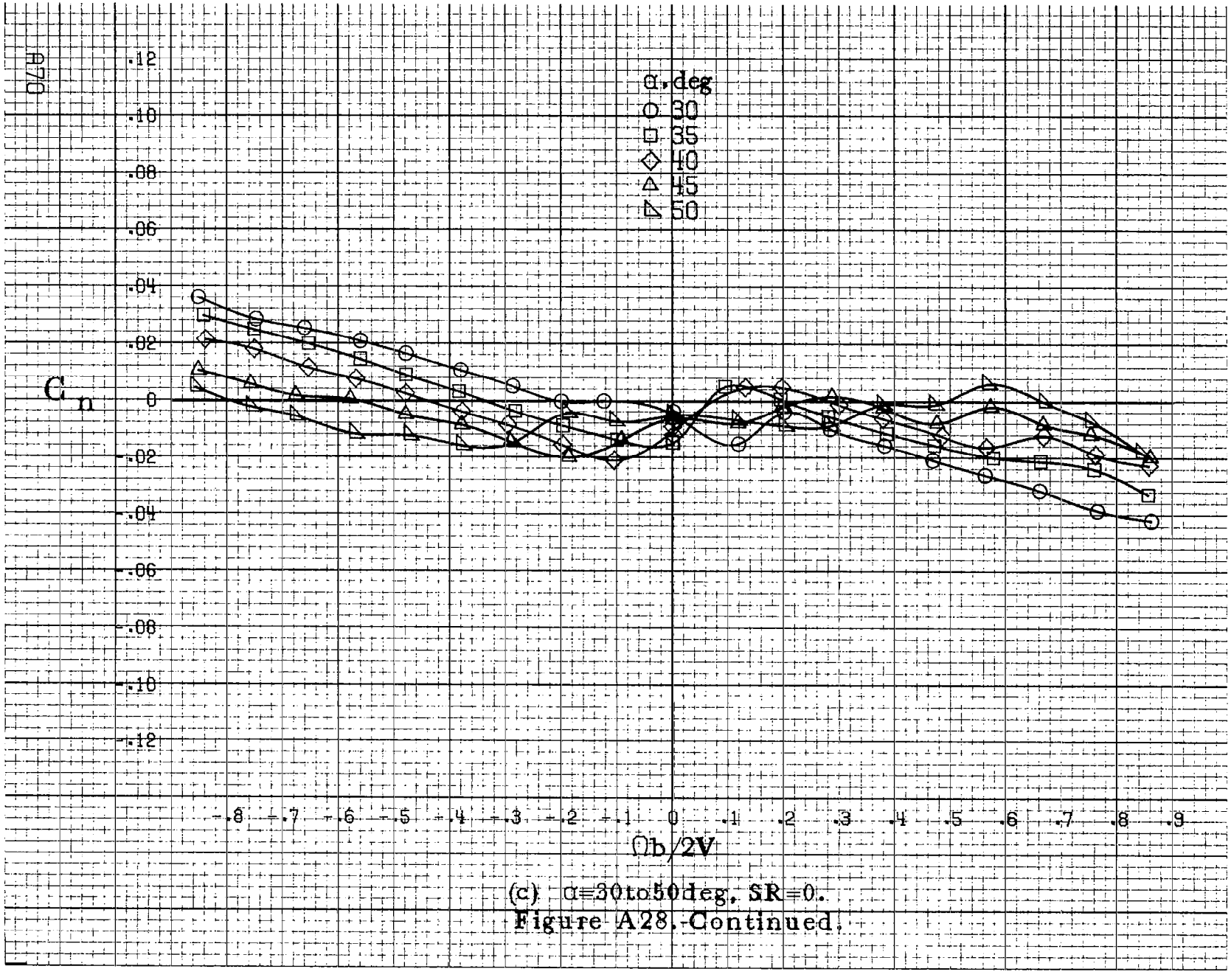

(c) α=30 to 50 deg, SR=0.

Figure A28.-Continued.

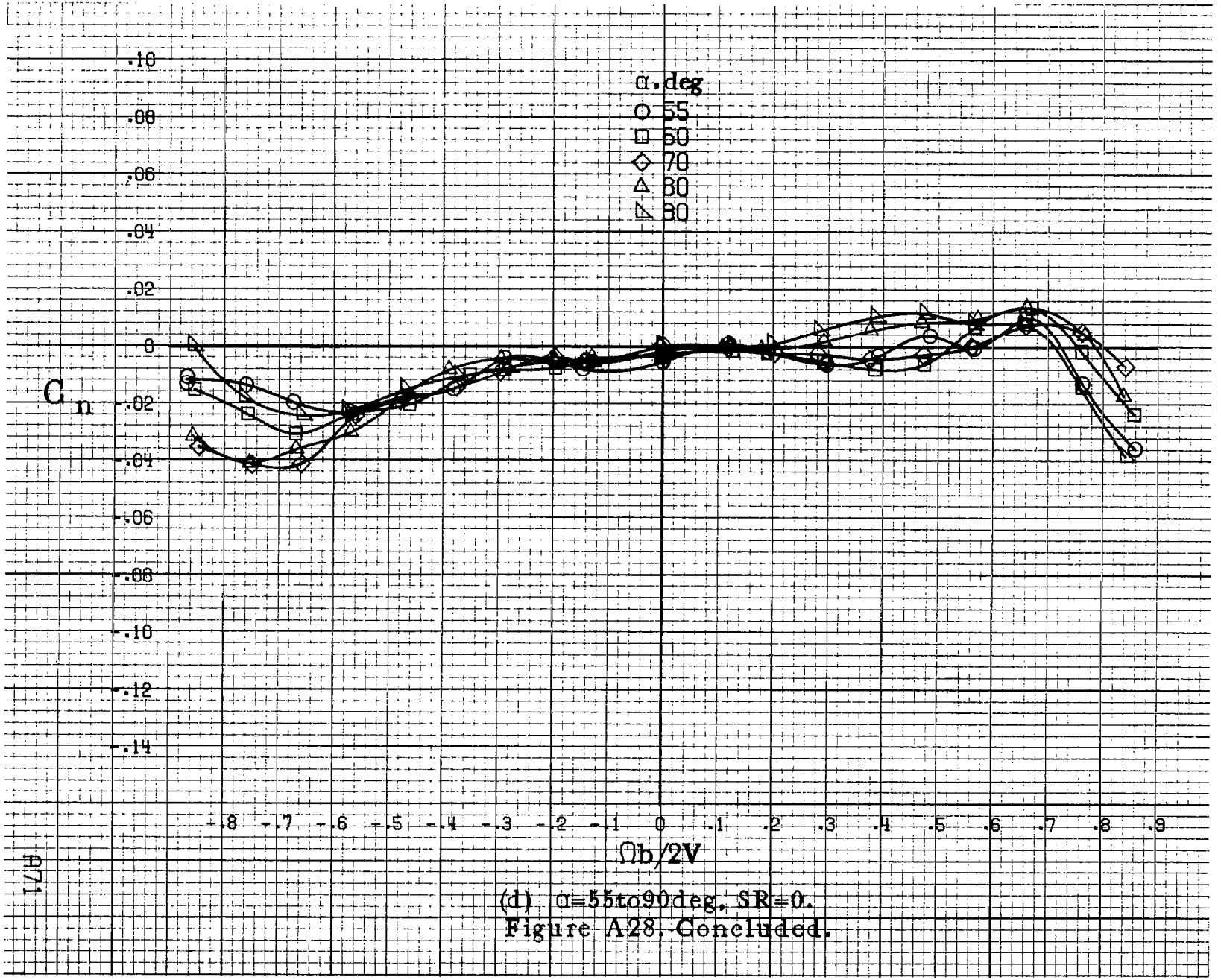

(d) α=55to90deg, SR=0.

Figure A28. Concluded.

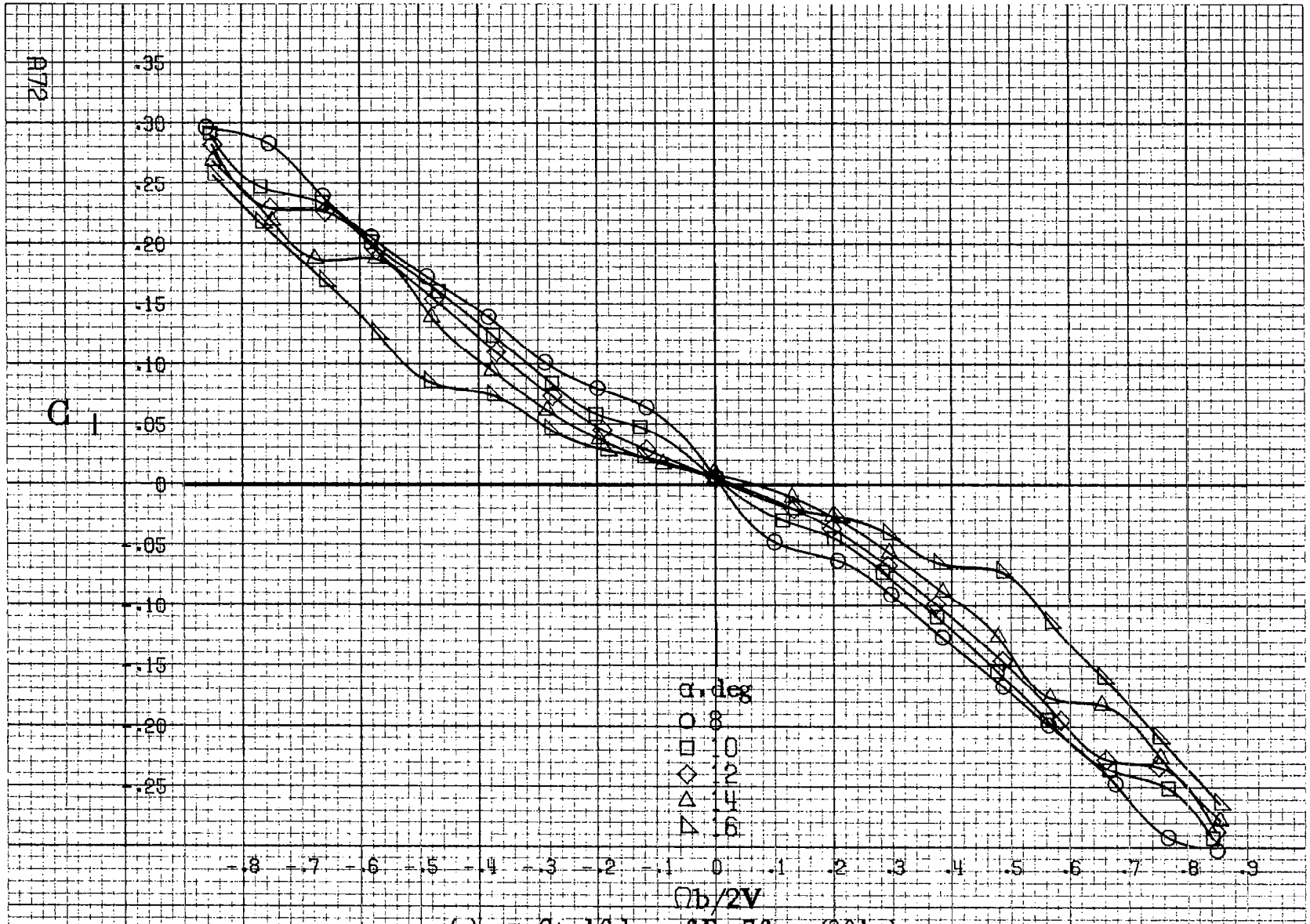

(a) α=8to16deg, SR=76cm(30in).

Figure A29.-Effect of rotation rate and angle of attack on rolling-moment coefficient for configuration having outboard LE wing drop with large nose radius. $\delta_e = 0°$, $\delta_a = 0°$, $\delta_r = 0°$, $\beta = 0°$.

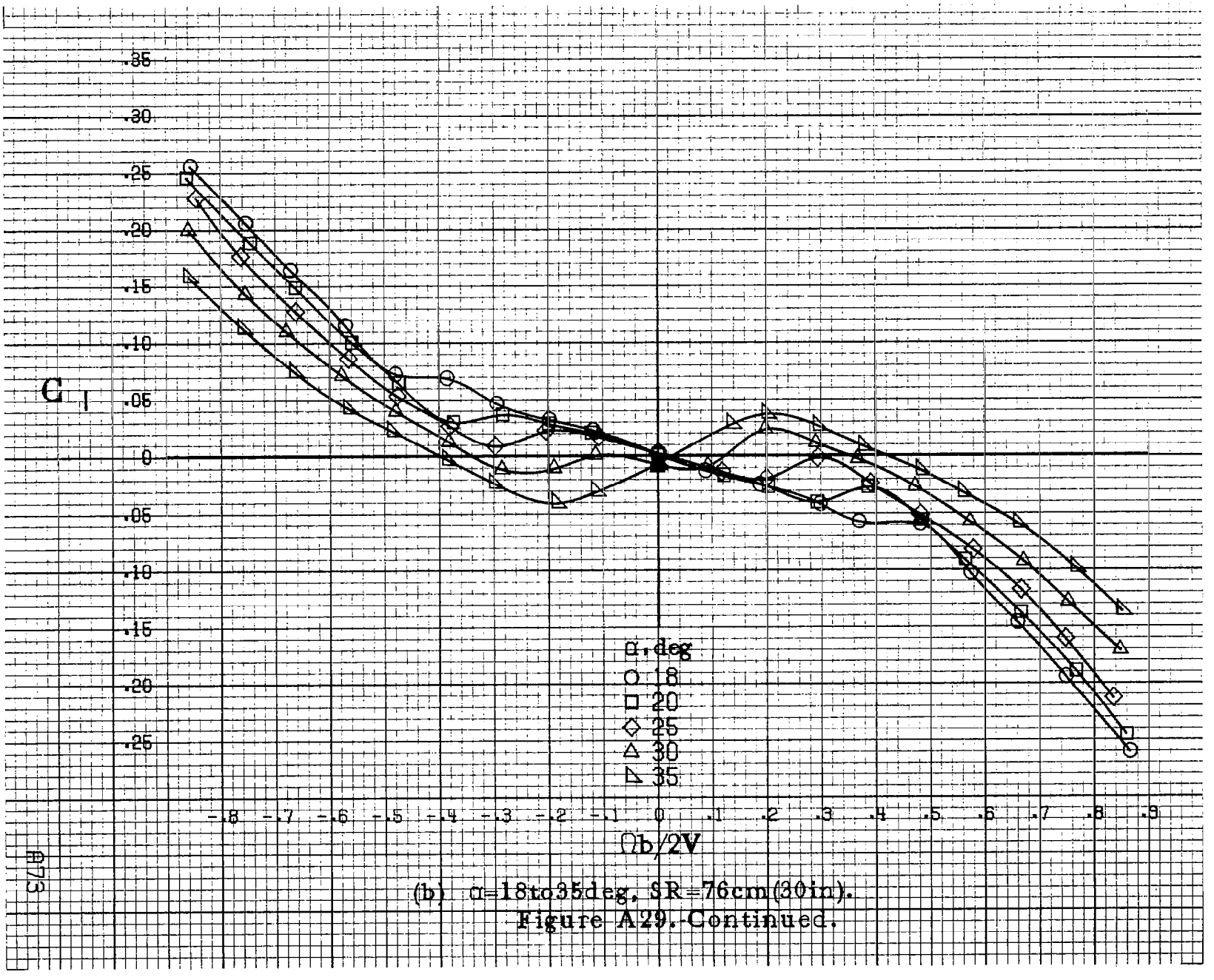

(b) α=18to35deg, SR=76cm(30in).

Figure A29.-Continued.

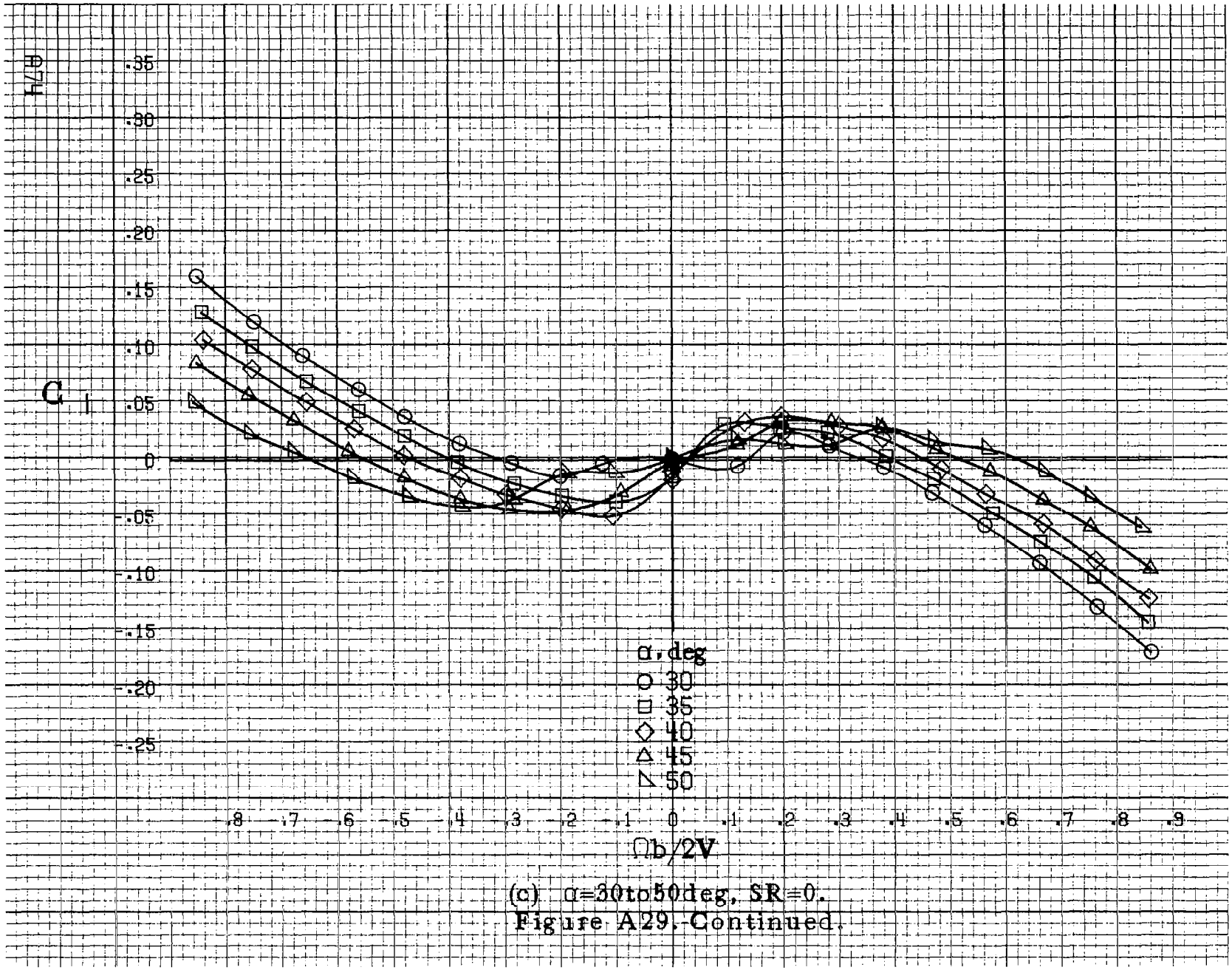

(c) α=30to50deg, SR=0.

Figure A29.-Continued.

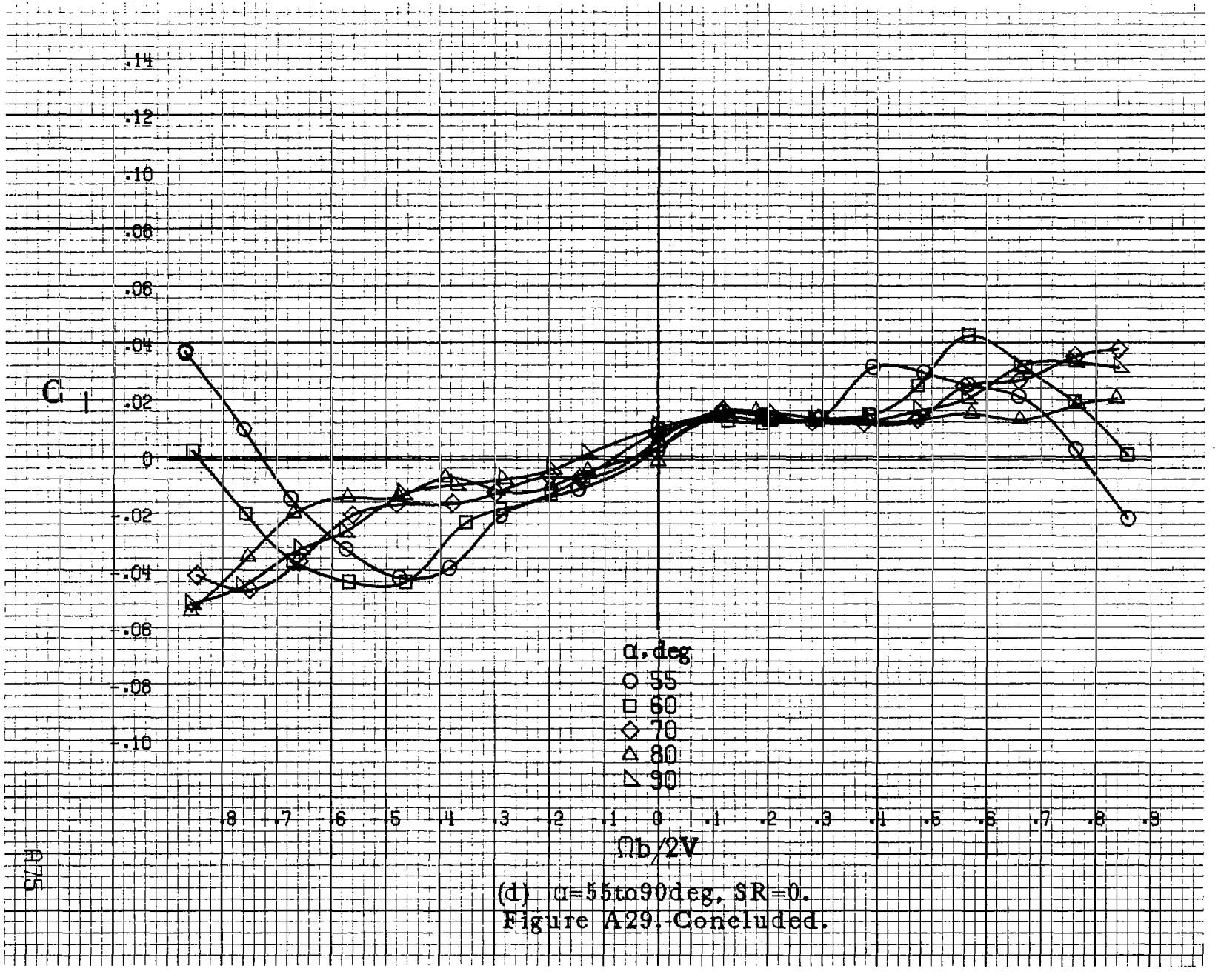

(d) α=55to90deg, SR=0.

Figure A29. Concluded.

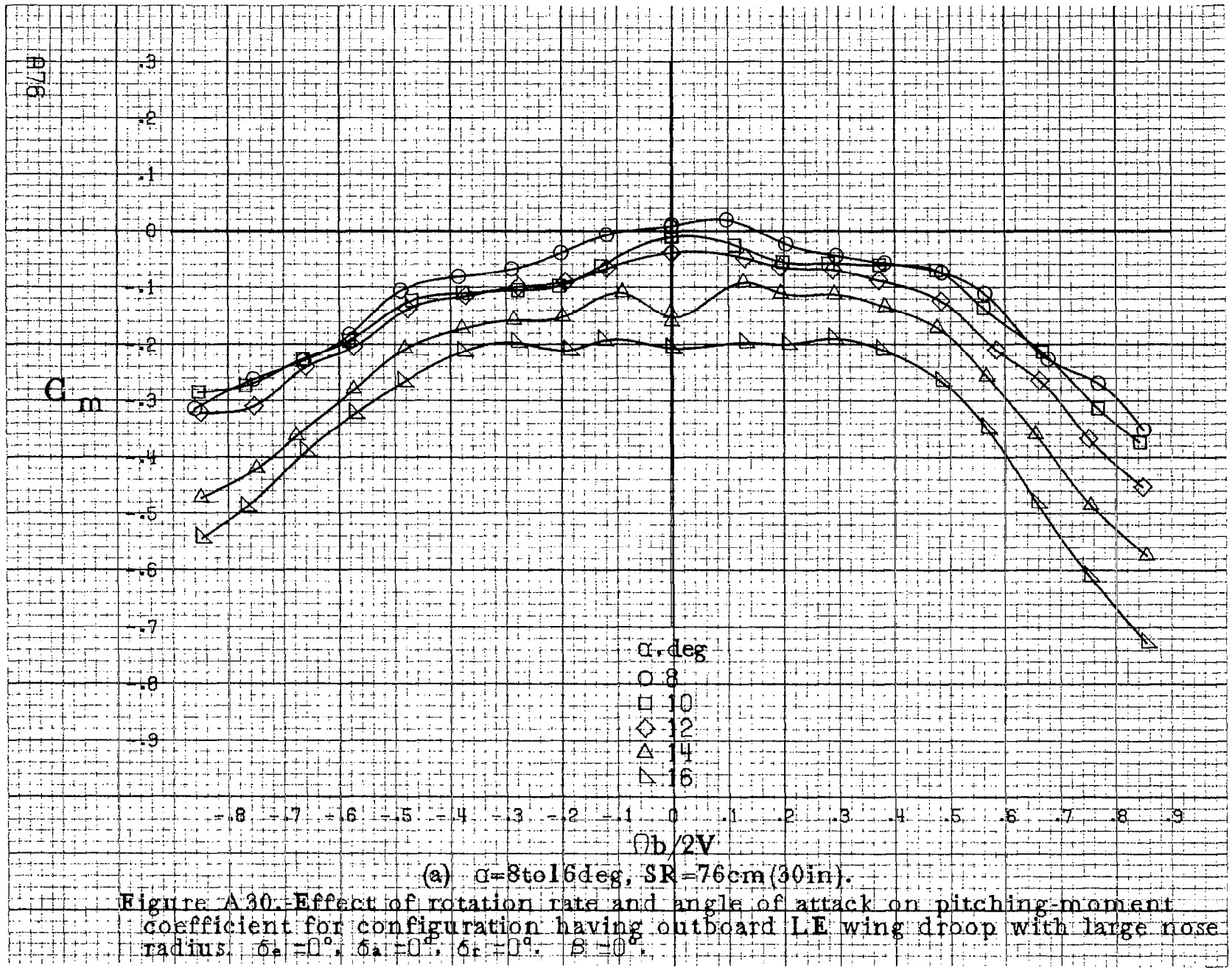

(a) α=8to16deg, SR=76cm(30in).

Figure A30.-Effect of rotation rate and angle of attack on pitching-moment coefficient for configuration having outboard LE wing droop with large nose radius. δ_e=0°, δ_a=0°, δ_r=0°, β=0°.

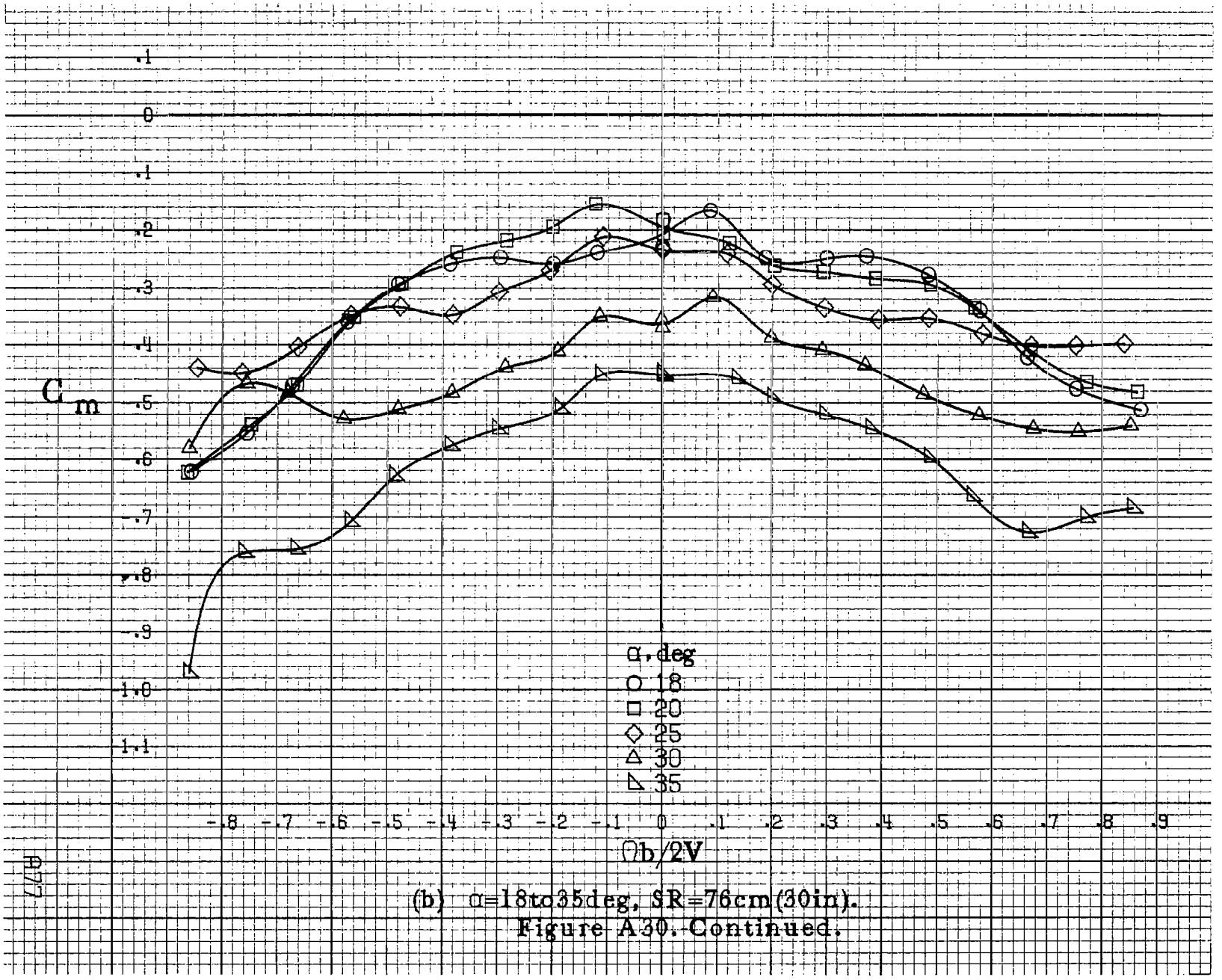

(b) α=18to35deg, SR=76cm(30in).

Figure A30. Continued.

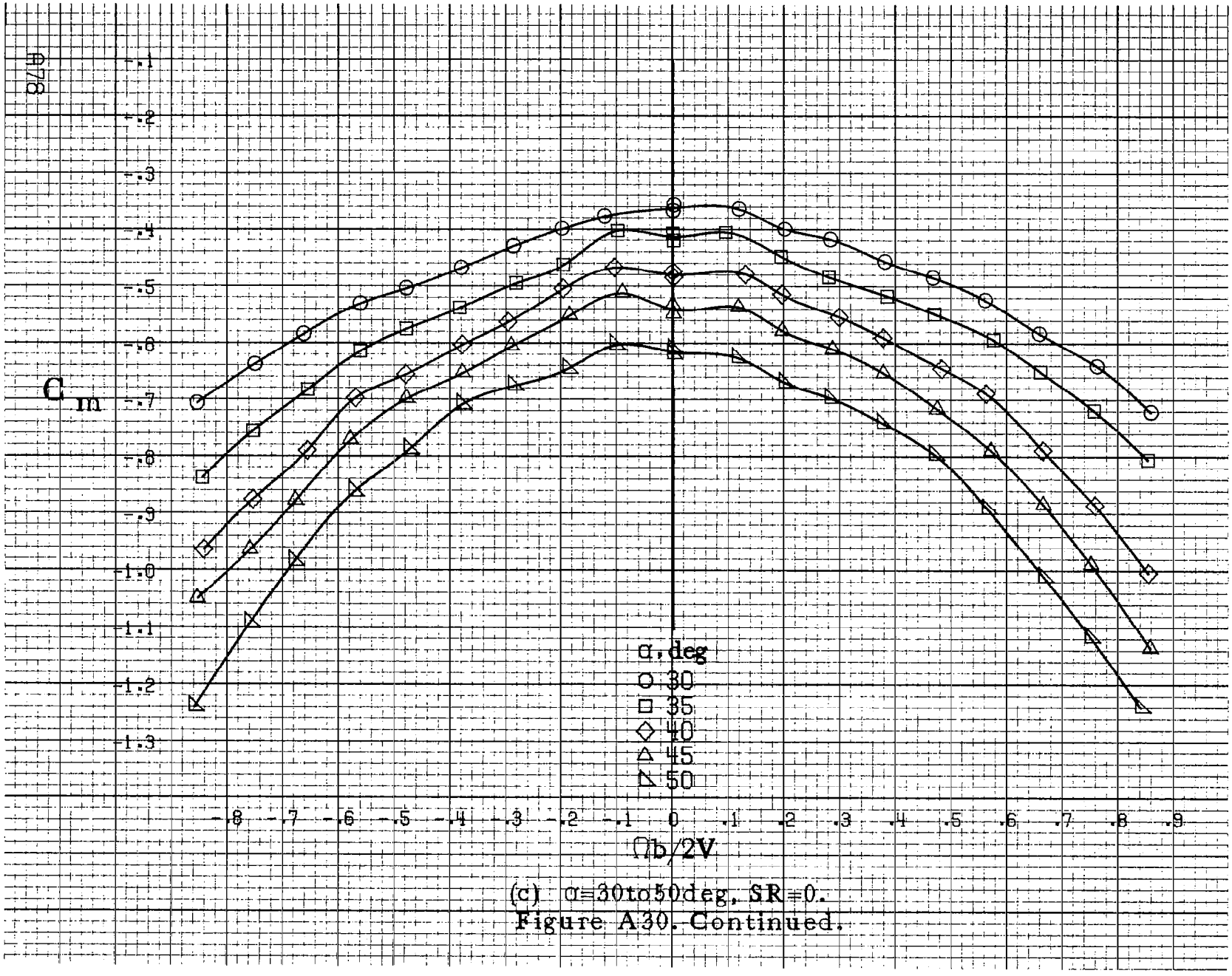

(c) α=30to50deg, SR=0.

Figure A30. Continued.

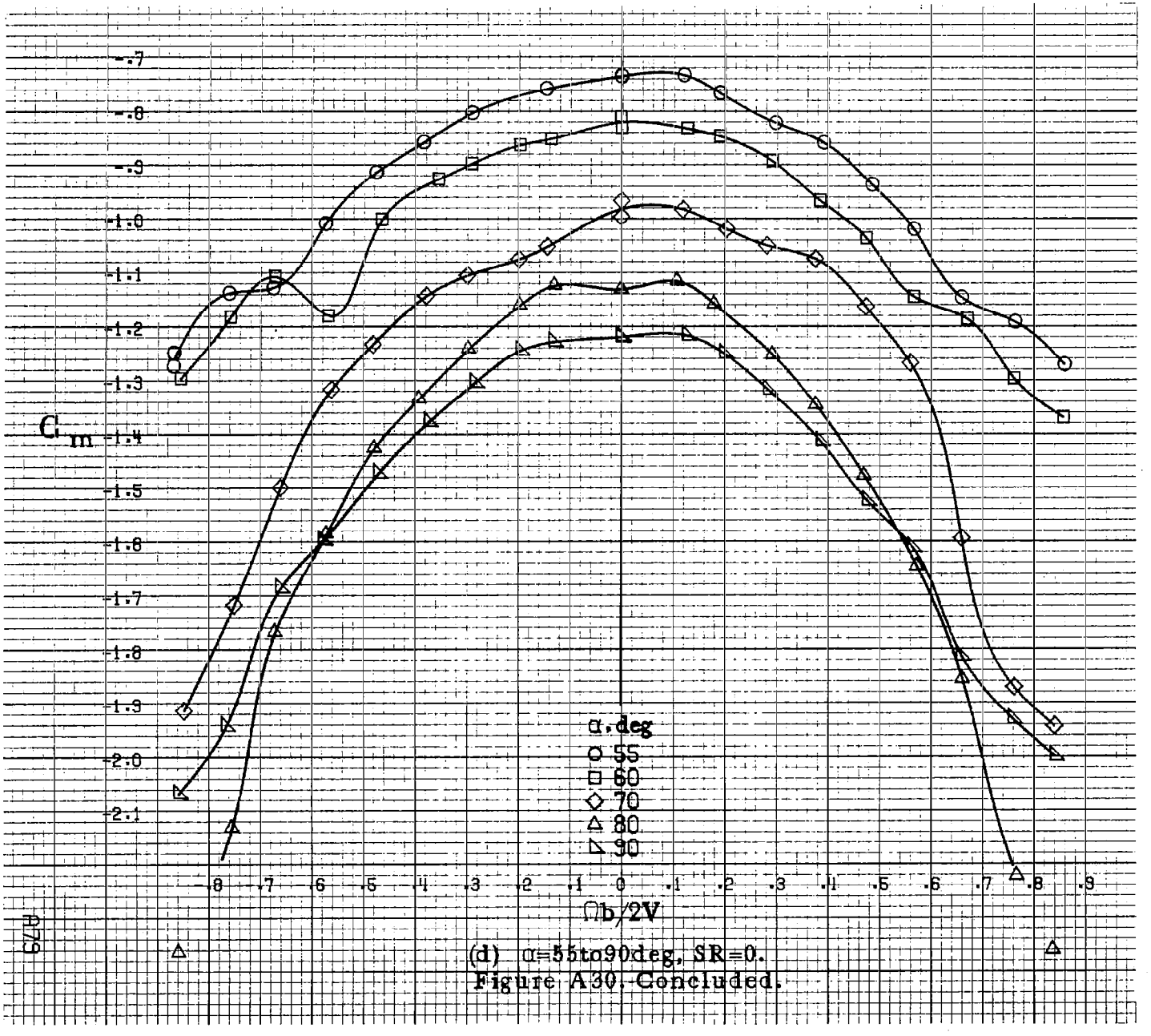

(d) α=55to90deg, SR=0.

Figure A30.-Concluded.

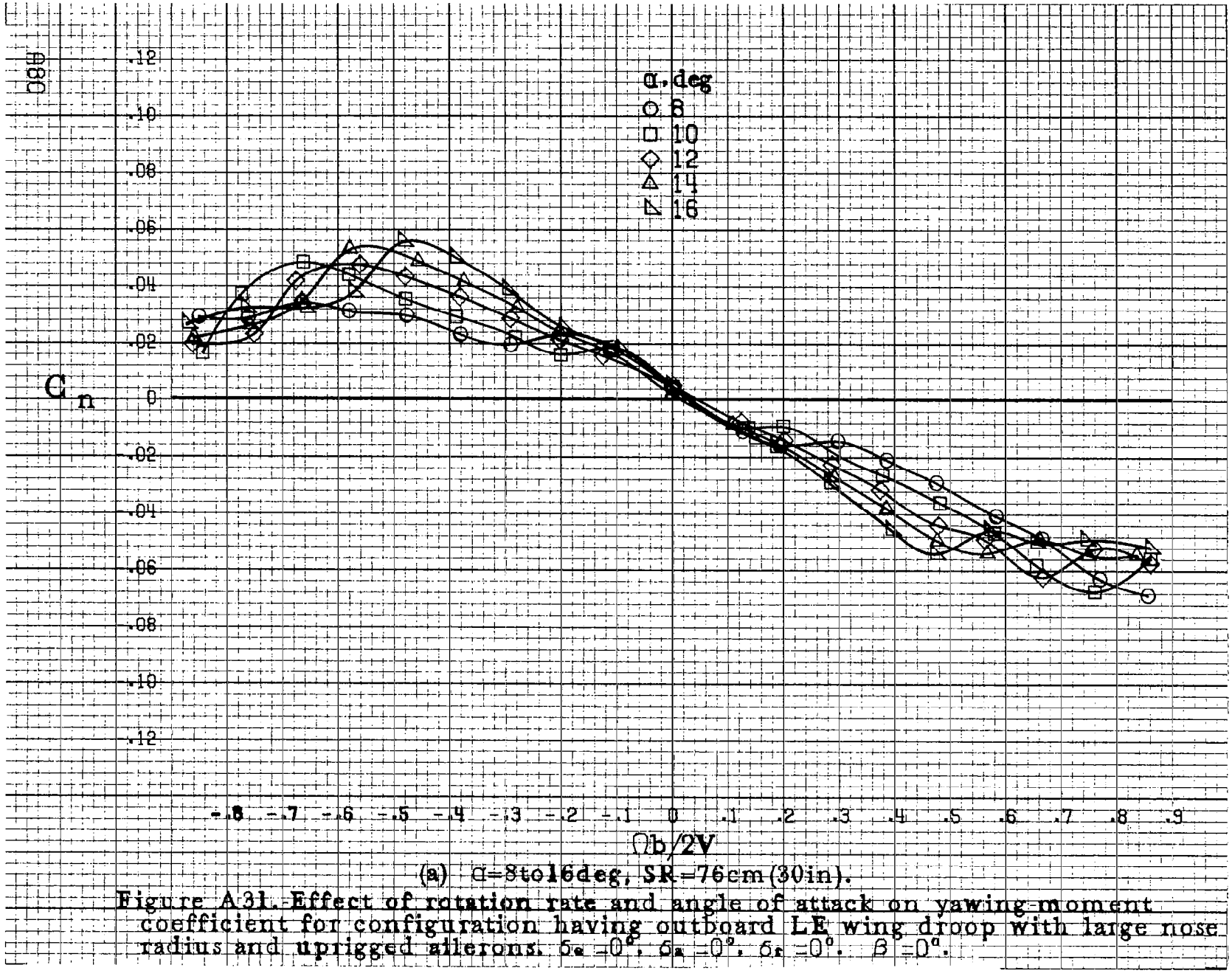

(a) α=8to16deg, SR=76cm(30in).

Figure A31. Effect of rotation rate and angle of attack on yawing-moment coefficient for configuration having outboard LE wing droop with large nose radius and uprigged ailerons. $\delta_a = 0°$, $\delta_s = 0°$, $\delta_r = 0°$, $\beta = 0°$.

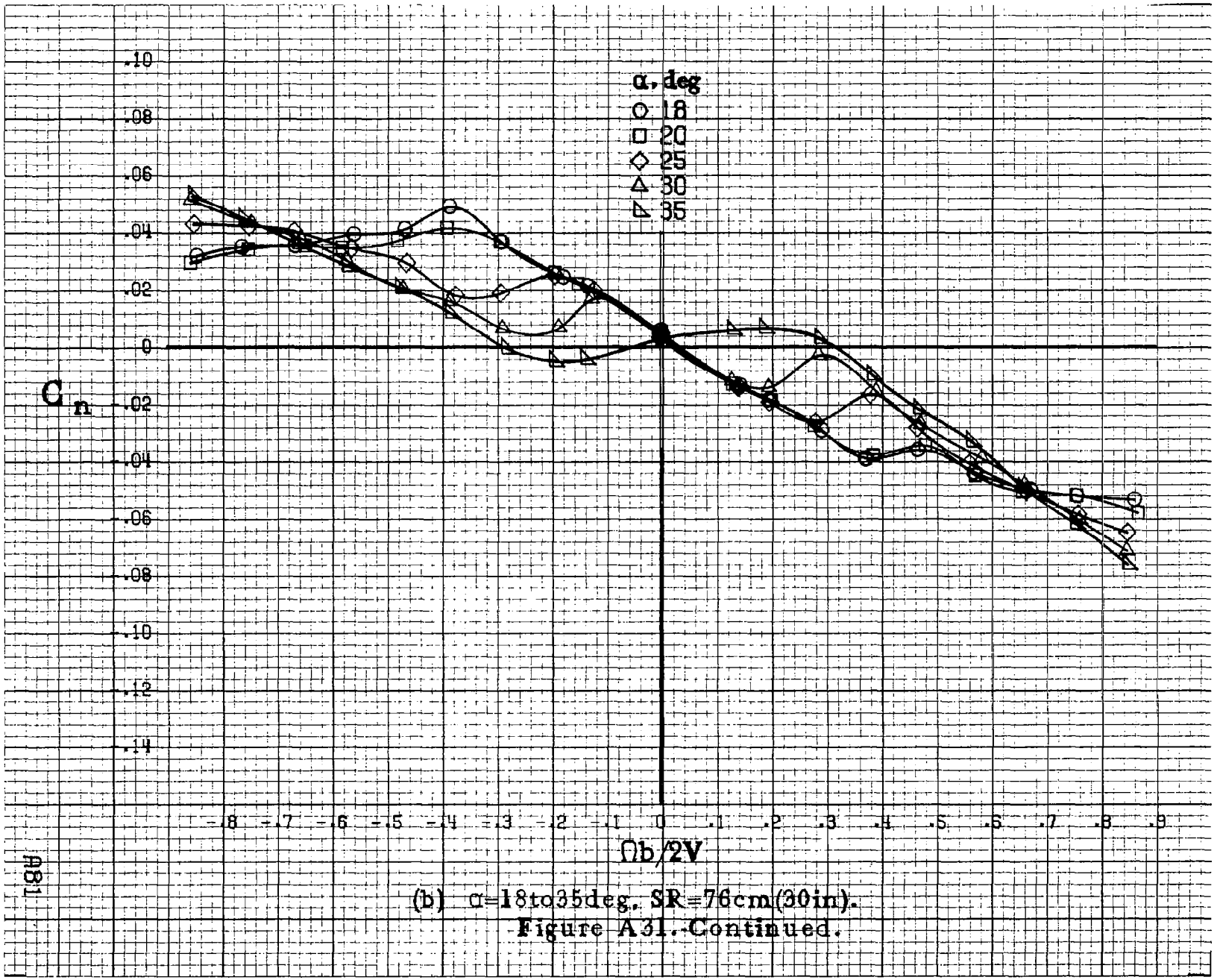

(b) α=18to35deg, SR=76cm(30in).

Figure A31.-Continued.

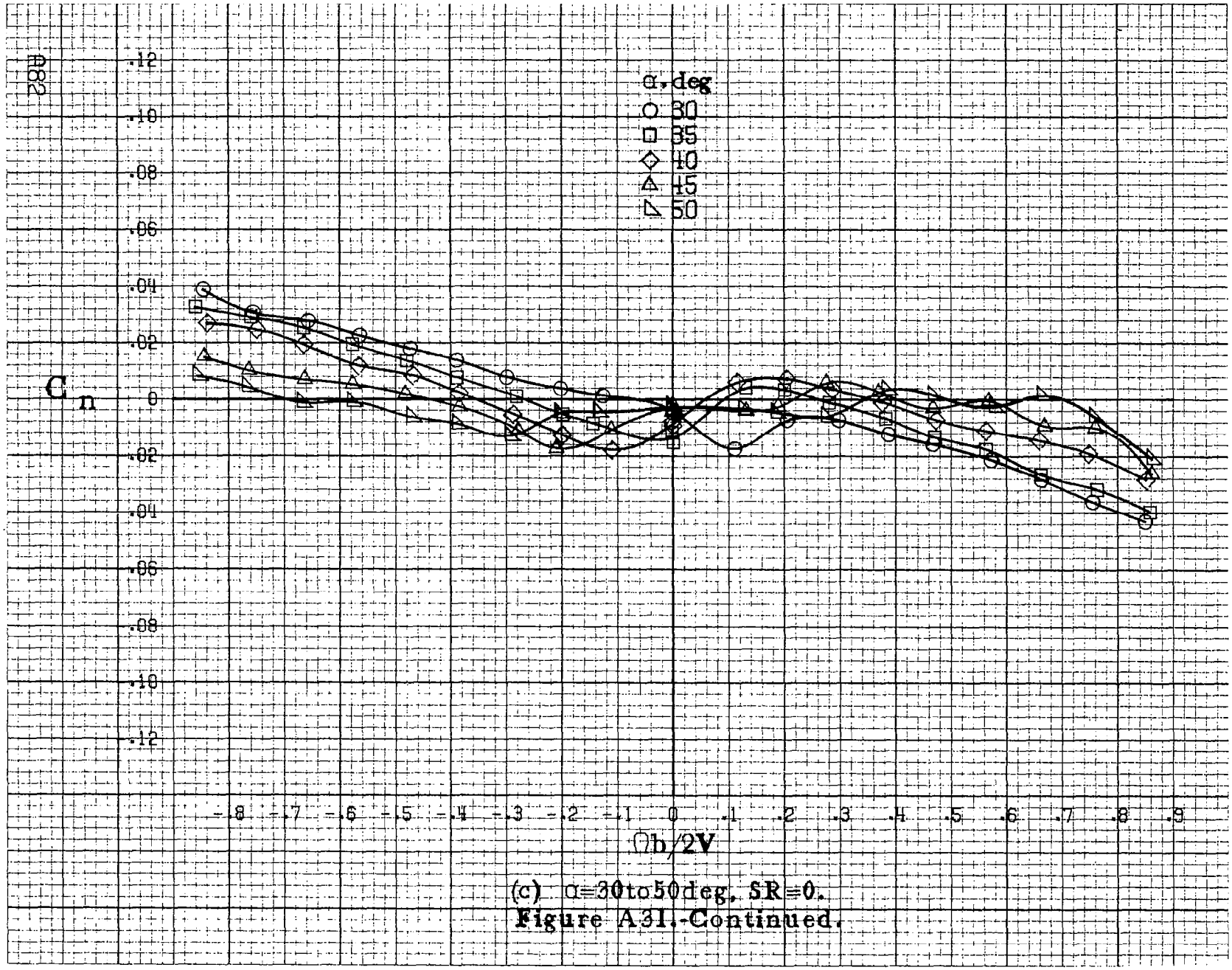

(c) $\alpha = 30$ to 50 deg, SR = 0.

Figure A31.-Continued.

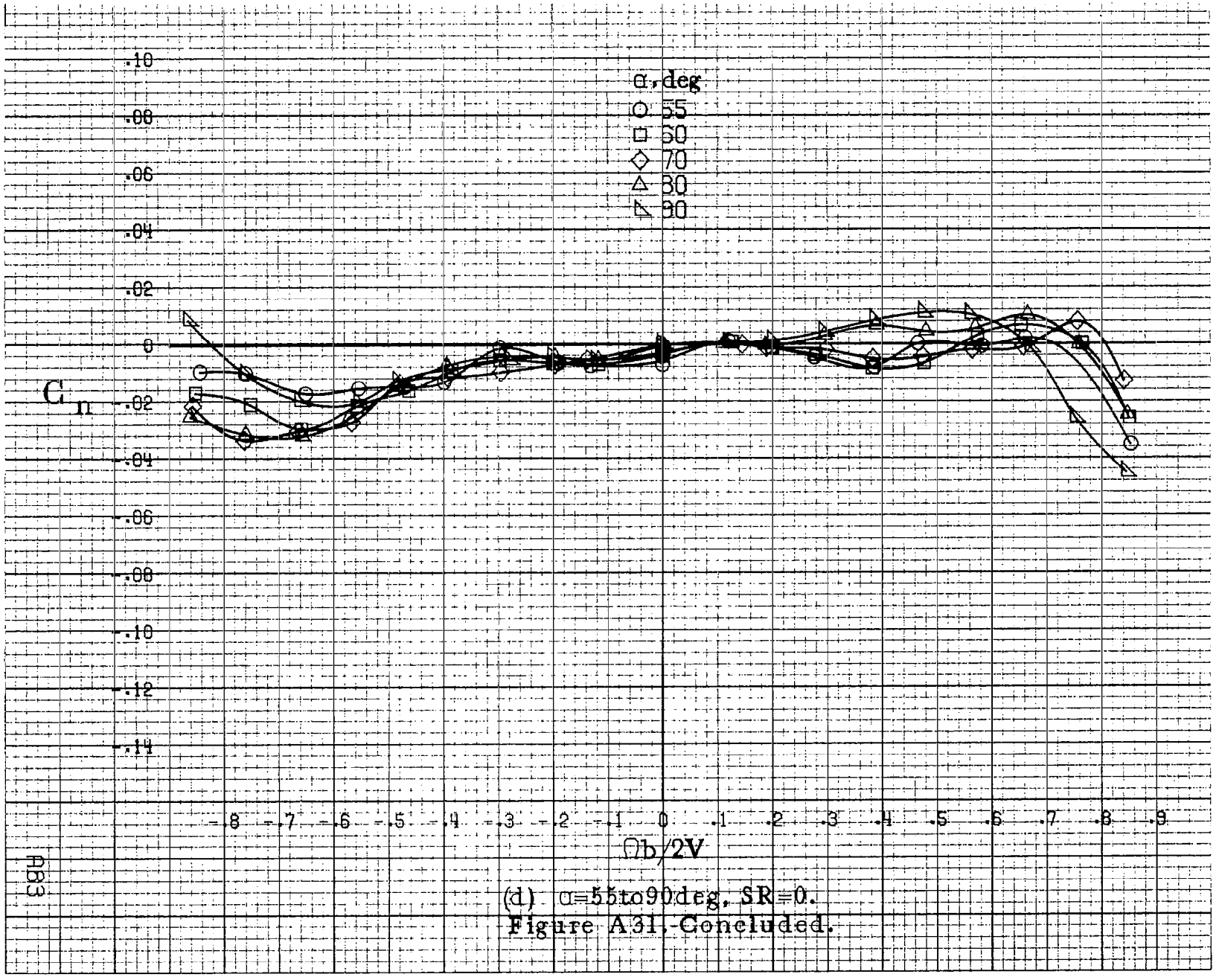

(d) α=55to90deg, SR=0.

Figure A31.-Concluded.

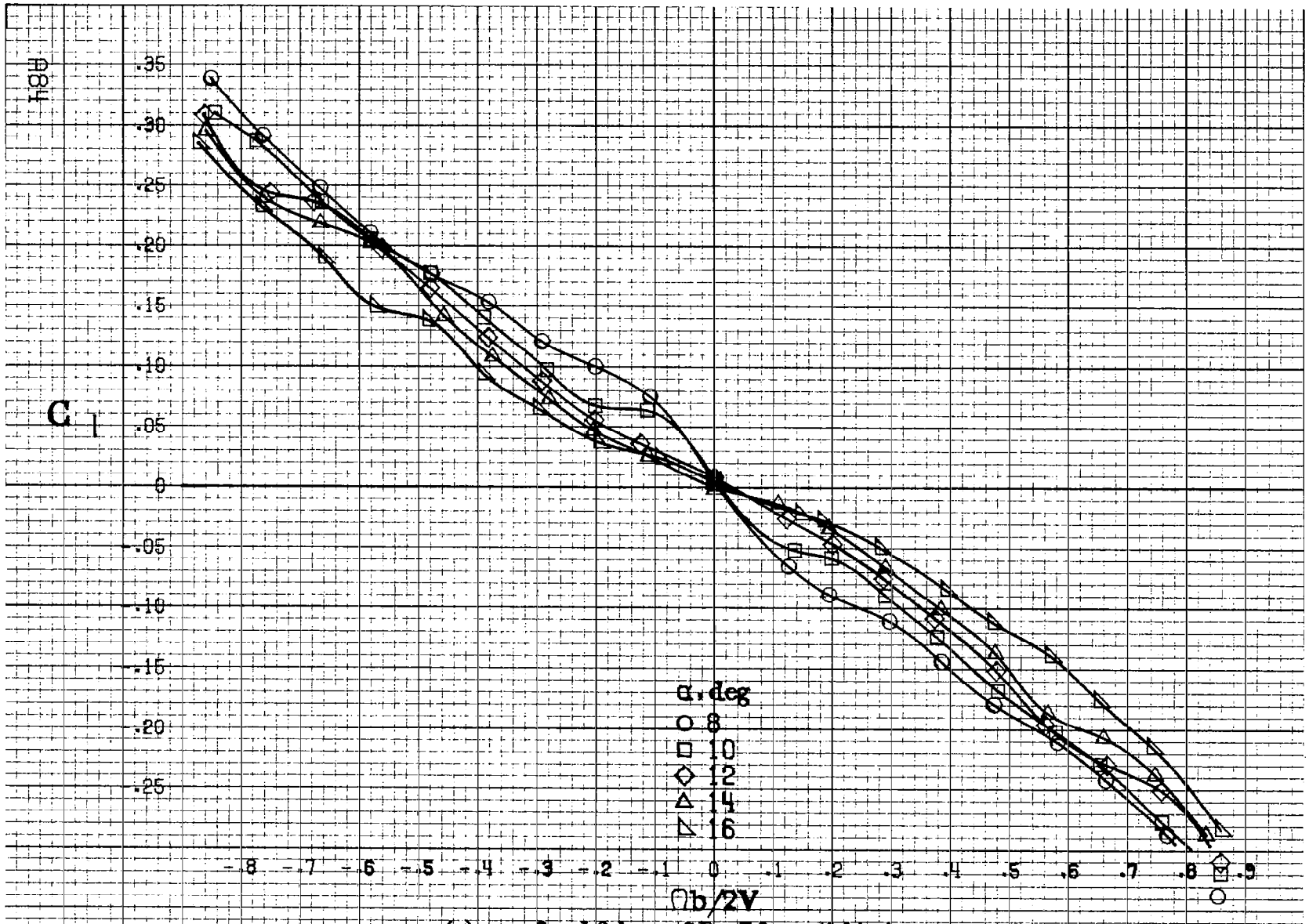

(a) α=8to16deg, SR=76cm(30in).

Figure A32. Effect of rotation rate and angle of attack on rolling-moment coefficient for configuration having outboard LE wing droop with large nose radius and uprigged ailerons. $\delta_e = 0°$, $\delta_a = 0°$, $\delta_r = 0°$, $\beta = 0°$.

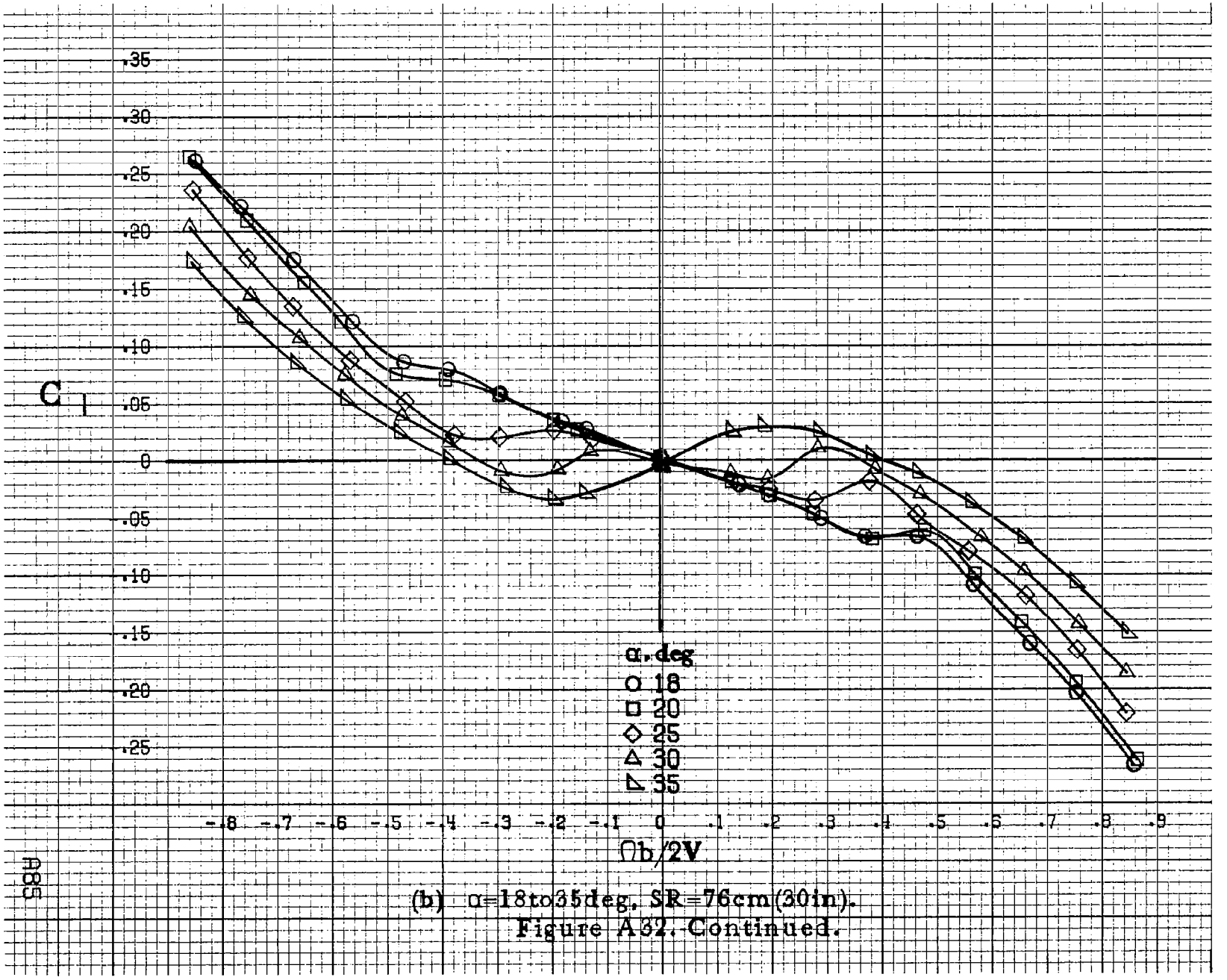

(b) α=18to35deg, SR=76cm(30in).

Figure A32. Continued.

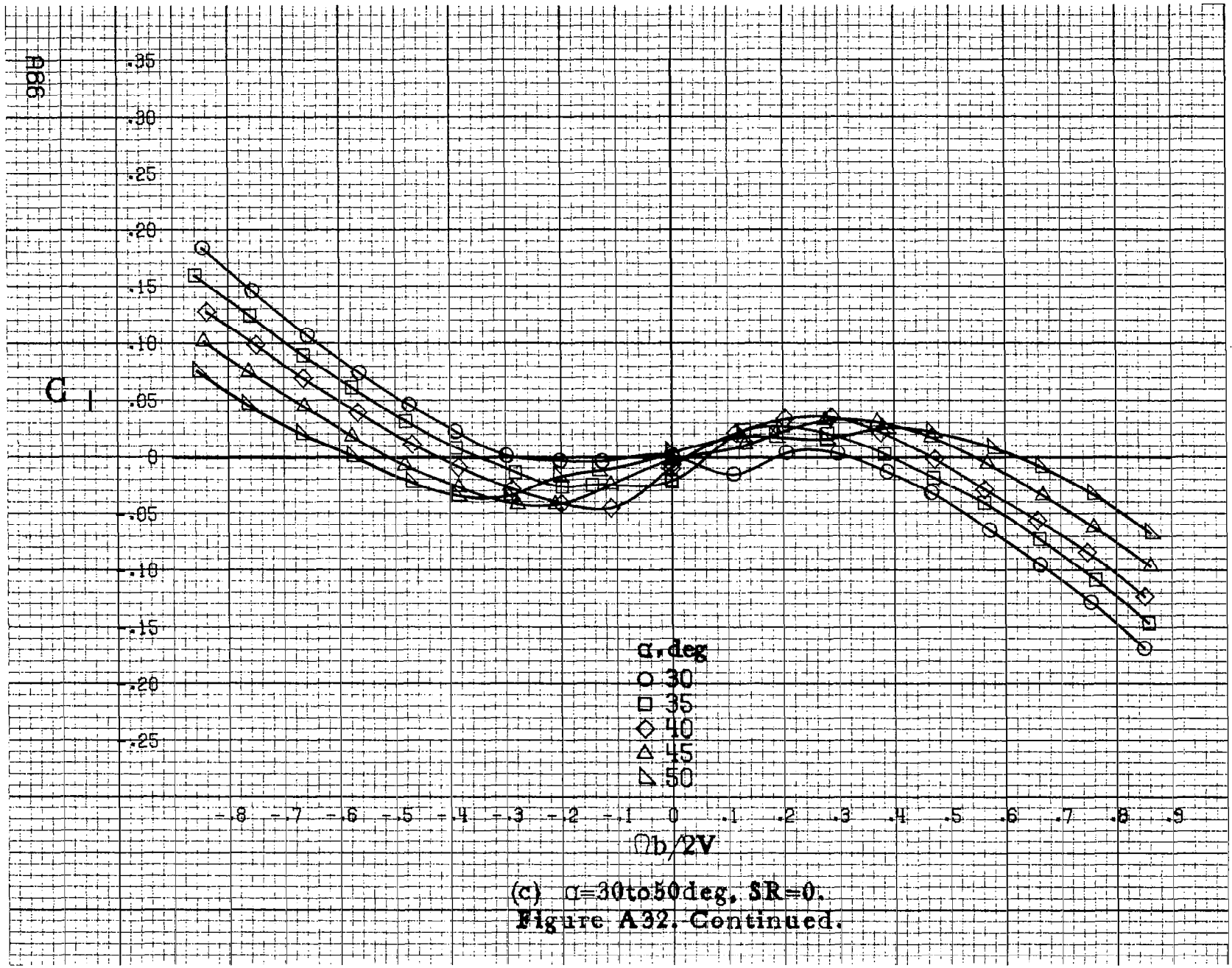

(c) α=30to50deg, SR=0.

Figure A32. Continued.

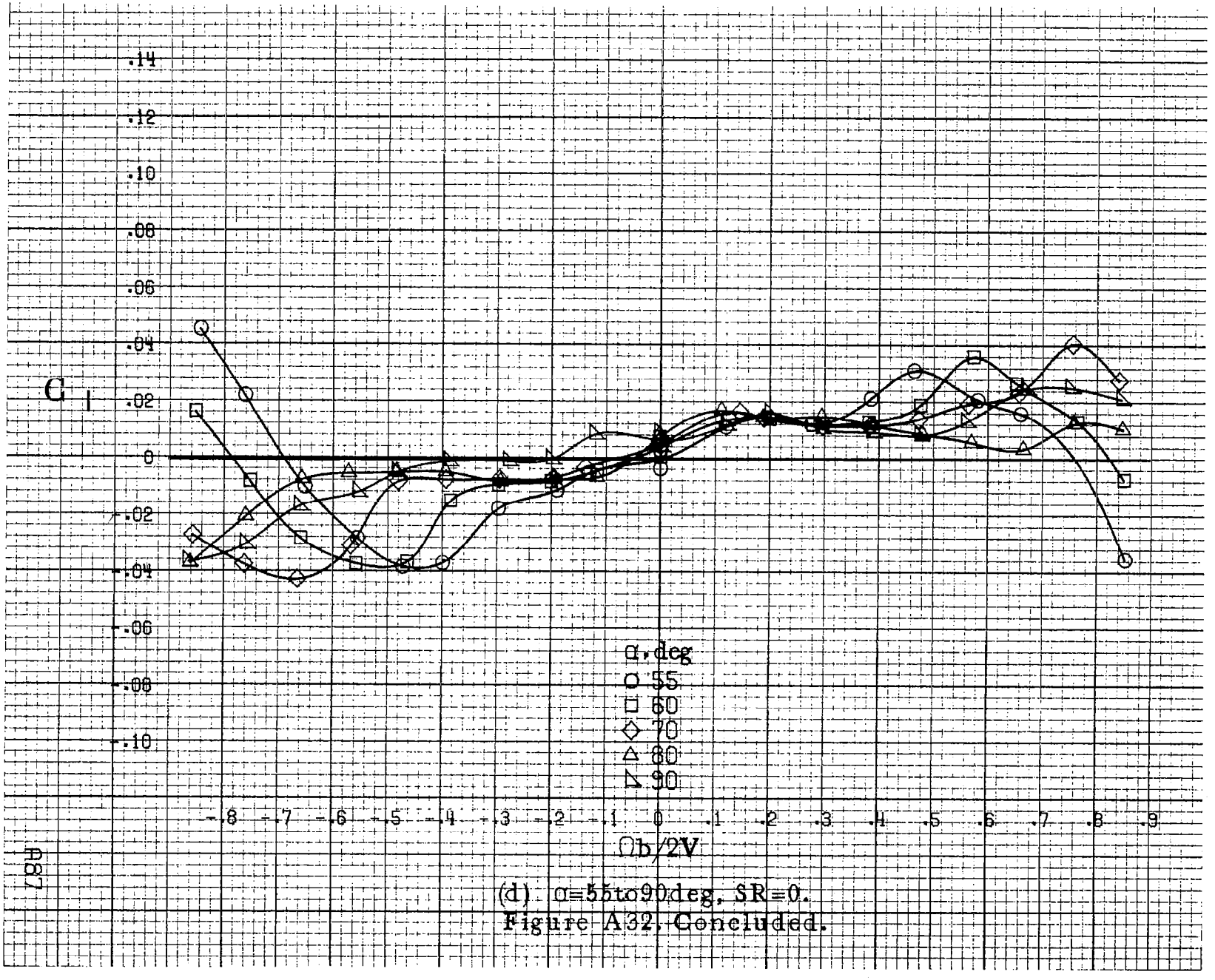

(d) α=55to90deg, δ_R=0.

Figure A32. Concluded.

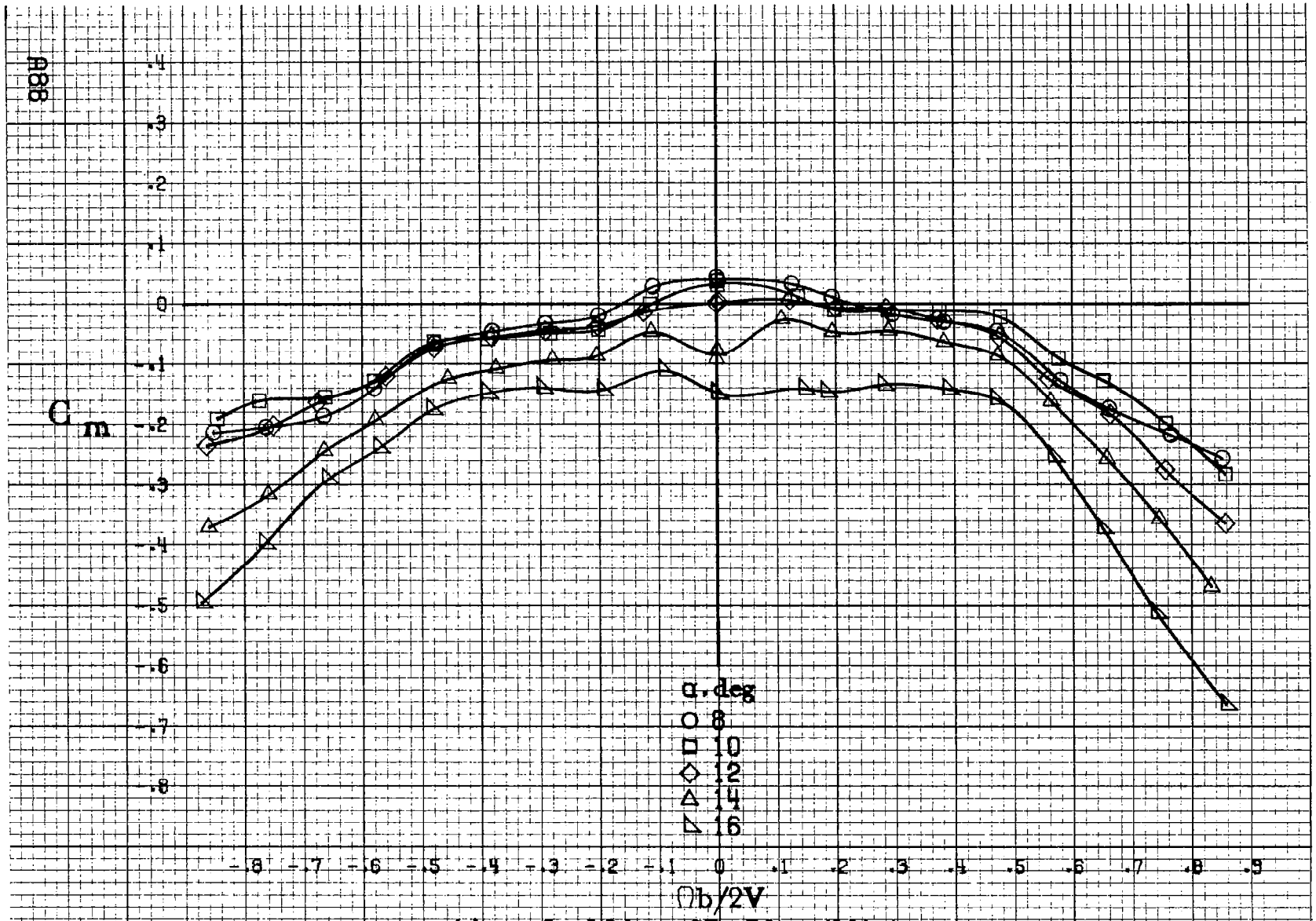

(a) α=8to16deg, SR=76cm(30in).

Figure A33. Effect of rotation rate and angle of attack on pitching-moment coefficient for configuration having outboard LE wing droop with large nose radius and uprigged ailerons. $\delta_e = 0°$, $\delta_a = 0°$, $\delta_r = 0°$, $\beta = 0°$.

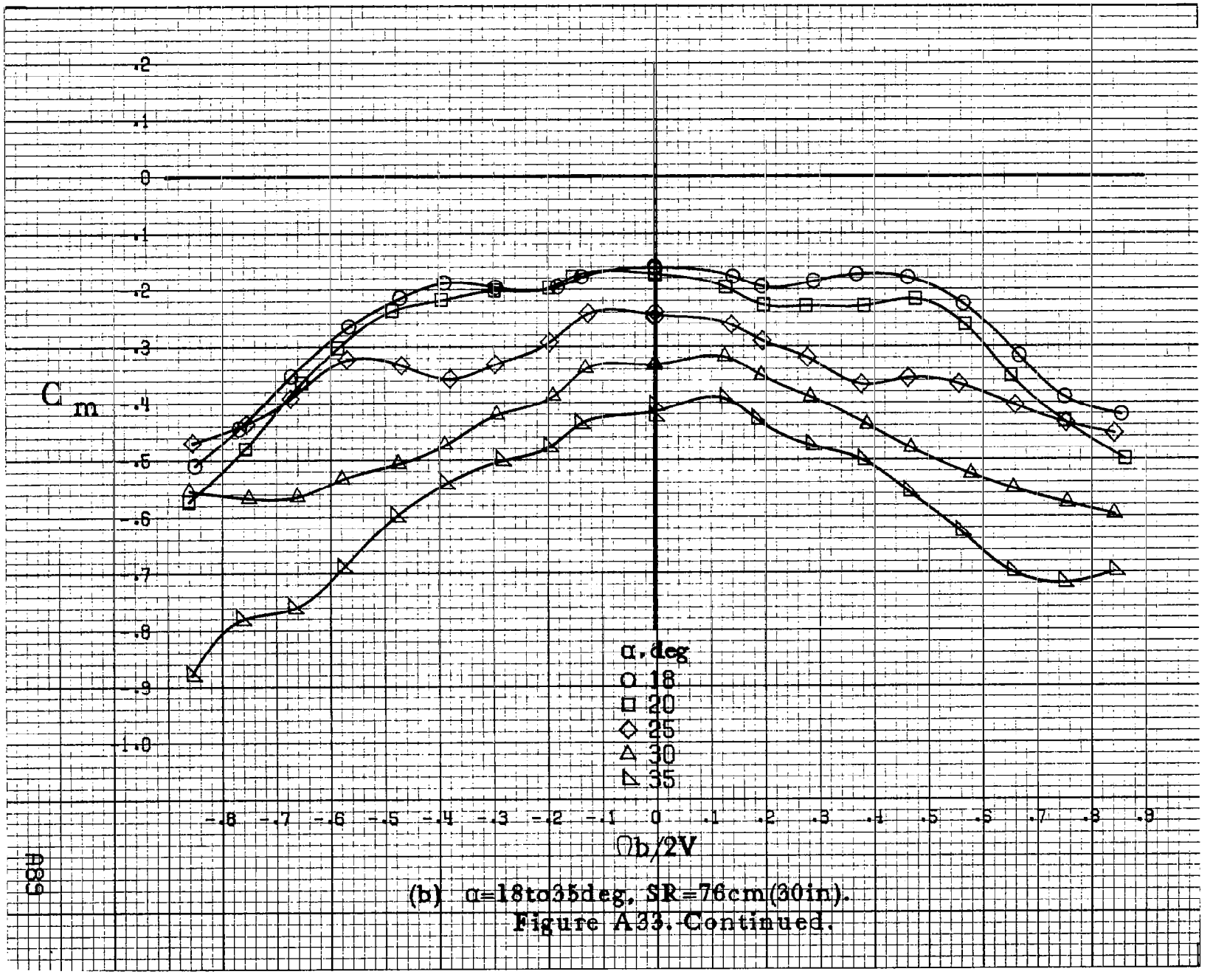

(b) α=18to35deg, SR=76cm(30in).

Figure A33. Continued.

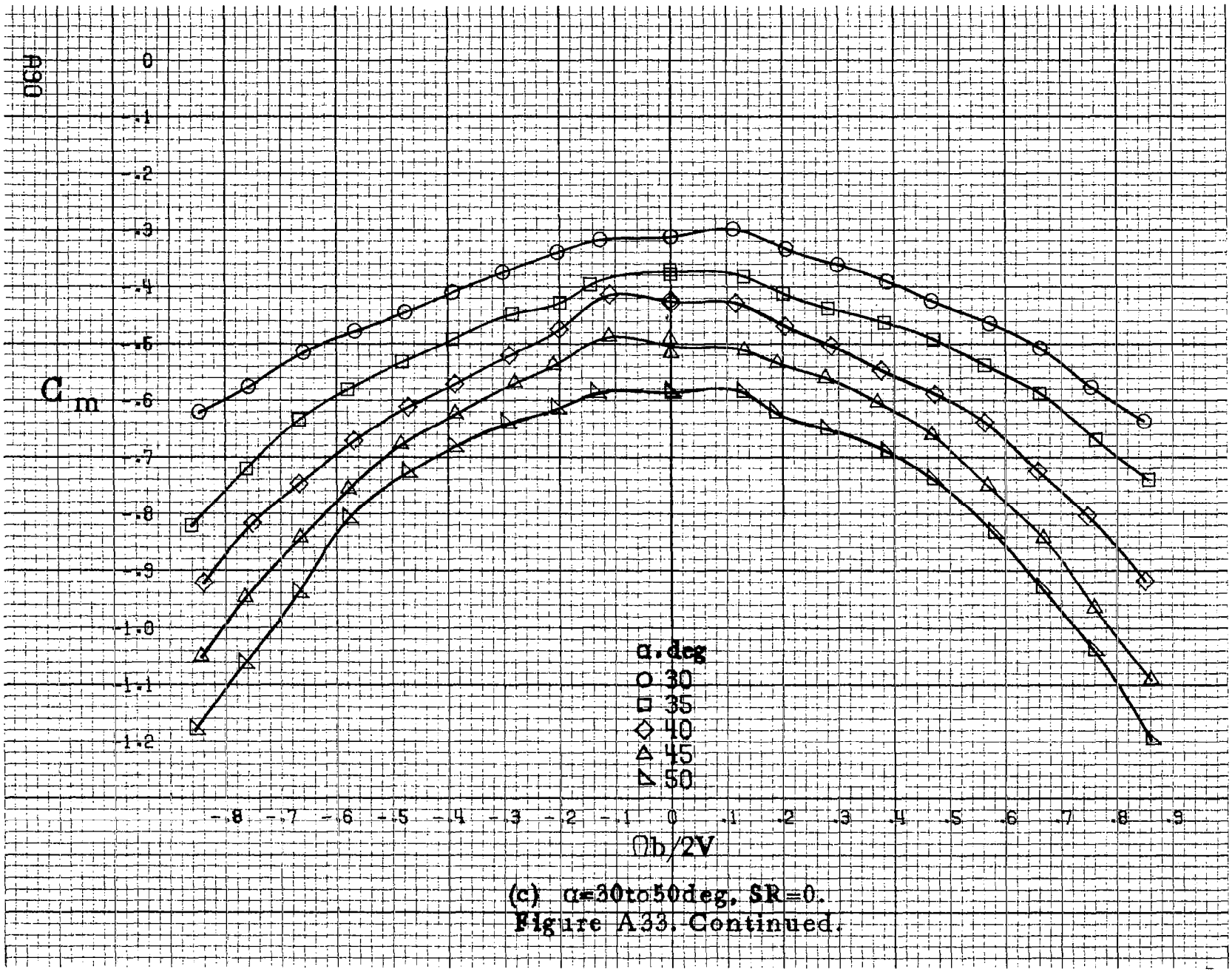

(c) α=30to50deg, SR=0.

Figure A33.-Continued.

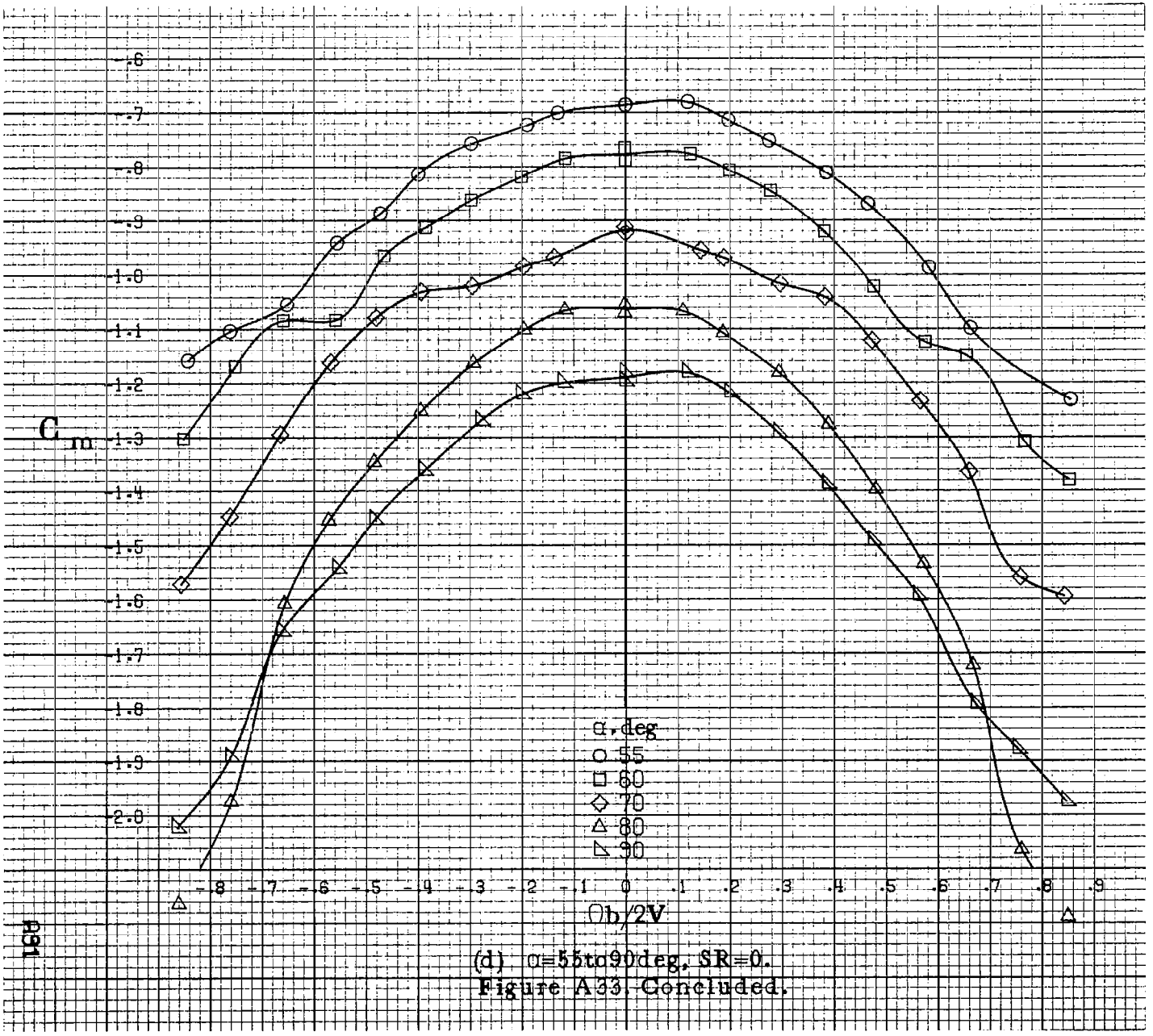

(d) α=55 to 90 deg, SR=0.

Figure A33. Concluded.

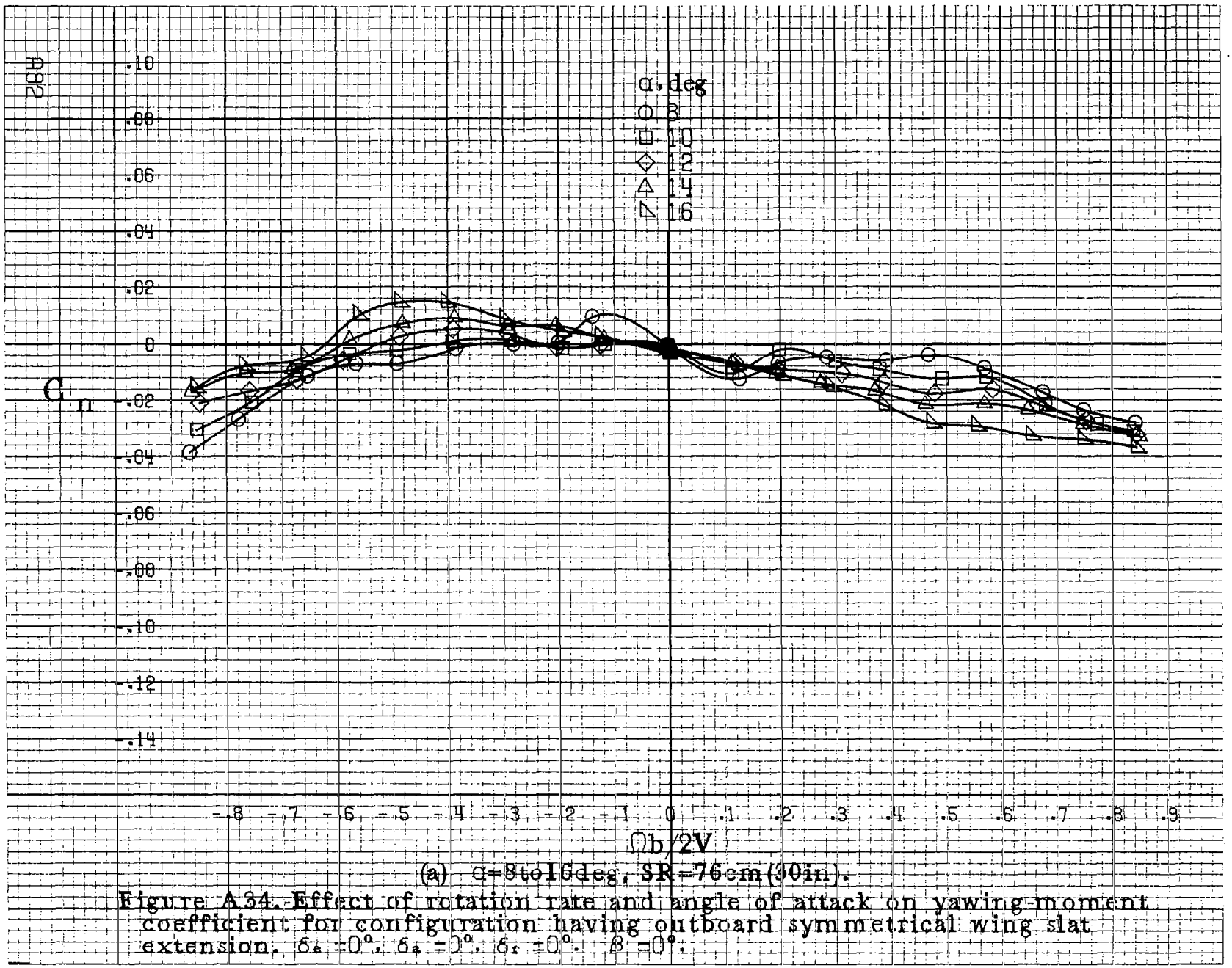

(a) α=8to16deg, SR=76cm(30in).

Figure A.34.-Effect of rotation rate and angle of attack on yawing-moment coefficient for configuration having outboard symmetrical wing slat extension. $\delta_e = 0°$, $\delta_a = 0°$, $\delta_r = 0°$, $\beta = 0°$.

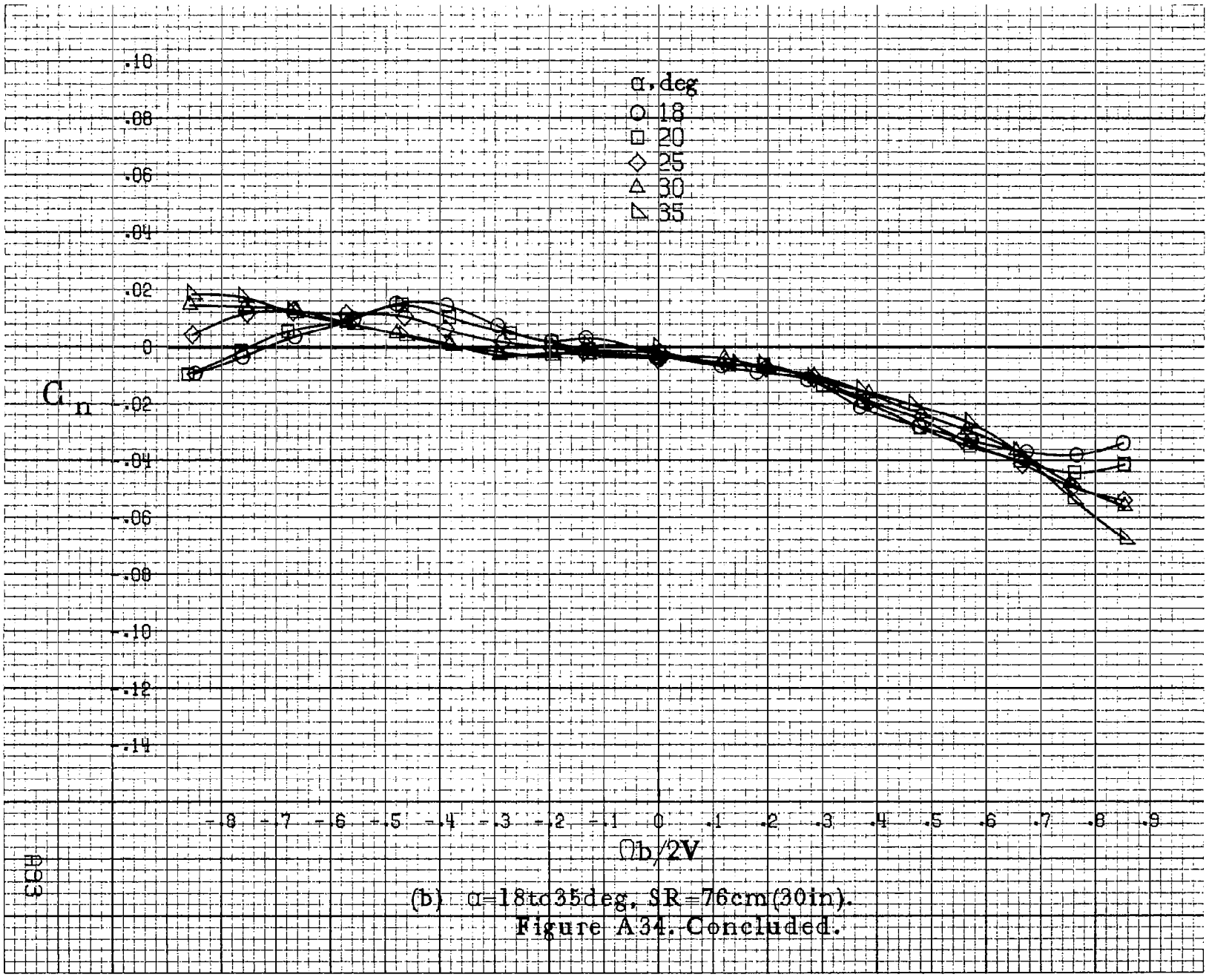

(b) α=18to35deg, SR=76cm(30in).

Figure A34. Concluded.

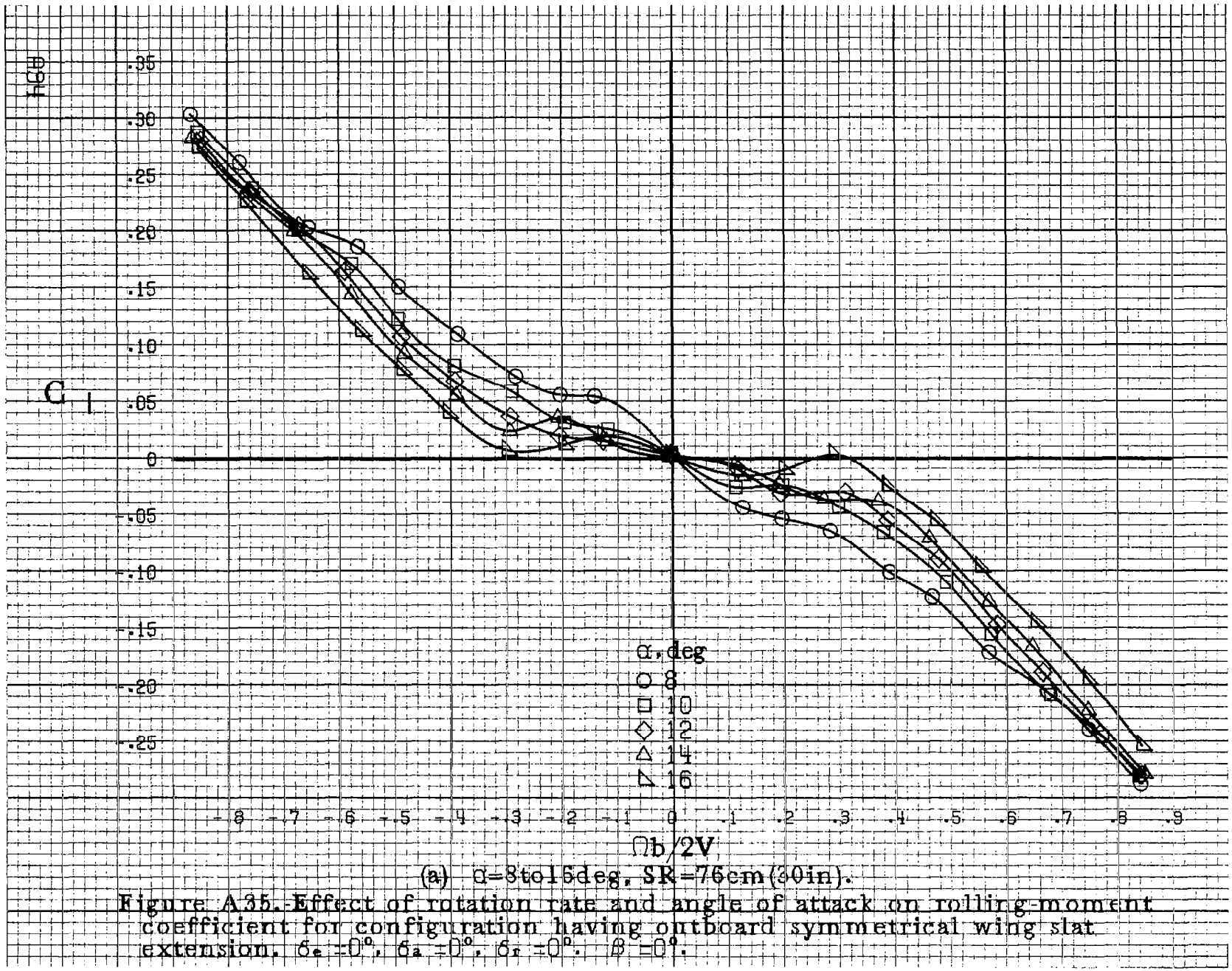

(a) α=8to16deg, SR=76cm(30in).

Figure A35.-Effect of rotation rate and angle of attack on rolling-moment coefficient for configuration having outboard symmetrical wing slat extension. $\delta_e = 0°$, $\delta_a = 0°$, $\delta_r = 0°$. $\beta = 0°$.

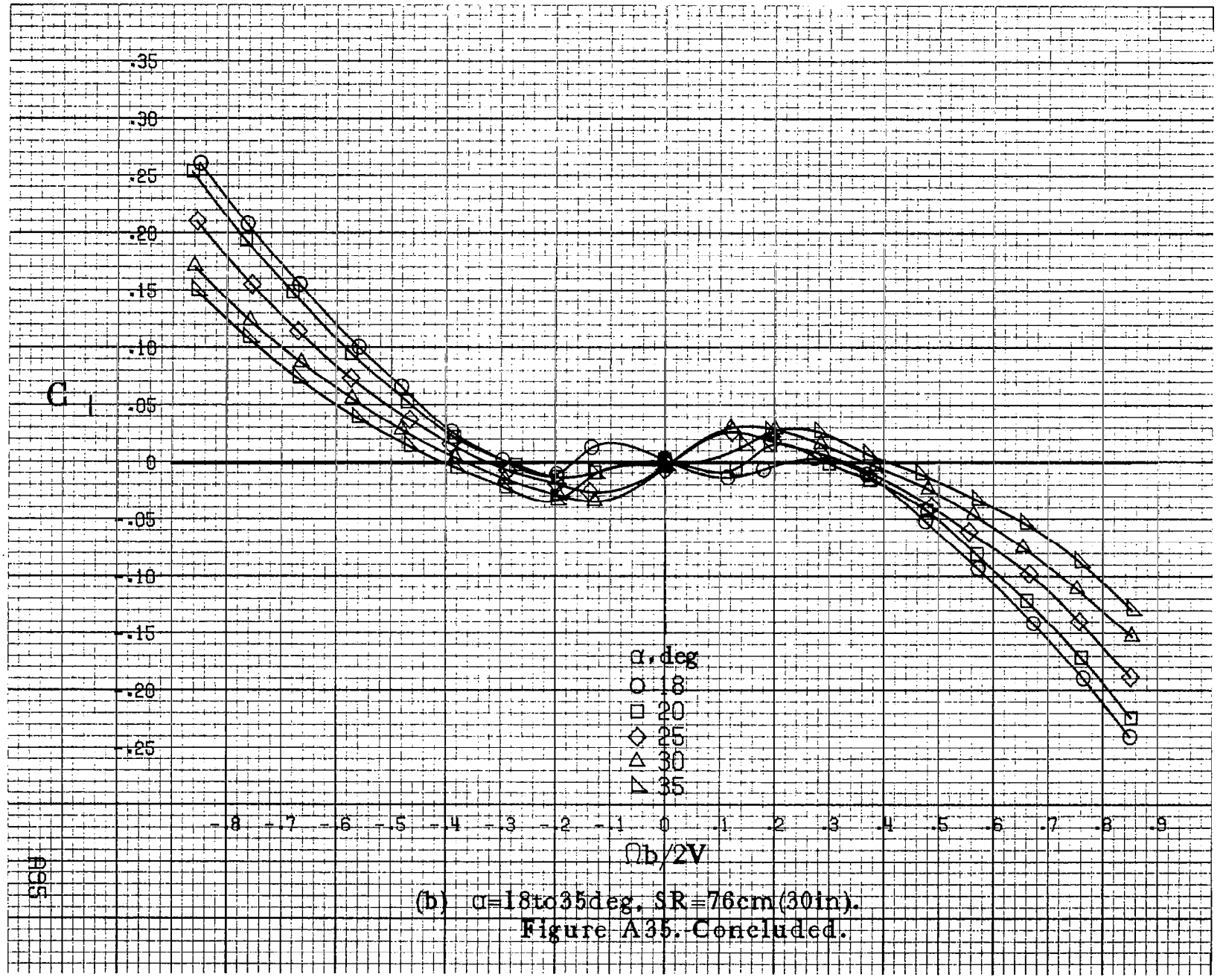

(b) α=18to35deg, SR=76cm(30in).

Figure A35.-Concluded.

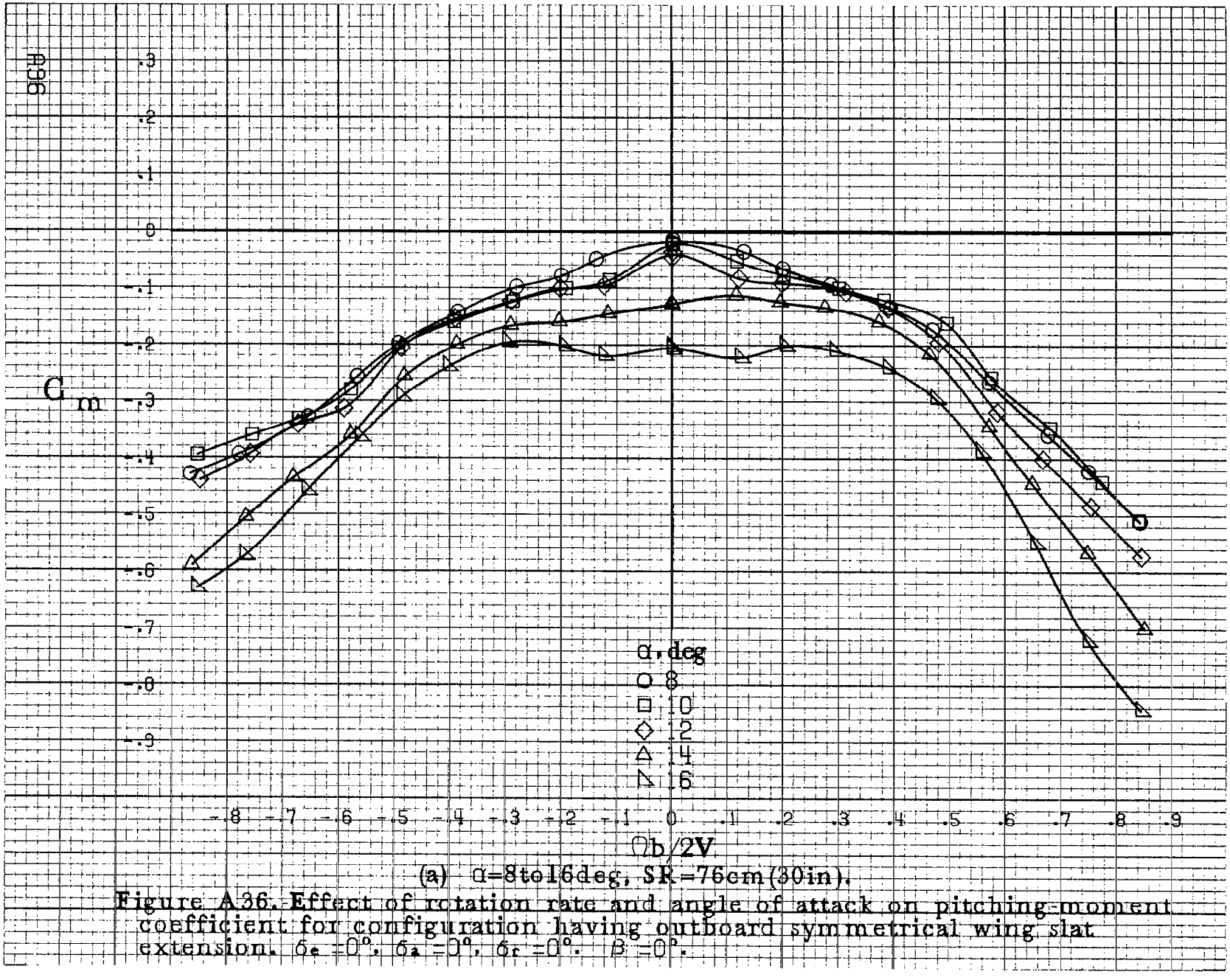

(a) α=8to16deg, SR=76cm(30in).

Figure A36. Effect of rotation rate and angle of attack on pitching-moment coefficient for configuration having outboard symmetrical wing slat extension. $\delta_e = 0°$, $\delta_a = 0°$, $\delta_r = 0°$. $\beta = 0°$.

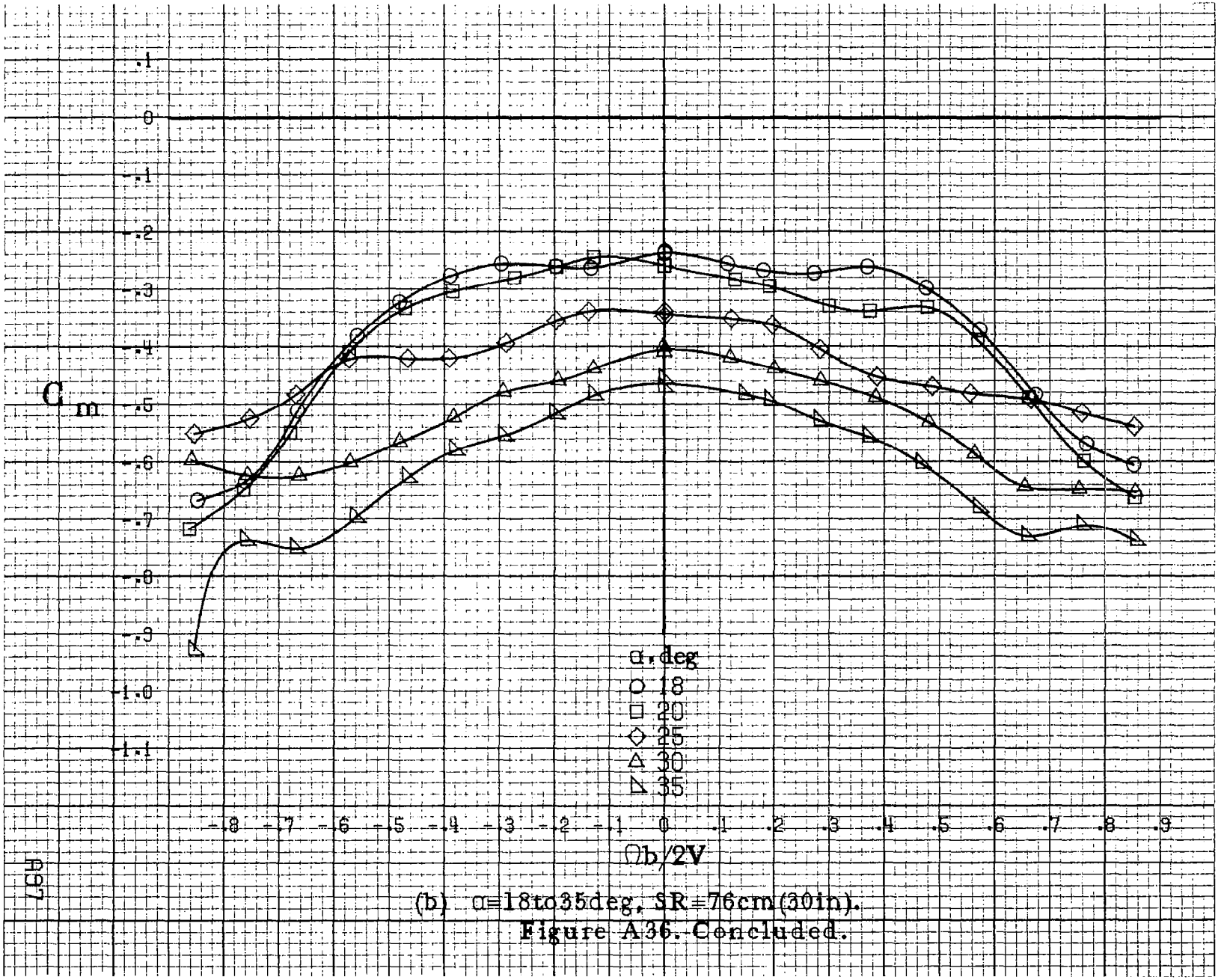

(b) α=18to35deg, SR=76cm(30in).

Figure A36. Concluded.

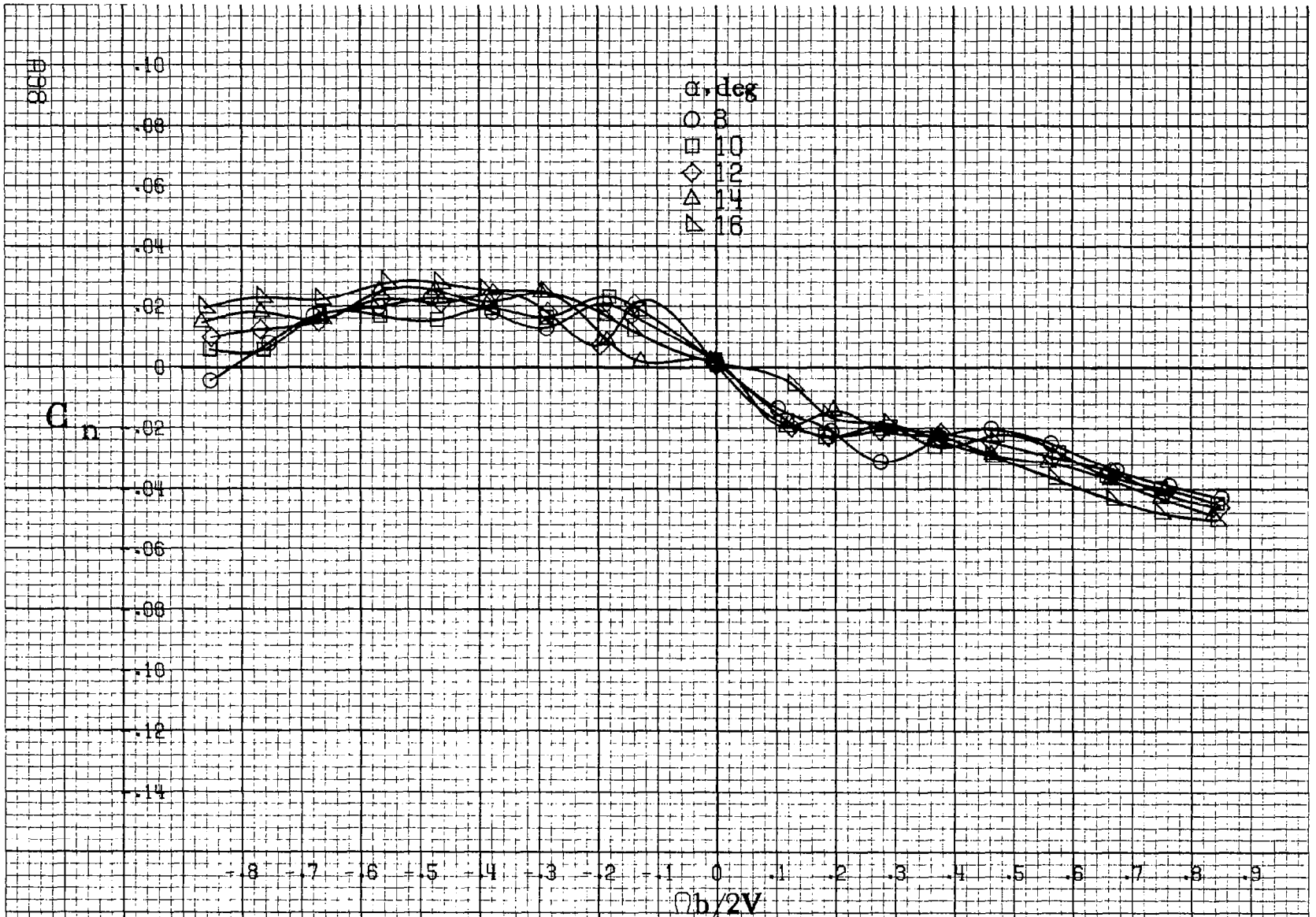

(a) α=8to16deg, SR=76cm(30in).

Figure A37.-Effect of rotation rate and angle of attack on yawing-moment coefficient for configuration having full-span LE wing droop with outboard spoiler strip. $\delta_e = 0°$, $\delta_a = 0°$, $\delta_r = 0°$, $\beta = 0°$.

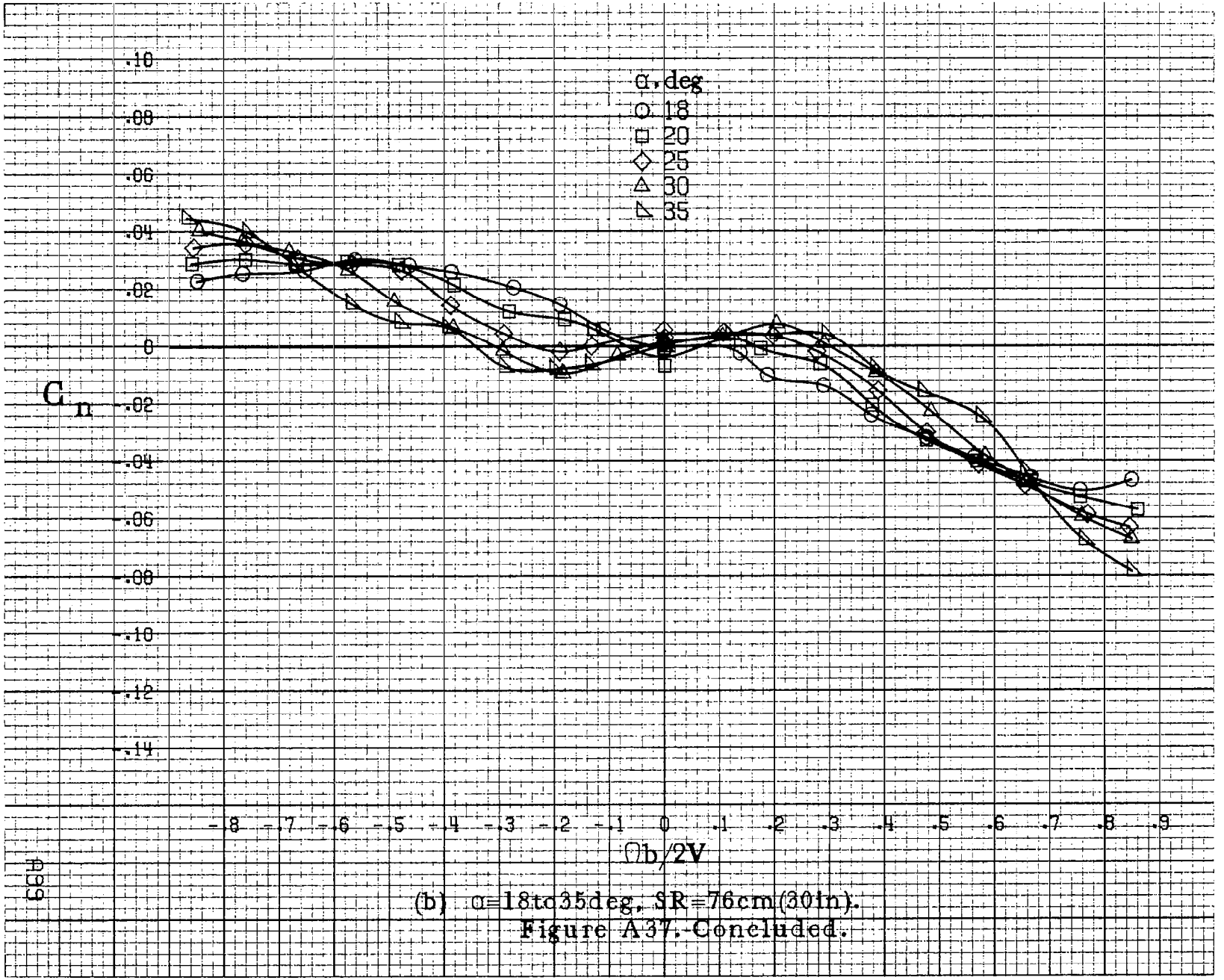

(b) α=18to35deg, SR=76cm(30in).

Figure A37.-Concluded.

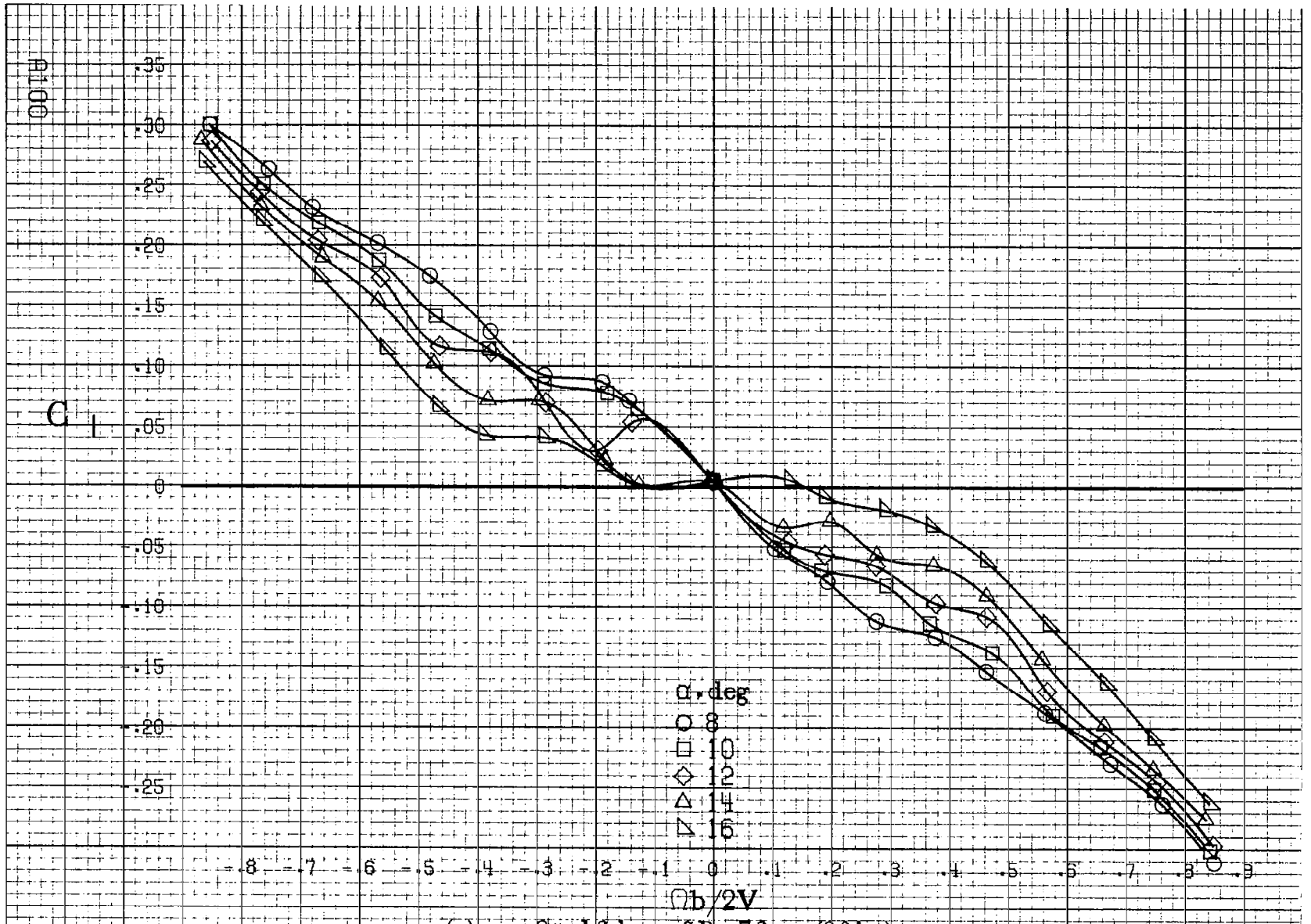

(a) α=8to16deg, SR=76cm(30in).

Figure A.38. Effect of rotation rate and angle of attack on rolling-moment coefficient for configuration having full-span LE wing droop with outboard spoiler strip. $\delta_e = 0°$, $\delta_a = 0°$, $\delta_r = 0°$, $\beta = 0°$.

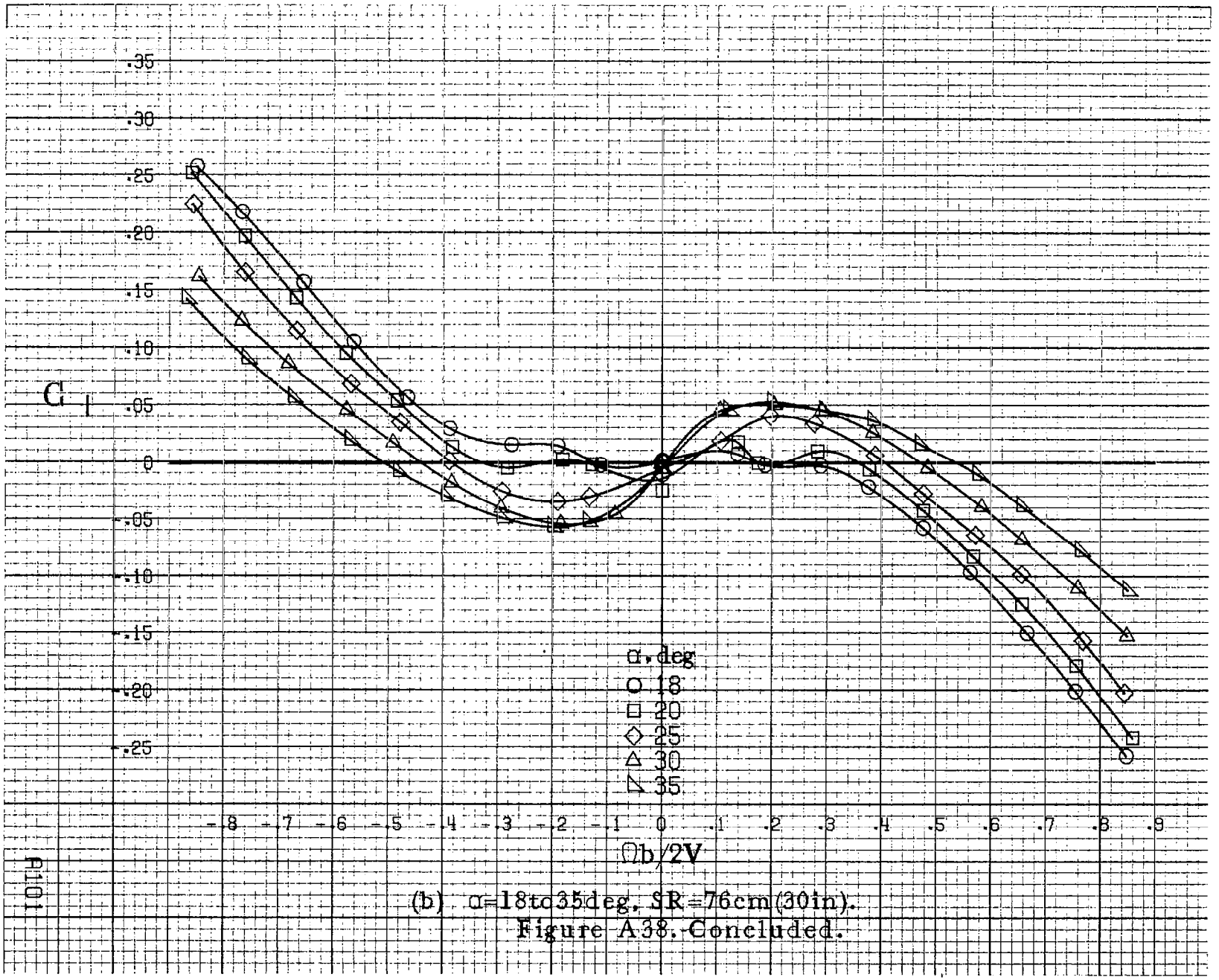

(b) α=18to35deg, SR=76cm(30in).

Figure A38.-Concluded.

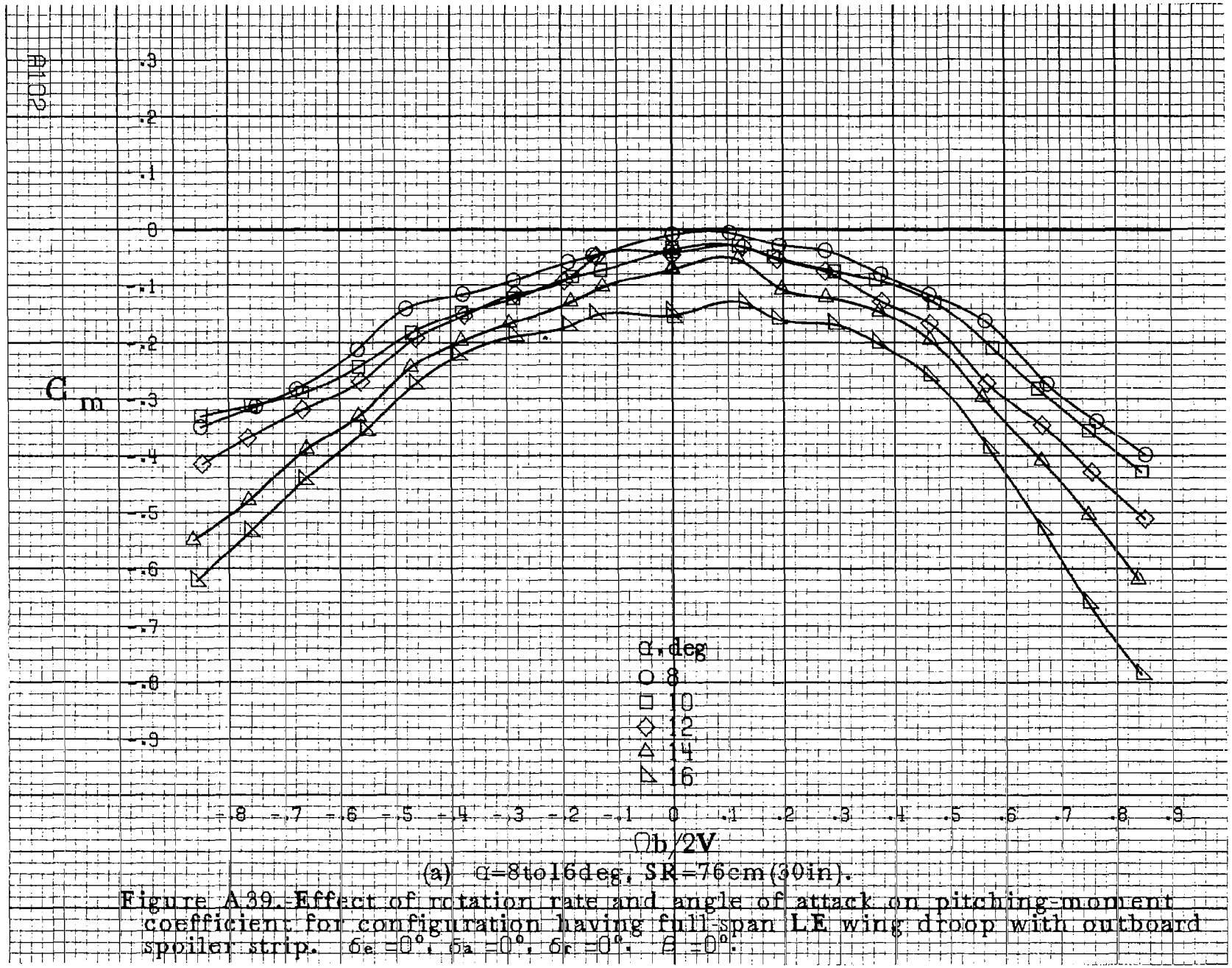

(a) α=8to16deg, SR=76cm(30in).

Figure A39.-Effect of rotation rate and angle of attack on pitching-moment coefficient for configuration having full-span LE wing droop with outboard spoiler strip. $\delta_e = 0°$, $\delta_a = 0°$, $\delta_r = 0°$, $\beta = 0°$.

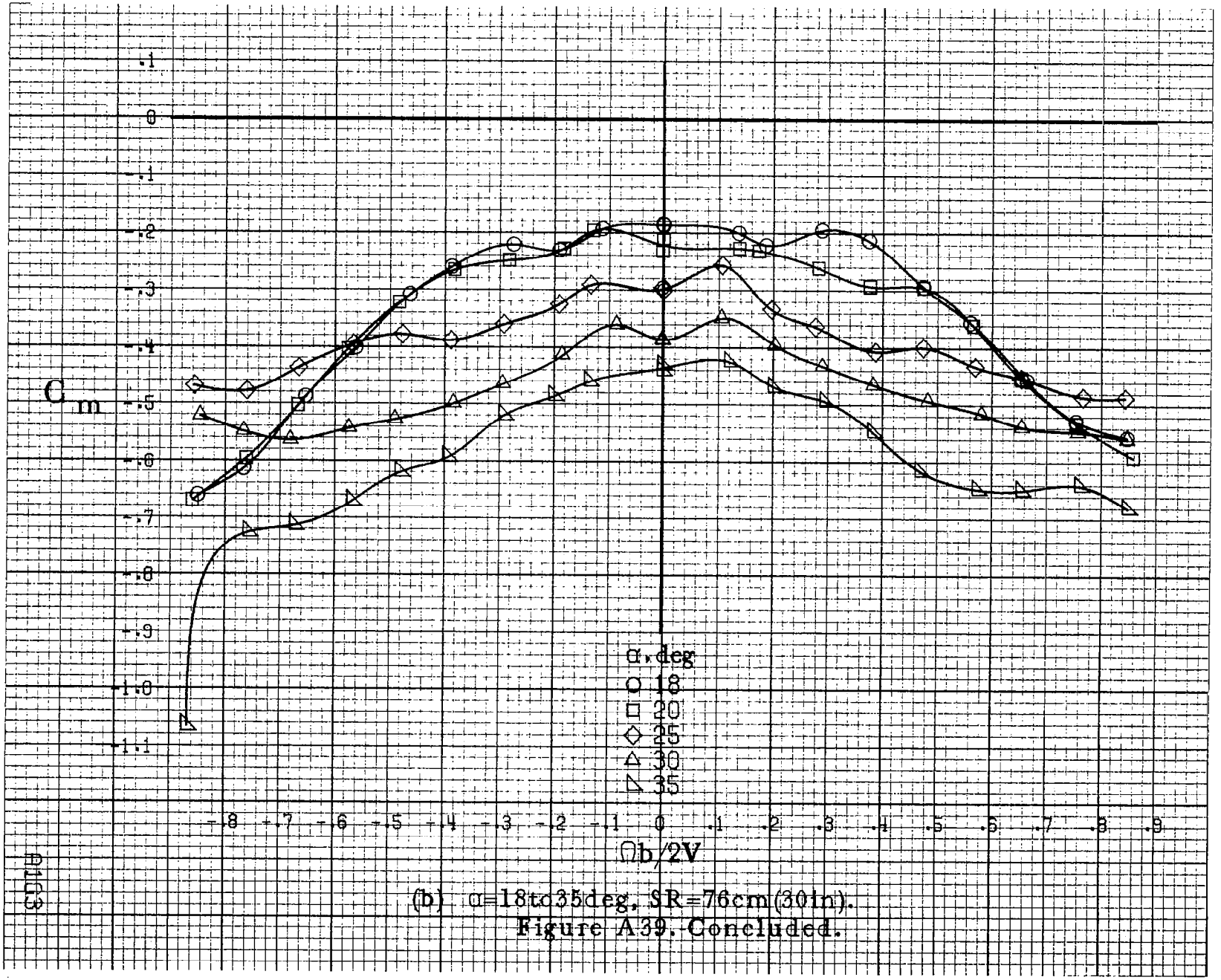

Figure A39.-Concluded.

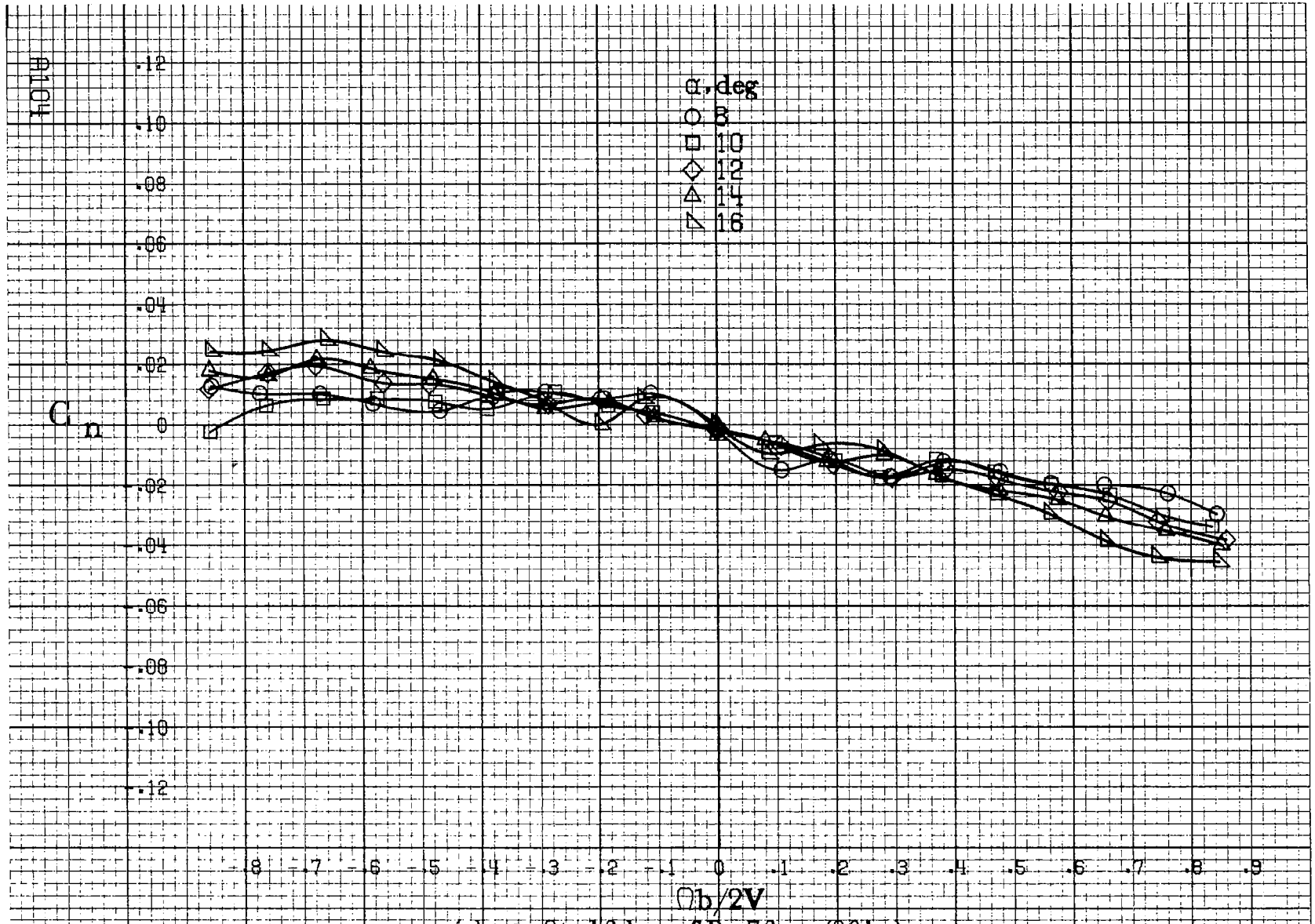

(a) α=8to16deg, SR=76cm(30in).

Figure A40. Effect of rotation rate and angle of attack on yawing-moment coefficient for configuration having segmented LE wing droop with 16.3cm (6.4in) gap. $\delta_e = 0^\circ$, $\delta_a = 0^\circ$, $\delta_r = 0^\circ$. $\beta = 0^\circ$.

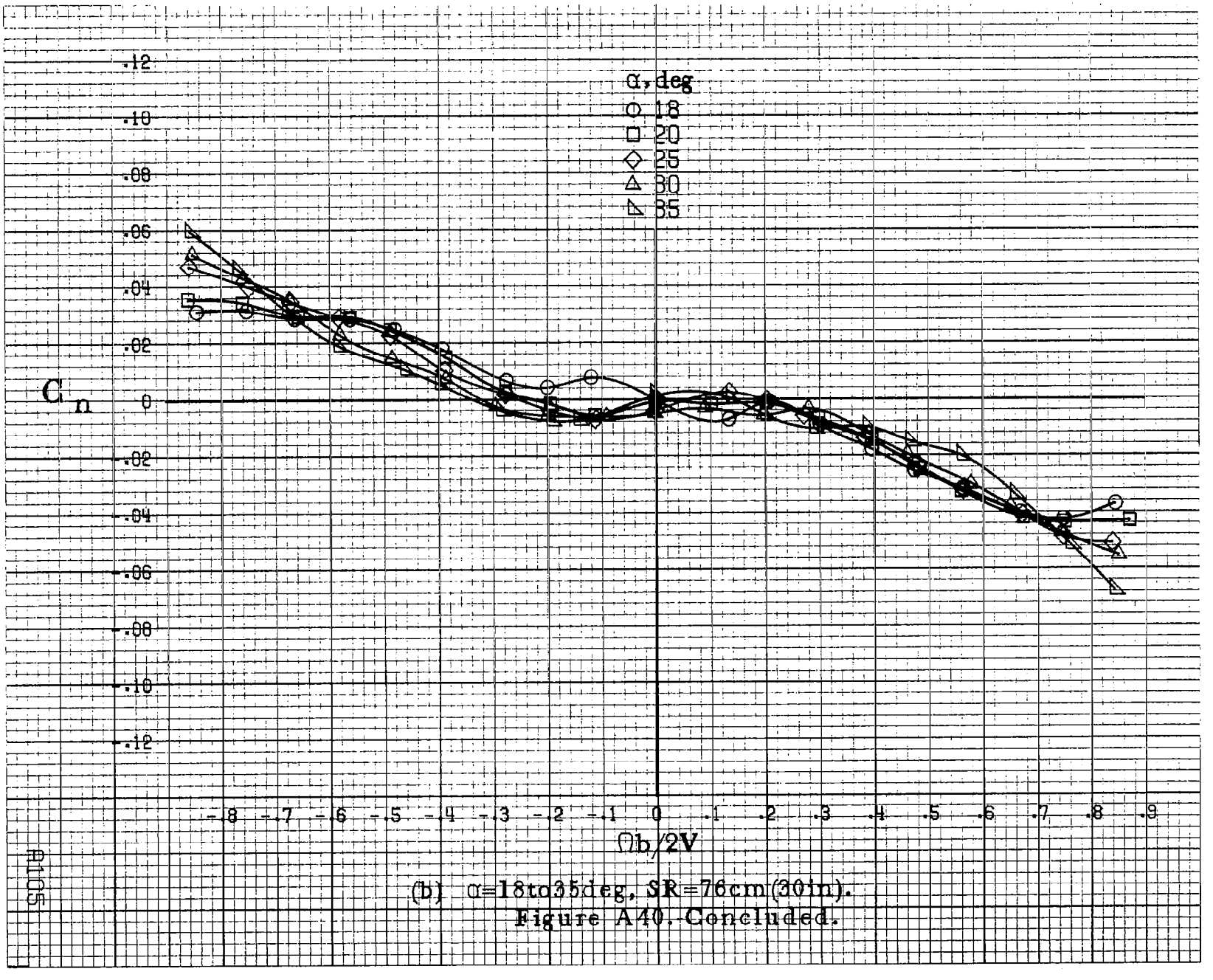

(b) α=18to35deg, SR=76cm(30in).

Figure A40. Concluded.

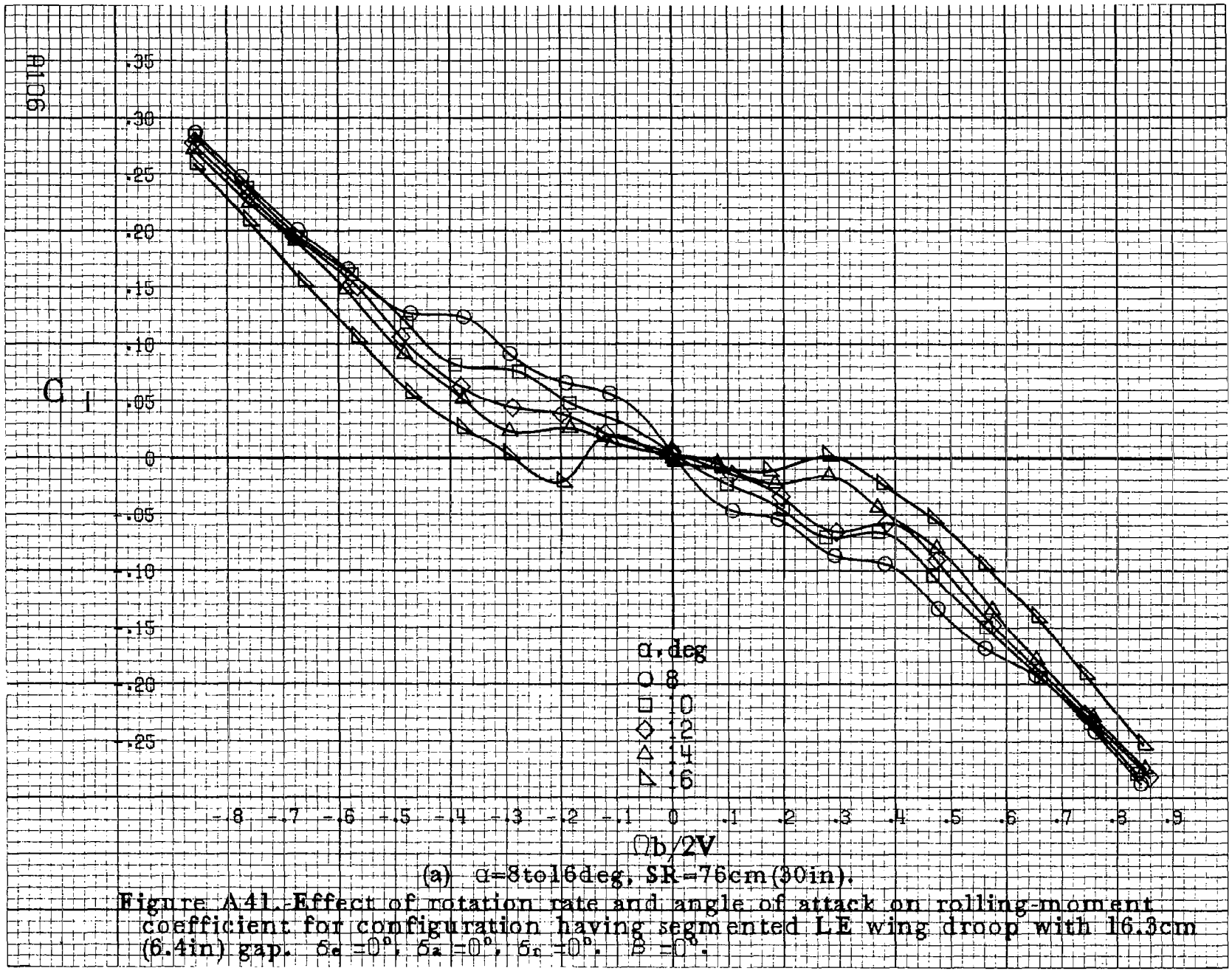

(a) α=8to16deg, SR=76cm(30in).

Figure A41.-Effect of rotation rate and angle of attack on rolling-moment coefficient for configuration having segmented LE wing droop with 16.3cm (6.4in) gap. $\delta_e = 0^\circ$, $\delta_a = 0^\circ$, $\delta_r = 0^\circ$. $\beta = 0^\circ$.

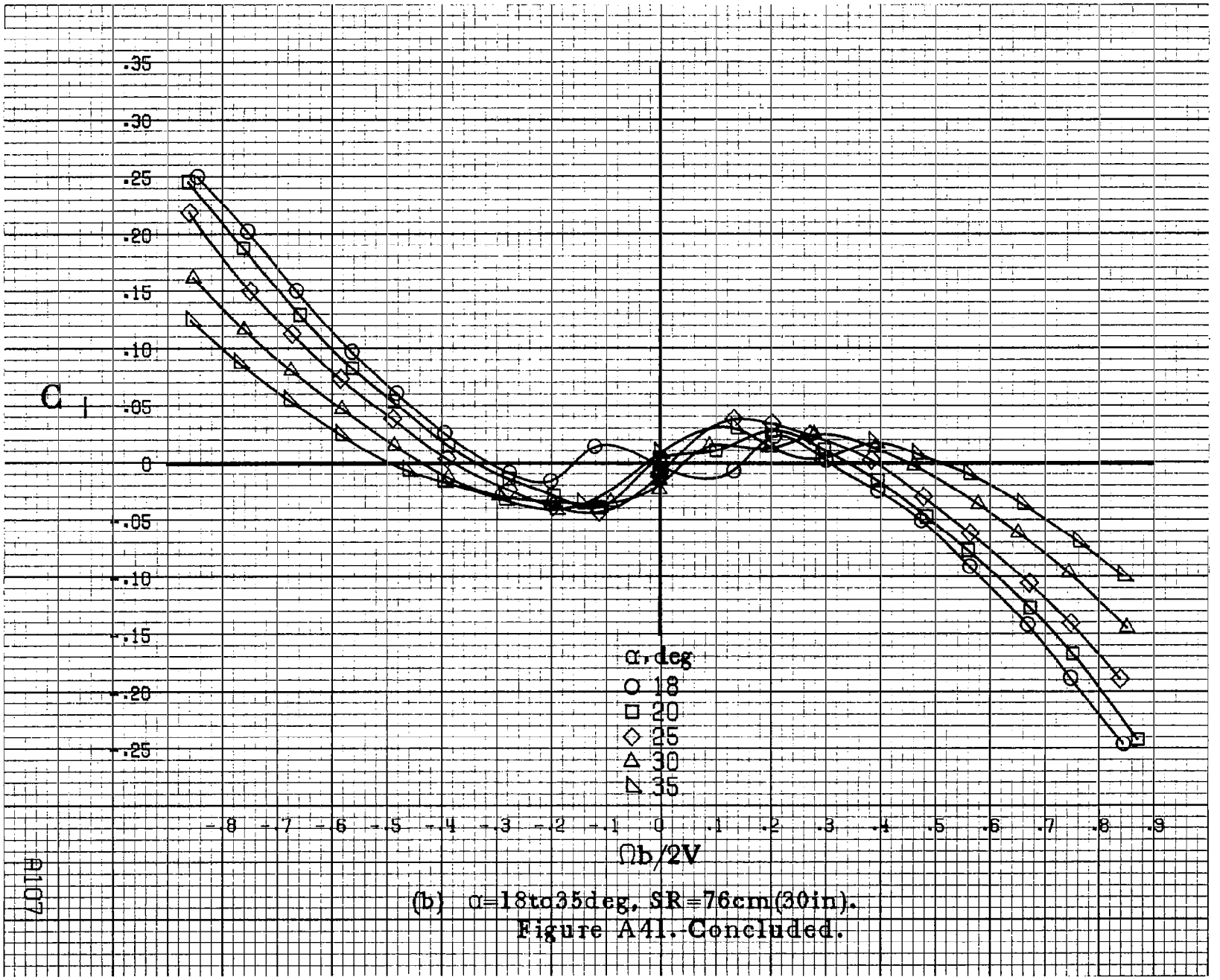

(b) α=18to35deg, SR=76cm(30in).

Figure A41.-Concluded.

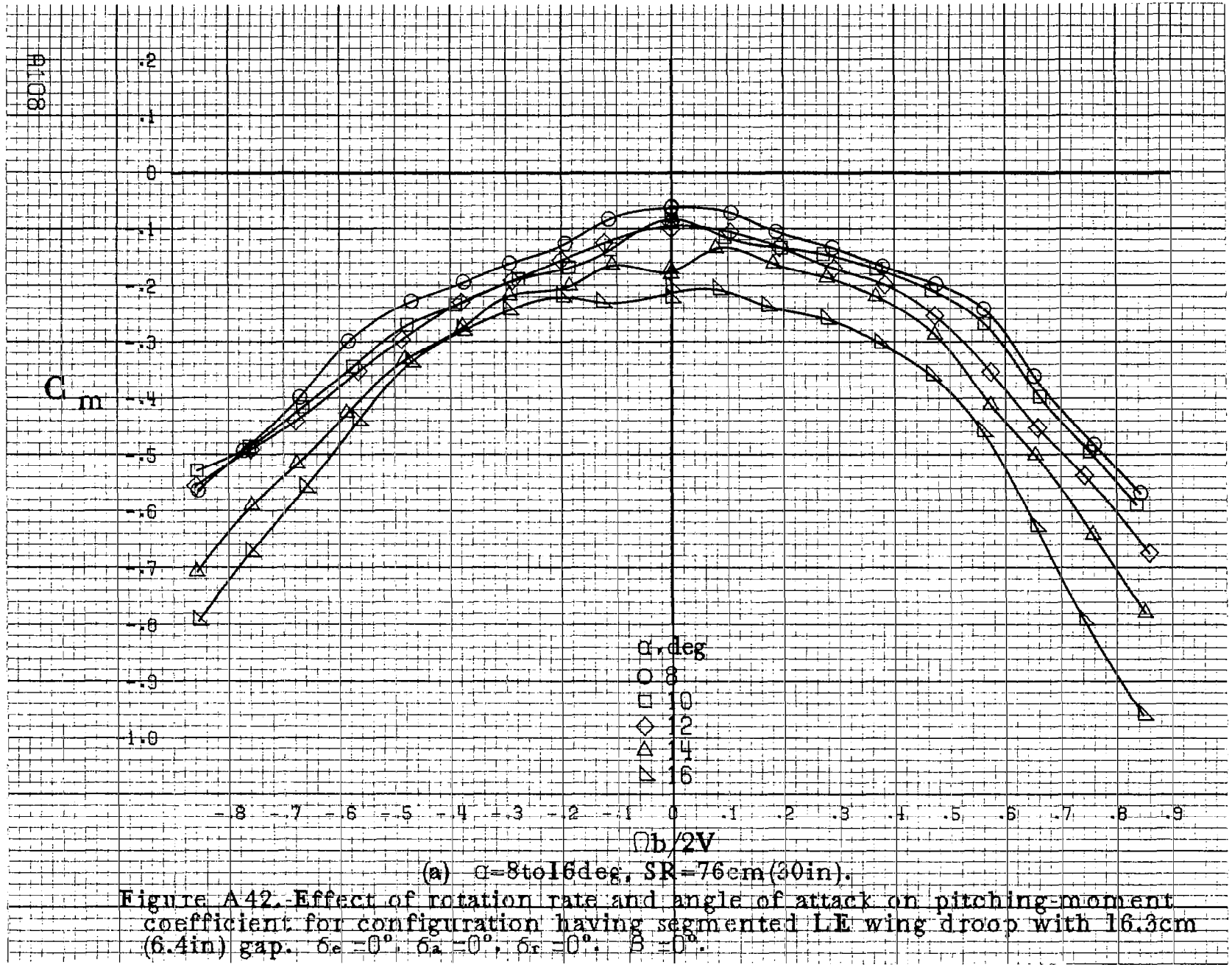

(a) α=8to16deg, SR=76cm(30in).

Figure A42.-Effect of rotation rate and angle of attack on pitching-moment coefficient for configuration having segmented LE wing droop with 16.3cm (6.4in) gap. $\delta_e = 0°$, $\delta_a = 0°$, $\delta_r = 0°$, $\beta = 0°$.

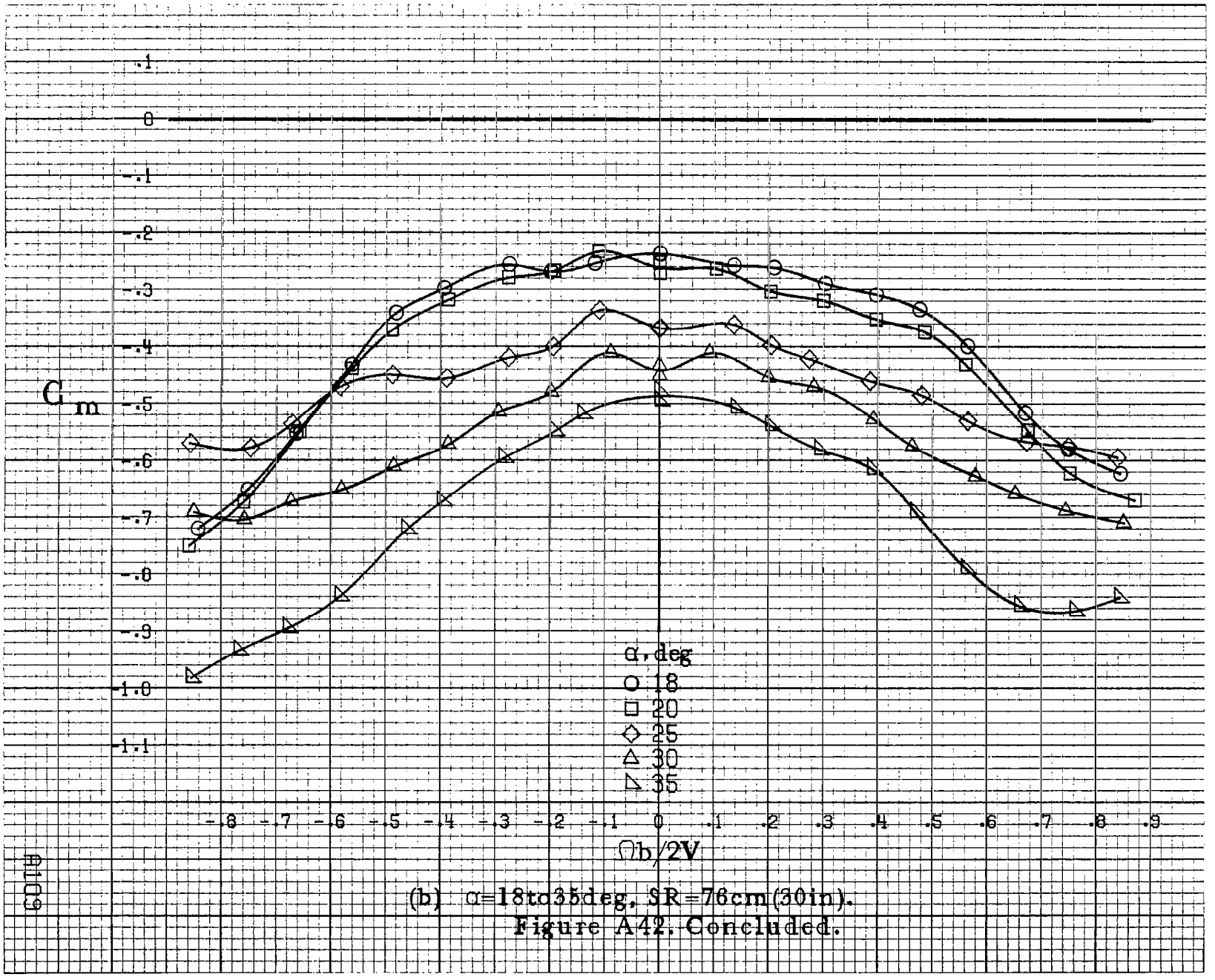

(b) α=18to35deg, SR=76cm(30in).

Figure A42. Concluded.

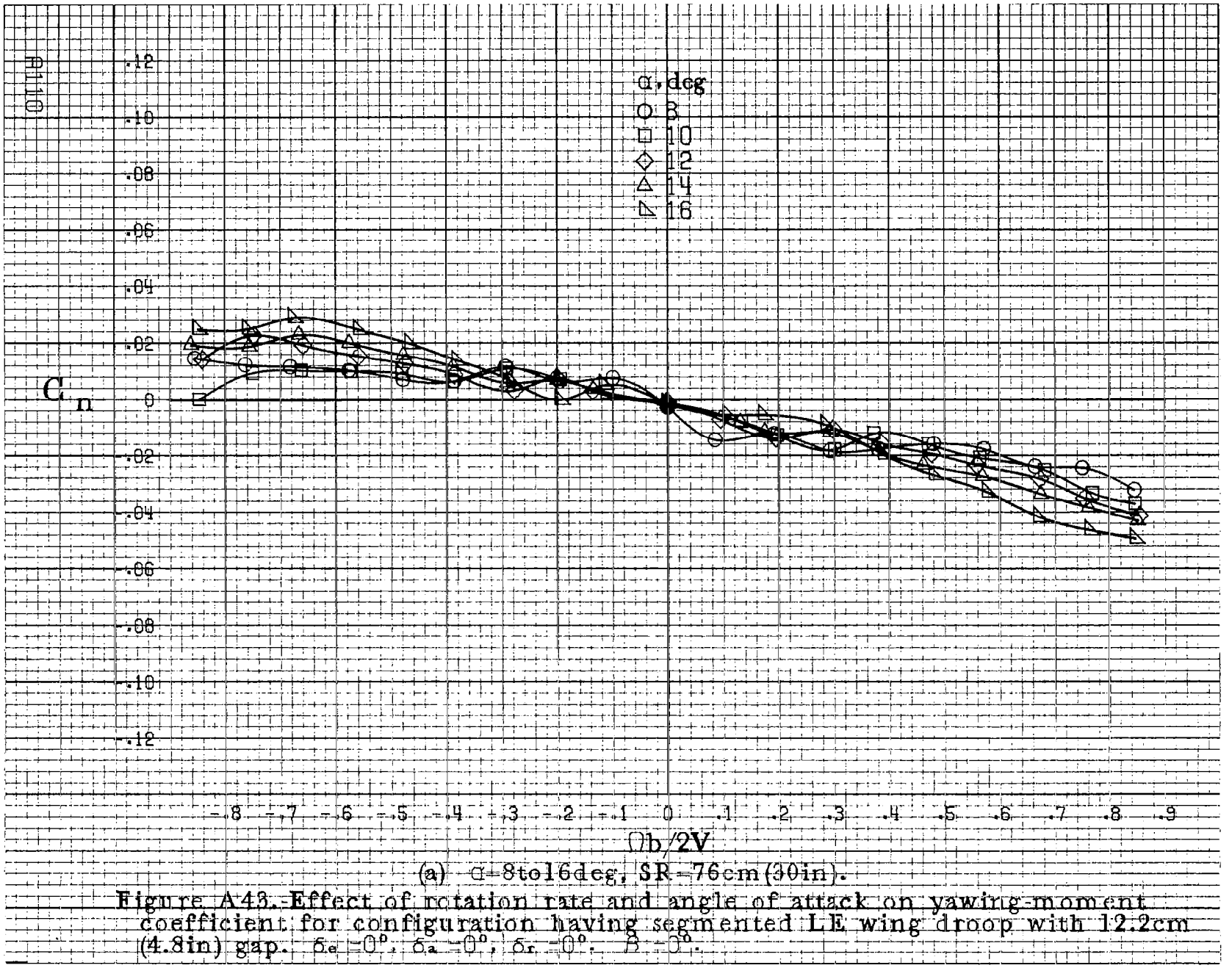

(a) α=8to16deg, SR=76cm(30in).

Figure A43.-Effect of rotation rate and angle of attack on yawing-moment coefficient for configuration having segmented LE wing droop with 12.2cm (4.8in) gap. $\delta_e = 0^\circ$, $\delta_a = 0^\circ$, $\delta_r = 0^\circ$, $\beta = 0^\circ$.

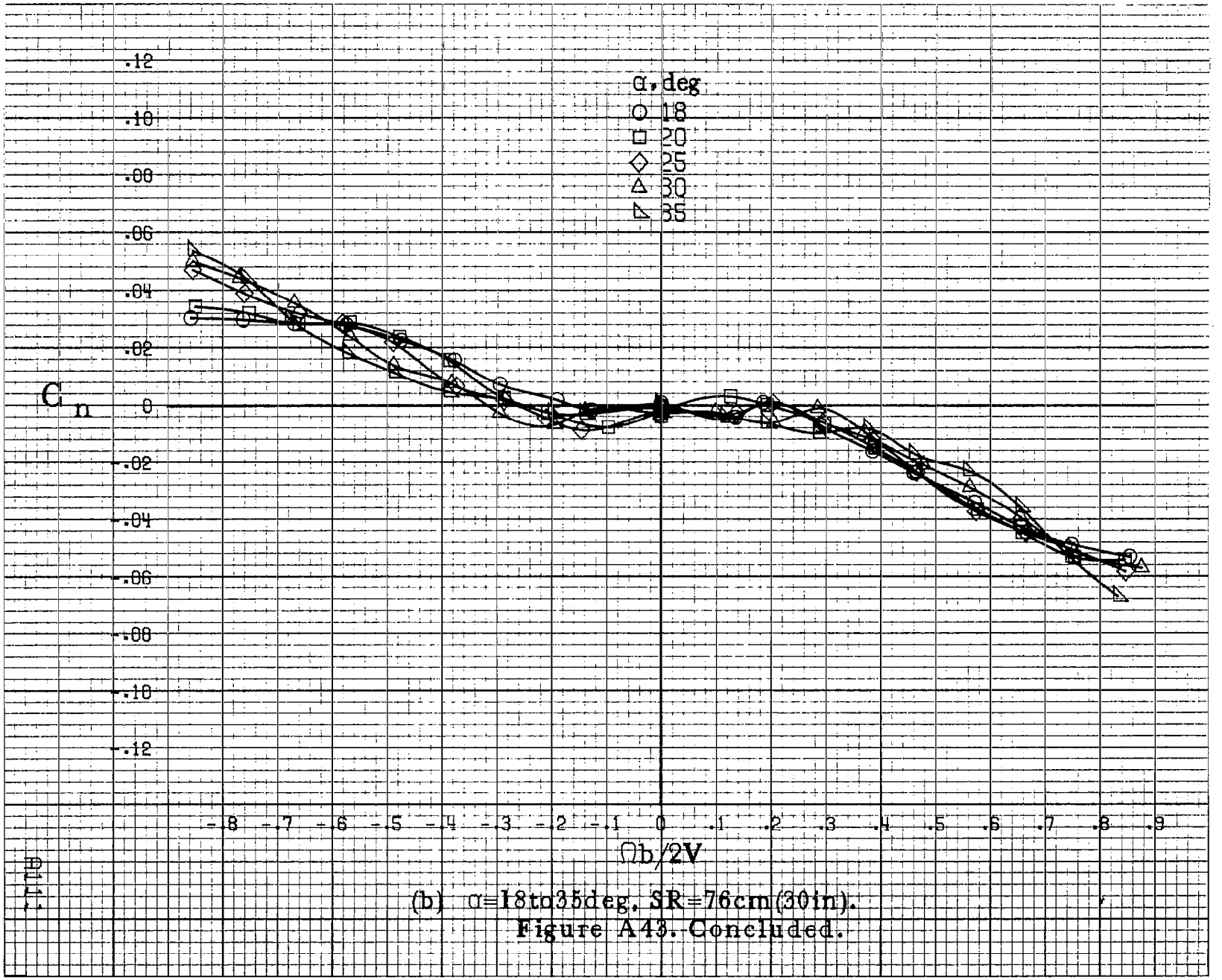

(b) α=18to35deg, SR=76cm(30in).

Figure A43.-Concluded.

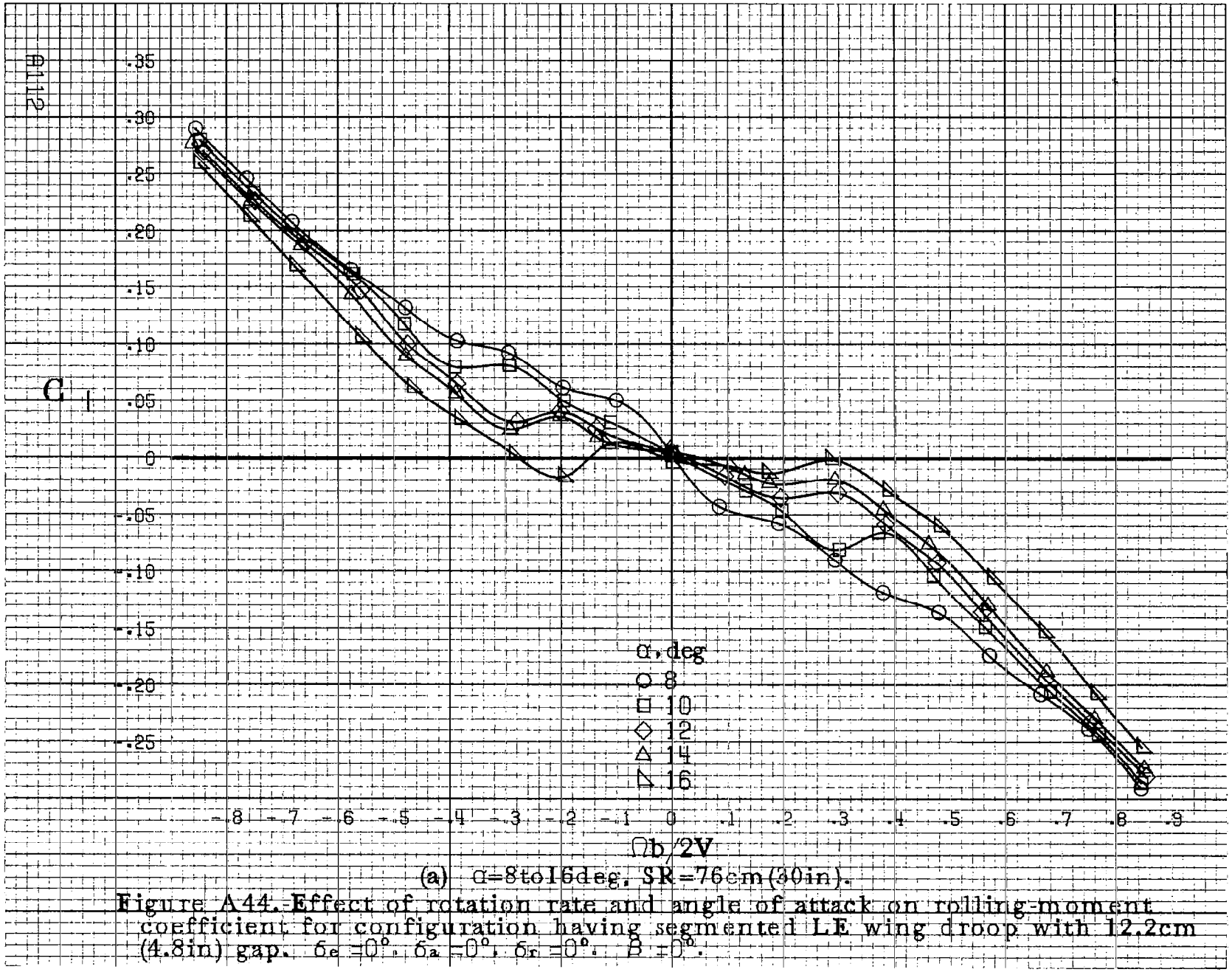

(a) α=8to16deg, SR=76cm(30in).

Figure A44.-Effect of rotation rate and angle of attack on rolling-moment coefficient for configuration having segmented LE wing droop with 12.2cm (4.8in) gap. $\delta_e = 0°$, $\delta_a = 0°$, $\delta_r = 0°$, $\beta = 0°$.

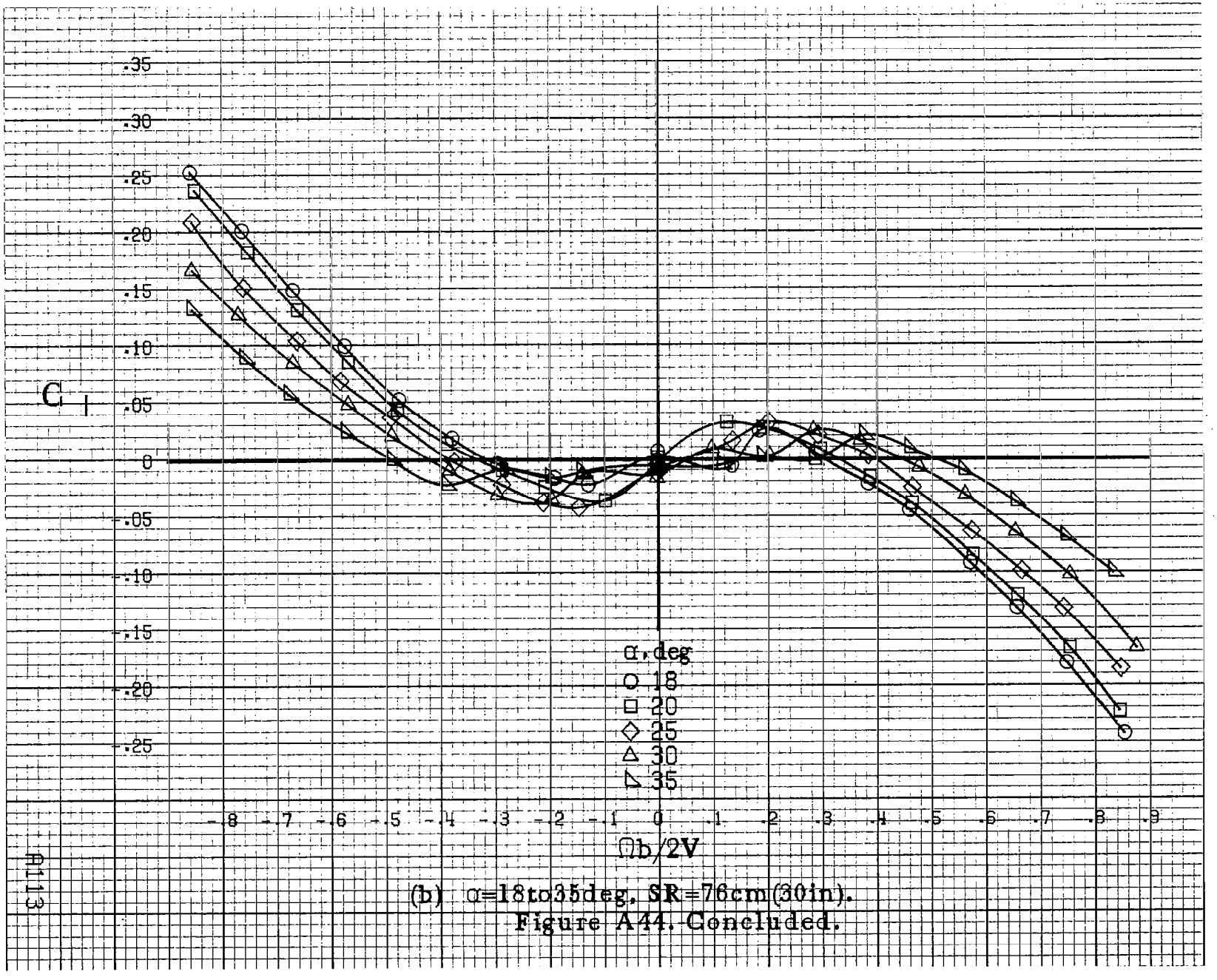

(b) α=18to35deg, SR=76cm(30in).

Figure A44. Concluded.

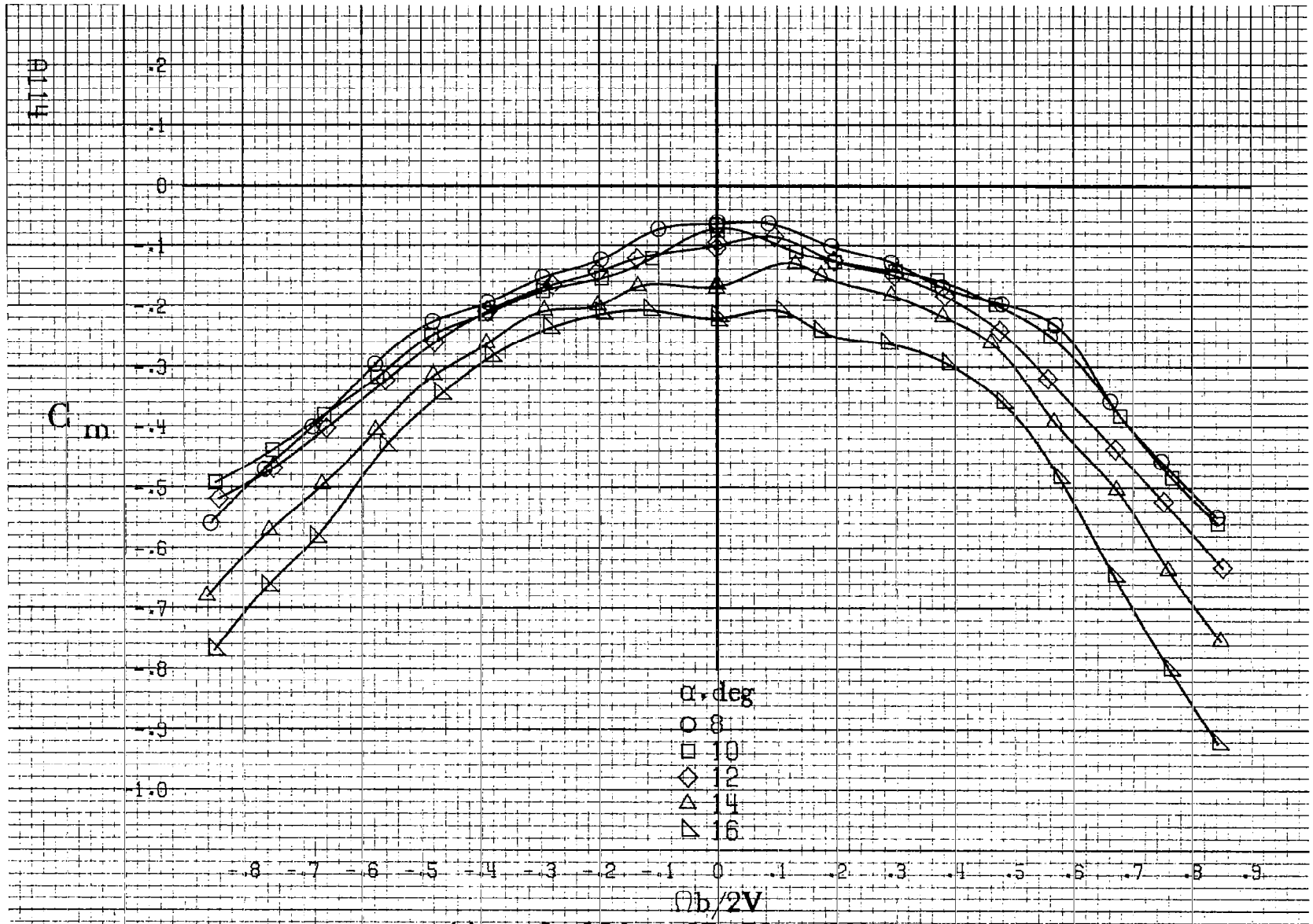

(a) α=8to16deg, SR=76cm(30in).

Figure A45. Effect of rotation rate and angle of attack on pitching-moment coefficient for configuration having segmented LE wing droop with 12.2cm (4.8in) gap. $\delta_e = 0°$, $\delta_a = 0°$, $\delta_r = 0°$, $\beta = 0°$.

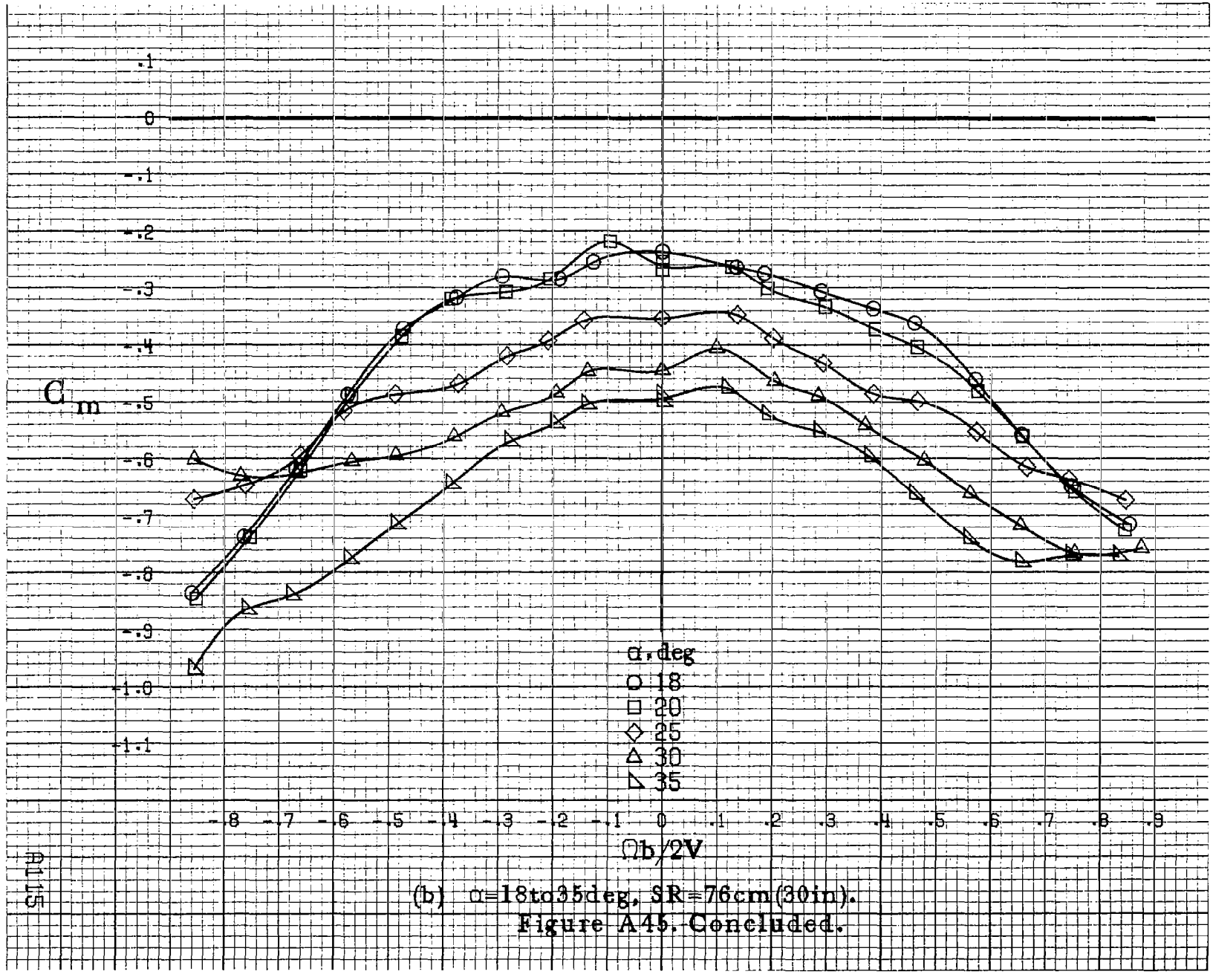

(b) α=18to35deg, SR=76cm(30in).

Figure A45. Concluded.

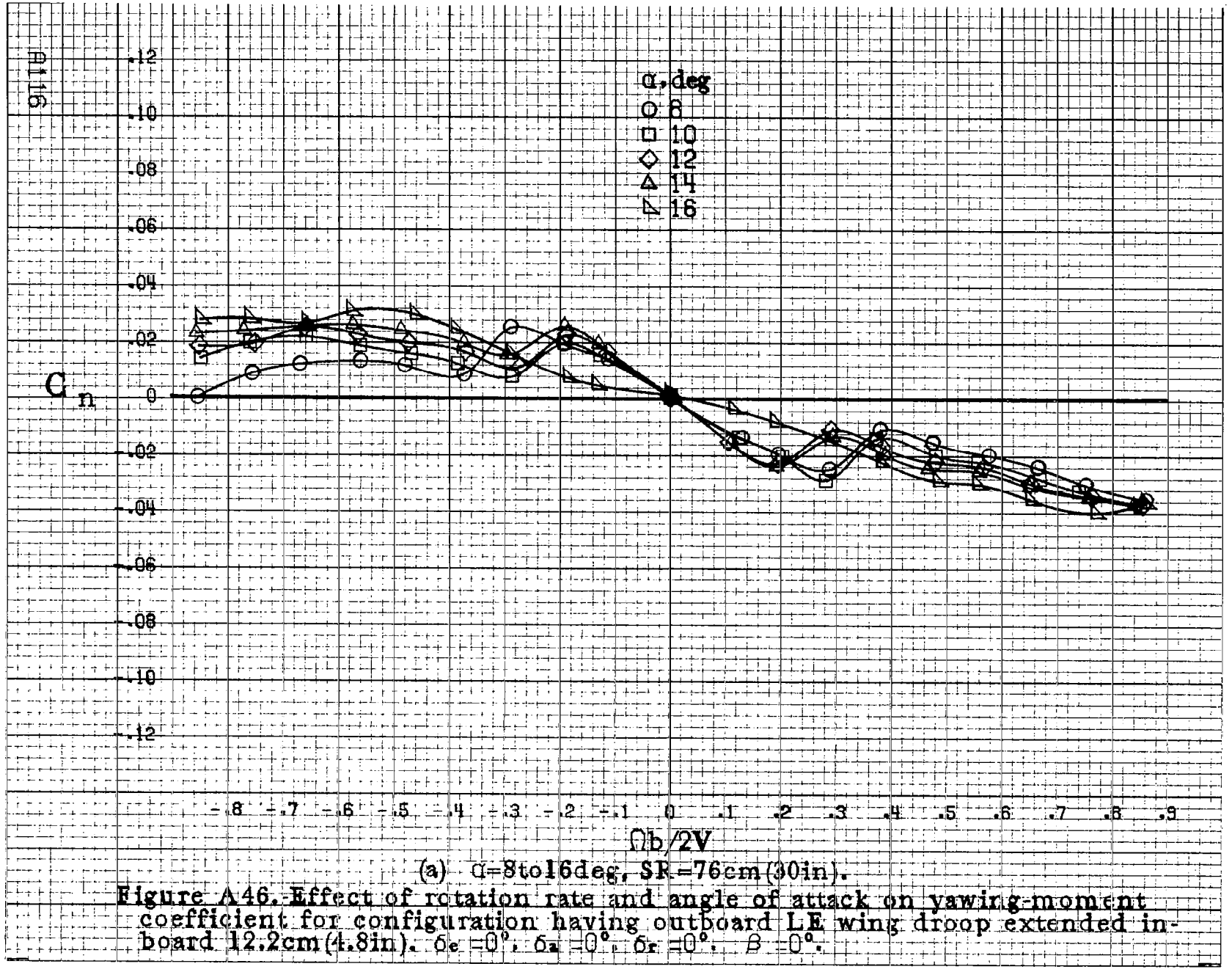

(a) α=8to16deg, SR=76cm(30in).

Figure A46. Effect of rotation rate and angle of attack on yawing-moment coefficient for configuration having outboard LE wing droop extended inboard 12.2cm(4.8in). δ_e =0°, δ_a =0°, δ_r =0°, β =0°.

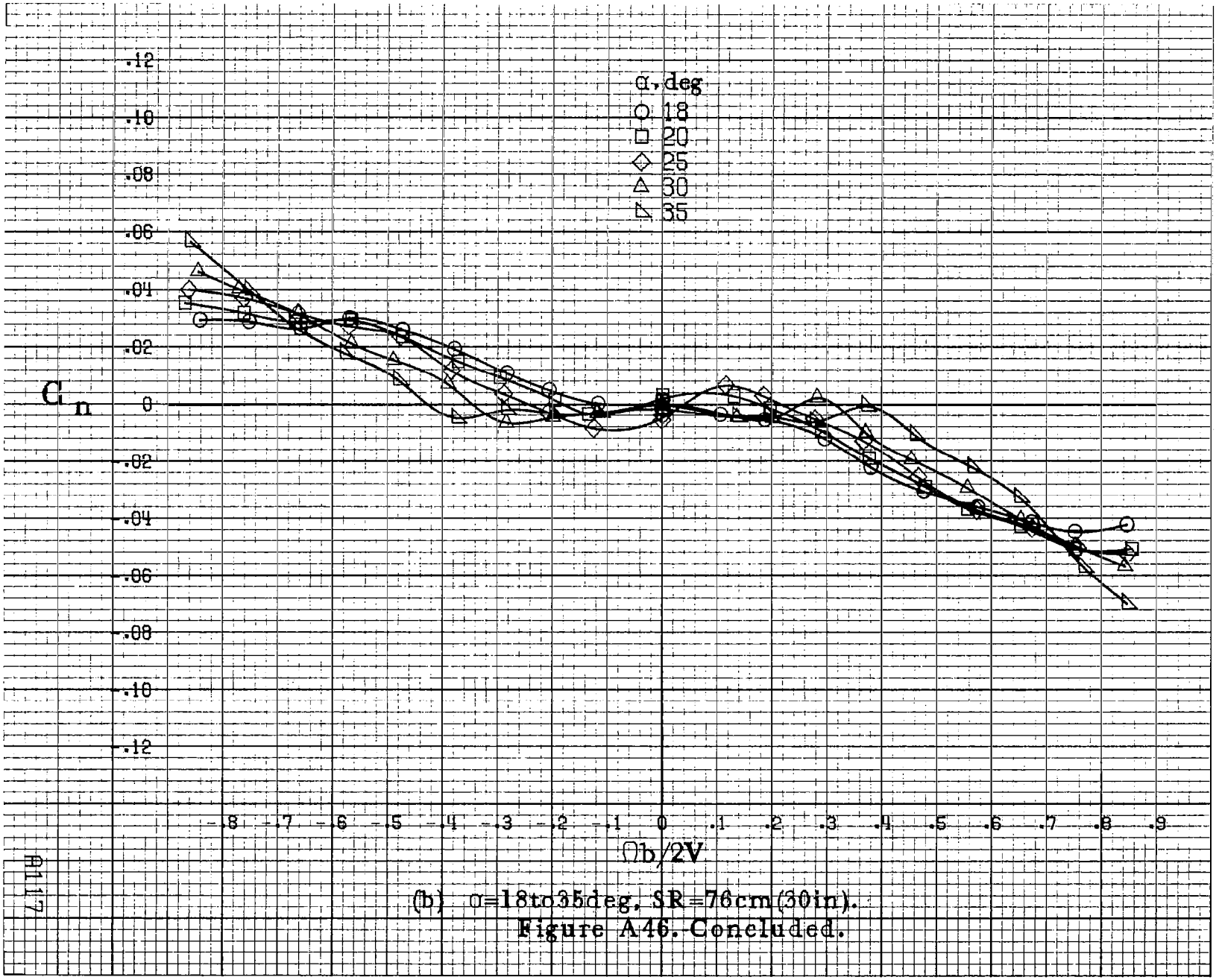

(b) α=18to35deg, SR=76cm(30in).

Figure A46. Concluded.

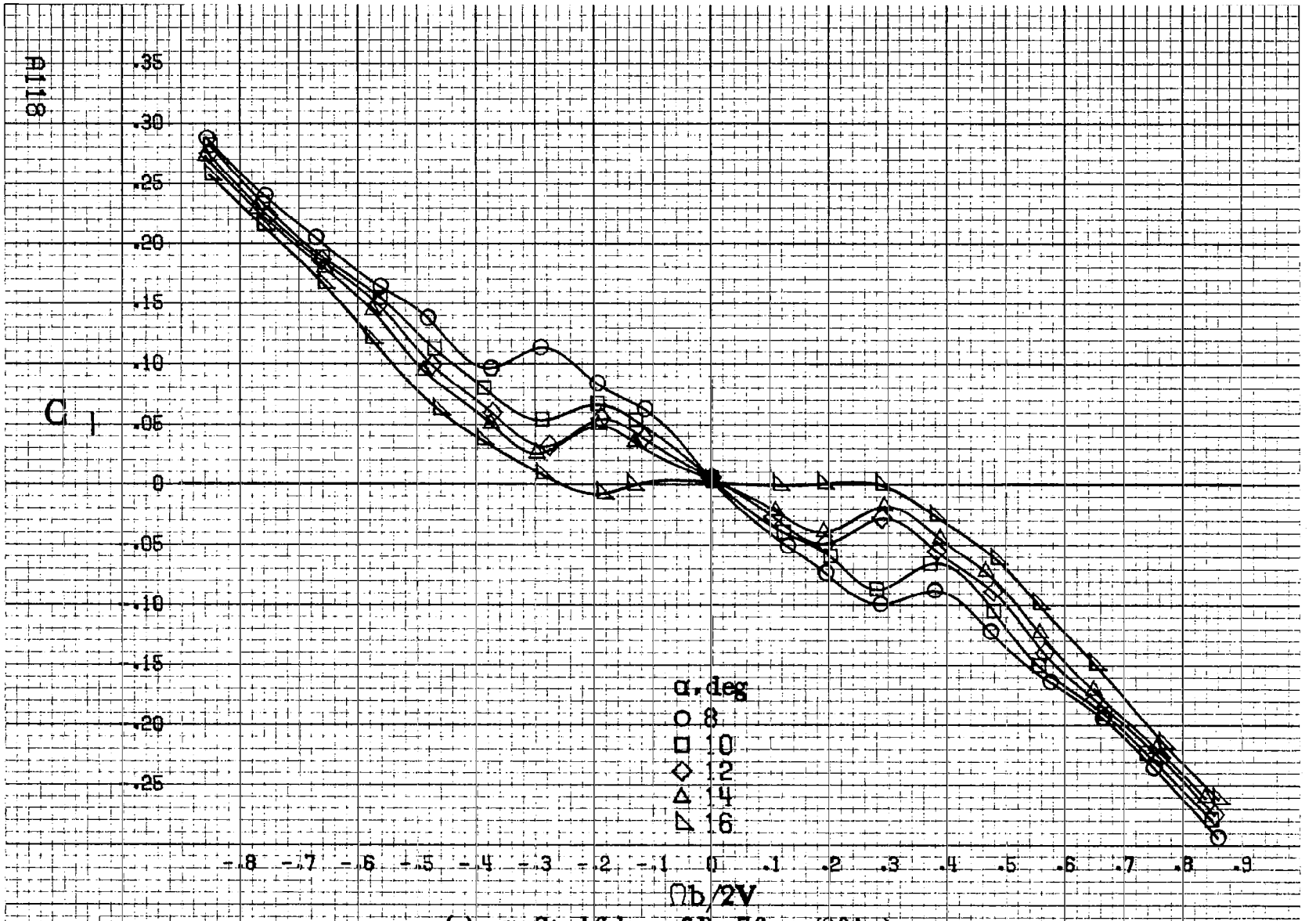

(a) α=8to16deg, SR=76cm(30in).

Figure A47. Effect of rotation rate and angle of attack on rolling-moment coefficient for configuration having outboard LE wing droop extended inboard 12.2cm(4.8in). $\delta_e = 0°$, $\delta_a = 0°$, $\delta_r = 0°$, $\beta = 0°$.

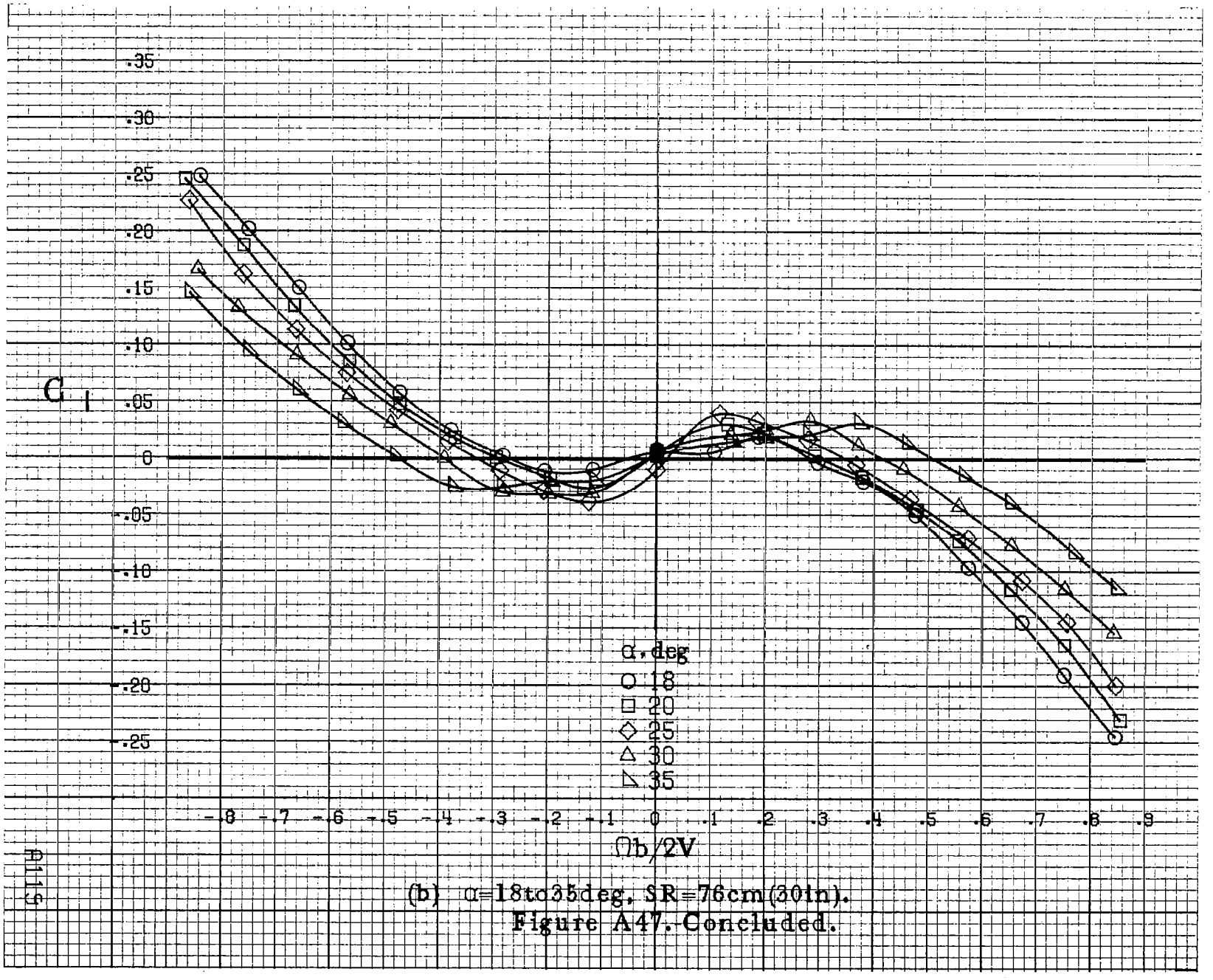

(b) α=18to35deg, SR=76cm(30in).

Figure A47.-Concluded.

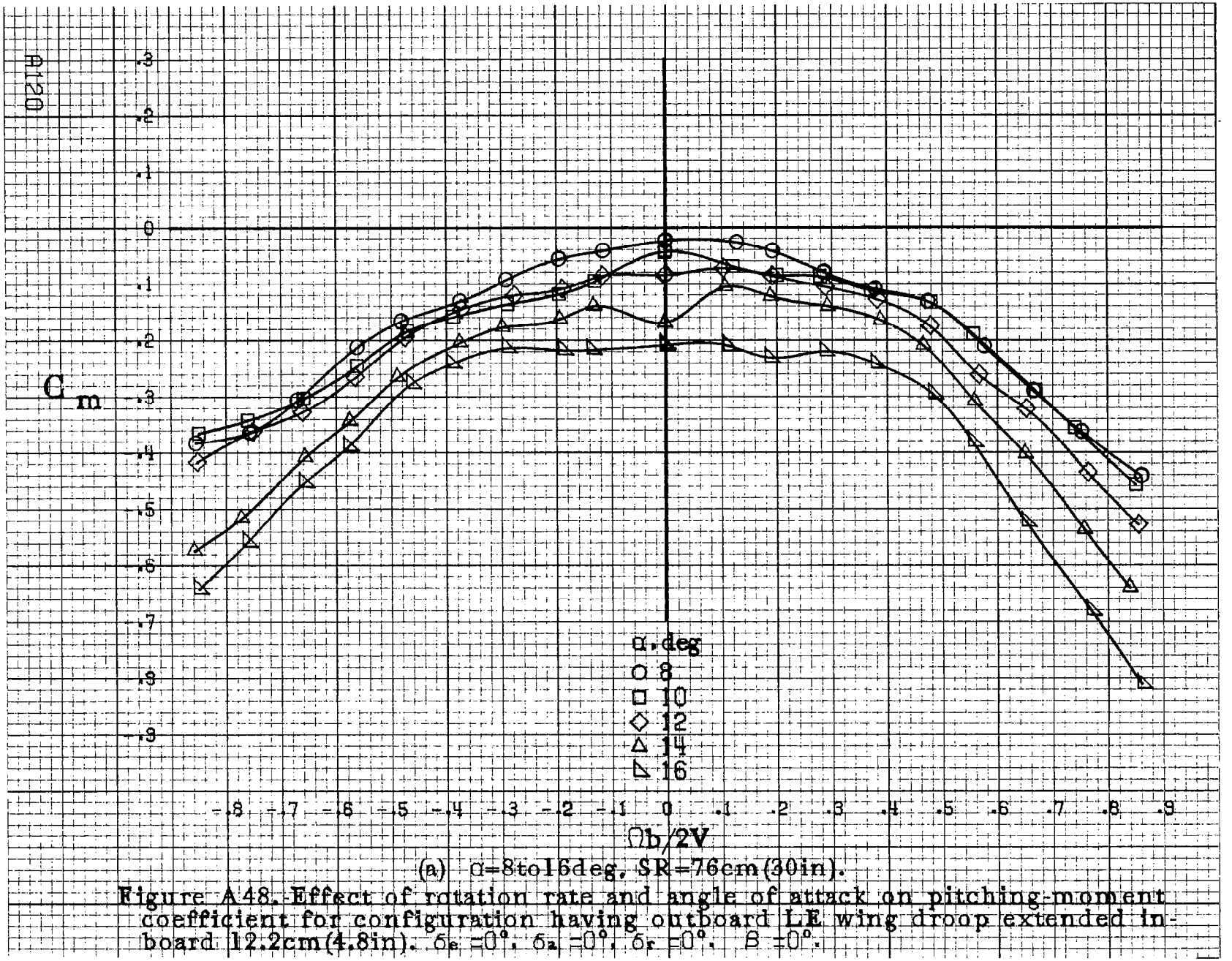

(a) α=8to16deg, SR=76cm(30in).

Figure A48.-Effect of rotation rate and angle of attack on pitching-moment coefficient for configuration having outboard LE wing droop extended inboard 12.2cm(4.8in). $\delta_e = 0°$, $\delta_a = 0°$, $\delta_r = 0°$, $\beta = 0°$.

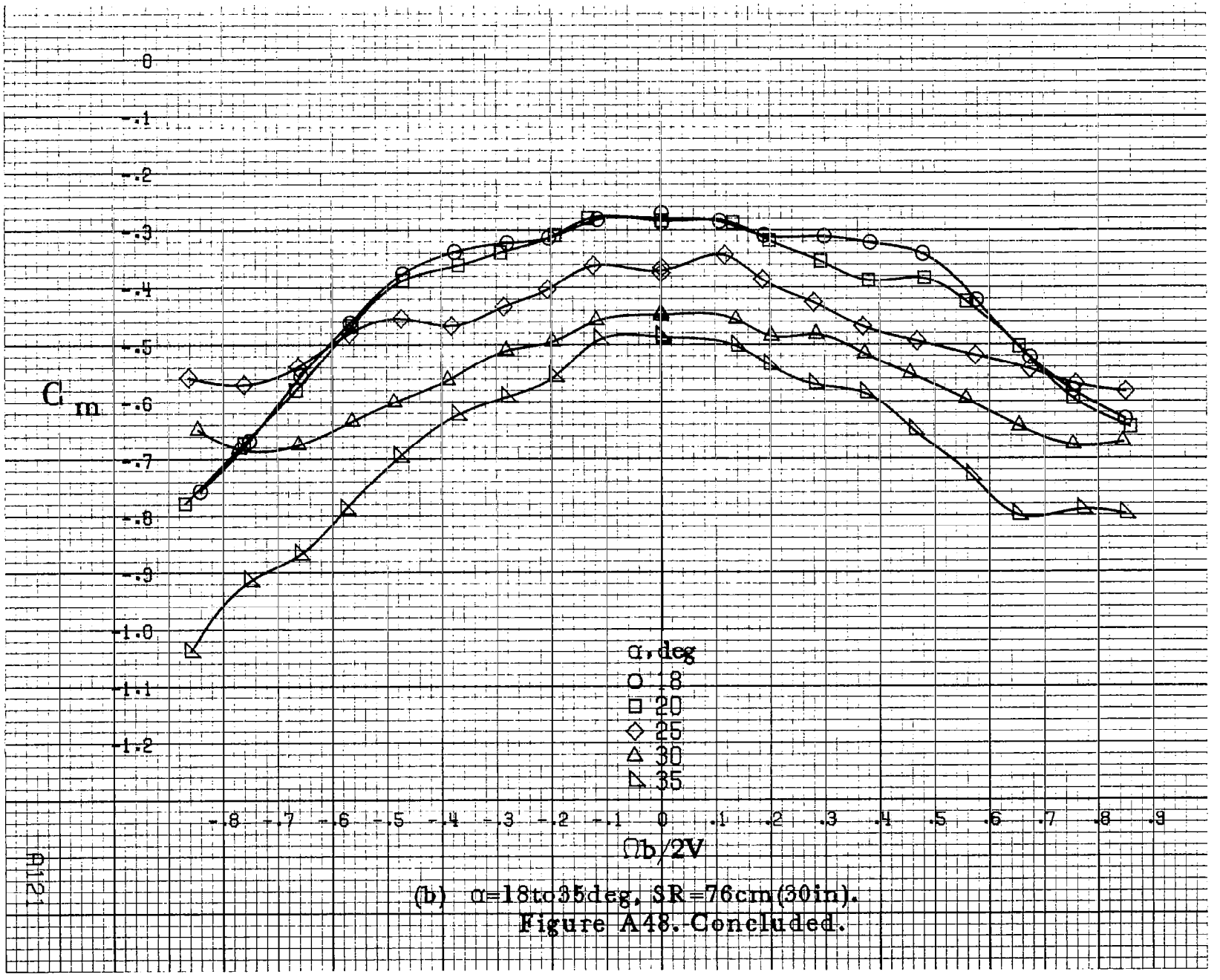

(b) α=18to35deg, SR=76cm(30in).

Figure A48.-Concluded.

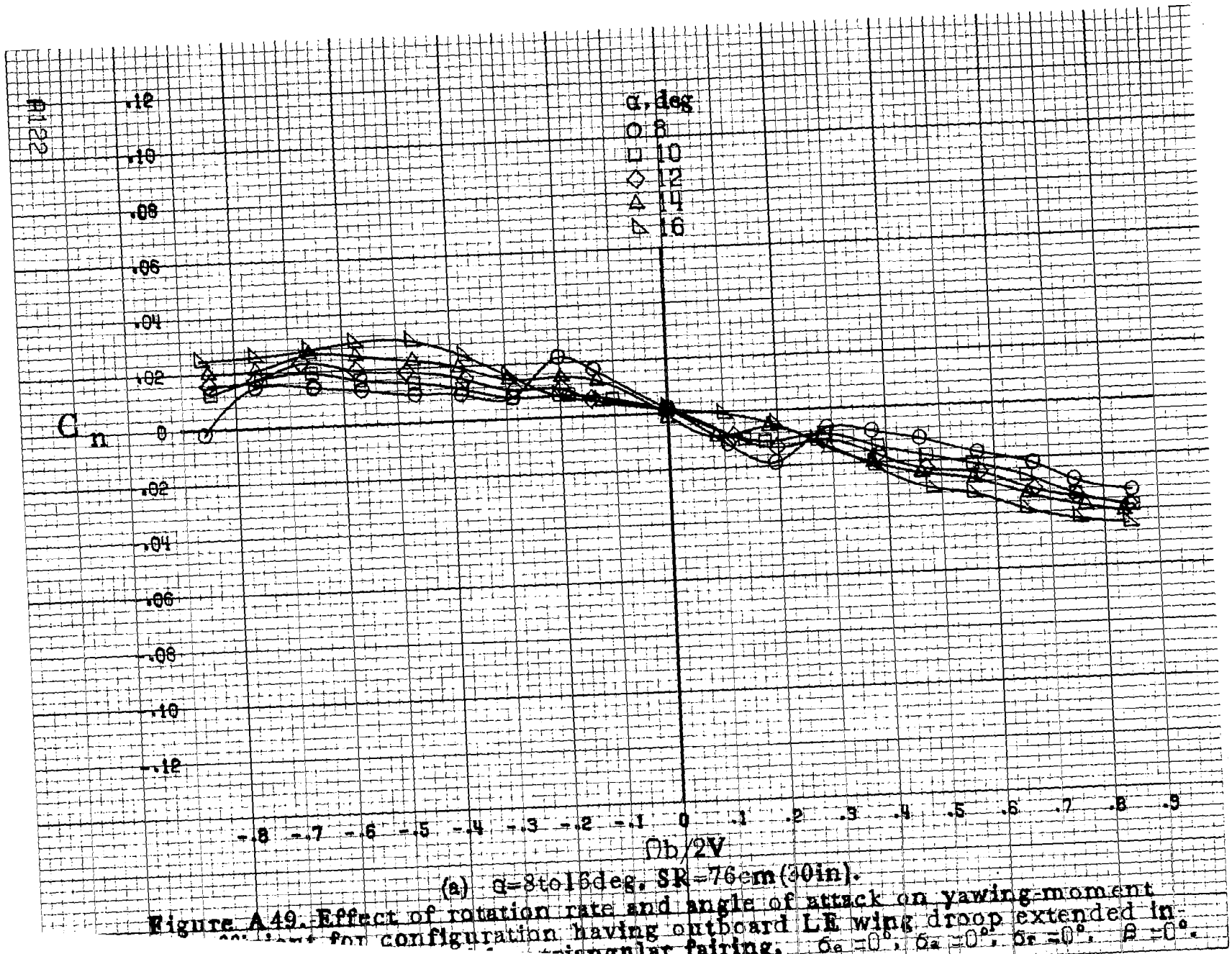

(a) α=8to16deg. SR=76cm(30in).

Figure A49. Effect of rotation rate and angle of attack on yawing-moment [illegible] for configuration having outboard LE wing droop extended in [illegible] triangular fairing. $\delta_e = 0°$, $\delta_a = 0°$, $\delta_r = 0°$, $\beta = 0°$.

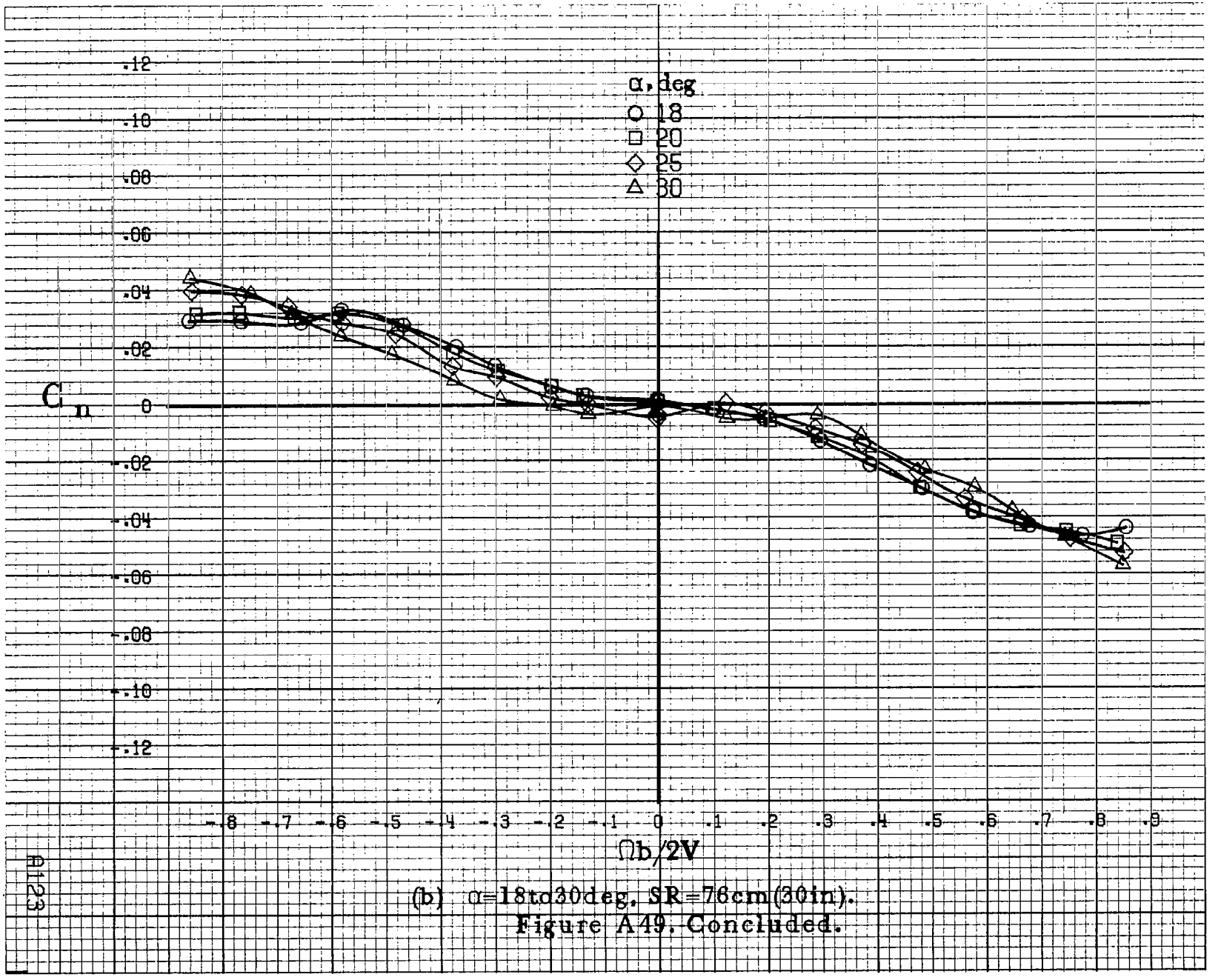

(b) α=18toα30deg, SR=76cm(30in).

Figure A49. Concluded.

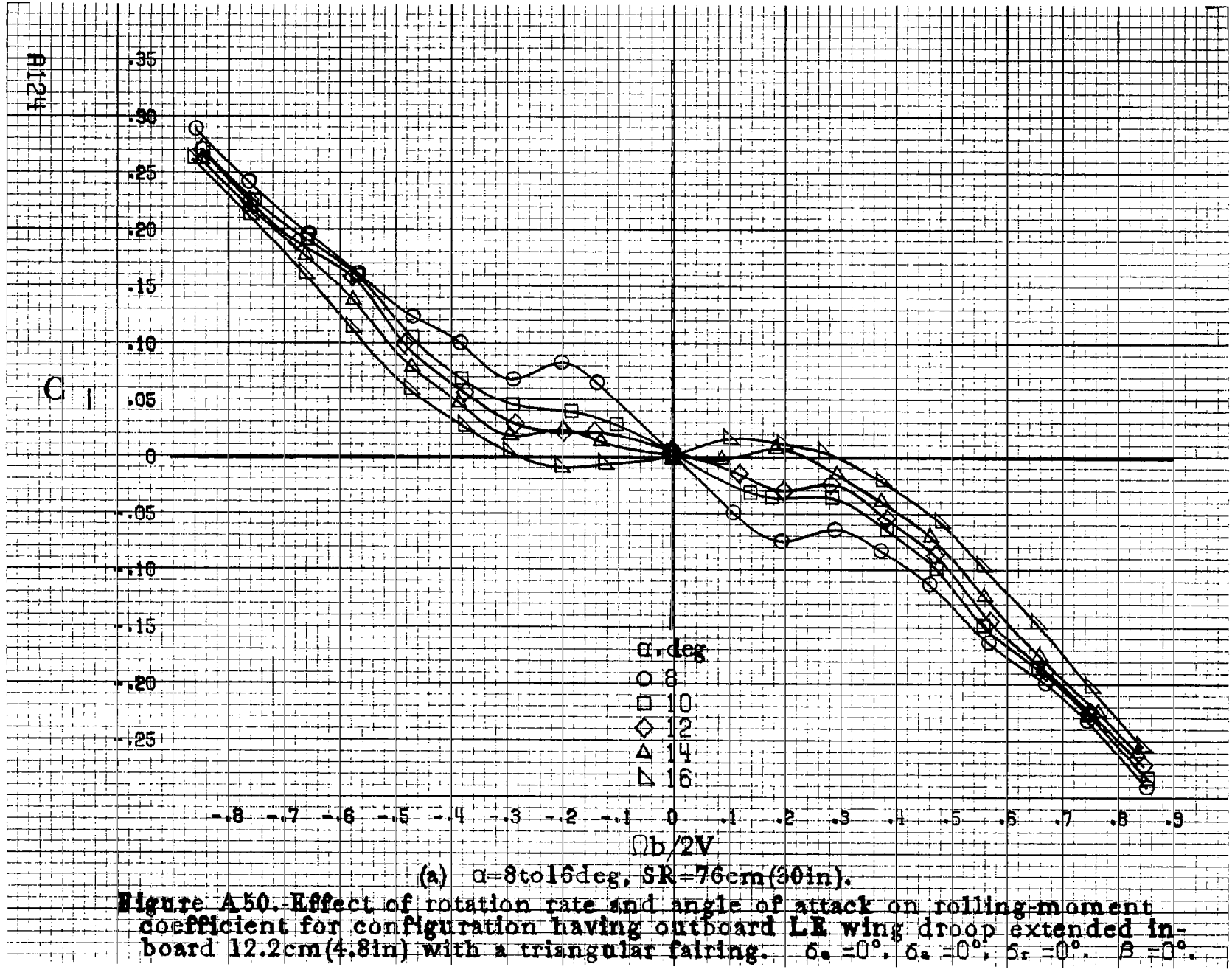

(a) α=8to16deg, SR=76cm(30in).

Figure A50.-Effect of rotation rate and angle of attack on rolling-moment coefficient for configuration having outboard LE wing droop extended inboard 12.2cm(4.8in) with a triangular fairing. $\delta_e = 0°$, $\delta_a = 0°$, $\delta_r = 0°$, $\beta = 0°$.

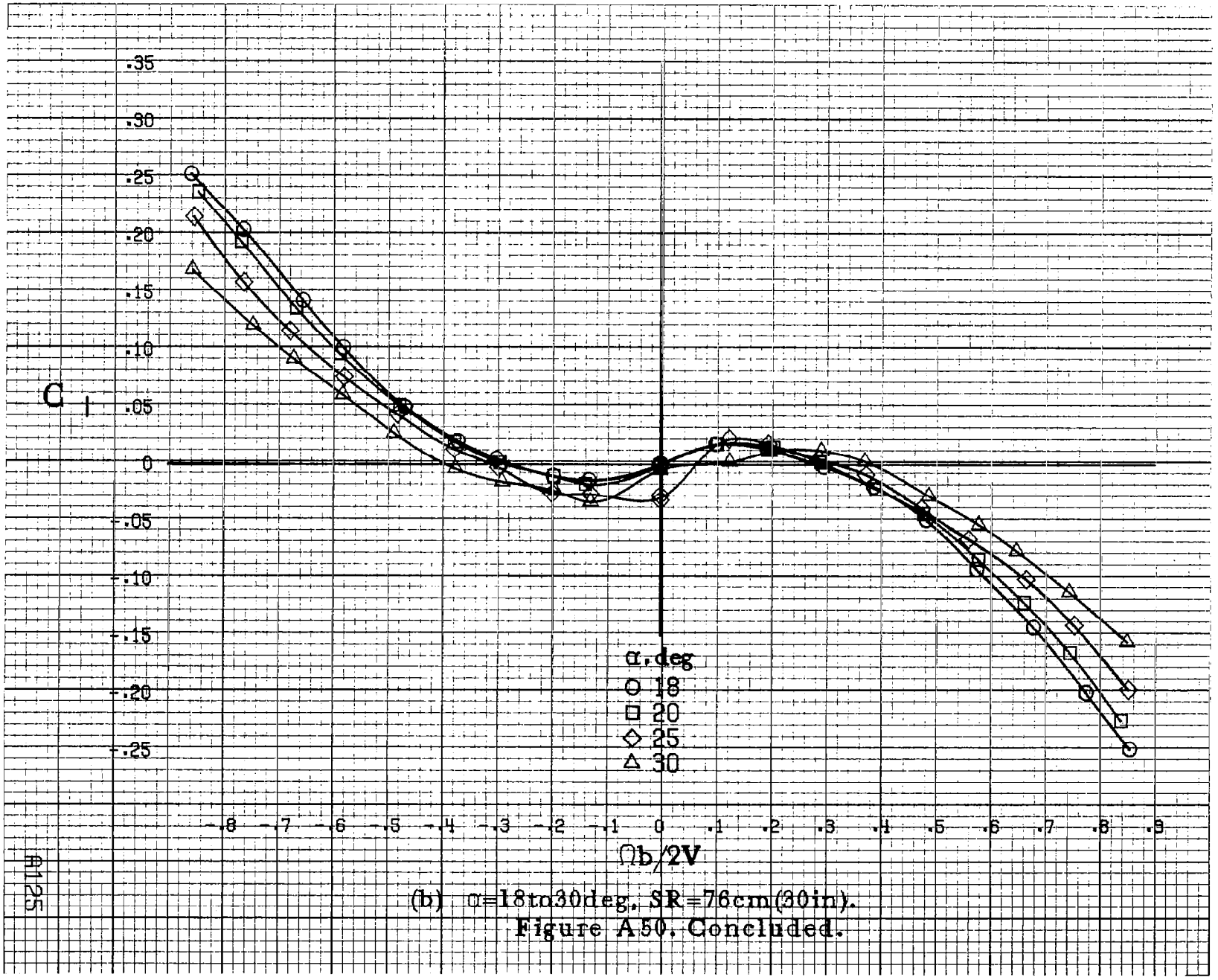

(b) α=18to30deg, SR=76cm(30in).

Figure A50. Concluded.

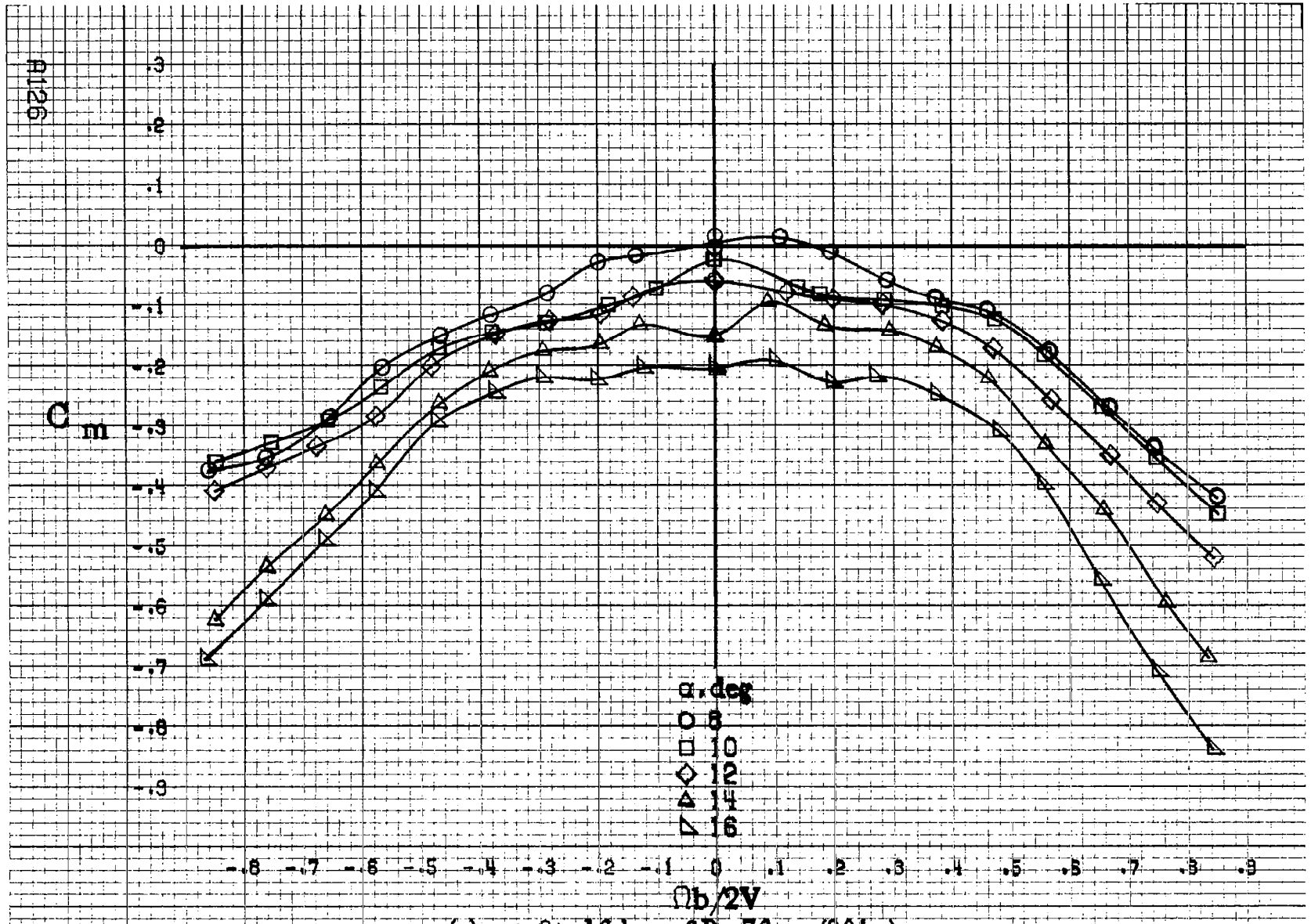

(a) α=8to16deg, SR=76cm(30in).

Figure A51.-Effect of rotation rate and angle of attack on pitching-moment coefficient for configuration having outboard LE wing droop extended inboard 12.2cm(4.8in) with a triangular fairing. $\delta_e = 0°$, $\delta_a = 0°$, $\delta_r = 0°$. $\beta = 0°$.

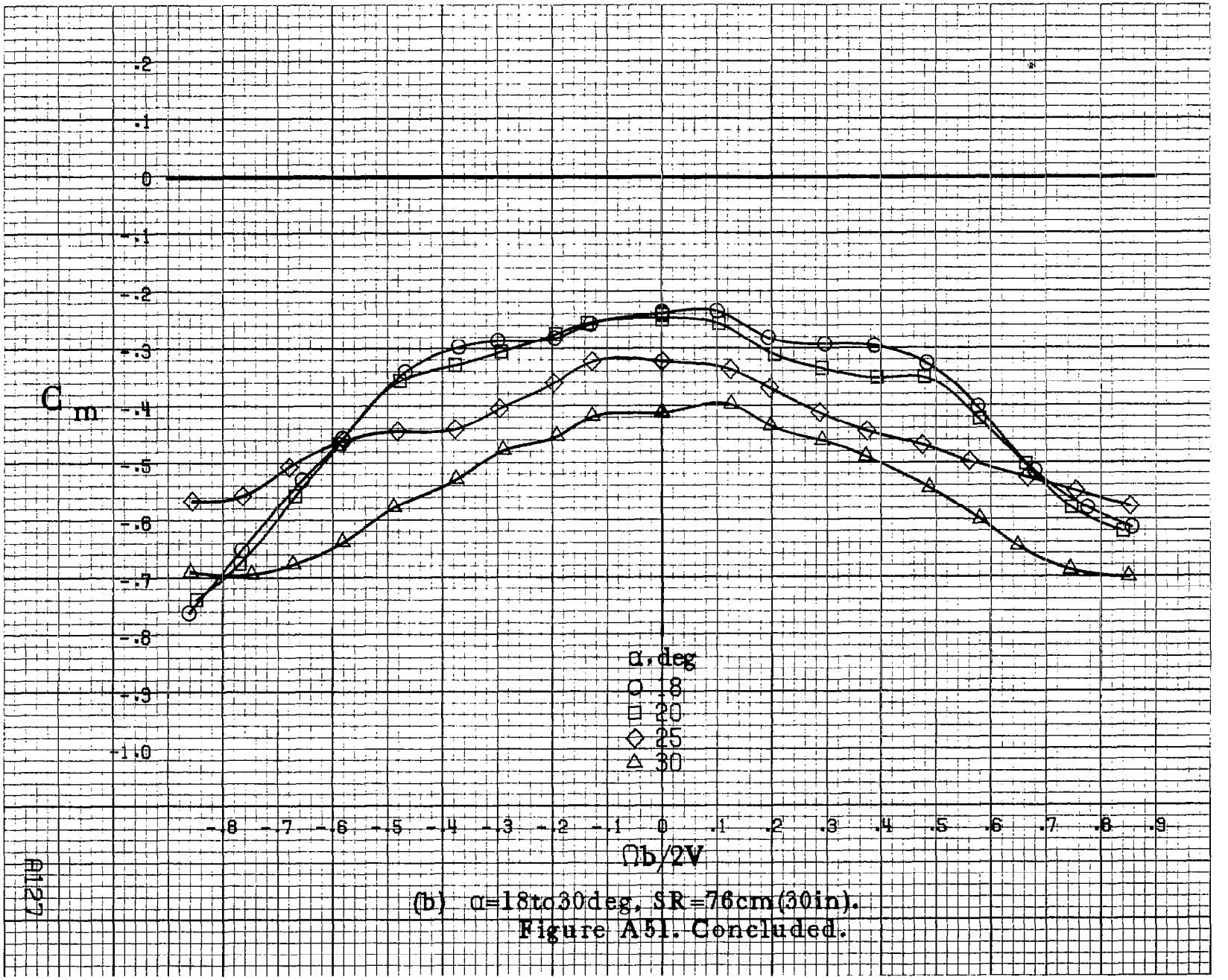

(b) α=18to30deg, SR=76cm(30in).

Figure A51. Concluded.

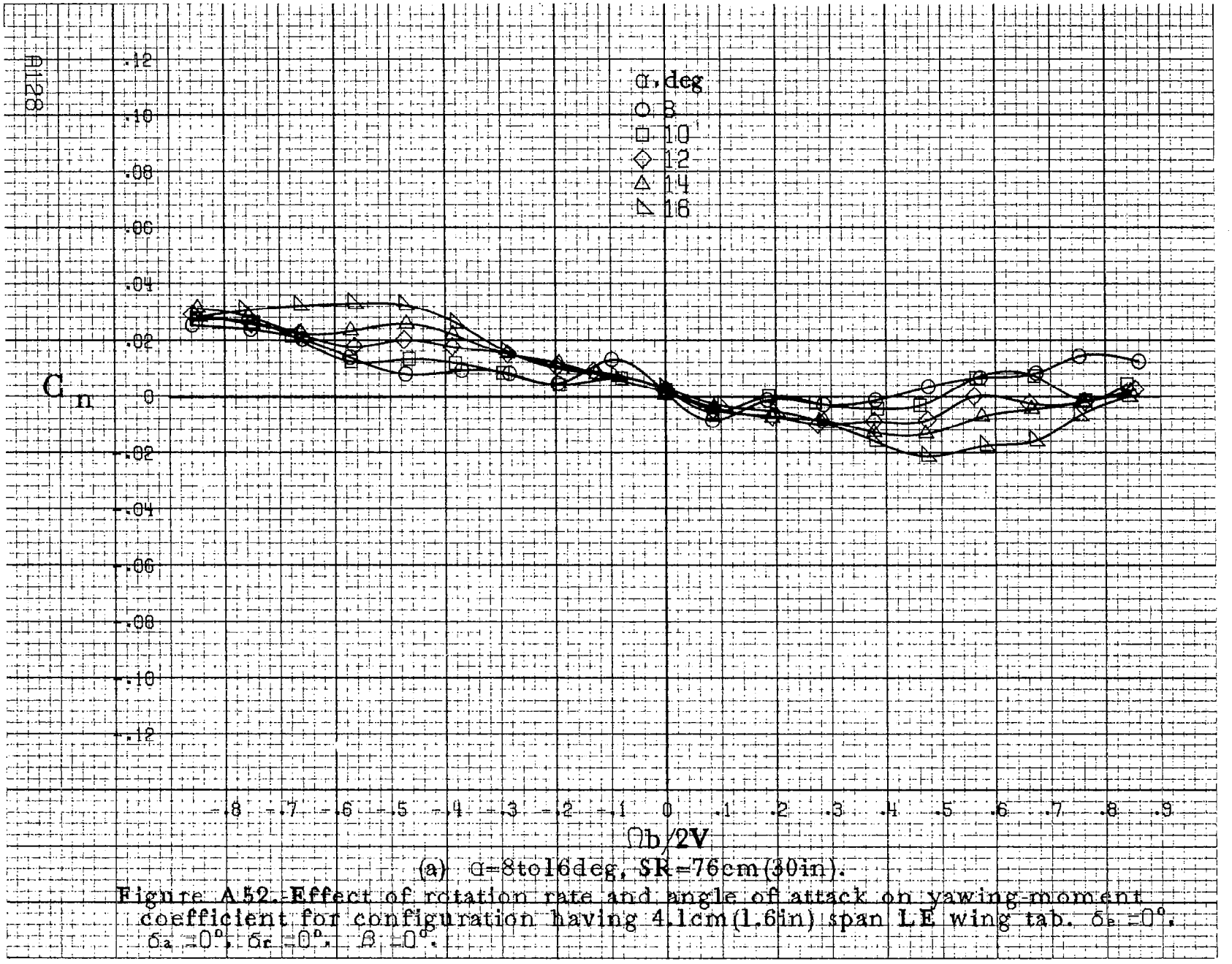

(a) α=8to16deg, SR=76cm(30in).

Figure A52.-Effect of rotation rate and angle of attack on yawing-moment coefficient for configuration having 4.1cm(1.6in) span LE wing tab. $\delta_e = 0°$, $\delta_a = 0°$, $\delta_r = 0°$, $\beta = 0°$.

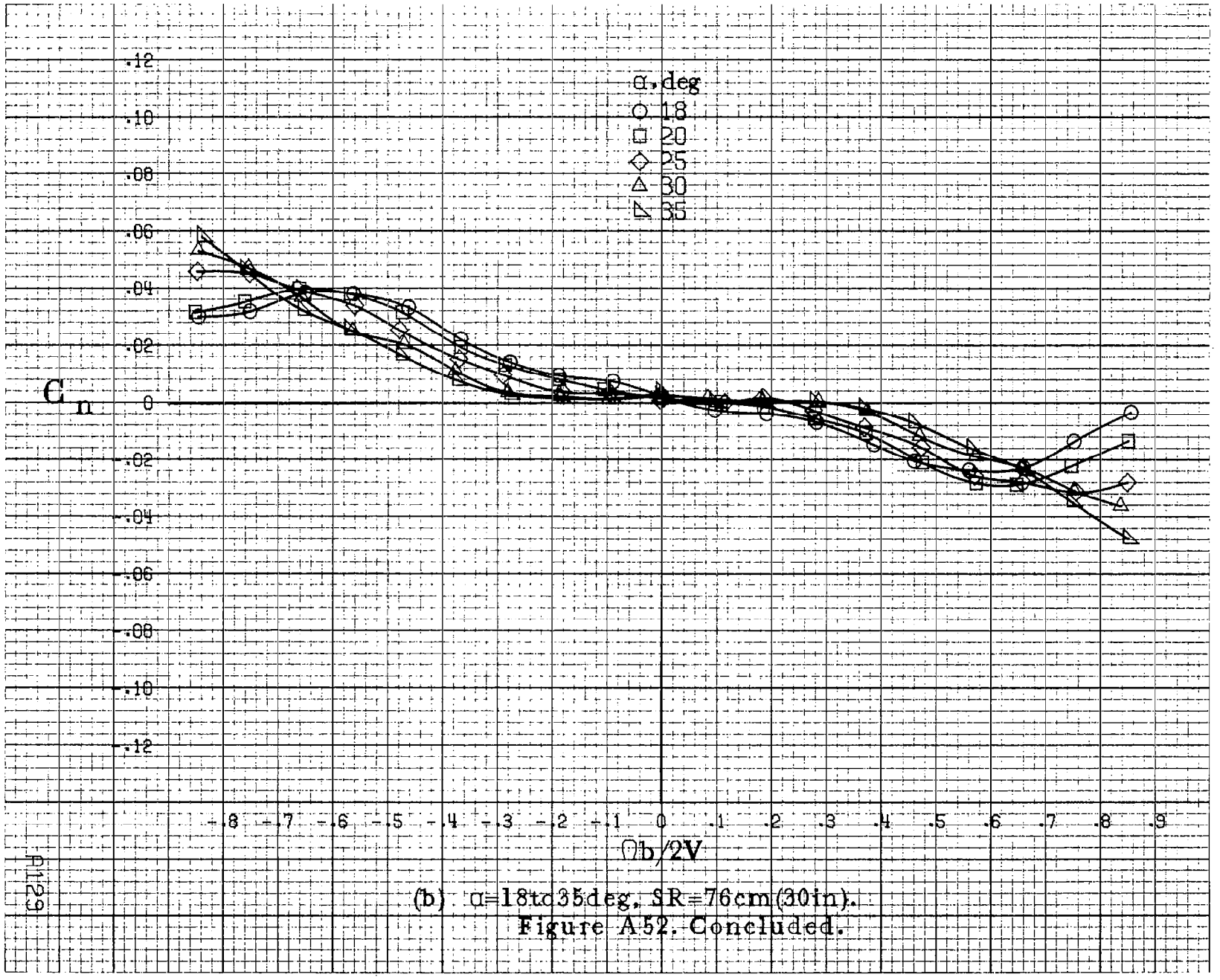

(b) α=18to35deg, SR=76cm(30in).

Figure A52. Concluded.

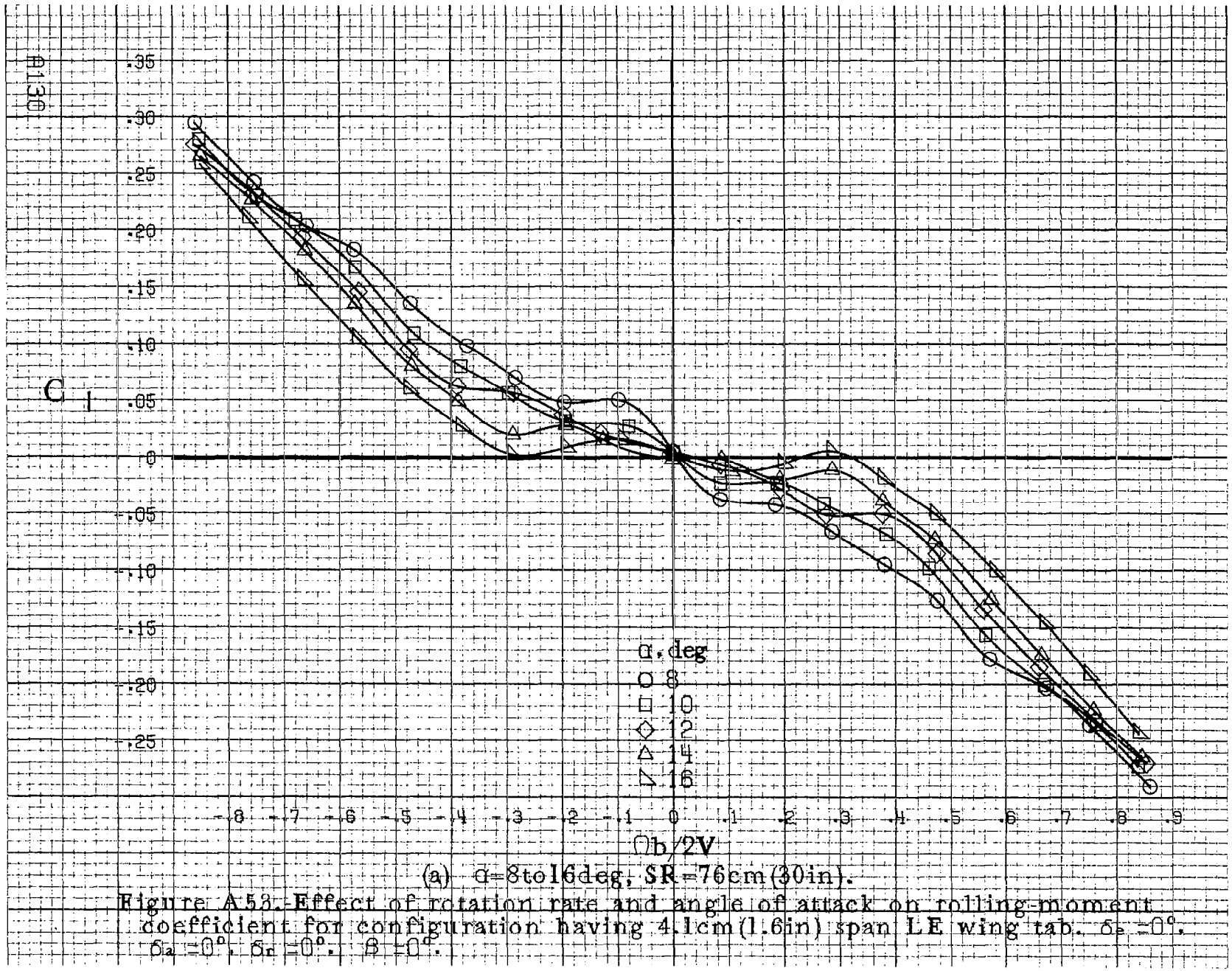

(a) α=8to16deg, SR=76cm(30in).

Figure A53.-Effect of rotation rate and angle of attack on rolling-moment coefficient for configuration having 4.1cm(1.6in) span LE wing tab. $\delta_e = 0°$, $\delta_a = 0°$, $\delta_r = 0°$, $\beta = 0°$.

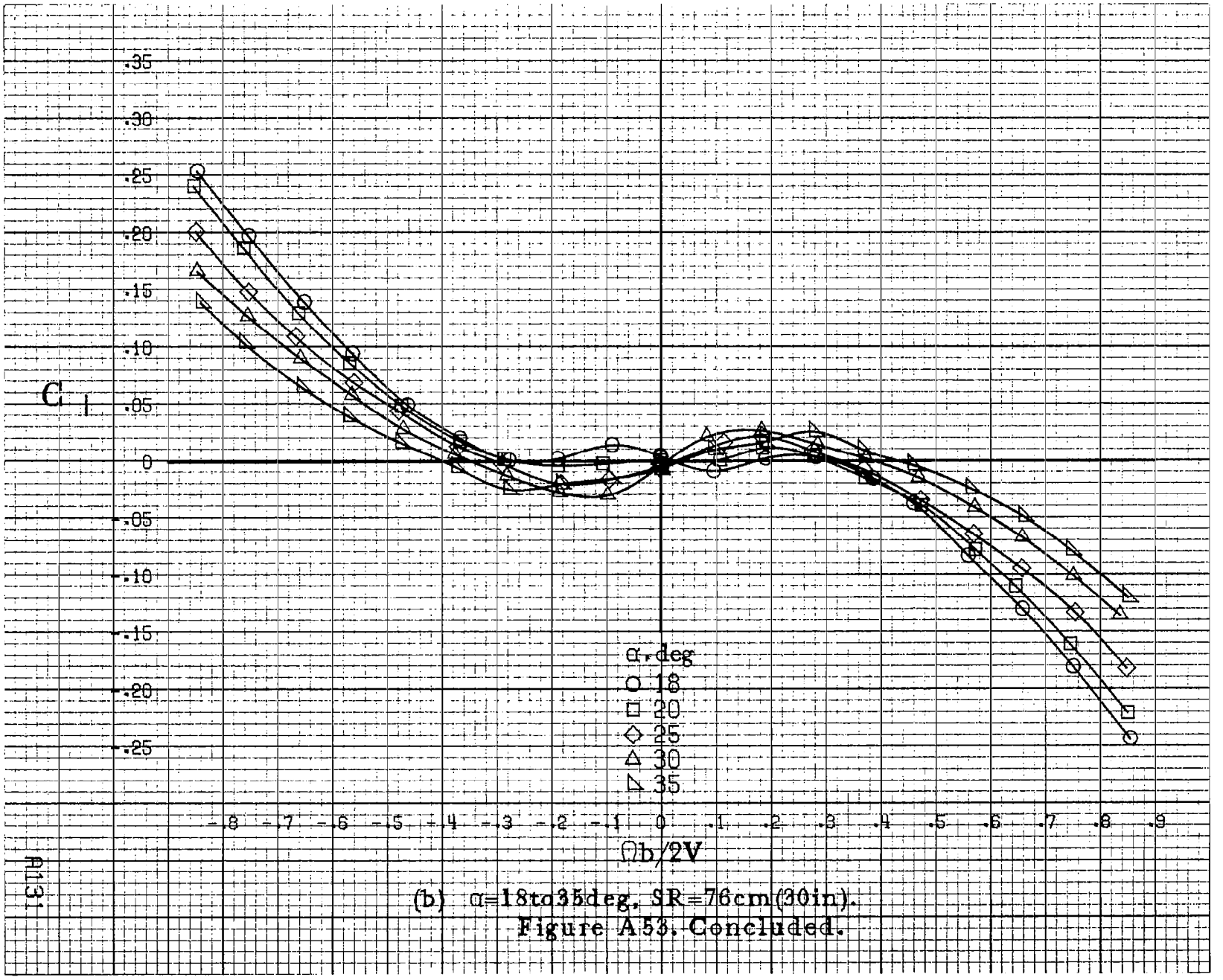

(b) α=18to35deg, SR=76cm(30in).

Figure A53. Concluded.

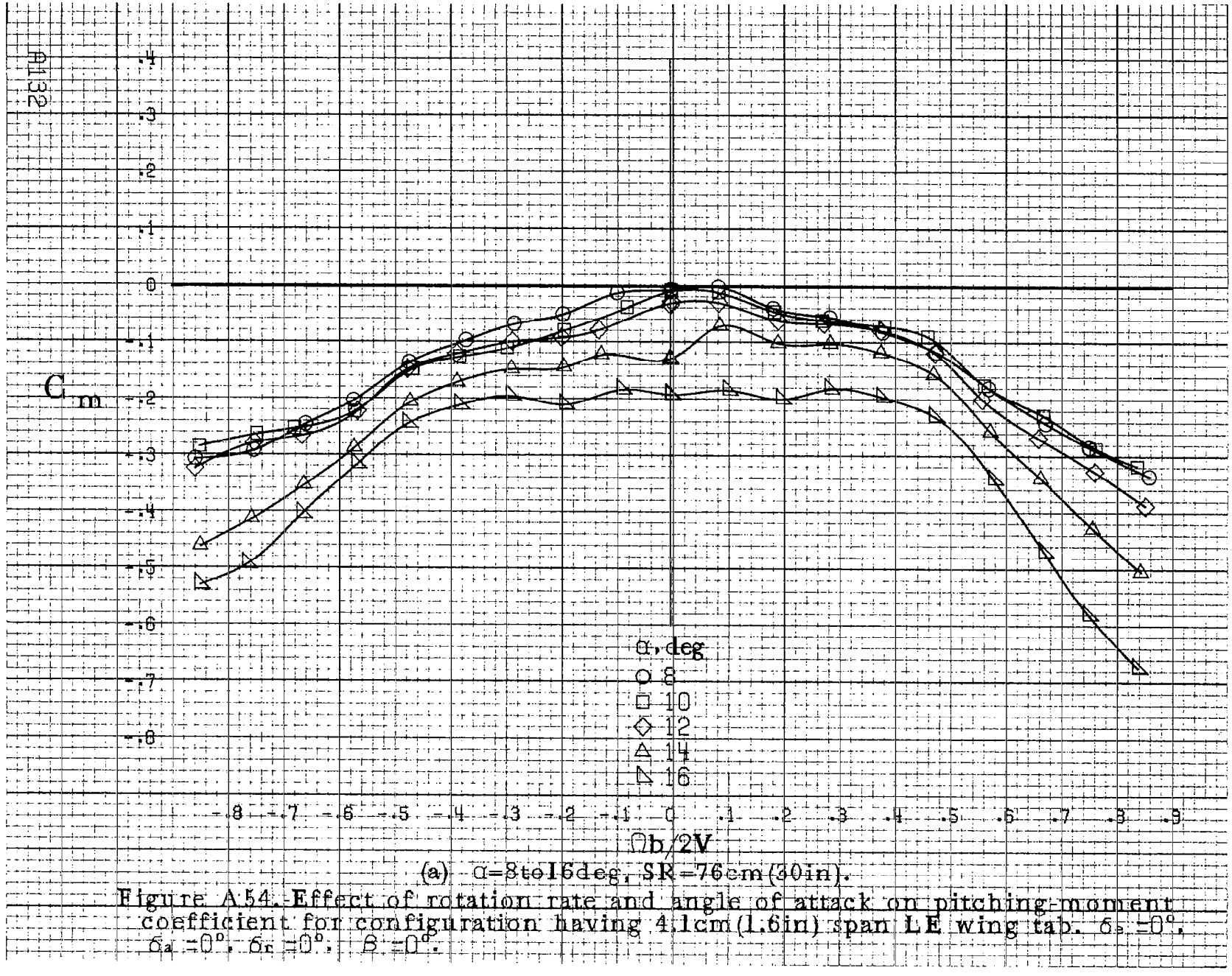

(a) α=8to16deg, SR=76cm(30in).

Figure A.54. Effect of rotation rate and angle of attack on pitching-moment coefficient for configuration having 4.1cm(1.6in) span LE wing tab. $\delta_s = 0°$, $\delta_a = 0°$, $\delta_r = 0°$, $\beta = 0°$.

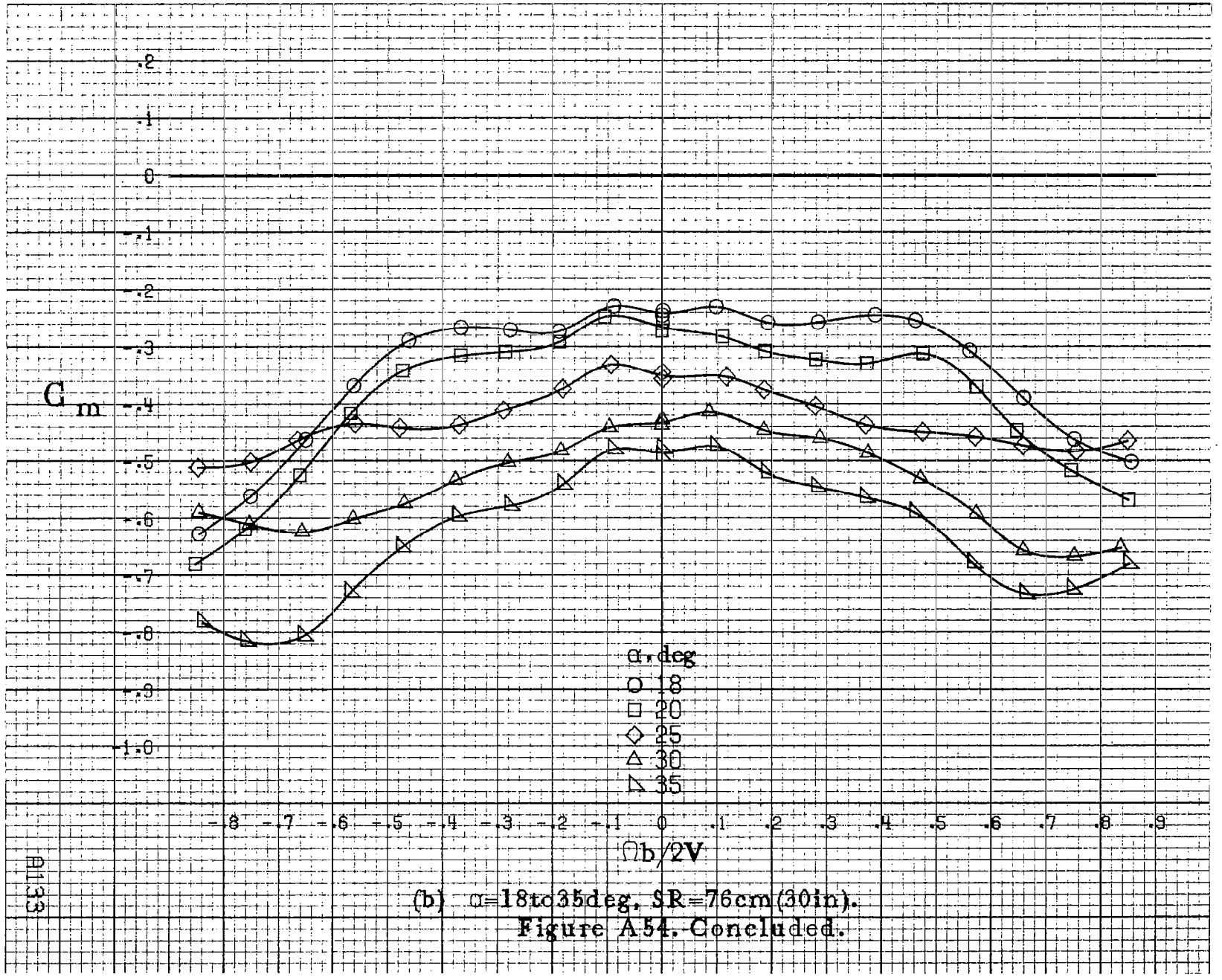

(b) α=18to35deg, SR=76cm(30in).

Figure A54.-Concluded.

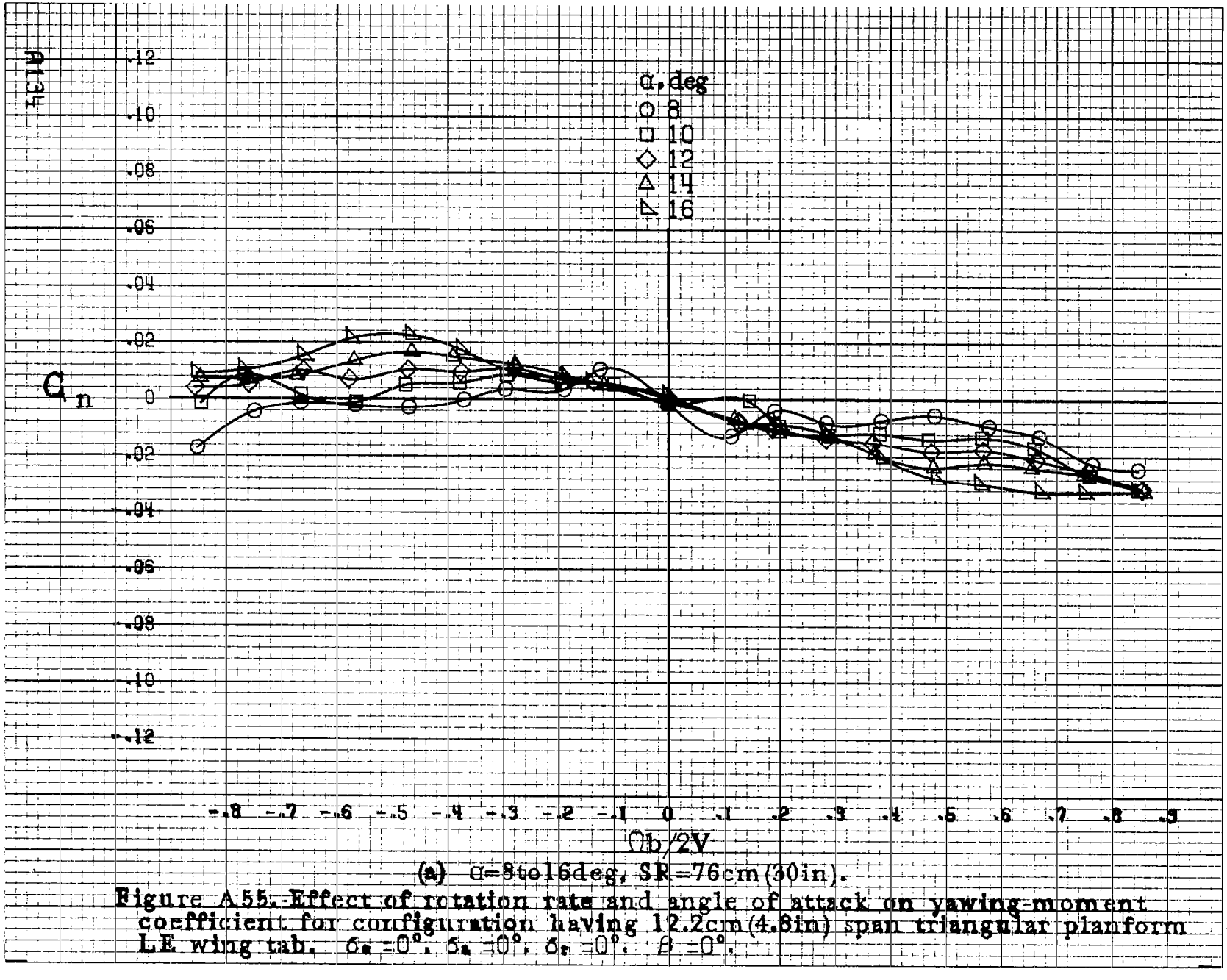

(a) α=8to16deg, SR=76cm(30in).

Figure A.55.-Effect of rotation rate and angle of attack on yawing-moment coefficient for configuration having 12.2cm(4.8in) span triangular planform LE wing tab. $\delta_e = 0°$, $\delta_a = 0°$, $\delta_r = 0°$, $\beta = 0°$.

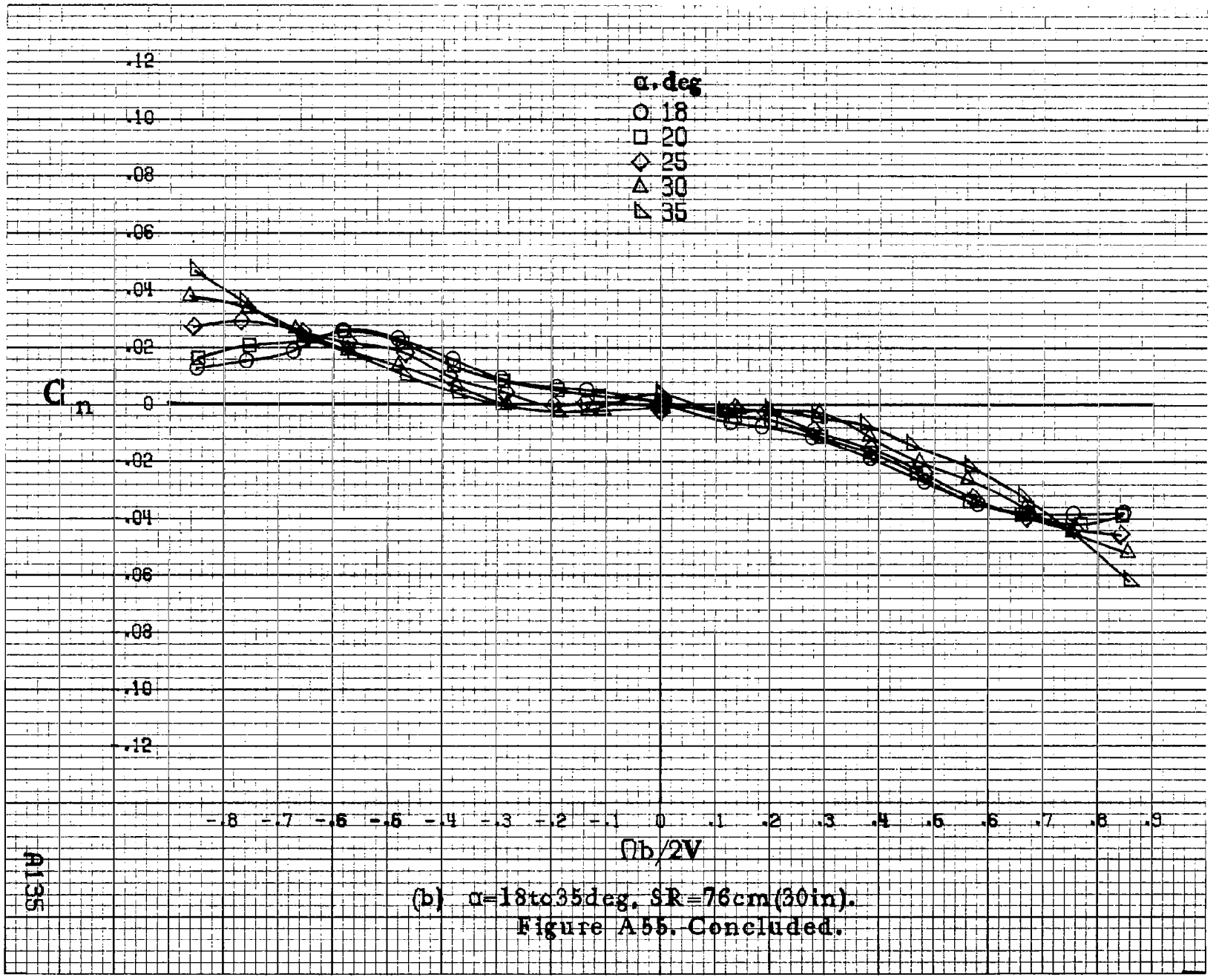

(b) α=18to35deg. SR=76cm(30in).

Figure A55.-Concluded.

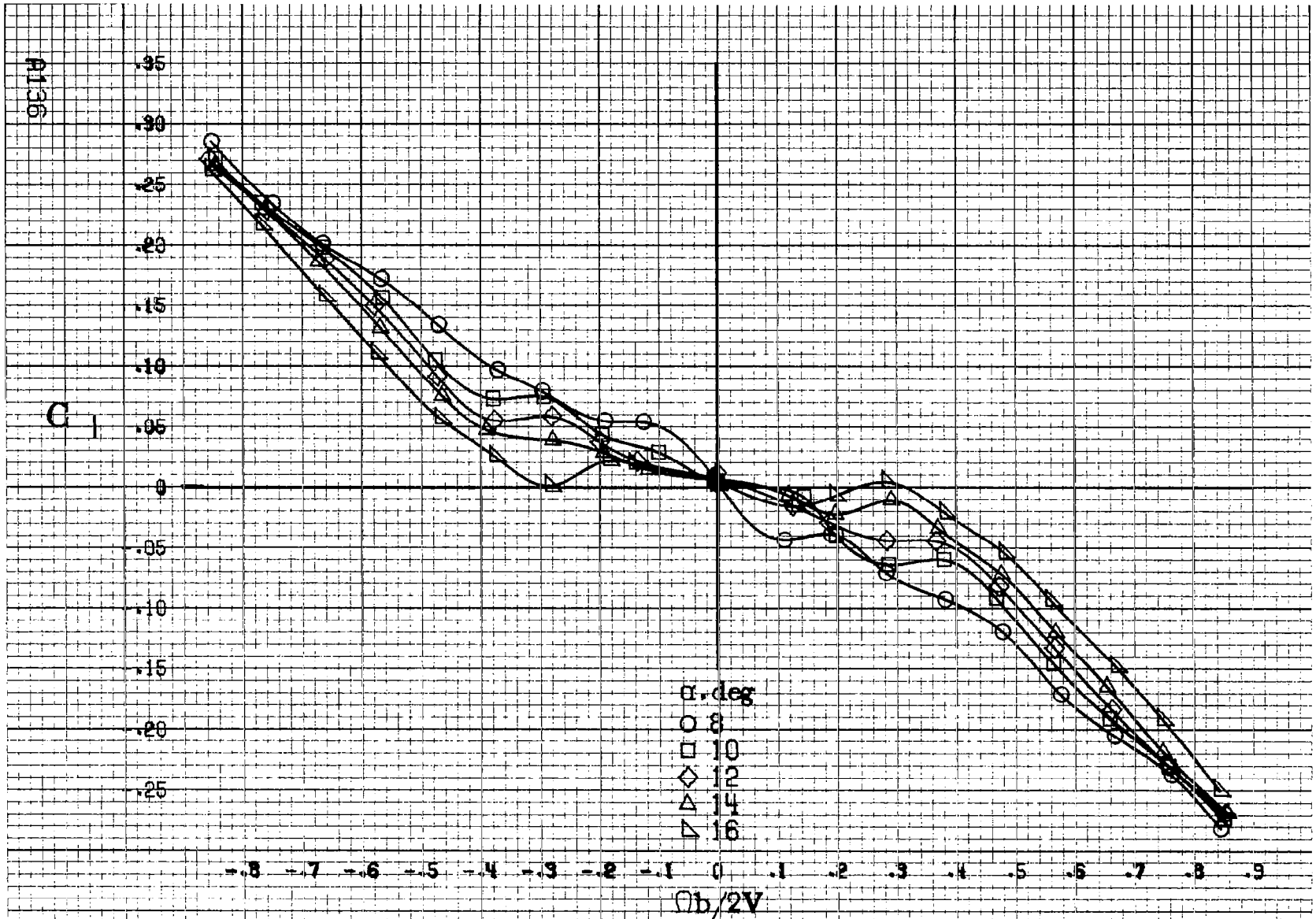

(a) α=8to16deg, SR=76cm(30in).

Figure A56.-Effect of rotation rate and angle of attack on rolling-moment coefficient for configuration having 12.2cm(4.8in) span triangular planform LE wing tab. $\delta_e = 0°$, $\delta_a = 0°$, $\delta_r = 0°$. $\beta = 0°$.

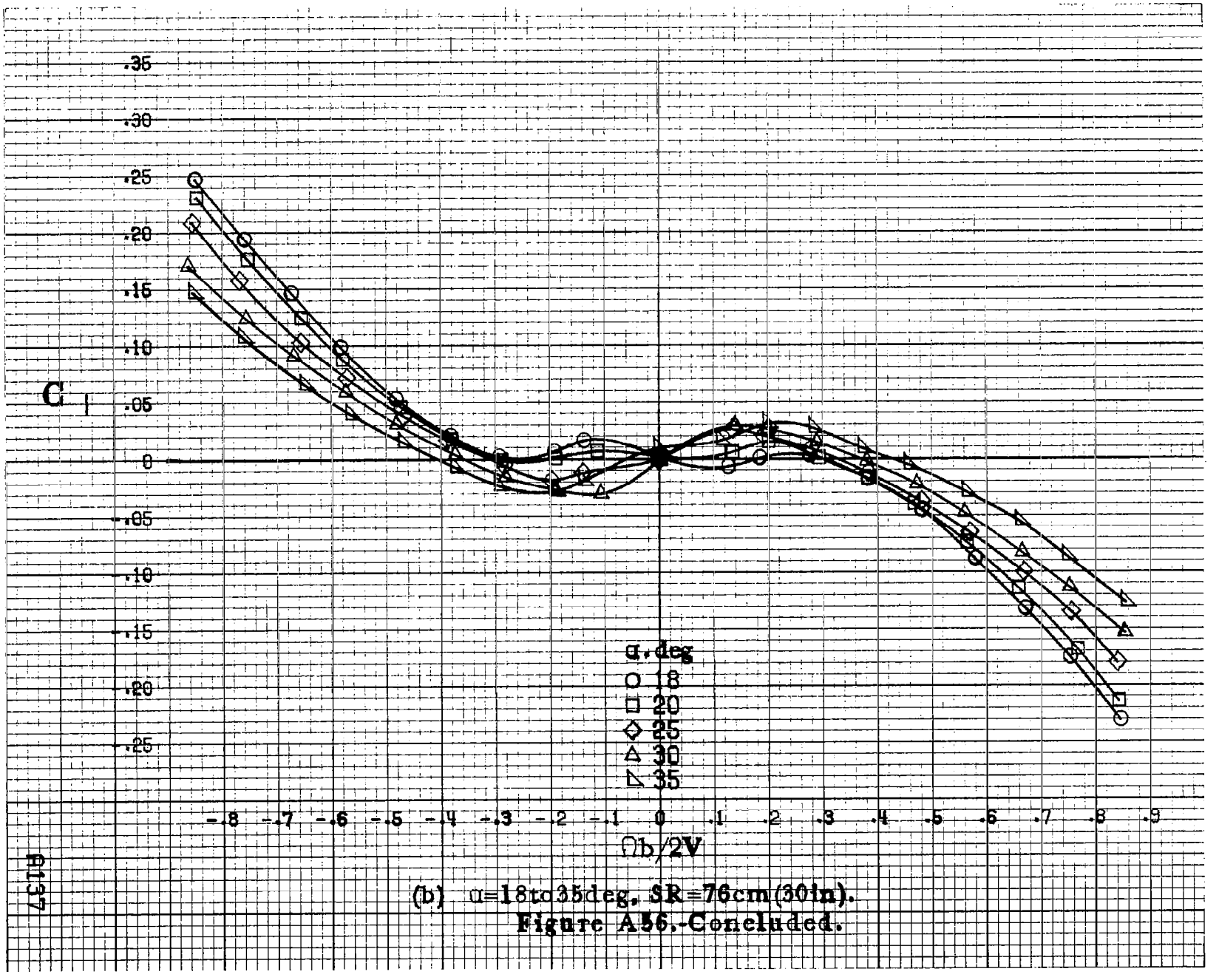

(b) α=18to35deg, SR=76cm(30in).

Figure A56.-Concluded.

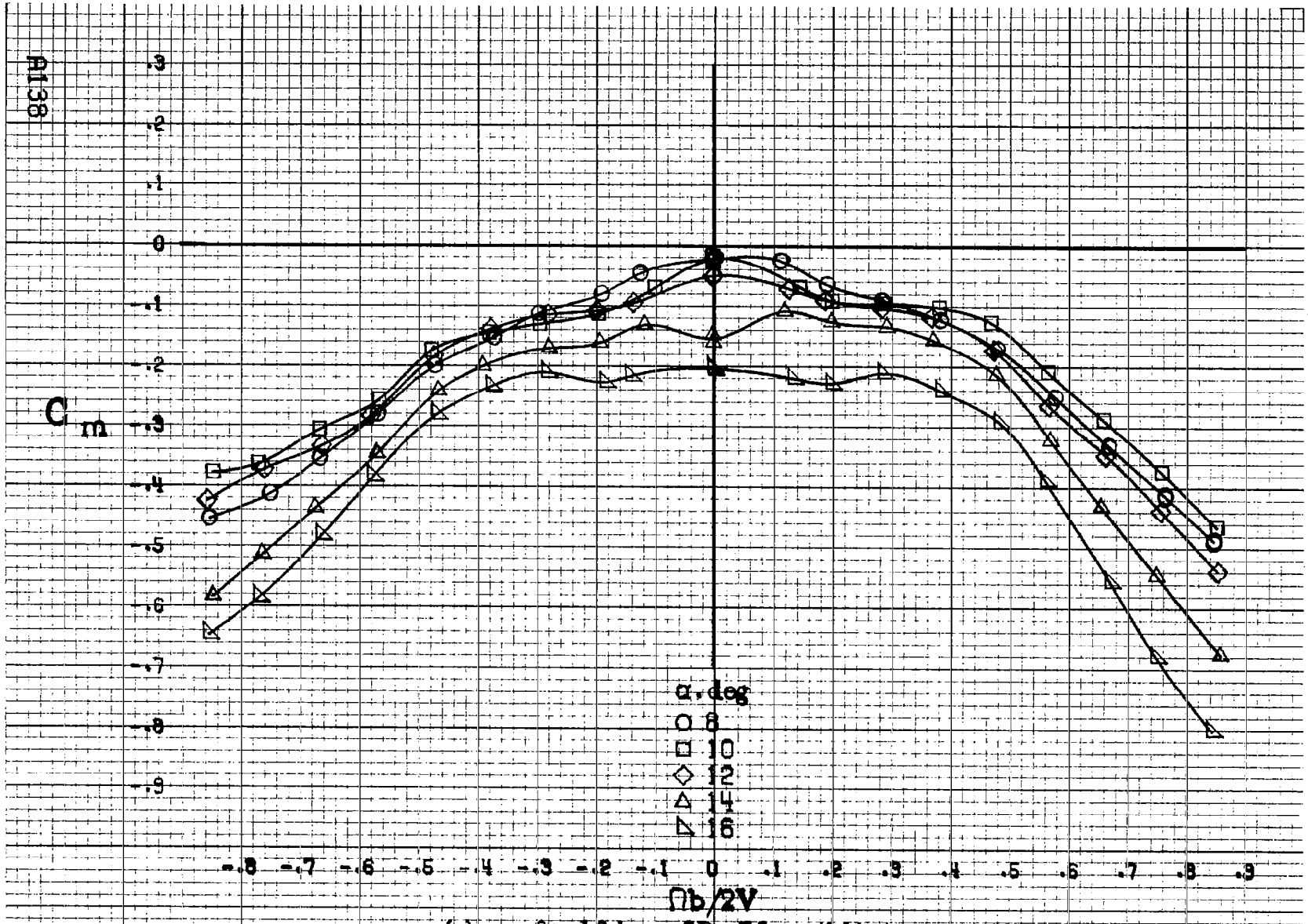

(a) α=8to16deg, SR=76cm(30in).

Figure A57.-Effect of rotation rate and angle of attack on pitching-moment coefficient for configuration having 12.2cm(4.8in) span triangular planform LE wing tab. $\delta_e = 0°$, $\delta_a = 0°$, $\delta_r = 0°$, $\beta = 0°$.

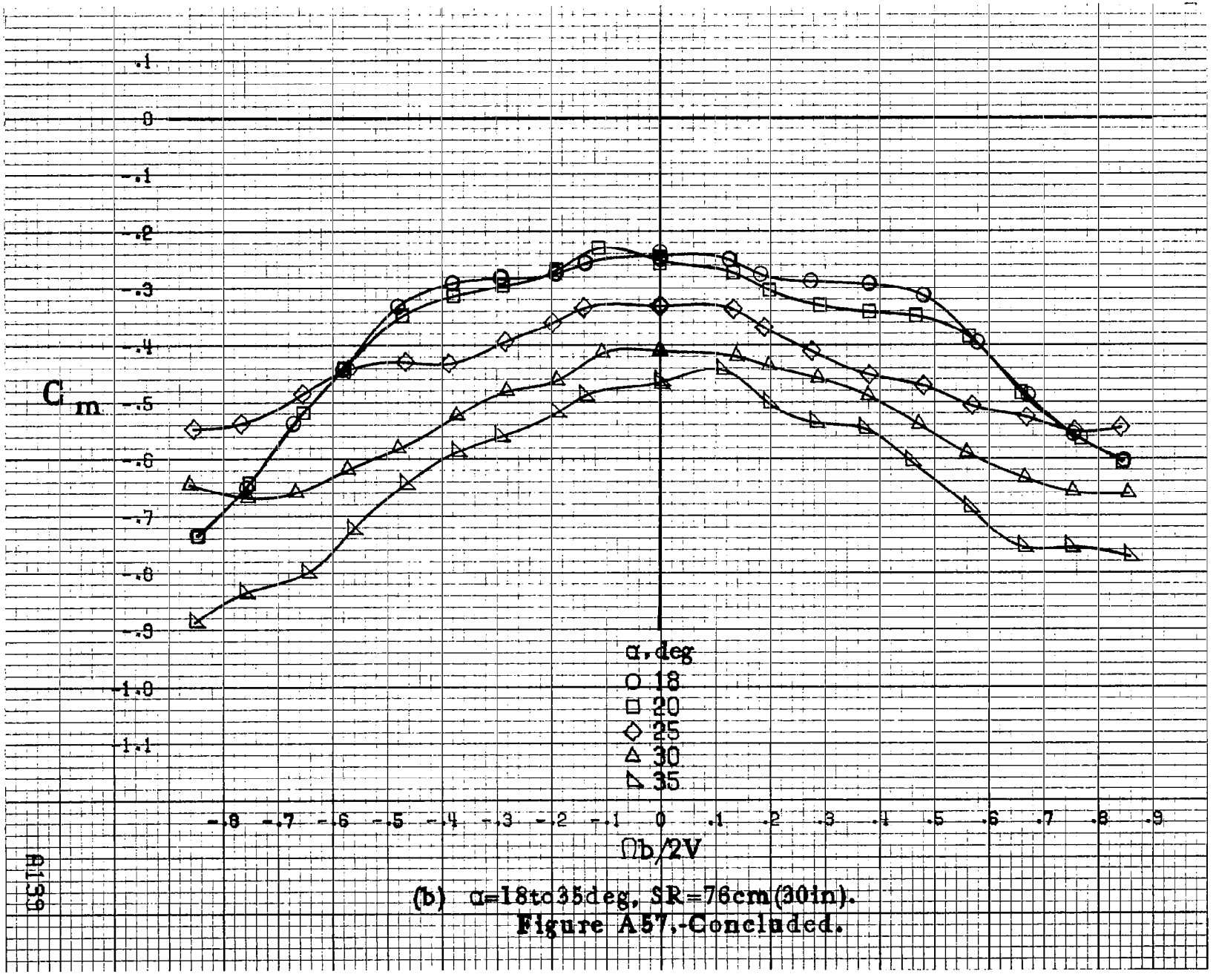

(b) α=18to35deg, SR=76cm(30in).

Figure A57.-Concluded.

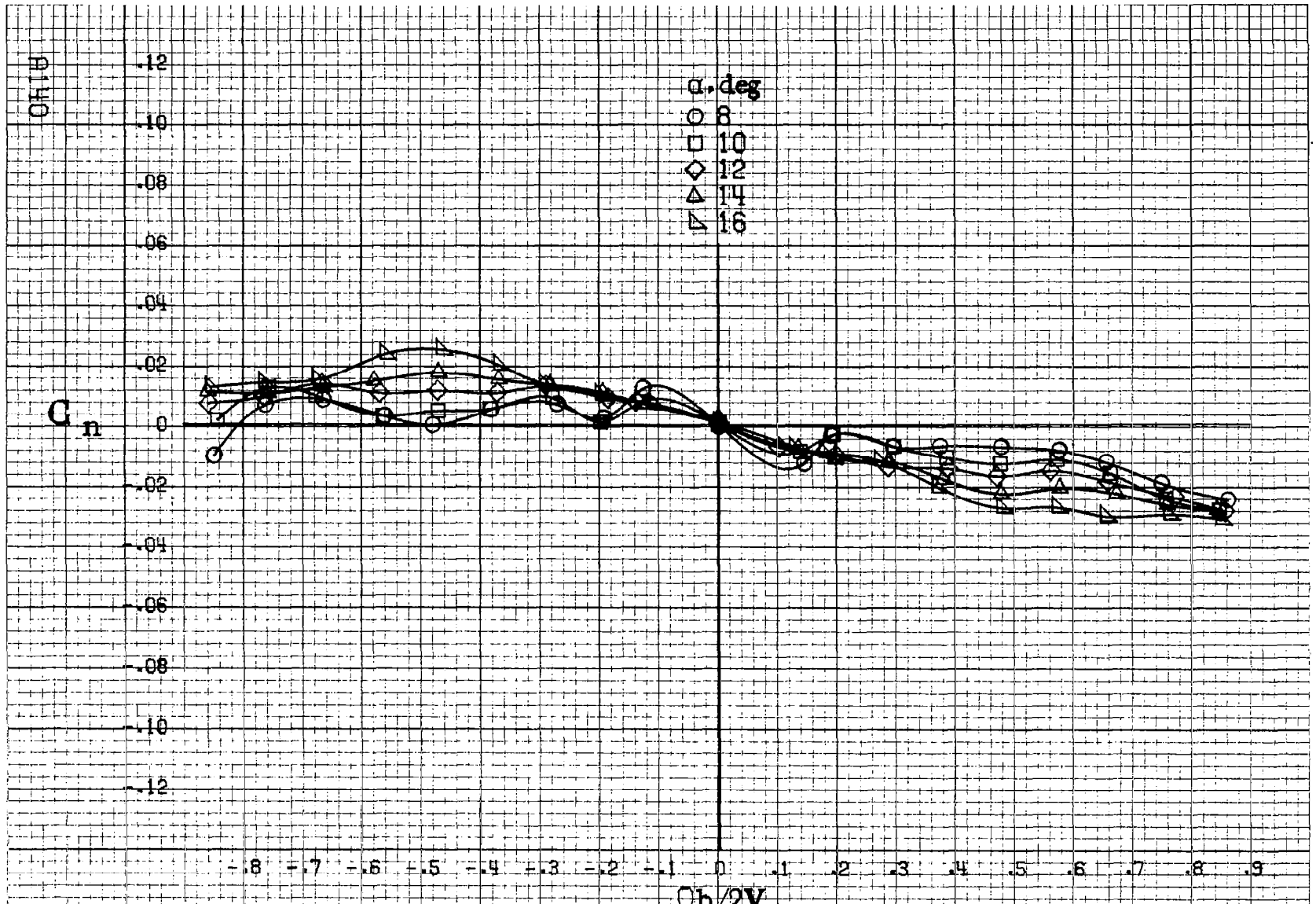

(a) α=8to16deg, SR=76cm(30in).

Figure A58.-Effect of rotation rate and angle of attack on yawing-moment coefficient for configuration having 4.1cm(1.6in) span LE wing tab extended outboard 12.2cm(4.8in) with a triangular fairing. $\delta_a = 0°$, $\delta_t = 0°$, $\delta_r = 0°$, $\beta = 0°$.

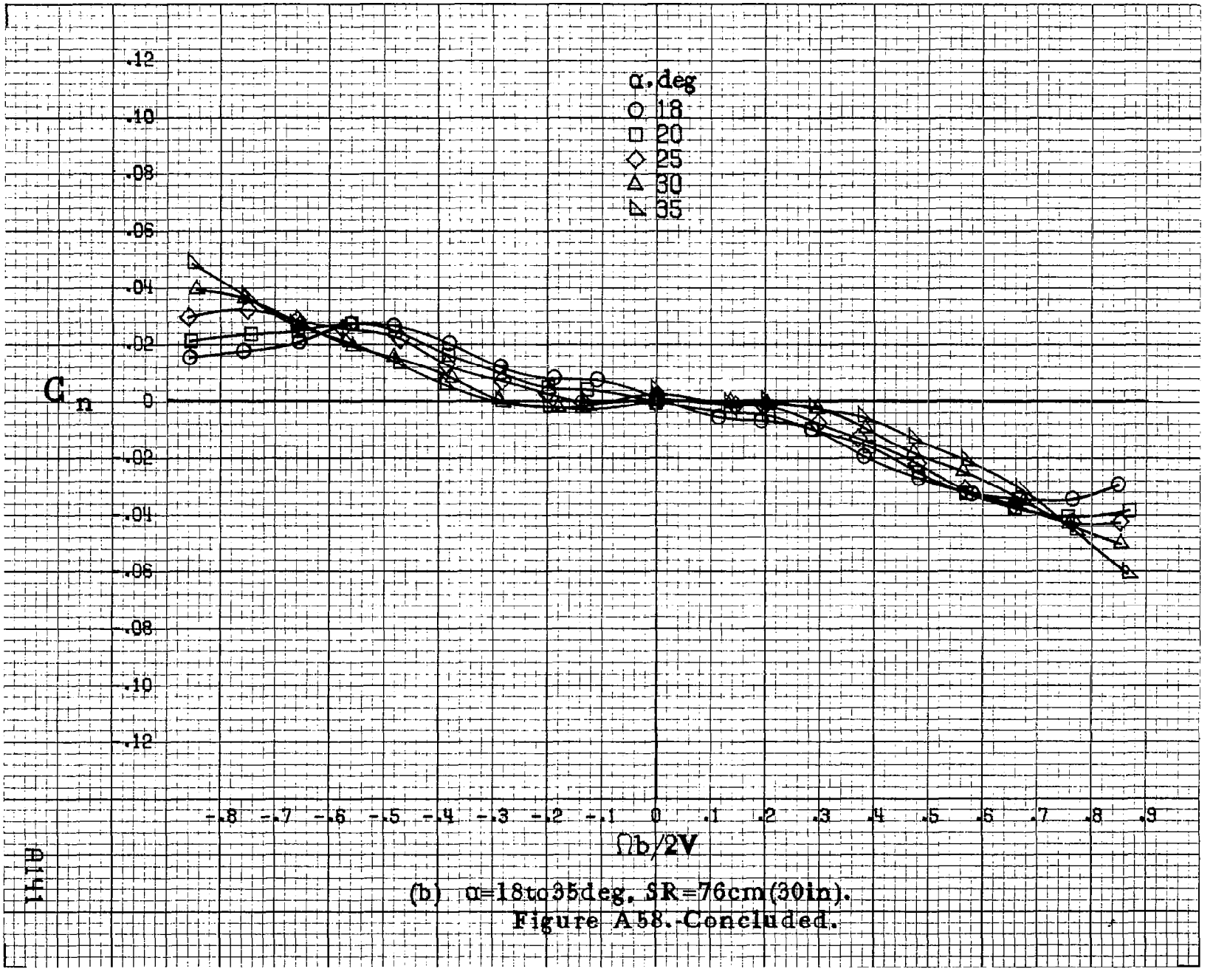

B1f1

(b) α=18to35deg, SR=76cm(30in).

Figure A58.-Concluded.

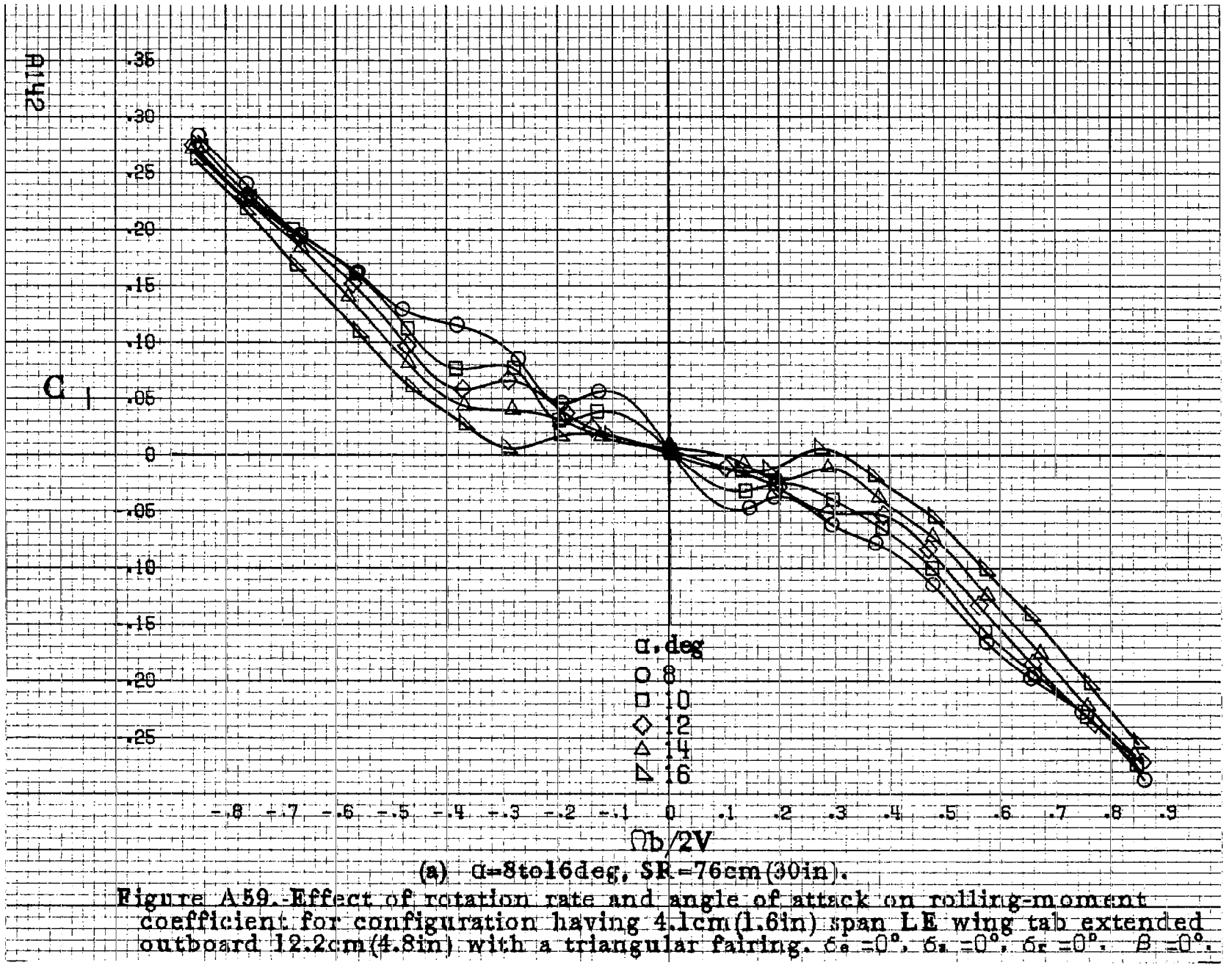

(a) α=8to16deg, SR=76cm(30in).

Figure A59.-Effect of rotation rate and angle of attack on rolling-moment coefficient for configuration having 4.1cm(1.6in) span LE wing tab extended outboard 12.2cm(4.8in) with a triangular fairing. $\delta_e = 0°$, $\delta_a = 0°$, $\delta_r = 0°$, $\beta = 0°$.

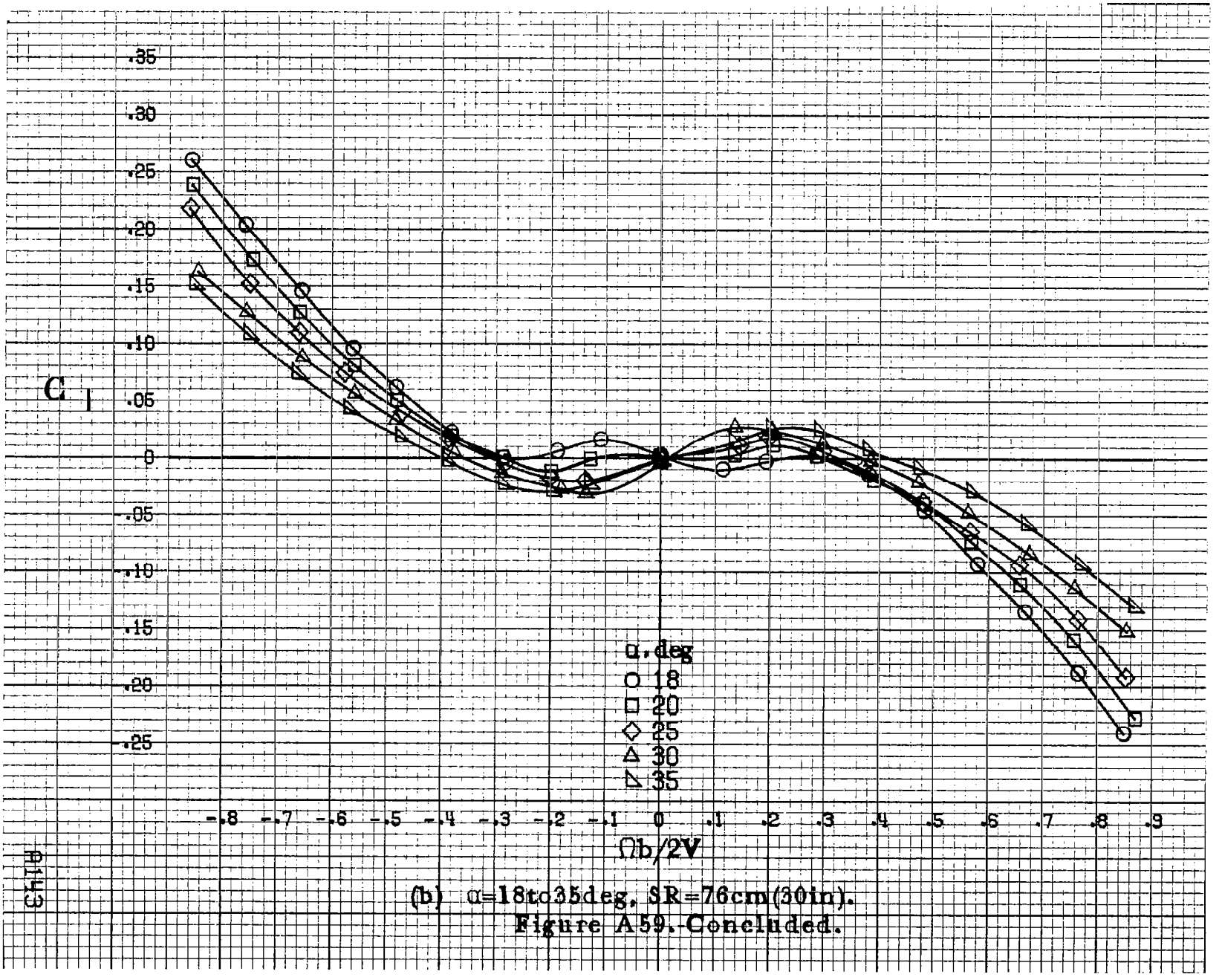

(b) α=18to35deg, SR=76cm(30in).

Figure A59.-Concluded.

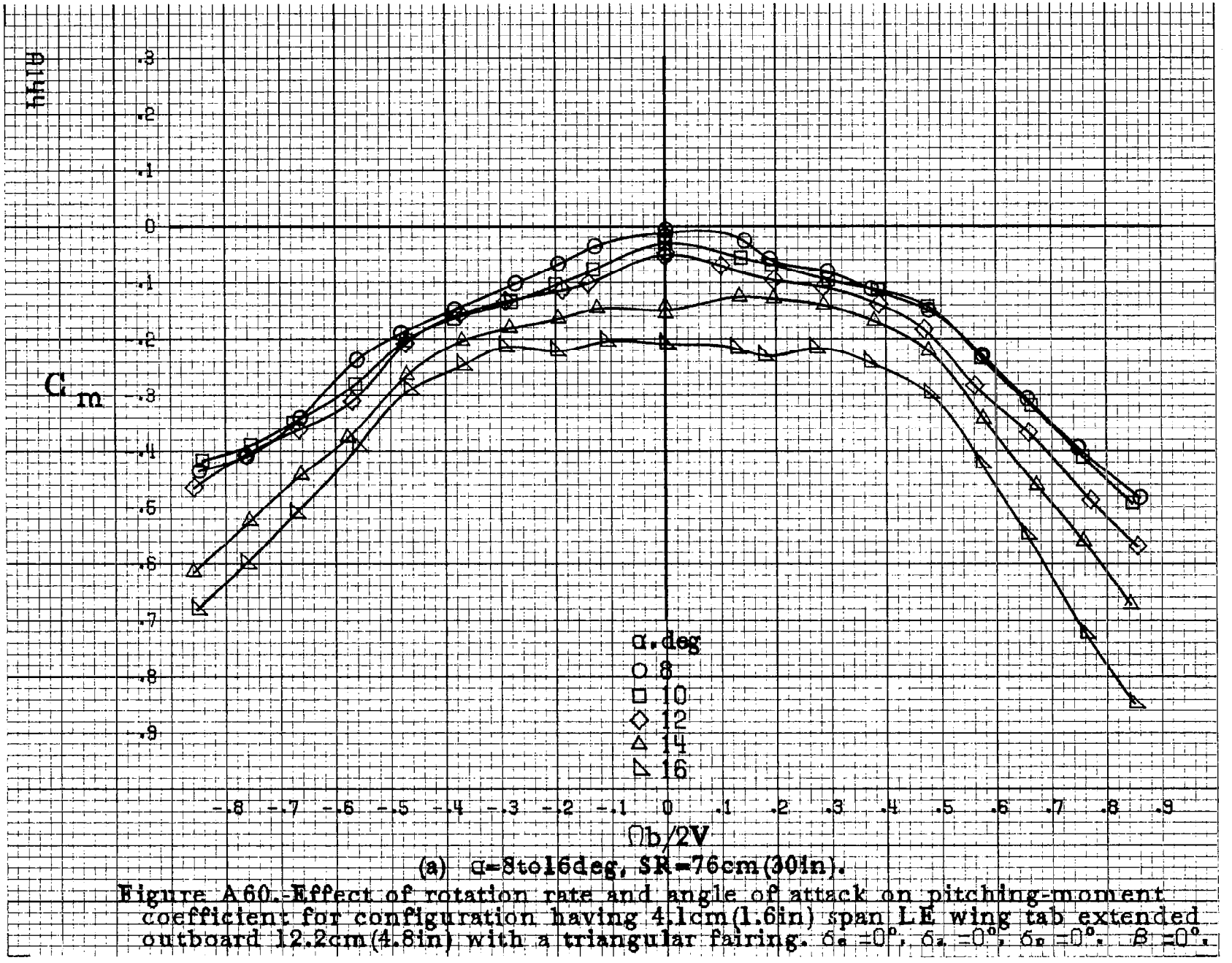

(a) α=8to16deg, SR=76cm(30in).

Figure A60.-Effect of rotation rate and angle of attack on pitching-moment coefficient for configuration having 4.1cm(1.6in) span LE wing tab extended outboard 12.2cm(4.8in) with a triangular fairing. δ_e =0°, δ_a =0°, δ_r =0°. β =0°.

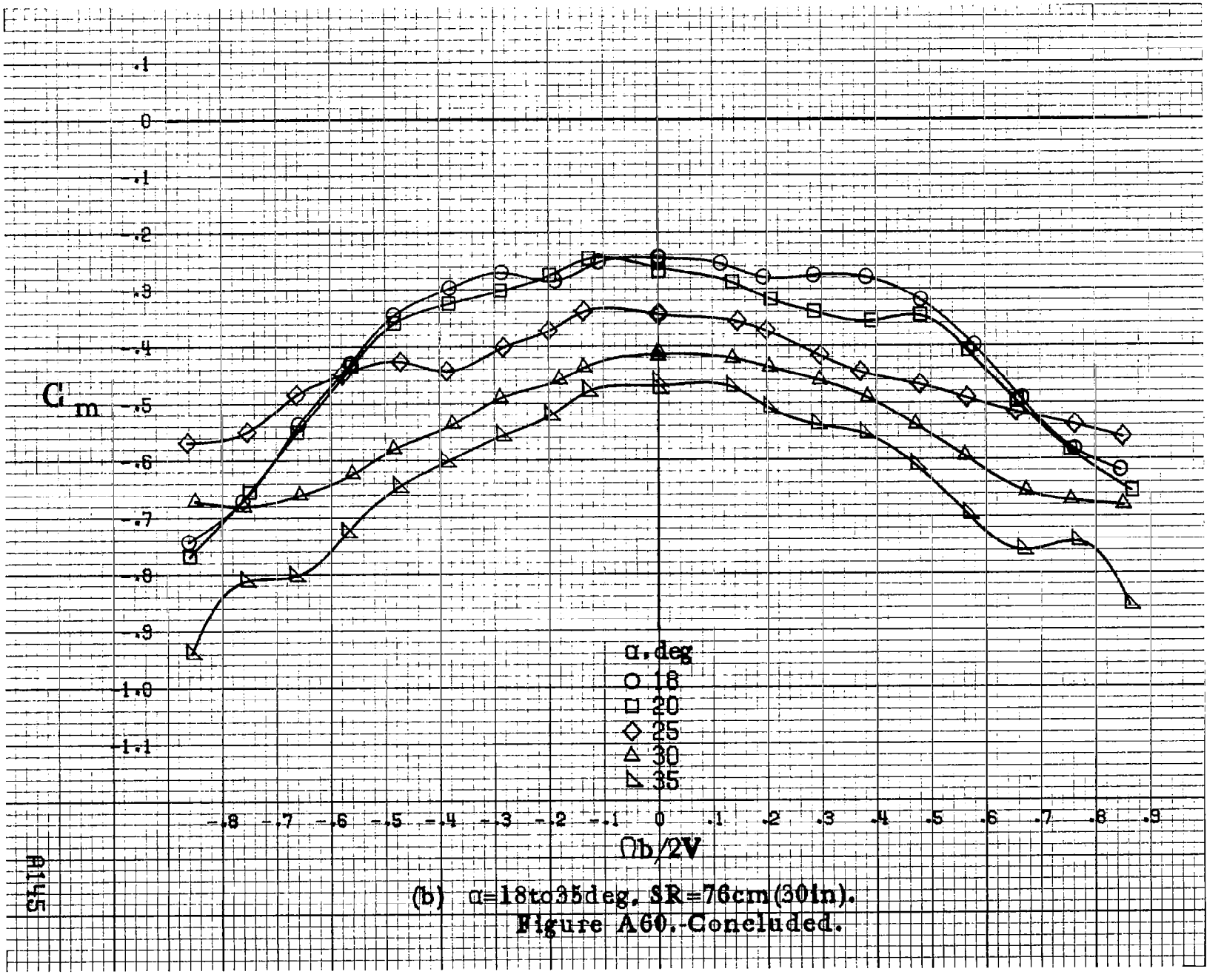

(b) α=18to35deg. SR=76cm(30in).

Figure A60.-Concluded.

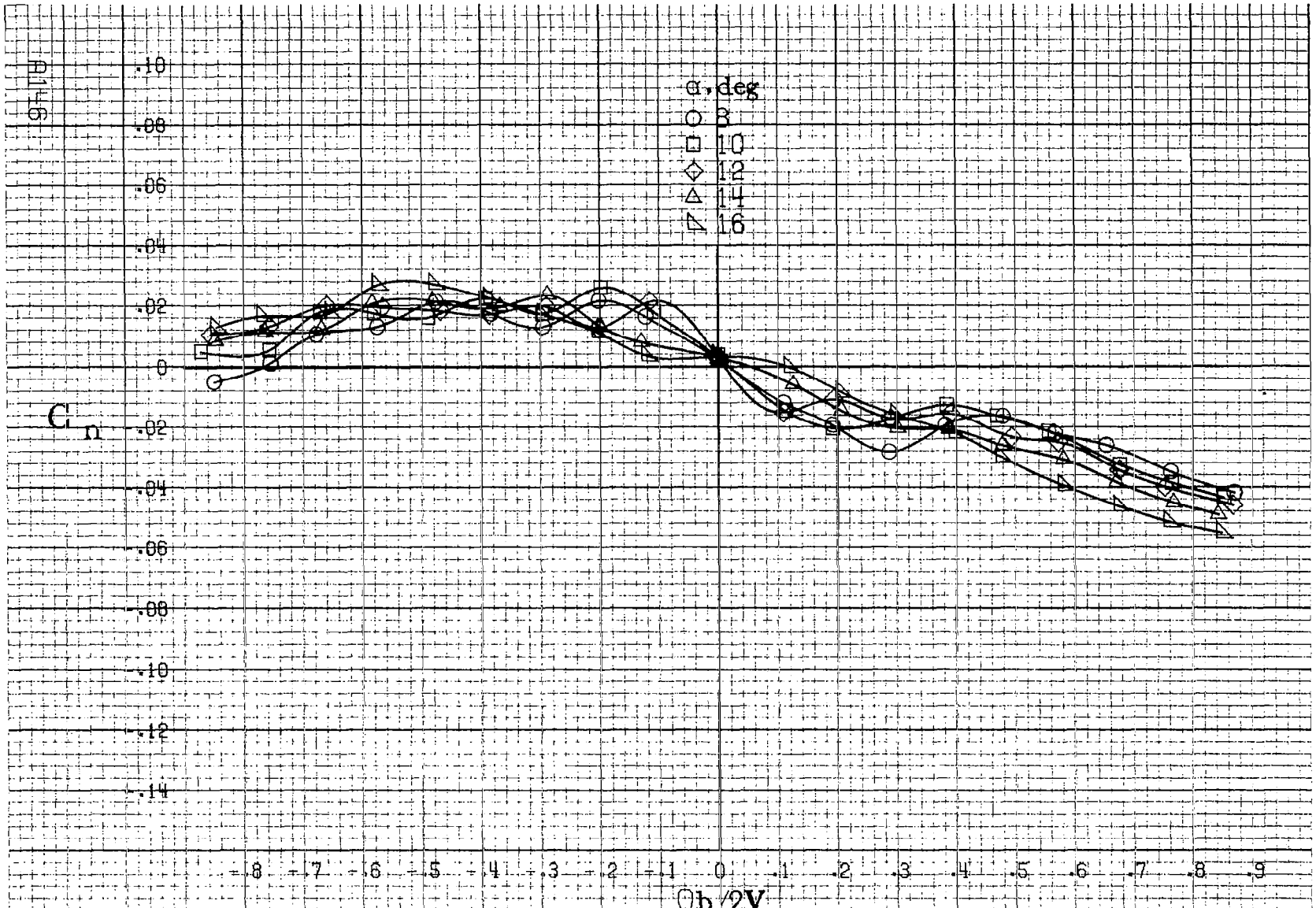

(a) α=8to16deg, SR=76cm(30in).

Figure A61.-Effect of rotation rate and angle of attack on yawing-moment coefficient for configuration having full-span LE wing droop with a 12.2cm (4.8in) span triangular planform LE wing tab. $\delta_e = 0°$, $\delta_a = 0°$, $\delta_r = 0°$, $\beta = 0°$.

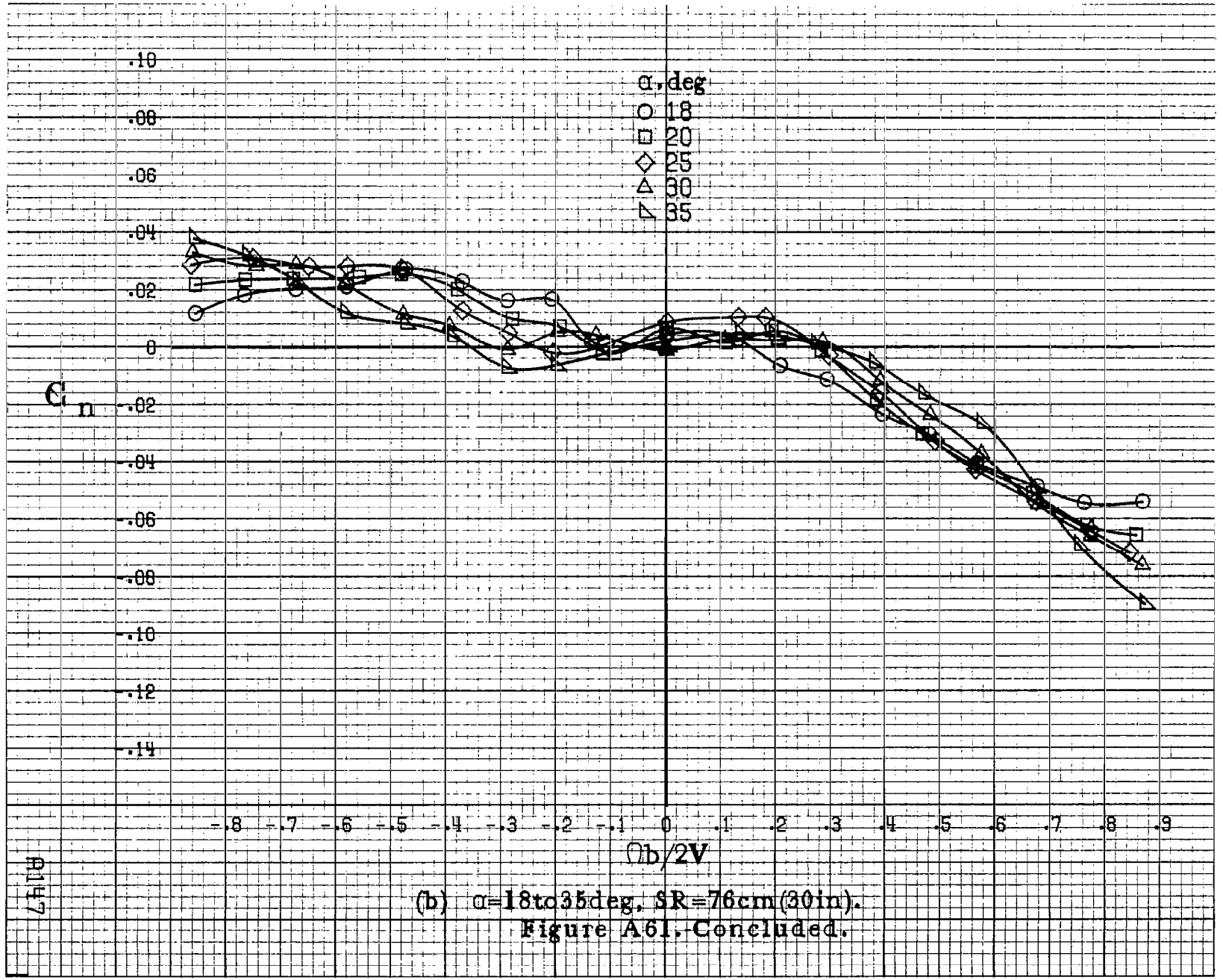

(b) α=18to35deg, SR=76cm(30in).

Figure A61. Concluded.

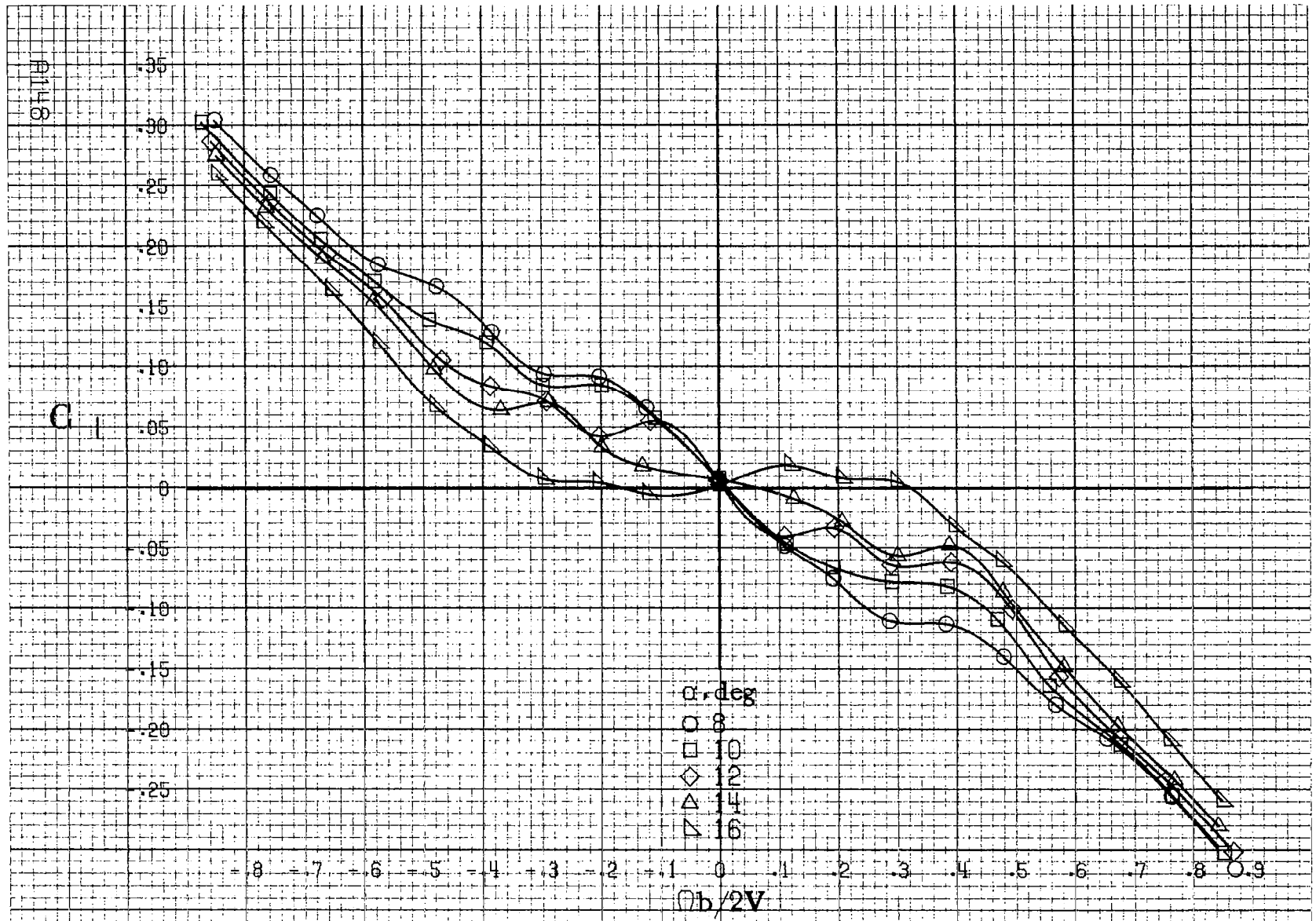

(a) α=8to16deg, SR=76cm(30in).

Figure A62.-Effect of rotation rate and angle of attack on rolling-moment coefficient for configuration having full span LE wing droop with a 12.2cm (4.8in) span triangular planform LE wing tab. $\delta_e = 0^\circ$. $\delta_a = 0^\circ$. $\delta_r = 0^\circ$. $\beta = 0^\circ$.

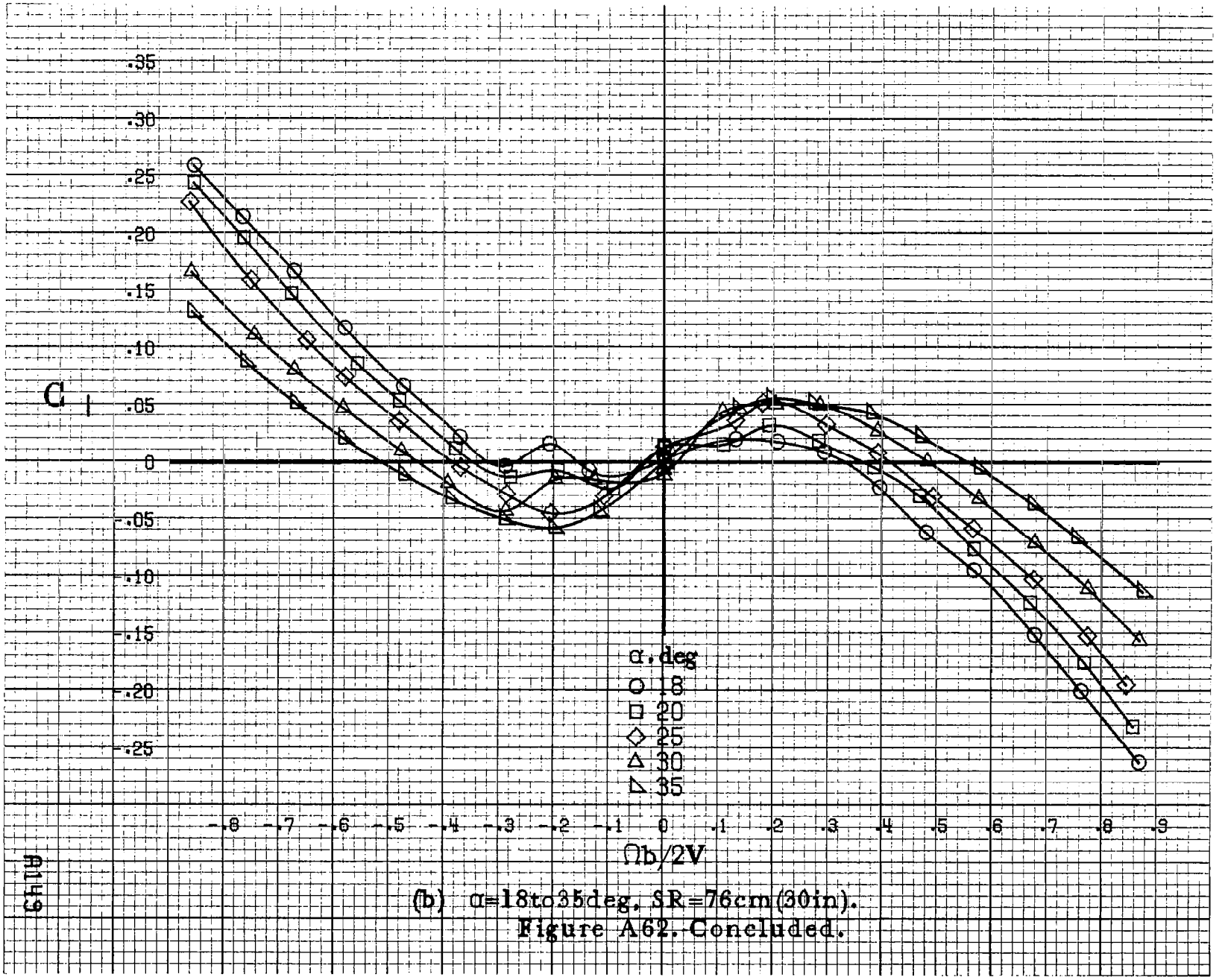

(b) α=18to35deg. SR=76cm(30in).

Figure A62. Concluded.

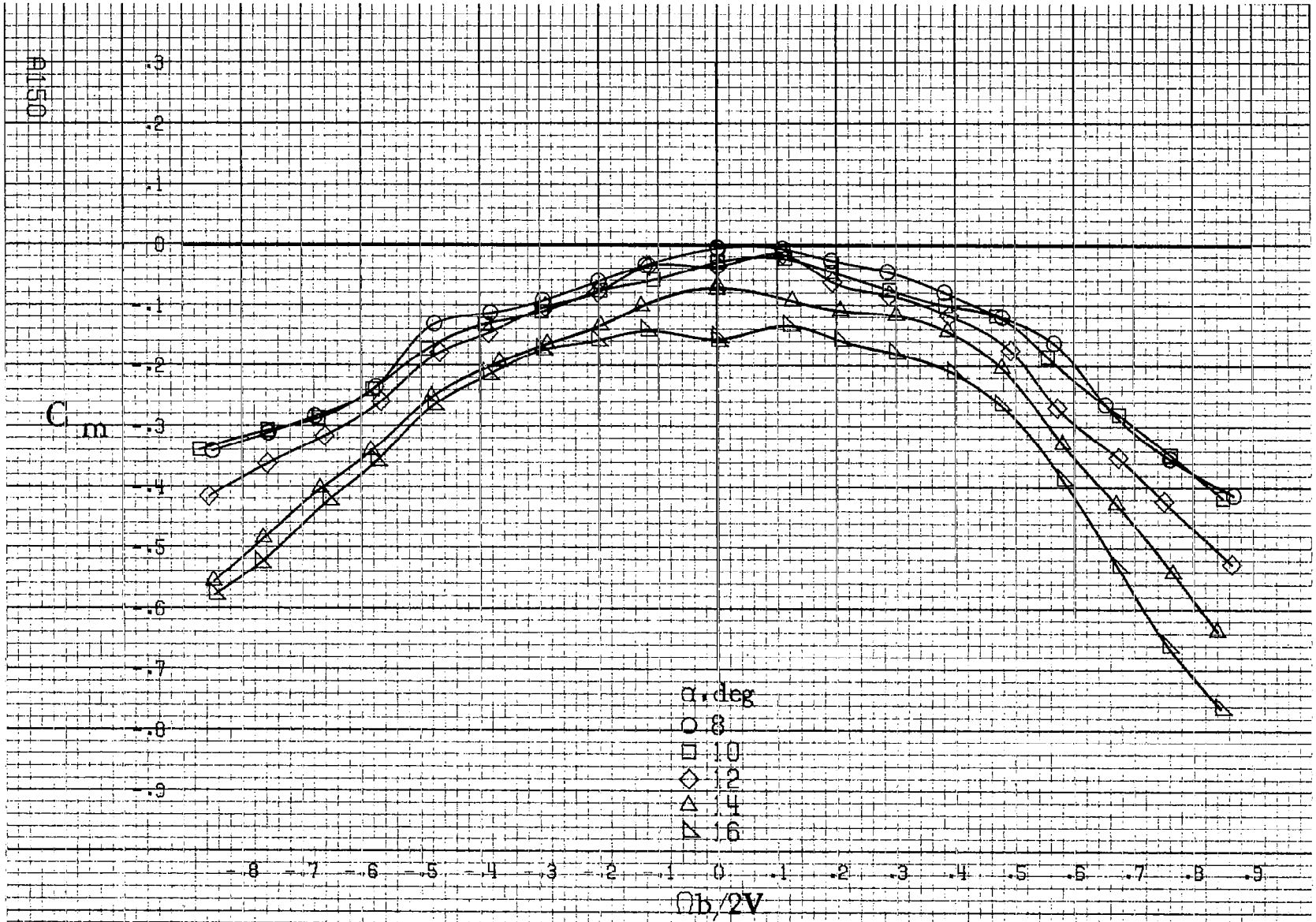

(a) α=8to16deg, SR=76cm(30in).

Figure A63. Effect of rotation rate and angle of attack on pitching moment coefficient for configuration having full-span LE wing droop with a 12.2cm (4.8in) span triangular planform LE wing tab. $\delta_e = 0°$, $\delta_a = 0°$, $\delta_r = 0°$, $\beta = 0°$.

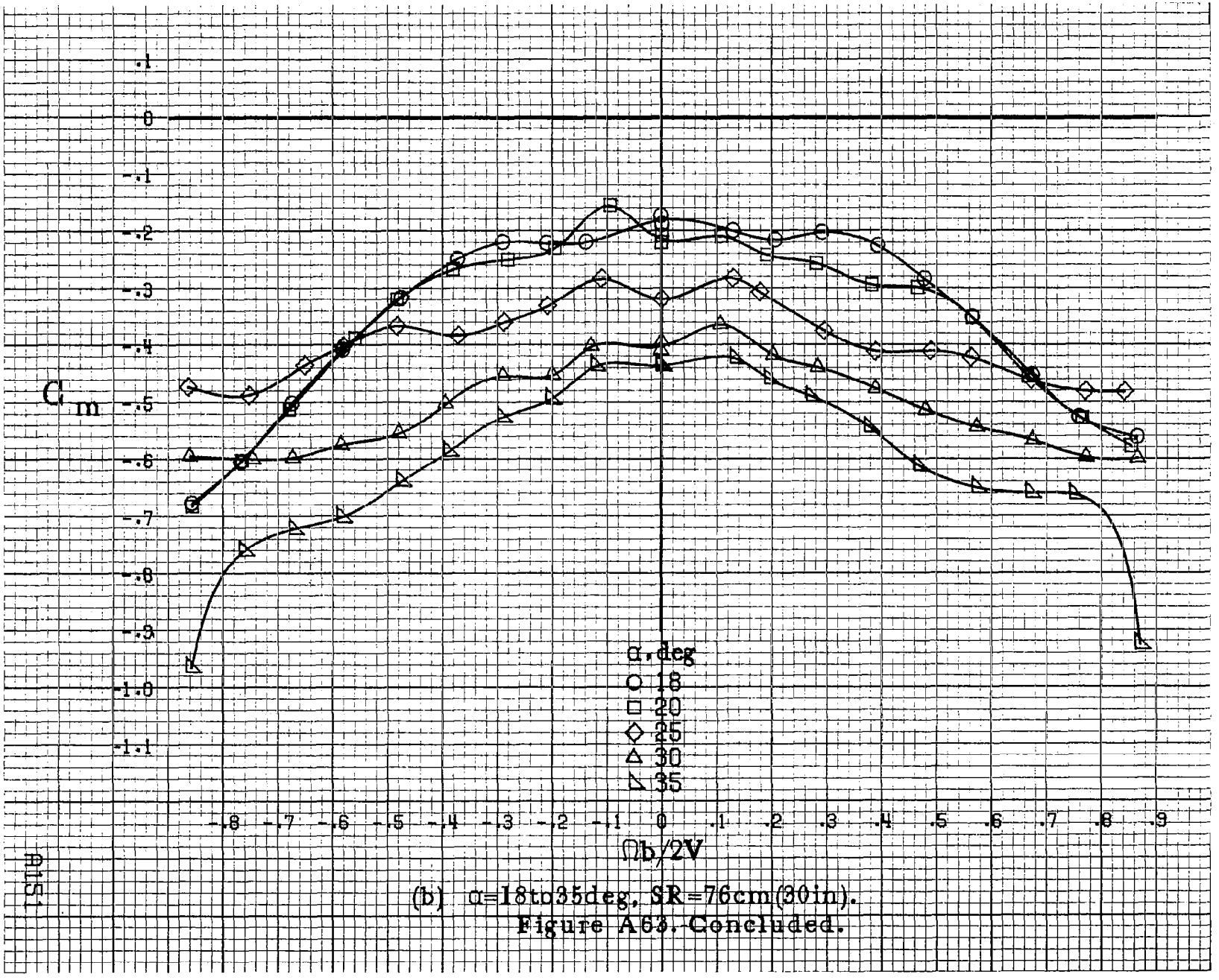

(b) α=18to35deg, SR=76cm(30in).

Figure A63. Concluded.

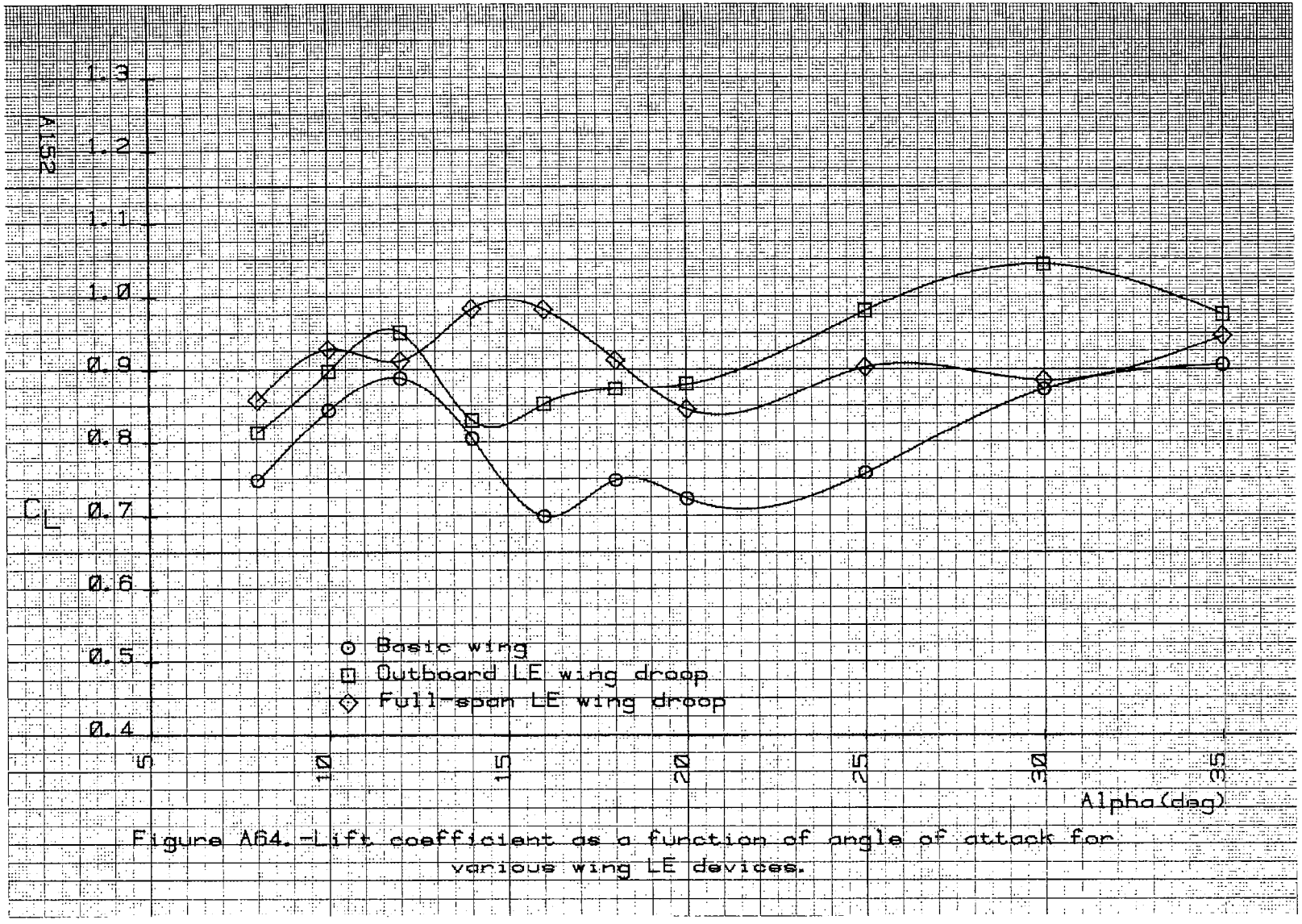

Figure A64.—Lift coefficient as a function of angle of attack for various wing LE devices.

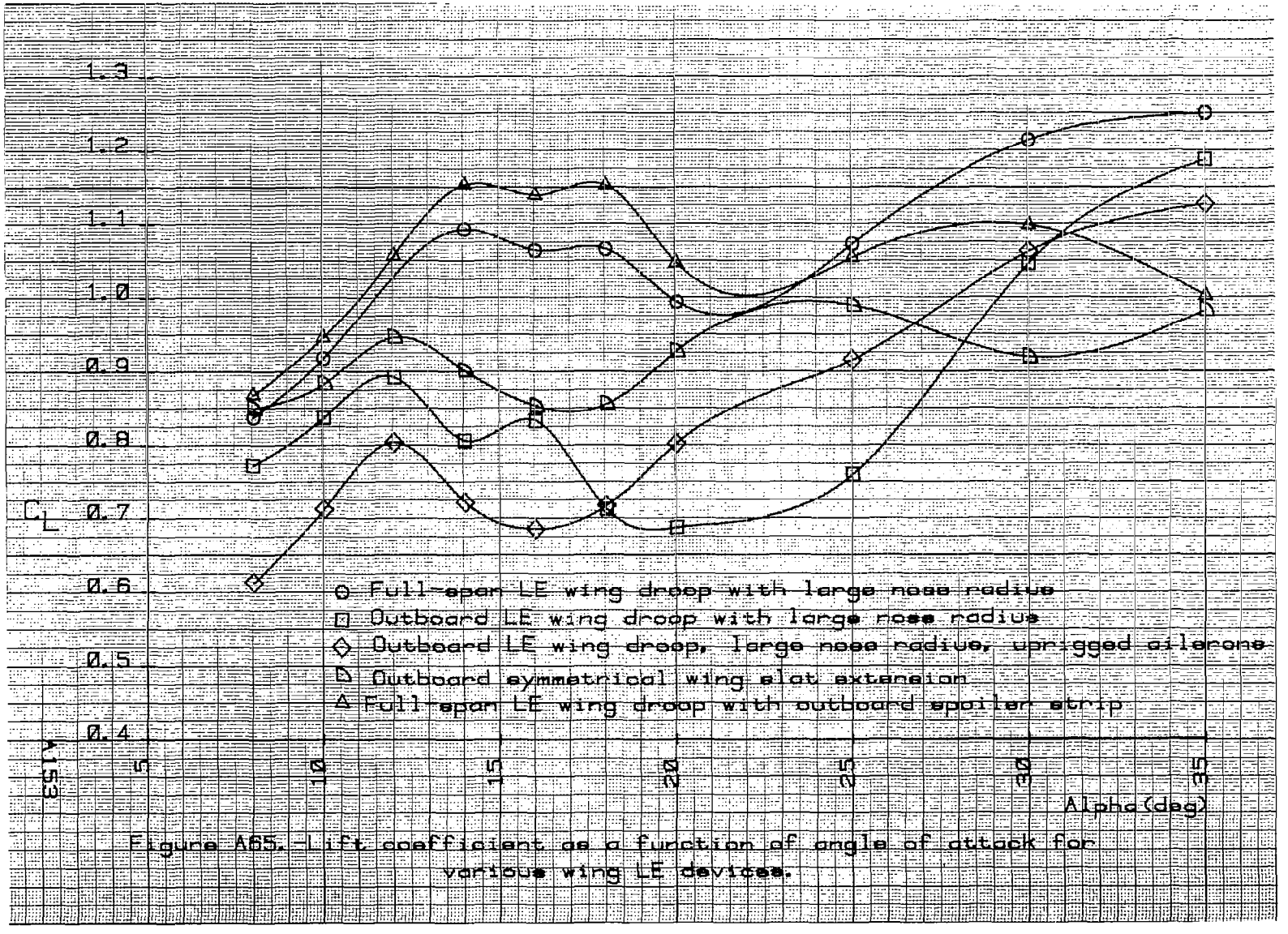

A153

Figure A65. Lift coefficient as a function of angle of attack for various wing LE devices.

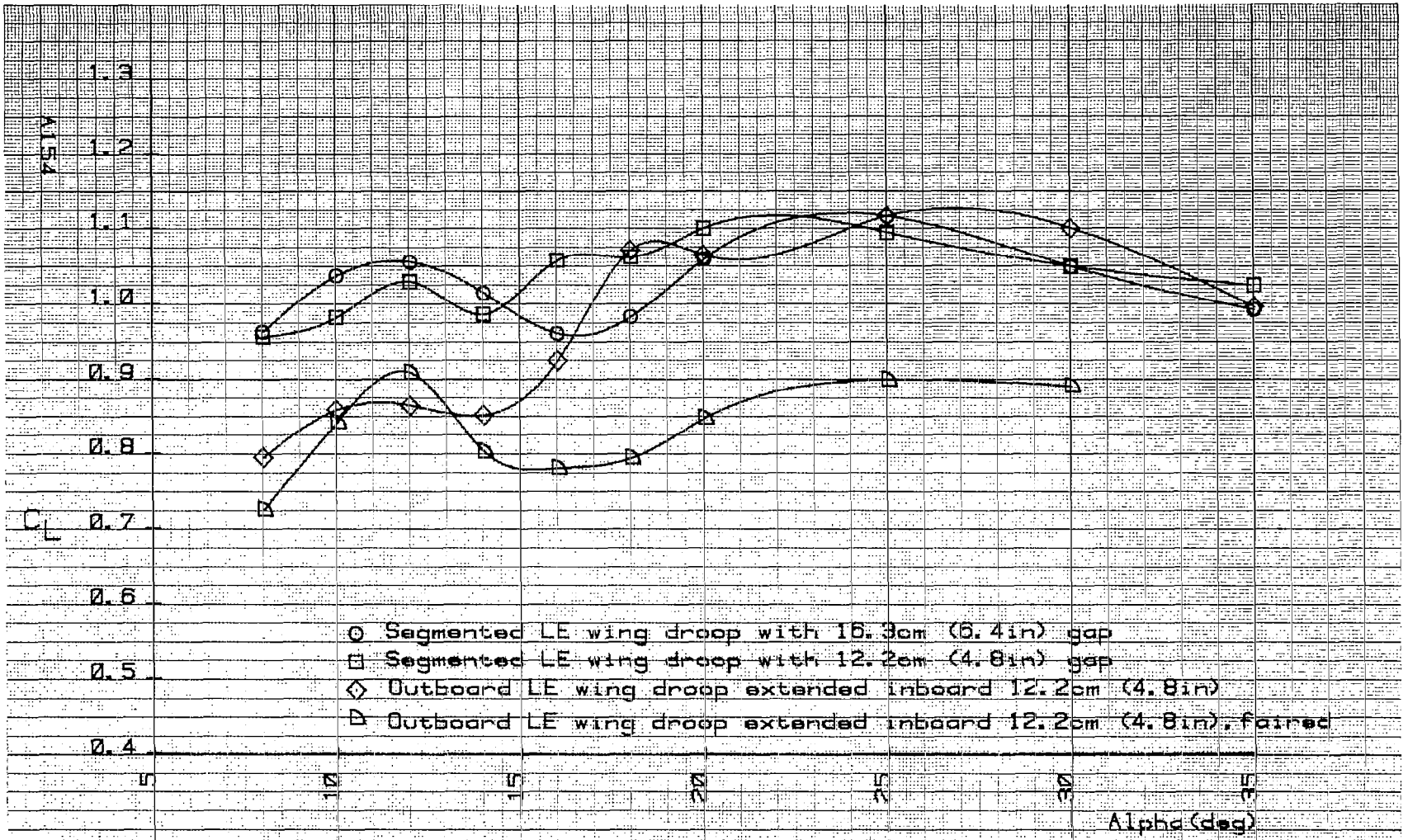

Figure A66.—Lift coefficient as a function of angle of attack for various wing LE devices.

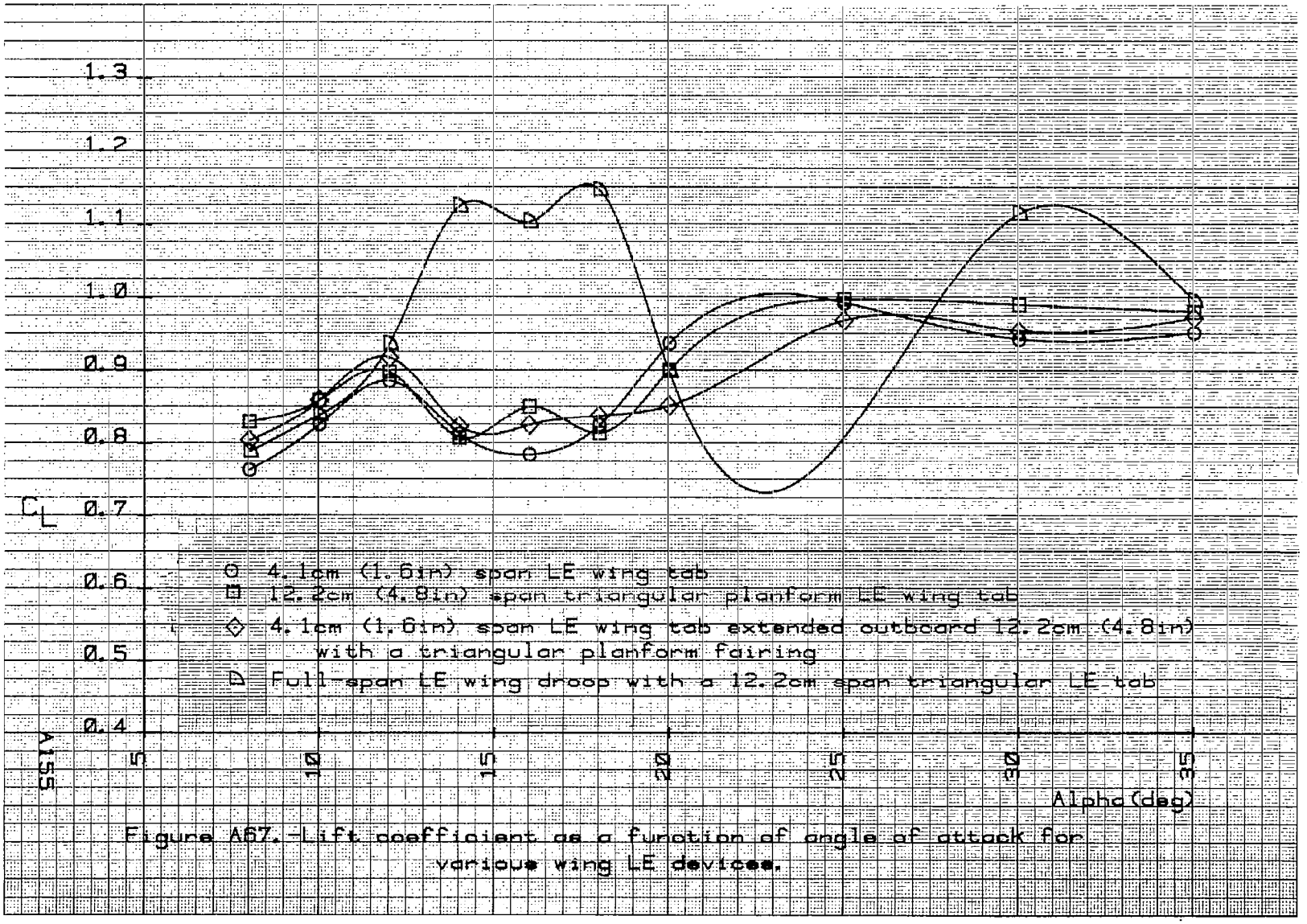

Figure A67.-Lift coefficient as a function of angle of attack for various wing LE devices.

1. Report No.	2. Government Accession No.	3. Recipient's Catalog No.
NASA CR-3102		

4. Title and Subtitle	5. Report Date
Rotary Balance Data for a Typical Single-Engine General Aviation Design for an Angle-of-Attack Range of 8^{o} to 35^{o}. III - Effect of Wing Leading-Edge Modifications Model A.	November 1979
	6. Performing Organization Code

7. Author(s)	8. Performing Organization Report No.
William Bihrle, Jr. William Mulcay	
	10. Work Unit No.
9. Performing Organization Name and Address	505-10-13-07
Bihrle Applied Research, Inc. 400 Jericho Turnpike Jericho, New York 11753	11. Contract or Grant No. NAS1-14849, Task 31
	13. Type of Report and Period Covered
12. Sponsoring Agency Name and Address	Contractor Report
National Aeronautics and Space Administration Washington, DC 20546	14. Sponsoring Agency Code

15. Supplementary Notes

Langley Technical Monitor: James S. Bowman, Jr.

Topical report

16. Abstract

Aerodynamic characteristics obtained in a rotational flow environment utilizing a rotary balance located in the Langley spin tunnel are presented in plotted form for a 1/5-scale, single-engine, low-wing, general aviation airplane model. The configurations tested included the basic airplane, sixteen wing leading-edge modifications and lateral-directional control settings. Data are presented for all configurations without analysis for an angle-of-attack range of 8^{o} to 35^{o} and clockwise and counter-clockwise rotations covering an $\frac{\Omega b}{2V}$ range from 0 to 0.85. Also, data are presented above 35^{o} angle of attack for some configurations.

17. Key Words (Suggested by Author(s))	18. Distribution Statement
General Aviation Spinning Rotary Balance High angle-of-attack wind tunnel data	Unclassified - Unlimited Subject Category 02

19. Security Classif. (of this report)	20. Security Classif. (of this page)	21. No. of Pages	22. Price*
Unclassified	Unclassified	173	$8.00

* For sale by the National Technical Information Service, Springfield, Virginia 22161

NASA-Langley, 1979